

THE $2p^2\ ^3P$ STATE OF SOME He-LIKE SYSTEMS:
ELECTRON CORRELATION EFFECTS

Thesis submitted for the degree of
Doctor of Philosophy
at the University of Leicester

by

David Robert Trevena Keeble
Department of Physics and Astronomy
University of Leicester

April 1990

UMI Number: U025912

All rights reserved

INFORMATION TO ALL USERS

The quality of this reproduction is dependent upon the quality of the copy submitted.

In the unlikely event that the author did not send a complete manuscript and there are missing pages, these will be noted. Also, if material had to be removed, a note will indicate the deletion.



UMI U025912

Published by ProQuest LLC 2015. Copyright in the Dissertation held by the Author.
Microform Edition © ProQuest LLC.

All rights reserved. This work is protected against
unauthorized copying under Title 17, United States Code.



ProQuest LLC
789 East Eisenhower Parkway
P.O. Box 1346
Ann Arbor, MI 48106-1346



7500491788

7751645183

ACKNOWLEDGEMENTS

I wish to thank Professor K.A. Pounds for the opportunity to work in the Department of Physics and Astronomy at the University of Leicester.

The receipt of a Science and Engineering Research Council maintenance grant is gratefully acknowledged.

I am indebted to Miss B.M. Trevena, Mr L.B. Keeble and Mrs R. Christmas for their help in the preparation of this thesis.

I should like to express my gratitude for the assistance given by the staff of the Computer Centre and for the help given by all the members of the Quantum Molecular Physics Research Group at the University of Leicester. In particular, the advice of Dr P.K. Youngman has been unstinting and invaluable.

It is a pleasure to acknowledge the assistance of Professor G. Drake of the University of Windsor, Ontario and also Professor C.A. Nicolaides and Dr G. Aspromallis of the National Hellenic Research Foundation, Athens who provided many of the wavefunctions analysed in this thesis.

Above all, special thanks must go to Dr K.E. Banyard for his patience, help and encouragement throughout the course of this research.

D.R.T. Keeble

Contents

I	Introduction	4
1	General Introduction	5
1.1	The Correlation Problem	5
1.2	Examination of Correlation Effects	10
2	The $2p^2\ ^3P$ State	13
2.1	Doubly Excited States	13
2.2	Experimental Evidence for the $2p^2\ ^3P$ State	14
2.3	Wavefunctions for the $2p^2\ ^3P$ State	16
II	Electron Correlation Effects in Position Space	19
3	Wavefunctions	20
3.1	Introduction	20
3.2	Hartree-Fock Wavefunctions	21
3.3	Drake Wavefunctions	22
3.4	Nicolaides and Aspromallis Wavefunctions	23
4	Evaluation of Correlation Properties	27
4.1	Introduction	27
4.2	Radial Functions and Properties	28
4.3	$f(r_{12})$ and Related Functions and Properties	34
4.4	Interangular Functions and Properties	38

5	Discussion of Position Space Results	43
5.1	Introduction	43
5.2	Total Correlation Effects	45
5.3	Z-Dependent Trends	56
5.4	The Drake Wavefunctions Compared to the NA-CI Wavefunctions . . .	64
5.5	The Natural Expansions and the NA-CI Wavefunctions	71
5.6	Summary	83
6	Position Space Results: Tables and Figures	85
6.1	Introduction	85
6.2	Position Space Results: Tables	87
6.3	Position Space Results: Figures	97
III	Electron Correlation Effects in Momentum Space	132
7	Momentum Space	133
7.1	Introduction	133
7.2	Wavefunctions	137
7.3	Evaluation of Correlation Properties	139
8	Discussion of Momentum Space Results	145
8.1	Introduction	145
8.2	Total Correlation Effects	147
8.3	Z-Dependent Trends	156
8.4	The Natural Expansions and the NA-CI Wavefunctions	163
8.5	Summary	175
9	Momentum Space Results: Tables and Figures	179
9.1	Introduction	179
9.2	Momentum Space Results: Tables	181
9.3	Momentum Space Results: Figures	188

IV	Appendices	216
A	Curve-Fitting	217
A.1	Introduction	217
A.2	Fitting Procedure	218
A.3	Tests of Goodness-of-Fit	220
A.4	Discussion	222
A.5	Table and Figures	224
B	Gram-Schmidt Orthogonalization	228
C	Natural Orbital Analysis	230
C.1	Introduction	230
C.2	Method	232
	Bibliography	237

Part I
Introduction

Chapter 1

General Introduction

1.1 The Correlation Problem

Quantum theory, the foundations of which were principally developed in the first three decades of this century, is based upon the Schrödinger wave equation [1]. For an N-electron atomic system, the non-relativistic, time-independent Schrödinger equation is given by:

$$\left(-\frac{1}{2} \sum_{i=1}^N \nabla_i^2 - Z \sum_{i=1}^N \frac{1}{r_i} + \sum_{i<j}^N \frac{1}{r_{ij}}\right) \Psi = E \Psi, \quad (1.1)$$

where r_i is the distance of electron i from the nucleus, r_{ij} is the distance between electron i and electron j , Ψ is the wavefunction representing the system, Z is the atomic number and E is the energy of the system. This equation is expressed in atomic units [2], which will be used throughout this thesis except where otherwise explicitly stated.

In any system containing more than one electron the wave equation cannot be solved in a closed analytic form owing to the presence of the $\frac{1}{r_{ij}}$ terms. This therefore means that any quantum mechanical investigation of such a system must use approximation techniques. The principal, but not the only, function of such an approximation will generally be to produce the most accurate energy possible.

Some early attempts to surmount the problem of the $\frac{1}{r_{ij}}$ terms in equation 1.1 were due to Hartree [3] and to Fock [4], and the culmination of their efforts came to be known as the ‘Hartree-Fock technique’. The essence of their method was to assume that the

interelectronic potential could be modelled by a static average potential, experienced by each electron. This static potential evolves by a self-consistent procedure, whereby an approximate independent-particle wavefunction is used to calculate an approximate potential which is then used to produce an improved wavefunction. This procedure is then iterated until no further significant change is observed in the wavefunction, and hence in the potential field. This independent-particle wavefunction is termed the ‘Hartree-Fock wavefunction’. In order to take account of the Pauli exclusion principle, the Hartree-Fock wavefunction must be written in Slater-determinantal form [5], which ensures that the wavefunction is antisymmetric.

It is clear, however, that the Hartree-Fock procedure can never produce a wavefunction which is exactly correct. This is because in reality the instantaneous position of each electron is *correlated* with the instantaneous position of every other electron, due to the electrostatic force between them. The correlation energy of a system is usually defined as being the difference between the exact non-relativistic energy of the system and the Hartree-Fock energy of the system:

$$E_{\text{Correlation}} = E_{\text{Exact}} - E_{\text{HF}}. \quad (1.2)$$

This definition, which is due to Löwdin [6], only encompasses *Coulombic* correlation, as the antisymmetric nature of the Hartree-Fock wavefunctions ensures that parallel electrons experience what is known as ‘Fermi correlation’. In general, we will take the term ‘correlation’ to mean only Coulombic correlation, unless otherwise stated. Coulombic correlation may be visualized as a region of depleted electron density surrounding each electron—the so-called ‘Coulomb hole’ [7]. Likewise, each electron can be surrounded by a ‘Fermi hole’ [8] where the density of parallel electrons is reduced.

The Hartree-Fock method frequently produces energies that are within 1% of the exact energy, and it might therefore be questioned whether it is necessary to make further attempts to improve upon this approximation method. Unfortunately, however, the correlation energy turns out to be of a significant magnitude in very many chemical applications. This is because it is usually the *change* in energies in a given process that is relevant, and this is obviously smaller than the magnitudes of the actual energies.

If the Hartree-Fock energies are used, the energy change predicted will often be very inaccurate, and may even be of the wrong sign. For example, in this thesis the $2p^2\ ^3P$ state of the H^- ion, amongst others, will be studied. The Hartree-Fock energy predicts, wrongly, that this system will not be bound and so more sophisticated calculations are required. A circumstance of particular inadequacy for Hartree-Fock calculations is encountered when molecules where the constituent nuclei are significantly displaced from their equilibrium positions are considered. Here, the Hartree-Fock energies tend to be especially inaccurate [9].

Wavefunctions which go beyond the Hartree-Fock approximation in the accuracy of their energies are known as *correlated* wavefunctions. Two of the most important kinds were first employed by Hylleraas [10,11] in the late 1920's. Each employs the variation method [12], whereby a trial wavefunction is constructed containing unknown parameters, which are then varied to produce the minimum energy. It may be shown that this energy is then the best possible approximation for a wavefunction of this form, and that it constitutes an upper bound to the true energy. The Löwdin definition can be used to assess the degree to which the energy, E_{Approx} , of an approximate correlated wavefunction bridges the gap between the Hartree-Fock energy and the exact energy. The percentage of the correlation energy recovered by an approximate wavefunction is defined:

$$\%E_{CORR} = 100 \frac{E_{Approx} - E_{HF}}{E_{Correlation}}, \quad (1.3)$$

where E_{HF} and $E_{Correlation}$ are defined as in equation 1.2.

The first type of approximations are known as 'Hylleraas-type' or 'explicitly-correlated' wavefunctions. These contain powers of the interelectronic distances r_{ij} . An example of a Hylleraas-type wavefunction may be seen in equation 3.6 in chapter 3. As the purpose of using correlated wavefunctions is to represent the interelectronic interactions accurately, it is natural to expect a wavefunction containing interelectronic distances to be rapidly convergent in energy as the number of terms used in the wavefunction, and hence its flexibility, is increased. This is indeed so [13], and the most accurate non-relativistic energy approximations for the ground state of helium use Hylleraas-type

trial wavefunctions. The impressive calculations of Pekeris and Frankowski [14,15]

in the 1950's and 1960's remained unsurpassed with respect to the energies obtained until the 1984 work of Freund, Huxtable and Morgan [16]. All of these workers used explicitly-correlated wavefunctions of various kinds. Unfortunately, it proves difficult to extend the explicitly-correlated method to species containing more than two electrons, and although there have been results reported for three-electron systems [17], the vast bulk of variational results for systems containing three or more electrons use the second method of wavefunction approximation.

This second form of wavefunction is most commonly known as a 'configuration-interaction' (CI) wavefunction. The wavefunction comprises terms called 'configurations', each of which consists of a summation of Slater determinants, the elements of which are one-electron functions called spin-orbitals. The spin-orbitals are given by:

$$\varphi(r, \theta, \phi)_{nlmm_s} = R_{nl}(r)Y_l^m(\theta, \phi)\chi_{m_s}, \quad (1.4)$$

where $R_{nl}(r)$ is a function of r , the distance of the electron from the nucleus, $Y_l^m(\theta, \phi)$ is a spherical harmonic angular function, and χ_{m_s} is a function representing the spin-state of an electron. ' n ', ' l ' and ' m ' denote the principal, azimuthal and magnetic quantum numbers respectively. m_s is the quantum number corresponding to the eigenfunctions of the spin angular momentum operator, \hat{S}_z . In atomic calculations, the radial functions, $R_{nl}(r)$, are most usually composed of the radial parts of 'Slater-type orbitals' (STO's) [18], which bear a close resemblance to the radial parts of hydrogen-like wavefunctions, (see equations 3.3 and 7.4). All spherical harmonics used in this thesis employ the Condon-Shortley [19] phase convention, whereby,

$$Y_l^{-m}(\theta, \phi) = (-1)^m Y_l^{m*}(\theta, \phi), \quad (1.5)$$

where '*' denotes complex conjugation. An example of a configuration interaction wavefunction is given by equations 3.12 and 3.13 in chapter 3.

At first sight, a configuration interaction wavefunction may not appear very suitable for the incorporation of correlation effects, as it contains no direct reference to

interelectronic distances. But if we consider the expansion of $\frac{1}{r_{ij}}$ in terms of spherical harmonics [20]:

$$\frac{1}{r_{ij}} = \sum_{l=0}^{\infty} \sum_{m=-l}^{m=+l} \frac{4\pi}{2l+1} \frac{r_{<}^l}{r_{>}^{l+1}} (-1)^m Y_l^m(\theta_i, \phi_i) Y_l^{m*}(\theta_j, \phi_j), \quad (1.6)$$

where ‘ $r_{>}$ ’ and ‘ $r_{<}$ ’ denote respectively the larger and the smaller of r_i and r_j , it may be seen that the interelectronic distance is included in CI wavefunctions, albeit indirectly. This indirectness is responsible for the extremely slow convergence of CI wavefunctions [13].

In principle, both of the above methods may achieve results of any required accuracy, at the non-relativistic approximation, providing enough terms in the trial wavefunctions are used. Clearly, the more complex a wavefunction is, the more computation is required to achieve a variational minimum for the corresponding energy. It was only in the 1950’s that the widespread introduction of digital electronic computers made possible accurate calculations on any but the simplest systems. In this sense, advances in atomic and molecular calculations may still be said to be driven by advances in computer technology. Nevertheless, despite huge increases in the amount of computing power available, there is a multitude of problems remaining to be solved. There is thus a great need for an understanding of *how* accurate wavefunctions may be constructed. Because it is now possible to obtain the Hartree-Fock wavefunction with the use of relatively little computer time for many systems, especially atomic systems [21], efficient wavefunction construction depends primarily on an understanding of *correlation* effects. As Sinanoğlu and Brueckner [22] have written:

The effects [of correlation] are large, so that without them a quantitative theory of atomic structures would not be possible.

More recently, Feng and Dahl [23] have made similar comments:

The study of the electron correlation problem has always been one of the most important subjects in quantum chemistry and is central to our understanding of the electronic structure of atoms and molecules.

Sinanoğlu [24] has suggested a method of writing the exact wavefunction for a system in a manner that makes the correlation effects explicit. Following this scheme, one may write for an N-electron system:

$$\Psi(1, 2, \dots, N) = c\mathcal{A}[(\phi_1, \phi_2, \dots, \phi_i, \dots, \phi_N)(1 + \sum_i^N \frac{f(i)}{\phi_i} + \frac{1}{\sqrt{(2!)}} \sum_{i>j}^N \frac{U_{ij}}{\phi_i\phi_j} + \frac{1}{\sqrt{(3!)}} \sum_{i>j>k}^N \frac{U_{ijk}}{\phi_i\phi_j\phi_k} + \dots)], \quad (1.7)$$

where \mathcal{A} is the antisymmetrizer and $(\phi_1, \phi_2, \dots, \phi_i, \dots, \phi_N)$ is generally a product of N normalized Hartree-Fock spin-orbitals. Each $f(i)$ function provides a correction to the i th Hartree-Fock orbital. The U_{ij} functions are electron-pair correlations and the higher terms describe multi-electron correlations. The precise nomenclature used here is that of Taylor and Banyard [25].

As the simplest atomic species in which correlation effects are present, helium-like systems have always played an important role in quantum mechanics. Hylleraas' pioneering studies were carried out on such systems. They are simple enough for highly accurate calculations to be carried out on them, yet contain essentially the same kinds of correlation effects as do more complex systems. Hence they are ideal candidates for examinations of correlation effects.

1.2 Examination of Correlation Effects

There have been a number of correlation studies on different systems, using a variety of methods. One of the first quantitative examinations was conducted by Coulson and Neilson in 1961 [7]. These authors considered, for the helium atom, the function $\Delta f(r_{12})$, which is defined as the change in the interelectronic distribution function, $f(r_{12})$, due to electron correlation. It therefore comprises the Hartree-Fock interelectronic distribution function subtracted from the equivalent correlated function, in accordance with the Löwdin [6] conception of correlation effects stated in equation 1.2. As this function shows the depletion in electron density near to an electron due to Coulombic correlation effects, Coulson and Neilson considered it to be a definition of the Coulomb hole. The

form of their Coulomb hole showed that correlation effects reduces the value of the $f(r_{12})$ function for small r_{12} , but increases it for large r_{12} .

There have since been at least two different definitions of the Coulomb hole employed by various workers. Gilbert [26] proposed in 1963 that the above definition should be weighted by a factor of r_{12}^{-1} , on the grounds that the effect of correlation on the interelectronic potential energy would thereby be shown directly. In 1974 Tatewaki and Tanaka [27] published correlation studies concerning Be, B⁺ and C⁺⁺ where the $\Delta f(r_{12})$ function was divided by r_{12}^2 in order to yield the change in average probability per unit volume. This function is effectively the same as the correlation-induced change in the intracule function of Thakkar [28]. None of these later functions possesses simple normalization properties, whereas the $f(r_{12})$ of Coulson and Neilson normalizes to unity. The approaches of Gilbert and of Tatewaki and Tanaka do not seem to have found as much favour in the literature as that of Coulson and Neilson. In 1965, Curl and Coulson [29] examined the Coulomb holes for some members of the helium series, H⁻, He, Li⁺ and O⁶⁺, concluding, as did Lester and Krauss [30], that their depth was independent of charge.

The $\Delta f(r_{12})$ function inevitably presents a limited view of correlation effects, and various authors have examined other correlation functions. In 1973 Boyd and Coulson [31] presented the *partial* Coulomb hole, where a test electron is held at a fixed distance r_1 from the nucleus, and the effects of correlation on the behaviour of the other electron is examined. In 1978, Banyard and Reed [32] assembled these types of partial holes into a surface, thus greatly increasing the ease of interpretation.

In atomic systems, correlation effects may be viewed as a combination of *radial* correlation, where electrons correlate by assuming different radial positions, and *angular* correlation, where the electrons change their mutual angular disposition [33]. In an effort to gain insight into the nature of angular correlation, Banyard and Ellis [34] defined an angular hole, which exhibits the change in the interangular distribution function due to correlation. They examined the ground and several singly-excited states of helium, finding that correlation increases the average angle between the electrons.

Banyard and Youngman [35] have conducted extensive studies of correlation effects in singly-excited states of helium. They produced Coulomb holes and partial Coulomb holes of a highly complex form, quite different from those for the ground state. Boyd and Coulson [31], and Thakkar [36], have produced some similar results.

Following the work of Banyard and Mashat [37], which utilized the many-electron-theory of Sinanoğlu [22] mentioned above, it has been possible to examine correlation effects in systems with more than two electrons by partitioning the wavefunction into functions of two electrons. Using this approach, the ground state of beryllium has been subjected to a correlation study by Banyard and Mobbs [38]. Liu, Zhang and Zhao [39] later investigated the same system, using a form of many-body theory in their study. The ground state and an excited state of some lithium-like ions have been investigated by Banyard and Al-Bayati [40,41] .

In recent years there has been an ever-growing general interest in the properties of atomic and molecular species in *momentum* space [42]. Following their definition of the momentum space analogue of the Coulomb hole—the Coulomb shift, Banyard and Reed [32] found that in the ground state of helium-like systems momentum space correlation effects were more complicated and more informative than those in position space. Radial and angular correlation effects were found to act in opposition, whereas in position space they had been shown to act in unison. These observations have, in the main, been repeated in momentum space correlation studies of singly-excited helium, lithium-like-ions and beryllium carried out by Banyard and co-workers [43,44,45,46].

In an effort to extend and enhance the conclusions reached in previous studies, we have conducted an extensive study of electron correlation effects in the $2p^2\ ^3P$ doubly excited state of H^- , He, Li^+ and Be^{++} . In view of the fruitfulness of examining such effects in momentum space in previous studies, we have investigated correlation effects in *both* spaces for these systems. In chapter 2 we shall briefly survey some previous work concerning these systems.

Chapter 2

The $2p^2\ 3P$ State

2.1 Doubly Excited States

In recent years there has been a great deal of interest in the doubly excited states (DES) of atomic systems (see, for example, [47,48,49,50,51,52,53,54,55]). They are generally said to be highly correlated [56] and, for our purposes, this is their most interesting attribute. A simple argument to this end was given by Berry [57]. The idea is that the electrons in DES will, on average, be a long way from the nucleus compared to ground state systems. They will consequently tend to have low momenta, and therefore low velocities. A low velocity electron will be relatively more susceptible to the fluctuation potential [58] due to the other electrons, and will therefore be more highly correlated than a fast electron.

Sinanoğlu, Herrick and Kellman [59,60], among others, have applied a supermultiplet classification theory to DES. An outcome of this group-theoretical work has been the idea of defining new quantum numbers, K , T and A which express the important role of correlation in these states. The K and T quantum numbers relate to the angular correlation, whereas the A quantum number is related to the radial correlation. These quantum numbers can be used to label approximate wavefunctions expressed in hyperspherical coordinates [56,61]. The reason for using hyperspherical coordinates is that the wavefunction is 'quasiseparable' [62] when written as a function of them.

Berry and co-workers [63,64,65,66] have conducted extensive theoretical investigations into DES. Much of this work was carried out in the context of a theory in which atoms in DES are considered as being analogous to trilinear ‘floppy molecules’ [60], whereby atoms are classified in a similar fashion to molecules, and vibrational, rotational and bending quantum numbers assigned to each state. Krause, Morgan and Berry [64] found that the $2p^2\ ^3P$ state had 1 quantum of bending vibration.

In view of the spate of theoretical interest in DES, it is perhaps somewhat surprising that no fully-fledged correlation study in the spirit of that of Coulson and Neilson [7] mentioned in chapter 1 appears to have been conducted. Although Berry and co-workers (see references above) and Nicolaides and co-workers [67,68] have evaluated conditional probability densities for some correlated DES wavefunctions, no corresponding investigation of the Hartree-Fock functions was undertaken.

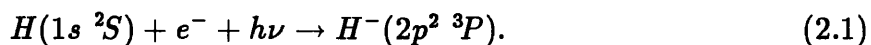
2.2 Experimental Evidence for the $2p^2\ ^3P$ State

Before experimental evidence can be discussed, the stability of the $2p^2\ ^3P$ state must be considered. Most DES, being embedded in the continuum, are autoionizing states [13], but parity and angular momentum conservation considerations prevent the $2p^2\ ^3P$ state from undergoing Coulombic autoionization [69]. Thus we can say that it is *metastable*. Autoionization can occur at significant rates [70] for $2p^2\ ^3P$ systems where the atomic number is large, and LS-coupling breaks down, but this is not important for the low- Z systems considered in this thesis. What Nicolaides has called ‘radiative autoionization’ [71] can occur, however. In this scheme, the system emits an electron *and* a photon, leaving the resulting hydrogen-like system in its ground state. The most important decay mechanism is the radiative transition to the $1s2p\ ^3P$ state [69]. The line corresponding to this transition in helium was first observed by Kruger in 1930 [72]. His tentative assignment of this observed line to the $2p^2\ ^3P$ - $1s2p\ ^3P$ transition was substantiated theoretically by Wu in 1944 [73]. The best experimental energy for the $2p^2\ ^3P$ state in helium, which was obtained by measuring this transition, is due to Tech and Ward [74] and was reported in 1971. These workers reported an energy of $481\ 301.5 \pm 1.2$

cm⁻¹ for this system. This result can be compared with the many theoretical values for the energy of this system, some of which we will discuss in the next section. When relativistic, mass-polarization, and radiative corrections were taken into account, using the highly-accurate calculations of Aashamar [75], a total theoretical estimate of 481 301.6 cm⁻¹ with respect to the ground state for the level was produced—an impressive agreement. It is also possible to investigate the $2p^2\ ^3P$ state by means of electron impact excitation, in which incident electrons excite ground state systems into this state. The first unambiguous demonstration of this phenomenon, in He, was made by Westerveld et al. in 1979 [76]. The earlier (1970) results of Burrow [77] were later shown to be erroneous [78]. Transitions involving the $2p^2\ ^3P$ state of Li⁺ and Be⁺⁺ [79,80] have also been observed and agree with theoretical results to the somewhat limited level of accuracy quoted for these experimental results. It should be noted that the $2p^2\ ^3P$ state has been routinely identified and discussed in high-*Z* systems which are frequently produced in nuclear fusion plasma experiments [70,81,82,83,84,85].

The case of H⁻ in this state is of much theoretical and experimental interest. Although all of the recent correlated calculations summarized below show the $2p^2\ ^3P$ state to be bound for H⁻, no conclusive evidence of its existence has yet emerged. This is presumably related to the fact that the calculated binding energy of this state is extremely low, being only 0.0096 eV (calculated using the most accurate theoretical energy, due to Jáuregui and Bunge [86]). In 1975 Nagata [87] suggested that a small peak in a translational energy spectrum of H⁻ ions formed from the passage of H⁺ through potassium vapour might be due to the $2p^2\ ^3P$ state. However, an experiment specifically designed for the detection of H⁻ in this state [89,88] by means of crossing a beam of ground state H⁻ ions with a beam of mercury atoms had a negative result.

It is well known that processes involving the ground state of H⁻ are responsible for continuous absorption in solar spectra [90,91]. It has been suggested [92] that the following process could also be significant:



That is, a hydrogen atom in the ground state, an electron and a photon combine to

form a doubly excited state. This process is the reverse of the ‘radiative autoionization’ mentioned earlier [71]. An absorption feature identified as corresponding to this transition has been observed in the spectra of the stars ζ Tau [93] and Θ^2 Ori A [94]. The wavelength at which this feature is located is in accord with the theoretical predictions of Drake [92,95] and of Jacobs, Bhatia and Temkin [96,97]. Clearly the existence and properties of this state in the H^- system are of some astrophysical interest.

2.3 Wavefunctions for the $2p^2 \ ^3P$ State

Many wavefunctions have been calculated for the $2p^2 \ ^3P$ state, and we lay emphasis here on highly-accurate variational calculations. The first quantum mechanical calculations that we have found reported [73,98,99] were conducted in the 1930’s and 1940’s on the He system and were performed with a view to establishing the correctness of the attribution of the line observed by Kruger [72] which we mentioned earlier. The approximate energies reported by these workers were, owing to the lack of digital computers at the time, poor in comparison to later theoretical results, but they were sufficiently accurate for this purpose. Another early investigation was reported by Hylleraas in 1950 [100]. He was interested in whether or not a second bound state of H^- exists. With the limited facilities for calculation available to him, he reached the conclusion that the $2p^2 \ ^3P$ state would not be bound in this system.

There appears to have been, with an occasional exception [101], an hiatus in theoretical work on this state until the early 1970’s. At this time, Holøien and co-workers conducted a number of studies on the $2p^2 \ ^3P$ state [75,102,103,104]. Especially notable amongst these was the 1970 study of Aashamar [75] where relativistic, radiative and mass-polarization corrections for the ions $Z=1$ to 10 were reported. These corrections are small, and will not in general be considered in this thesis, excepting the mass polarization corrections which can be compared to some of our momentum space results (see equation 7.34 in chapter 7 and table III.5 in chapter 9). These workers all reached the conclusion that the H^- system *is* bound in the $2p^2 \ ^3P$ state. In 1970, Drake [105] produced a study of the state in H^- using Hylleraas-type wavefunctions which defini-

tively established that it was bound. Also in 1970, Bhatia [106] reported highly-accurate energies for H^- and He, again using Hylleraas-type functions. The He value remains the best variational energy to date. In contrast to these explicitly-correlated studies, in 1978 Beck and Nicolaides [107] produced an energy for H^- by means of configuration interaction calculations. In addition, by employing the Froese Fischer numerical Hartree-Fock program [108] to obtain Hartree-Fock energies for H^- and He, and by using the experimental energy for He due to Tech and Ward [74] mentioned above, they were able to report that the correlation energies for H^- and He are approximately the same. Jáuregui and Bunge [86] produced a highly-accurate natural expansion wavefunction for H^- in 1979. This constitutes the best variational energy yet obtained for this system. Unfortunately, it did not prove possible to obtain this natural expansion for our analysis.

Drake has recently [109,110] produced a series of extremely accurate Hylleraas-type wavefunctions for H^- , He, Li^+ and Be^{++} in the $2p^2 \ ^3P$ state. The Li^+ and Be^{++} energies are the best that we have seen reported, and those for H^- and He are not markedly inferior to the most accurate reported. Accordingly we have used these wavefunctions in our correlation analysis. We have also used configuration interaction wavefunctions for the same systems, calculated by Nicolaides and Aspromallis [111]. These recover a high proportion of the correlation energy (see equation 1.3) and hence are suitable for a study of correlation effects, although they are not of quite the same quality as the Drake wavefunctions. We have performed a natural orbital analysis on these configuration interaction wavefunctions (see Appendix C) in order to study the manner in which the different components of electron correlation produce the total correlation effect. By selecting wavefunctions of *different* forms, we will be able to assess the strengths and weaknesses of each kind of wavefunction.

The energies of all the wavefunctions that we have used are displayed in table II.1 in chapter 6. Because of the lack of accurate experimental energies for H^- , Li^+ and Be^{++} , we take the best theoretical values as the exact non-relativistic energies for this table. In the interests of consistency, we have adopted the same procedure for He. In chapter 3 the forms of the wavefunctions we employ are discussed.

Part II
Electron Correlation Effects
in Position Space

Chapter 3

Wavefunctions

3.1 Introduction

In order to understand correlation effects in the $2p^2\ ^3P$ state of helium-like systems, it is important to understand the structure of the wavefunctions that we use in our analysis. Each of the wavefunctions discussed below has been investigated in four systems of differing atomic number— H^- , He, Li^+ and Be^{++} . Throughout this chapter we consider the state such that the total magnetic quantum number, M , is equal to 1. It should be noted that at the non-relativistic level all these wavefunctions are degenerate with respect to the energy for this quantum number.

Three distinct types of wavefunction have been utilized in our work. As correlation effects are usually considered relative to the Hartree-Fock (HF) level [6], we have employed such wavefunctions as the reference for our analysis. The energetically best wavefunctions used are highly-accurate Hylleraas-type functions, produced by Drake [109,110], and henceforth referred to as ‘Drake wavefunctions’. These wavefunctions recover much more than 99% of the correlation energy in all cases. The other type of correlated wavefunction that we have examined is a configuration interaction (CI) wavefunction due to Nicolaides and Aspromallis [111], which, for brevity, we will designate the ‘NA-CI wavefunction’. Although not of the same calibre as the Drake wavefunctions, all of the NA-CI wavefunctions, apart from that for H^- , attain more than 99%

of the correlation energy. Even the H^- wavefunction achieves almost 98% of the correlation energy. Full details of the energy of each wavefunction are given in table II.1 in chapter 6. In order to facilitate our study of correlation effects, a natural orbital (NO) analysis has been performed on each NA-CI wavefunction.

3.2 Hartree-Fock Wavefunctions

These wavefunctions were produced by us using the most recent Froese Fischer code [112]. The radial part of the wavefunction is given *numerically* by this program, and this wavefunction is thus referred to as the ‘numerical Hartree-Fock’ wavefunction. It comprises only one determinant, and is given by:

$$\Psi_{HF}^{NUM}(\mathbf{r}_1, \mathbf{r}_2) = \frac{1}{\sqrt{2}} \begin{vmatrix} m=1 \phi_{HF}^{NUM}(\mathbf{r}_1) & m=0 \phi_{HF}^{NUM}(\mathbf{r}_1) \\ m=1 \phi_{HF}^{NUM}(\mathbf{r}_2) & m=0 \phi_{HF}^{NUM}(\mathbf{r}_2) \end{vmatrix}. \quad (3.1)$$

The vectors \mathbf{r}_1 and \mathbf{r}_2 denote the positions of the two electrons. The orbitals may be written in a more detailed form; for example:

$$m=1 \phi_{HF}^{NUM}(\mathbf{r}_1) = R_{HF}^{NUM}(r_1) Y_{l=1}^{m=1}(\theta_1, \phi_1), \quad (3.2)$$

where $R_{HF}^{NUM}(r_1)$ is the numerically-defined radial part of the wavefunction, and $Y_{l=1}^{m=1}(\theta_1, \phi_1)$ is a standard spherical harmonic function. The spin-dependent part of the wavefunction may be factored out from the spatial part as we are dealing with a two-electron system, and has not been included in the wavefunctions in this chapter as it plays no significant role in this study.

In order to facilitate our ability to manipulate and produce results from the HF wavefunctions, the numerical radial part, $R_{HF}^{NUM}(r_1)$, was fitted with a linear combination of the radial parts of Slater-type orbitals (STO’s), (see Appendix A for further details). We therefore write:

$$R_{HF}^{STO}(r_1) = \sum_i^{NSTO} C_i^{STO} r_1^{n_i} e^{-\zeta_i r_1}, \quad (3.3)$$

where C_i^{STO} and ζ_i are adjustable parameters produced by the fitting process, and n_i is

a positive integer. These are tabulated at the end of Appendix A. We now have,

$$\Psi_{HF}^{NUM}(\mathbf{r}_1, \mathbf{r}_2) \simeq \Psi_{HF}^{STO}(\mathbf{r}_1, \mathbf{r}_2) = \frac{1}{\sqrt{2}} \begin{vmatrix} {}^{m=1}\phi_{HF}^{STO}(\mathbf{r}_1) & {}^{m=0}\phi_{HF}^{STO}(\mathbf{r}_1) \\ {}^{m=1}\phi_{HF}^{STO}(\mathbf{r}_2) & {}^{m=0}\phi_{HF}^{STO}(\mathbf{r}_2) \end{vmatrix}, \quad (3.4)$$

where ${}^{m=1}\phi_{HF}^{STO}(\mathbf{r}_1) = R_{HF}^{STO}(r_1)Y_{l=1}^{m=1}(\theta_1, \phi_1)$. We will call $\Psi_{HF}^{STO}(\mathbf{r}_1, \mathbf{r}_2)$ the ‘fitted Hartree-Fock’ wavefunction.

Because the radial parts of the two orbitals are the same, we may factor the wavefunction into radial and angular parts:

$$\Psi_{HF}^{STO}(\mathbf{r}_1, \mathbf{r}_2) = R_{HF}^{STO}(r_1)R_{HF}^{STO}(r_2) \times \frac{1}{\sqrt{2}} \left[Y_{l=1}^{m=1}(\theta_1, \phi_1)Y_{l=1}^{m=0}(\theta_2, \phi_2) - Y_{l=1}^{m=0}(\theta_1, \phi_1)Y_{l=1}^{m=1}(\theta_2, \phi_2) \right]. \quad (3.5)$$

It should be noted that the Hartree-Fock wavefunction, as with the other wavefunctions for this state, is antisymmetric in its spatial part. This has the important consequence of giving rise to *Fermi* correlation in this state. The complete wavefunction is normalized to unity, as are the individual orbitals. Beck and Nicolaides [107] and Nicolaides and Aspromallis [111] have obtained the same energies for the systems under consideration by using an earlier version of the Froese Fischer code [108].

3.3 Drake Wavefunctions

The wavefunctions due to Drake are Hylleraas-type, or explicitly-correlated wavefunctions. They are of the form:

$$\Psi_{Drake}(\mathbf{r}_1, \mathbf{r}_2) = (1 - \mathbf{P}_{12}) \sum_{i,j,k}^{N_{Drake}} A_{ijk} r_1^i r_2^j r_{12}^k e^{-\alpha r_1 - \beta r_2} \mathcal{Y}_{l_1=1, l_2=1, L=1}^{M=1}(\theta_1, \phi_1, \theta_2, \phi_2), \quad (3.6)$$

where

$$\mathcal{Y}_{l_1=1, l_2=1, L=1}^{M=1}(\theta_1, \phi_1, \theta_2, \phi_2) = \frac{1}{\sqrt{2}} (Y_{l=1}^{m=1}(\theta_1, \phi_1)Y_{l=1}^{m=0}(\theta_2, \phi_2) - Y_{l=1}^{m=0}(\theta_1, \phi_1)Y_{l=1}^{m=1}(\theta_2, \phi_2)). \quad (3.7)$$

\mathbf{P}_{12} is a permutation operator designed to ensure the antisymmetry of the wavefunction; A_{ijk} , α and β are adjustable parameters used in the variational process, where i , j and

k are non-negative integers. The labels l_1 and l_2 are the azimuthal quantum numbers of the electrons, and L is the azimuthal quantum number for the whole system.

Drake has produced several wavefunctions for each system, each of which has a different number of terms, N_{Drake} . In every case, the integers i , j and k for a given term obey the relations,

$$i + j + k \leq N \quad (3.8)$$

$$i \geq 1 \quad (3.9)$$

$$j \geq 1 \quad (3.10)$$

$$k \geq 0, \quad (3.11)$$

where N is an integer fixed for each wavefunction. For the H^- wavefunctions, which were calculated first, all terms fulfilling these equations are included, but for He, Li^+ and Be^{++} a term with $i = x$, $j = y$ will not be included if the term with $i = y$, $j = x$ is already present. This procedure was found to be more computationally efficient than including all terms satisfying equations 3.8-11 [110].

We have examined two Drake wavefunctions for each system. We have naturally chosen the energetically best wavefunction for each system, which we will call the ‘best Drake’. We have also chosen the wavefunction with the fewest terms, which we will call the ‘short Drake’. A 70-term function, for example, will be referred to as the ‘Drake-70’ wavefunction. For H^- , the Drake-20 and Drake-84 wavefunctions were used. The Drake-13 and Drake-70 were used for the other systems.

It should be noted that $\mathcal{Y}_{l_1=1, l_2=1, L=1}^{M=1}(\theta_1, \phi_1, \theta_2, \phi_2)$ in equation 3.7 is identical to the angular part of the Hartree-Fock wavefunction. Although this function is normalized, no simple orthogonality relationship exists between the different terms in equation 3.6, owing to the presence of the r_{12}^k factors.

3.4 Nicolaides and Aspromallis Wavefunctions

The NA-CI wavefunctions comprise 50 configurations, constructed from a set of basis-functions, amongst which are 18 different radial parts. The types of basis functions are

shown in table II.2 in chapter 6. These wavefunctions are complete within the basis-set used in the sense that every possible configuration is included in the expression. Each NA-CI wavefunction is written:

$$\Psi_{NA-CI}(\mathbf{r}_1, \mathbf{r}_2) = \sum_{i=1}^{50} C_i \Phi_i(\mathbf{r}_1, \mathbf{r}_2), \quad (3.12)$$

where $\Phi_i(\mathbf{r}_1, \mathbf{r}_2)$ is the i^{th} configuration. A given configuration may be expanded in terms of its constituent determinants:

$$\Phi_i(\mathbf{r}_1, \mathbf{r}_2) = \frac{1}{\sqrt{2}} \sum_{j=1}^{N_i} K_{ij} \begin{vmatrix} {}^a\phi_{ij}(\mathbf{r}_1) & {}^b\phi_{ij}(\mathbf{r}_1) \\ {}^a\phi_{ij}(\mathbf{r}_2) & {}^b\phi_{ij}(\mathbf{r}_2) \end{vmatrix}, \quad (3.13)$$

where ${}^a\phi_{ij}$ and ${}^b\phi_{ij}$ are basis orbitals, and K_{ij} are coefficients which ensure that the total configuration is a correct eigenfunction of the L^2 operator. It should be noted that the labels a , b , i and j only label the position of the orbitals within the wavefunction. We use ‘a’ and ‘b’ to distinguish the two different orbitals in the determinant. These labels are *not* quantum numbers. It is also possible, however, to label the orbitals by their quantum numbers. We can write:

$$\phi_{ij}(\mathbf{r}_1) = \phi_{nlm}(\mathbf{r}_1), \quad (3.14)$$

where n , l and m have their usual meanings, and then expand the orbital thus:

$$\phi_{nlm}(\mathbf{r}_1) = R_{nl}(r_1)Y_l^m(\theta_1, \phi_1). \quad (3.15)$$

In fact, $\phi_{nlm}(\mathbf{r}_1)$ is an orthonormalized STO.

Each configuration contains two different types of orbitals, defined by the n and l quantum numbers. These types are denoted $2p$, $3d$ etc. In a given configuration the two kinds of orbital have the same quantum number l . In each determinant the m quantum numbers of the two orbitals always add up to 1, as is required to produce a total M quantum number of 1 for the wavefunction. The determinants are coupled together to form an appropriate eigenfunction, as mentioned above.

The first configuration, $\Phi_1(\mathbf{r}_1, \mathbf{r}_2)$, in the wavefunctions of Nicolaides and Aspromallis is the numerical Hartree-Fock wavefunction produced by the Froese Fischer program,

(see above). It contains 2p orbitals. For ease of analysis, we have employed the *fitted* radial part of the numerical Hartree-Fock in all calculations involving the NA-CI wavefunctions.

The orbitals $\phi_{nlm}(r_1)$ form an orthonormal set. That is to say,

$$\langle \phi_{n_1 l_1 m_1}(r_1) | \phi_{n_2 l_2 m_2}(r_1) \rangle = \int \phi_{n_1 l_1 m_1}^*(r_1) \phi_{n_2 l_2 m_2}(r_1) d\tau_1 = \delta_{n_1 n_2} \delta_{l_1 l_2} \delta_{m_1 m_2}, \quad (3.16)$$

where $d\tau_1$ is the volume element, and integration takes place over all possible values. For orbitals of different symmetry, the orthogonality property of spherical harmonics ensures that this condition is automatically fulfilled. Unfortunately, however, the radial parts of STO's are not orthogonal and thus the radial parts of orbitals of the same angular symmetry must be *made* orthonormal by means of the Gram-Schmidt orthogonalization method. Because we use the fitted radial part of the Hartree-Fock as the first configuration, we have re-performed the orthogonalization procedure, in order to ensure that all radials are precisely orthonormal, (see Appendix B for details). The upshot of this is that the $R_{nl}(r_1)$ in equation 3.15 are in general a summation of the radial parts of STO's.

The entire wavefunction, $\Psi_{NA-CI}(r_1, r_2)$, is itself normalized to unity. The individual configurations are orthonormal in the sense,

$$\langle \Phi_p(r_1, r_2) | \Phi_q(r_1, r_2) \rangle = \int \Phi_p^*(r_1, r_2) \Phi_q(r_1, r_2) d\tau_1 d\tau_2 = \delta_{pq}. \quad (3.17)$$

A consequence of this is that the sum of the squares of the configuration coefficients is equal to unity, that is,

$$\sum_{i=1}^{50} C_i^2 = 1. \quad (3.18)$$

A natural orbital analysis has been performed upon the NA-CI wavefunction. Details of the procedure for obtaining an approximate natural expansion from the NA-CI wavefunction, together with a discussion of the significance and uses of such an expansion may be found in Appendix C. We will confine ourselves here to a consideration of the *structure* of the NA-CI wavefunction in its natural form. It should be noted that performing a natural orbital analysis does not change the wavefunction: the natural

expansion is, in totality, equal to the original wavefunction. What has happened is that the orbitals have been transformed to a new basis, and the configuration coefficients therefore make concomitant changes.

Whenever a function or quantity is to be taken as part of a natural expansion, it will have an appropriate superscript. Thus, when we write the NA-CI wavefunction in its natural form we have:

$$\Psi_{NA-CI}^{NC}(\mathbf{r}_1, \mathbf{r}_2) = \sum_{i=1}^{18} C_i^{NC} \Phi_i^{NC}(\mathbf{r}_1, \mathbf{r}_2), \quad (3.19)$$

where

$$\Phi_i^{NC}(\mathbf{r}_1, \mathbf{r}_2) = \frac{1}{\sqrt{2}} \sum_{j=1}^{N_i^{NC}} K_{ij}^{NC} \begin{vmatrix} {}^a\phi_{ij}^{NO}(\mathbf{r}_1) & {}^b\phi_{ij}^{NO}(\mathbf{r}_1) \\ {}^a\phi_{ij}^{NO}(\mathbf{r}_2) & {}^b\phi_{ij}^{NO}(\mathbf{r}_2) \end{vmatrix}. \quad (3.20)$$

$\Phi_i^{NC}(\mathbf{r}_1, \mathbf{r}_2)$ is called a ‘natural configuration’ (NC), and $\phi_{ij}^{NO}(\mathbf{r}_1)$ is called a ‘natural orbital’ (NO). It should be clear from the preceding comments that:

$$\Psi_{NA-CI}^{NC}(\mathbf{r}_1, \mathbf{r}_2) \equiv \Psi_{NA-CI}(\mathbf{r}_1, \mathbf{r}_2). \quad (3.21)$$

We can, as before, write the natural orbital in its detailed form:

$$\phi_{ij}^{NO}(\mathbf{r}_1) = \phi_{nlm}^{NO}(\mathbf{r}_1) = R_{nl}^{NO}(r_1) Y_l^m(\theta_1, \phi_1). \quad (3.22)$$

Note that no additional superscript is necessary on the spherical harmonics. The natural orbital analysis only alters the *radial* parts of the orbitals.

We will usually consider not the total natural expansion, but the expansion *truncated* to a specified number of natural configurations and renormalized. If we are referring to a truncation with, say, 3 natural configurations, then we will call this the ‘3 natural configuration’ (3NC) wavefunction. It should be noted that a truncation will contain a number of natural *radials* equal to the number of natural configurations.

All the orthogonality properties pertaining to the CI wavefunctions apply in the analogous natural cases. It is a property of this natural expansion that it only contains doubly-occupied configurations; that is, configurations where the two natural orbitals have the same radial part.

Chapter 4

Evaluation of Correlation Properties

4.1 Introduction

In order to investigate the effects of electron correlation it is necessary to evaluate various functions and properties derived from the wavefunctions under consideration. For the $2p^2\ ^3P$ system, the two-particle probability density function is given by:

$$\rho_2(\mathbf{r}_1, \mathbf{r}_2) = \Psi^*(\mathbf{r}_1, \mathbf{r}_2)\Psi(\mathbf{r}_1, \mathbf{r}_2), \quad (4.1)$$

and is a function of six independent variables. The arguments \mathbf{r}_1 and \mathbf{r}_2 are vectors representing the positions of the electrons. Clearly, it is not feasible to plot such a function in its entirety. In practice, we must integrate over most of the variables in order to produce functions which are only dependent on a few quantities. A function of one variable may be plotted as a curve, whereas a function dependent on two variables can be represented as a surface.

In any study of correlation effects it is to be expected that two-particle functions and expectation values will be especially susceptible to correlation-induced changes. Accordingly, we have focused on two-particle properties in our study. Nevertheless, we shall occasionally examine one-particle attributes, in order to present a full picture of the quantum mechanical description of the system.

It should be noted that the functions presented below are *probability* density functions, and not electron density functions. Consequently, they are normalized to unity.

Multiplication by two will recover the corresponding electron density functions.

In our account of how the various functions and expectation values were obtained the natural orbital wavefunction will not be separately examined; the analysis is essentially the same as for the Nicolaides and Aspromallis (NA-CI) wavefunction, because their fundamental structures are the same, (see chapter 3). A useful test of the correctness of our natural orbital analysis is provided by the fact that any property calculated using the *full* natural expansion must be the same as when calculated with the original NA-CI wavefunction.

When we refer to the Hartree-Fock (HF) wavefunction, we will not, in general, specify whether the radial part is numerically defined, or is represented by a summation of the radial parts of Slater-type orbitals (STO's). This will only be stated if it has a bearing on the evaluation techniques used. Although the vast majority of the Hartree-Fock results in chapter 6 and chapter 9 are produced using the STO-fitted functions, it is useful to evaluate some results using the numerical Hartree-Fock wavefunctions as well, in order to assess the quality of the fitted functions.

4.2 Radial Functions and Properties

One of the simplest functions characterizing an atomic system is the radial distribution function, given by:

$$D(r_1) = \int \Psi^*(\mathbf{r}_1, \mathbf{r}_2) \Psi(\mathbf{r}_1, \mathbf{r}_2) \frac{d\tau_1 d\tau_2}{dr_1}, \quad (4.2)$$

where r_1 is the distance of electron 1 from the nucleus, and $d\tau_1 d\tau_2$ is the product of the volume elements for the two electrons. The integration is performed over all possible values of the relevant variables. This may be assumed of all the integrations shown in this chapter where the limits are not explicitly given. The physical interpretation of this function is that $D(r_1)dr_1$ represents the probability of electron 1 being found at a distance from the nucleus between r_1 and $r_1 + dr_1$. Clearly, $D(r_1)$ normalizes to unity. We may investigate the correlation-induced changes to $D(r_1)$ by forming the radial hole:

$$\Delta D(r_1) = D(r_1)_{CORR} - D(r_1)_{HF}, \quad (4.3)$$

where $D(r_1)_{CORR}$ represents the radial distribution function produced by using a correlated wavefunction, and $D(r_1)_{HF}$ represents the same quantity calculated when using the Hartree-Fock description. The procedure of subtracting a Hartree-Fock function from a correlated function to demonstrate the effects of electron correlation is a powerful technique, and will be encountered many times in this chapter. It corresponds to the Löwdin [6] definition of the correlation energy given in chapter 1. As a means of assessing the proportion of the distribution function shifted by electron correlation we have evaluated the quantity:

$$\Upsilon_{r_1} = \frac{1}{2} \int_0^\infty |\Delta D(r_1)| dr_1. \quad (4.4)$$

It is very simple to obtain the $D(r_1)$ for the Hartree-Fock wavefunction. The volume element is expressed in spherical polar coordinates:

$$d\tau_1 d\tau_2 = r_1^2 dr_1 \sin \theta_1 d\theta_1 d\phi_1 r_2^2 dr_2 \sin \theta_2 d\theta_2 d\phi_2. \quad (4.5)$$

The product of the HF wavefunction (see equation 3.5) with its complex conjugate will produce an angular function that integrates to unity. As the HF radial function is normalized, we have:

$$D(r_1)_{HF} = r_1^2 R^2(r_1)_{HF}. \quad (4.6)$$

The procedure for the Drake wavefunction is surprisingly complicated. This is due to the presence of powers of r_{12} , the interelectronic distance given by $r_{12} = |\mathbf{r}_2 - \mathbf{r}_1|$. These powers of r_{12} prevent orthogonality properties from being relevant. Many of the procedures and concepts that we encounter in the following analysis will be found to be of great use in evaluating a number of the other quantities described in this chapter. First, we must re-express the volume element, $d\tau_1 d\tau_2$, in a form which will accommodate the presence of terms in r_{12} . It can be written [113]:

$$d\tau_1 d\tau_2 = r_1 dr_1 r_2 dr_2 r_{12} dr_{12} \sin \theta_1 d\theta_1 d\phi_1 d\chi, \quad (4.7)$$

where χ is the angle of rotation of the second electron around the first electron.

If we examine equation 3.6, it is apparent that we may write the Drake wavefunction as the product of an angular function $\mathcal{Y}_{l_1=1, l_2=1, L=1}^{M=1}(\theta_1, \phi_1, \theta_2, \phi_2)$ and a quantity which

is only a function of r_1 , r_2 and r_{12} :

$$\Psi(\underline{r}_1, \underline{r}_2)_{Drake} = \mathcal{Y}_{l_1=1, l_2=1, L=1}^{M=1}(\theta_1, \phi_1, \theta_2, \phi_2) S(r_1, r_2, r_{12}). \quad (4.8)$$

From the definition of $D(r_1)$ it follows that one may write,

$$D(r_1)_{Drake} = \int_0^\infty \int_{|r_1-r_2|}^{r_1+r_2} r_1 r_2 r_{12} S^2(r_1, r_2, r_{12}) \int_{ANG} \mathcal{Y}_{l_1=1, l_2=1, L=1}^{M=1, *}(\theta_1, \phi_1, \theta_2, \phi_2) \times \mathcal{Y}_{l_1=1, l_2=1, L=1}^{M=1}(\theta_1, \phi_1, \theta_2, \phi_2) d\Omega dr_{12} dr_2, \quad (4.9)$$

where $d\Omega = d\chi d\phi_1 \sin\theta_1 d\theta_1$. The angular integrations reduce to a linear combination of four integrals of the form,

$$I_{ANG} = \int_{ANG} Y_{l_1}^{m_1*}(\theta_1, \phi_1) Y_{l_2}^{m_2}(\theta_1, \phi_1) Y_{l_3}^{m_3*}(\theta_2, \phi_2) Y_{l_4}^{m_4}(\theta_2, \phi_2) d\Omega. \quad (4.10)$$

By expanding each product of spherical harmonics of the same argument as a sum of spherical harmonics, I_{ANG} may be further reduced to a sum of integrals of the form:

$$I = \int_{ANG} Y_l^m(\theta_1, \phi_1) Y_k^n(\theta_2, \phi_2) d\Omega. \quad (4.11)$$

Benesch [114], and Calais and Löwdin [115] have shown that

$$I = (-1)^m 2\pi \delta_{m-n} \delta_{lk} P_l(\cos\theta_{12}), \quad (4.12)$$

where $P_l(\cos\theta_{12})$ are *un-normalized* Legendre polynomials, and θ_{12} is the angle subtended at the nucleus by the two electrons. Using this relation, it may be shown that

$$\int_{ANG} \mathcal{Y}_{l_1=1, l_2=1, L=1}^{M=1, *}(\theta_1, \phi_1, \theta_2, \phi_2) \mathcal{Y}_{l_1=1, l_2=1, L=1}^{M=1}(\theta_1, \phi_1, \theta_2, \phi_2) d\Omega = \frac{1}{2}(1 - P_2(\cos\theta_{12})) \quad (4.13)$$

and thus equation 4.9 reduces to:

$$D(r_1)_{Drake} = \frac{1}{2} \int_0^\infty \int_{|r_1-r_2|}^{r_1+r_2} r_1 r_2 r_{12} S^2(r_1, r_2, r_{12}) (1 - P_2(\cos\theta_{12})) dr_{12} dr_2. \quad (4.14)$$

A further simplification is possible, using a recursion relation due to Drake [116], which implies that if, for convenience, we define a function:

$$J_l(r_{12}^{c+2}) = \int_{|r_1-r_2|}^{r_1+r_2} r_{12}^{c+2} P_l(\cos\theta_{12}) r_{12} dr_{12}, \quad (4.15)$$

then the following relationship can be established:

$$J_{l+1}(r_{12}^c) - J_{l-1}(r_{12}^c) = \frac{(2l+1)}{(c+2)r_1r_2} J_l(r_{12}^{c+2}). \quad (4.16)$$

As all the integrations with respect to r_{12} in equation 4.14 will be of the form of equation 4.15, and as $P_0(\cos \theta_{12}) = 1$, we may write:

$$D(r_1)_{Drake} = \frac{1}{2} \int_0^\infty \int_{|r_1-r_2|}^{r_1+r_2} r_1 r_2 r_{12} S^{2'}(r_1, r_2, r_{12}) P_1(\cos \theta_{12}) dr_{12} dr_2, \quad (4.17)$$

where $S^{2'}(r_1, r_2, r_{12})$ is a function of the same general form as $S^2(r_1, r_2, r_{12})$, but with different powers of r_1 , r_2 and r_{12} and different linear coefficients, determined by use of equation 4.16. As $P_1(\cos \theta_{12}) = \cos \theta_{12}$, whereas $P_2(\cos \theta_{12}) = \frac{1}{2}(3 \cos^2 \theta_{12} - 1)$, equation 4.17 is evidently simpler than equation 4.14. If the cosine rule is used to substitute for $\cos \theta_{12}$, ($\cos \theta_{12} = \frac{r_1^2 + r_2^2 - r_{12}^2}{2r_1r_2}$), it is clear that we have reduced the problem to one double integral of an integrand which comprises a large summation of similar terms. That is, we have:

$$D(r_1)_{Drake} = \int_0^\infty \int_{|r_1-r_2|}^{r_1+r_2} \sum_i B_i r_1^{a_i} r_2^{b_i} r_{12}^{c_i} e^{-\delta_i r_1 - \gamma_i r_2} dr_{12} dr_2, \quad (4.18)$$

where a_i , b_i and c_i are integers, and B_i are constants arising from the analysis. We can also consider equation 4.18 as the summation of a large number of integrals of the same form,

$$D(r_1)_{Drake} = \sum_i B_i \int_0^\infty \int_{|r_1-r_2|}^{r_1+r_2} r_1^{a_i} r_2^{b_i} r_{12}^{c_i} e^{-\delta_i r_1 - \gamma_i r_2} dr_{12} dr_2. \quad (4.19)$$

A general, analytical, expression for the double integrals in equation 4.19 is consequently required, and was produced, although the complex details of this are not presented in this thesis.

It is much easier to produce the $D(r_1)$ curve for the NA-CI wavefunction. If we consider equations 3.12 and 3.13, then it is evident that we may write:

$$D(r_1)_{NA-CI} = \sum_i D_i \int \phi_{n_1^i l_1^i m_1^i}^*(r_1) \phi_{n_2^i l_2^i m_2^i}(r_1) \phi_{n_3^i l_3^i m_3^i}^*(r_2) \phi_{n_4^i l_4^i m_4^i}(r_2) \times r_1^2 \sin \theta_1 d\theta_1 d\phi_1 r_2^2 \sin \theta_2 d\theta_2 d\phi_2, \quad (4.20)$$

where D_i are coefficients, and we have returned to the simpler expression for the volume element given in equation 4.5. Because the orbitals are orthonormal, each integration

over the position of electron 2 will have a result of either unity or zero, depending on the quantum numbers. The angular integrations for electron 1 will have the same simple form, due to the orthonormality of spherical harmonics. Thus the expression for $D(r_1)$ reduces to a summation of radial parts of orbitals, which may be easily evaluated.

It is useful to be able to characterize the $D(r_1)$ curves quantitatively, and to achieve this we have evaluated the radial expectation values,

$$\langle r_1^n \rangle = \int r_1^n \Psi^*(\mathbf{r}_1, \mathbf{r}_2) \Psi(\mathbf{r}_1, \mathbf{r}_2) d\tau_1 d\tau_2, \quad (4.21)$$

for n equal to $-2, -1, 0, +1, +2$. Clearly, the negative n values will emphasize the inner regions of the $D(r_1)$ curve, whereas the positive ones will emphasize the outer regions. The $n = 0$ expectation value is equal to unity by definition. It therefore provides an extremely valuable check on the correctness of the $D(r_1)$ curve, if it is obtained from numerical integration of this function. Some of these quantities are of practical interest. The value $\langle r_1^{-1} \rangle$ is present in the definition of the nuclear diamagnetic shielding factor [117]. Of course, the electron-nuclear potential energy is given by: $-2Z \langle r_1^{-1} \rangle$. In addition, the diamagnetic susceptibility [118] is a function of $\langle r_1^2 \rangle$. It is important to be able to measure the spread of the $D(r_1)$ curve, and to do this we have calculated σ_{r_1} , the standard deviation of r_1 , which is given by,

$$\sigma_{r_1} = \sqrt{\langle r_1^2 \rangle - \langle r_1 \rangle^2}. \quad (4.22)$$

In the case of the numerical Hartree-Fock functions, one must use numerical integration of the radial part of the wavefunction to evaluate the expectation values. For the fitted Hartree-Fock description, however, we can evaluate $\langle r_1^n \rangle$ using a simple analytical formula for the integrals involved. In the case of the Drake wavefunction, the problem may be thought of as one of determining $\langle r_1^l r_2^m r_{12}^n \rangle$ for $m = 0, n = 0$, and will be considered when the evaluation of $\langle r_{12}^n \rangle$ is discussed. For the NA-CI wavefunction, we must multiply the expression for $D(r_1)$ in equation 4.20 by the requisite power of r_1 and integrate with respect to r_1 . Although we cannot now use radial orthogonality properties for *this* integration, the analytical integrals are again simple.

The functions and quantities considered above are all related to the single-particle density. A function more directly related to correlation effects is the two-particle radial distribution function, given by:

$$D(r_1; r_2) = \int \Psi^*(\underline{r}_1, \underline{r}_2) \Psi(\underline{r}_1, \underline{r}_2) \frac{d\tau_1 d\tau_2}{dr_1 dr_2}. \quad (4.23)$$

The correlation surface may be formed:

$$\Delta D(r_1; r_2) = D(r_1; r_2)_{CORR} - D(r_1; r_2)_{HF}. \quad (4.24)$$

It is clear that these functions are related to the radial holes in a simple manner:

$$\Delta D(r_1) = \int_0^\infty \Delta D(r_1; r_2) dr_2. \quad (4.25)$$

The independent-particle nature of the Hartree-Fock representation results in a simple form for the two-particle radial function,

$$D(r_1; r_2) = D(r_1)_{HF} D(r_2)_{HF}. \quad (4.26)$$

In the case of the Drake wavefunction the essential modification to the $D(r_1)$ analysis is to not perform the r_2 integration in the routine which evaluates the integrals in equation 4.19. For the NA-CI case the analysis is only slightly different to that for the $D(r_1)$.

As with the $D(r_1)$ curves, it is useful to be able to describe the $D(r_1; r_2)$ curves by expectation values. These are defined by:

$$\langle r_1^n r_2^n \rangle = \int r_1^n r_2^n \Psi^*(\underline{r}_1, \underline{r}_2) \Psi(\underline{r}_1, \underline{r}_2) d\tau_1 d\tau_2, \quad (4.27)$$

and have been produced for $n = -2, -1, +1, +2$. In the case of the Hartree-Fock wavefunction, it is not actually necessary to calculate these values separately, as there exists a simple relationship between them and the single-particle expectation values:

$$\langle r_1^n r_2^n \rangle_{HF} = \langle r_1^n \rangle_{HF}^2. \quad (4.28)$$

For the correlated wavefunctions they may be evaluated in essentially the same way as the single-particle expectation values discussed above.

As a consequence of our investigation of electron correlation in the truncated natural expansions it became necessary to calculate the Sinanoğlu ‘f-functions’ discussed in chapter 1 from the NA-CI wavefunctions. One of these [25] is given by:

$${}^{m=1}f(\mathbf{r}_1) = \frac{\langle \Psi(\mathbf{r}_1, \mathbf{r}_2) | {}^{m=0}\phi_{HF}(\mathbf{r}_2) \rangle}{\langle \Psi(\mathbf{r}_1, \mathbf{r}_2) | {}^{m=0}\phi_{HF}(\mathbf{r}_2) {}^{m=1}\phi_{HF}(\mathbf{r}_1) \rangle} {}^{m=1}\phi_{HF}(\mathbf{r}_1), \quad (4.29)$$

where ‘ ${}^{m=1}\phi_{HF}(\mathbf{r}_1)$ ’ and ‘ ${}^{m=0}\phi_{HF}(\mathbf{r}_2)$ ’ are the two Hartree-Fock orbitals. Naturally, there is also an ${}^{m=0}f(\mathbf{r}_1)$ correction function. The common radial part of these f-functions is denoted by $f^{rad}(r_1)$ and this is the function which we have evaluated for each system. As an means of assessing the magnitude of the orbital correction functions, we have evaluated their norms, which are given by:

$$\|f(\mathbf{r}_1)\| = \sqrt{\langle f(\mathbf{r}_1) | f(\mathbf{r}_1) \rangle} = \sqrt{\int_0^\infty f^{rad}(r_1) {}^*f^{rad}(r_1) r_1^2 dr_1}. \quad (4.30)$$

4.3 $f(r_{12})$ and Related Functions and Properties

A function which is especially sensitive to the effects of correlation is the interelectronic distribution function, given by:

$$f(r_{12}) = \int \Psi^*(\mathbf{r}_1, \mathbf{r}_2) \Psi(\mathbf{r}_1, \mathbf{r}_2) \frac{d\mathbf{r}_1 d\mathbf{r}_2}{dr_{12}}, \quad (4.31)$$

where, as before, r_{12} is the magnitude of the interelectronic separation. If we form the correlation difference curve in the normal way,

$$\Delta f(r_{12}) = f(r_{12})_{CORR} - f(r_{12})_{HF}, \quad (4.32)$$

then we have what is known as the ‘Coulomb hole’. It was first defined and evaluated for the ground state of helium by Coulson and Neilson in 1961 [7]. The physical interpretation of the $\Delta f(r_{12})$ curve is that $\Delta f(r_{12}) dr_{12}$ represents the change in probability, due to electron correlation, of the interelectronic separation being between r_{12} and $r_{12} + dr_{12}$. To gauge the amount of the interelectronic distribution function displaced by correlation effects, or in other words the *size* of the Coulomb hole, we have evaluated the $\Upsilon_{r_{12}}$ which is defined, analogously to the Υ_{r_1} function, as

$$\Upsilon_{r_{12}} = \frac{1}{2} \int_0^\infty |\Delta f(r_{12})| dr_{12}. \quad (4.33)$$

In general, the calculation of the $f(r_{12})$ curves is much more complex and computationally expensive than for the radial functions described above. This is primarily because it is not possible to use orthogonality properties, as we did in the calculation of $D(r_1)$ and $D(r_1; r_2)$ for the NA-CI and HF wavefunctions.

We begin by writing the volume element in the form of equation 4.7, and substituting it into equation 4.31. For the Hartree-Fock,

$$f(r_{12})_{HF} = \int_0^\infty \int_{|r_1-r_{12}|}^{r_1+r_{12}} \int_{ANG} \Psi_{HF}^*(\underline{r}_1, \underline{r}_2) \Psi_{HF}(\underline{r}_1, \underline{r}_2) r_{12} r_2 dr_2 r_1 dr_1 \sin \theta_1 d\theta_1 d\phi_1 d\chi, \quad (4.34)$$

where we have made some of the limits of integration explicit. Substituting the expression for the HF wavefunction, equation 3.5, into this equation, and employing the relation for the angular integration, equation 4.13, we have,

$$f(r_{12})_{HF} = \frac{1}{2} \int_0^\infty \int_{|r_1-r_{12}|}^{r_1+r_{12}} r_1 r_2 r_{12} R_{HF}^2(r_1) R_{HF}^2(r_2) (1 - P_2(\cos \theta_{12})) dr_2 dr_1. \quad (4.35)$$

Substituting for $\cos \theta_{12}$ using the cosine rule gives an integrand which is only a function of r_1 , r_2 and r_{12} . We have thus reduced the problem to performing the double integral over r_1 and r_2 . Considering the STO-fitted Hartree-Fock, it was found that reducing the problem to a sum of primitive integrals, by expanding each $R_{HF}(r)$ in terms of its constituent STO's, and doing these analytically was prohibitively expensive in terms of computer time. Thus the integral in equation 4.35 was carried out *numerically*, using a routine from the Numerical Algorithm (NAG) Library [119]. To use such a routine, it is only necessary to express the integrand of equation 4.35 as a function of r_1 , r_2 and r_{12} . As the integral over r_1 has an upper limit of infinity, it was necessary to conduct extensive tests to determine an appropriate upper limit for the numerical integration, so that no significant regions were left out of the integration. The numerically defined Hartree-Fock was also used to calculate an $f(r_{12})$ function, and in this case there was no choice but to carry out the double integrals numerically.

The technique used for the Drake wavefunction was somewhat similar to that described above for the evaluation of the $D(r_1)$. We use the same expression for the volume element as was used in the $D(r_1)$ case, and by considering that the angular integral is

the same for this case we have:

$$f(r_{12})_{Drake} = \frac{1}{2} \int_0^\infty \int_{|r_1-r_{12}|}^{r_1+r_{12}} r_1 r_2 r_{12} S^2(r_1, r_2, r_{12}) (1 - P_2(\cos \theta_{12})) dr_2 dr_1. \quad (4.36)$$

Because no recursion relation is available in this case, we proceed directly to substitute for $\cos \theta_{12}$ using the cosine rule, thus obtaining:

$$f(r_{12})_{Drake} = -\frac{3}{16} \int_0^\infty \int_{|r_1-r_{12}|}^{r_1+r_{12}} r_1 r_2 r_{12} S^2(r_1, r_2, r_{12}) \times \left[\frac{r_1^2}{r_2^2} + \frac{r_2^2}{r_1^2} - 2 - \frac{2r_{12}^2}{r_2^2} - \frac{2r_{12}^2}{r_1^2} + \frac{r_{12}^4}{r_1^2 r_2^2} \right] dr_2 dr_1. \quad (4.37)$$

As with the $D(r_1)_{Drake}$, this is reduced to a summation of primitive double integrals:

$$f(r_{12})_{Drake} = \sum_i D_i K_i(r_{12}), \quad (4.38)$$

where D_i are constants, and,

$$K_i(r_{12}) = r_{12}^{c_i} \int_0^\infty \int_{|r_1-r_{12}|}^{r_1+r_{12}} r_1^{a_i} r_2^{b_i} e^{-\delta_i r_1 - \gamma_i r_2} dr_2 dr_1. \quad (4.39)$$

It should be noted that the a_i , b_i , c_i , δ_i and γ_i are not the same as the quantities in equation 4.19. It is possible to find a general expression for the determination of $K_i(r_{12})$. We produced such an expression and an equivalent formula was reported by Benesch [114]. It is interesting to note in passing that it would, instead, be possible to evaluate the double integral in equation 4.37 numerically, in a fashion similar to that used for the Hartree-Fock wavefunction.

In considering the evaluation of $f(r_{12})$ for the NA-CI wavefunction, the most salient point to note is the large number of angular functions present. If we expand the wavefunction as a summation of products of orbitals, and substitute into equation 4.31, we have:

$$f(r_{12})_{NA-CI} = \int_0^\infty \int_{|r_1-r_{12}|}^{r_1+r_{12}} \sum_i E_i r_1 r_2 r_{12} R_{n_1^i l_1^i}^*(r_1) R_{n_2^i l_2^i}(r_1) R_{n_3^i l_3^i}^*(r_2) R_{n_4^i l_4^i}(r_2) \times \int_{ANG} Y_{l_1^i}^{m_1^i*}(\theta_1, \phi_1) Y_{l_2^i}^{m_2^i}(\theta_1, \phi_1) Y_{l_3^i}^{m_3^i*}(\theta_2, \phi_2) Y_{l_4^i}^{m_4^i}(\theta_2, \phi_2) d\Omega dr_2 dr_1, \quad (4.40)$$

where E_i are constants originating from C_i and k_{ij} in equations 3.12-13. Clearly the angular parts should be evaluated first, and there will be many integrals of the form of

equation 4.11. Thus we have:

$$f(r_{12})_{NA-CI} = \int_0^\infty \int_{|r_1-r_{12}|}^{r_1+r_{12}} \sum_i F_i r_1 r_2 r_{12} R_{n_1^i l_1^i}^*(r_1) R_{n_2^i l_2^i}(r_1) \times \\ R_{n_3^i l_3^i}^*(r_2) R_{n_4^i l_4^i}(r_2) P_{l_i}(\cos \theta_{12}) dr_2 dr_1, \quad (4.41)$$

where $P_{l_i}(\cos \theta_{12})$ are Legendre polynomials, labelled by the index i . F_i are coefficients arising out of the analysis. If we were to substitute for $\cos \theta_{12}$, and expand this expression as a sum of primitive integrals of the form given by equation 4.39, the number of terms would turn out to be enormous, and we have thus adopted a numerical procedure, as with the Hartree-Fock wavefunction. It is straightforward to calculate the integrand in equation 4.41, because if there is a fixed r_1 , r_2 and r_{12} one can work out the values of the $P_{l_i}(\cos \theta_{12})$ via the cosine rule. It is again necessary to use great care in choosing the actual limit of the r_1 integration used. Because of the complexity of the integrand, the evaluation of $f(r_{12})$ for the NA-CI wavefunction is computationally time-consuming.

We have produced the expectation values associated with the $f(r_{12})$ curve, defined by

$$\langle r_{12}^n \rangle = \int r_{12}^n \Psi^*(r_1, r_2) \Psi(r_1, r_2) dr_1 dr_2, \quad (4.42)$$

where $n = -2, -1, 0, +1, +2$, and also the standard deviation, $\sigma_{r_{12}}$. As with the single-particle expectation values, $\langle r_{12}^0 \rangle$ must be equal to unity, and therefore constitutes a check on our $f(r_{12})$ functions. In the case of the Hartree-Fock and the NA-CI wavefunctions, these were evaluated by numerical integration of the $f(r_{12})$ curves. For the Drake wavefunction, a general routine was written to evaluate $\langle r_1^l r_2^m r_{12}^n \rangle$. This was done by analytically integrating the function in equation 4.39 with respect to r_{12} . If some minor modifications to the $f(r_{12})$ analysis are performed, in order to account for the powers of r_1 , r_2 , r_{12} that have been introduced in equations 4.21, 4.27 and 4.42, then an expectation value routine can be produced with very little effort. The $\langle r_{12}^{-1} \rangle$ value is naturally of interest as it is equal to the interelectronic potential energy.

Inevitably, the $f(r_{12})$ function loses much of the information about correlation, as both electronic coordinates have been integrated over all possible positions compatible with the value of r_{12} under consideration. A quantity which assesses the interparticle

distribution at a *fixed* radius of electron 1, is defined by:

$$g(r_{12}; r_1) = \int \Psi^*(\mathbf{r}_1, \mathbf{r}_2) \Psi(\mathbf{r}_1, \mathbf{r}_2) \frac{d\tau_1 d\tau_2}{dr_{12} dr_1}. \quad (4.43)$$

The *partial* Coulomb hole is therefore formed thus:

$$\Delta g(r_{12}; r_1) = g(r_{12}; r_1)_{CORR} - g(r_{12}; r_1)_{HF}, \quad (4.44)$$

and was initially defined by Boyd and Coulson in 1973 [31]. It was the *momentum* space analogue, the partial Coulomb shift, $\Delta g(p_{12}; p_1)$, (see chapter 7), however, which was first presented as a *surface* by Banyard and Reed in 1978 [32]. The partial Coulomb hole is related to the Coulomb hole by:

$$\Delta f(r_{12}) = \int_0^\infty \Delta g(r_{12}; r_1) dr_1, \quad (4.45)$$

and to the radial hole by:

$$\Delta D(r_1) = \int_0^\infty \Delta g(r_{12}; r_1) dr_{12}. \quad (4.46)$$

These relations provide a valuable means of checking that our results are consistent.

It is relatively simple to adapt the analysis and routines for $f(r_{12})$ evaluation to be used for the $g(r_{12}; r_1)$. Essentially, the double integral in equations 4.35, 4.39 and 4.41 will become a single integral with respect to r_2 . In the case of the Drake wavefunctions this necessitates providing a new integration routine. In the case of the Hartree-Fock and the NA-CI wavefunctions, the NAG double integral routine must be replaced by a single integral routine. Because the integral in question does not contain infinite limits, it is not necessary to carry out the extensive tests which were necessary for the determination of $f(r_{12})$ for these wavefunctions.

4.4 Interangular Functions and Properties

It is important to understand the angular component of the correlation effects. We have investigated the interangular distribution function defined by Youngman and Banyard [43]:

$$P(\theta_{12}) = \int \Psi^*(\mathbf{r}_1, \mathbf{r}_2) \Psi(\mathbf{r}_1, \mathbf{r}_2) \frac{d\tau_1 d\tau_2}{d\theta_{12}}. \quad (4.47)$$

We then form the associated angular hole,

$$\Delta P(\theta_{12}) = P(\theta_{12})_{CORR} - P(\theta_{12})_{HF}. \quad (4.48)$$

We have followed the above definition, rather than the definition of Ellis [120] which includes an additional factor of $\frac{1}{\sin \theta_{12}}$, in order to ensure that the resulting curve that we obtain possesses normalization properties; that is, because $P(\theta_{12})$ normalizes to unity, any area under the curve may be considered as a proportion of the probability distribution function. As with some of the other curves we have discussed, we have calculated the epsilon values:

$$\Upsilon_{\theta_{12}} = \frac{1}{2} \int_0^\pi |\Delta P(\theta_{12})| d\theta_{12}. \quad (4.49)$$

In order to evaluate the $P(\theta_{12})$ function, we must express the volume element $d\tau_1 d\tau_2$ in yet another form. Differentiation of the cosine rule, and substitution of the result into equation 4.7 gives,

$$d\tau_1 d\tau_2 = r_1^2 r_2^2 dr_1 dr_2 \sin \theta_{12} d\theta_{12} \sin \theta_1 d\theta_1 d\phi_1 d\chi. \quad (4.50)$$

It is significant that the radial part of this expression is identical to that in equation 4.5. This means that we will be able to use radial orthogonality properties, where appropriate. And even when this is not possible, the r_1 and r_2 integrations will usually be simple.

In the case of the Hartree-Fock representation, the fact that one can rearrange the product of the wavefunction with its complex conjugate into an angular part and a radial part means that we are able to obtain the simple expression:

$$P(\theta_{12})_{HF} = \frac{3}{4} \sin^3 \theta_{12}. \quad (4.51)$$

This expression applies for *all* values of the atomic number, Z and also holds for the 1 natural configuration (1NC) wavefunctions, and, for the H^- system, the 2NC wavefunction as well.

The analysis for the Drake wavefunction begins in the same fashion as for $D(r_1)$ and $f(r_{12})$ with the factorization of the wavefunction into an angular part and an

$S(r_1, r_2, r_{12})$ part, as in equation 4.8. The angular integral, equation 4.13, is handled in exactly the same fashion as before, producing an expression which is a function of only θ_{12} and which therefore requires no further integration. We thus have:

$$P(\theta_{12})_{Drake} = \frac{3}{4} \sin^3 \theta_{12} \int_0^\infty \int_0^\infty S^2(r_1, r_2, r_{12}) r_1^2 r_2^2 dr_1 dr_2. \quad (4.52)$$

The powers of r_{12} in $S^2(r_1, r_2, r_{12})$ present a problem. We must express these in terms of r_1, r_2 and $\cos \theta_{12}$, by means of the cosine rule. Unfortunately, however, the analytical integrals arising from this substitution are difficult to handle, and therefore we have evaluated the integral in equation 4.52 numerically, again paying close attention to the limits.

With the NA-CI wavefunction, the analysis again initially proceeds on a similar path to that for $f(r_{12})$, giving:

$$P(\theta_{12})_{NA-CI} = \sum_i G_i \int_0^\infty \int_0^\infty r_1^2 r_2^2 R_{n_1 l_1}^*(r_1) R_{n_2 l_2}(r_1) R_{n_3 l_3}^*(r_2) R_{n_4 l_4}(r_2) P_{l_i}(\cos \theta_{12}) dr_1 dr_2, \quad (4.53)$$

where G_i are constants. We note, again, that the Legendre polynomials $P_{l_i}(\cos \theta_{12})$ do not enter into the integrations in this equation. The radial integrations in this expression are thus simple, being uncontaminated by r_{12} terms, and are dealt with analytically. The $P(\theta_{12})$ computation therefore proceeds much faster than does that for the $f(r_{12})$.

In an effort to appraise the effects of angular correlation in different radial regions, we have calculated the angularly-dependent expectation values,

$$\langle r_1^n r_2^n \cos \theta_{12} \rangle = \int r_1^n r_2^n \cos \theta_{12} \Psi^*(r_1, r_2) \Psi(r_1, r_2) d\tau_1 d\tau_2, \quad (4.54)$$

for $n = -1, 0, +1$, and also the radially-independent quantity,

$$\langle \theta_{12} \rangle = \int \theta_{12} \Psi^*(r_1, r_2) \Psi(r_1, r_2) d\tau_1 d\tau_2. \quad (4.55)$$

It should be noted that the $n = 1$ value, together with $\langle r_1^2 \rangle$ and $\langle r_{12}^2 \rangle$ must obey the cosine rule. This acts as an essential test of our results. It is of note that the atomic dipole polarizability includes the expectation value $\langle r_1 \cdot r_2 \rangle$ in its definition [121].

When we evaluate these quantities for the Hartree-Fock wavefunctions and the 1NC wavefunctions (and the 2NC for H^-), then the radial part again separates out, leaving

an integration with respect to θ_{12} which is identically equal to zero. Thus, in these cases, the angular expectation values are all zero. For the correlated wavefunctions, if one multiplies the integrand of equation 4.47 by $\cos \theta_{12}$ and the appropriate powers of r_1 and r_2 , and then numerically integrates the resulting function of θ_{12} between 0 and π radians, the angular expectation values can be obtained relatively easily.

It has been found useful [32,34,37,38,122,123,124] in the understanding of correlation effects to consider the degree of *statistical* correlation in a system. Accordingly, we have produced various statistical correlation coefficients. These quantities were introduced into the analysis of electron correlation effects by Kutzelnigg, Del Re and Berthier [125] in 1968, and originate in the fields of probability theory and mathematical statistics. They assess the extent to which two variables are statistically correlated and are of great relevance to, although conceptually distinct from, the study of electron correlation as defined by Löwdin [6]. There are two kinds of correlation coefficients, radial and angular. The radial type are defined by:

$$\tau_r^{(n)} = \frac{\langle r_1^n r_2^n \rangle - \langle r_1^n \rangle^2}{\langle r_1^{2n} \rangle - \langle r_1^n \rangle^2}, \quad (4.56)$$

and we have evaluated these for $n = -1, +1$. The angular variety are given by:

$$\tau_{\theta_{12}}^{(n)} = \frac{\langle r_1^n r_2^n \cos \theta_{12} \rangle}{\langle r_1^{2n} \rangle}, \quad (4.57)$$

where we have taken $n = -1, 0, +1$. It is clear that we can evaluate all these correlation coefficients using quantities that have already been calculated. These values are bounded, fulfilling the relation: $-1 \leq \tau \leq +1$. A value of $+1$ corresponds to perfect *positive* correlation, whereas a value of -1 corresponds to perfect *negative* correlation. The value of n used in each case governs which radial region will be emphasized in the correlation coefficient. In their work concerning correlation coefficients, Banyard and co-workers have employed a different naming scheme for their τ values. This notation is related to that used here as follows:

$$\tau_r^{(-1)} = \tau_{1/r} \quad (4.58)$$

$$\tau_r^{(+1)} = \tau_r \quad (4.59)$$

$$\tau_{\theta_{12}}^{(-1)} = \tau_{\gamma'} \quad (4.60)$$

$$\tau_{\theta_{12}}^{(0)} = \tau_{\gamma''} \quad (4.61)$$

$$\tau_{\theta_{12}}^{(+1)} = \tau_{\gamma} \quad (4.62)$$

The correlation coefficients for the Hartree-Fock and the 1NC wavefunctions are always identically zero. For the angular coefficients, the numerator is always an expectation value which we have shown will be zero in these cases. Equation 4.28 shows that the numerator will also always be zero for the radial coefficients. The curves, surfaces and values defined in this chapter can be found in chapter 6 in sections 6.2 and 6.3.

Chapter 5

Discussion of Position Space Results

5.1 Introduction

Before the position space correlation effects can be discussed, it is necessary to deal with the general structure of the $2p^2\ ^3P$ state. This state, at the independent-particle approximation, comprises two 2p orbitals which are perpendicular to each other. We define one orbital to be situated along the z -axis. The other orbital is therefore located somewhere in the xy plane. The difference between the two orbitals is solely in their *angular* parts: their radial parts are identical, (see equation 3.5). This structure is illustrated schematically in figure II.1.

The $2p^2\ ^3P$ state is similar to the $1s^2\ ^1S$ ground state of helium-like systems, in that in each case the radial parts of the two orbitals are the same. This might imply *some* similarity between correlation effects in these two systems. On the other hand, the $2p^2\ ^3P$ state has the two-lobe angular structure described above, whereas the 1S system is spherically symmetric. One might therefore expect the $2p^2\ ^3P$ state to show some novel correlation effects.

In this analysis, we shall continually have need to refer to analogous results for the ground state 1S system. Although this is often possible, in some cases the relevant results have not been obtained. We shall therefore sometimes refer to results obtained for the $1s1s$ shell of lithium-like systems. These should serve as approximations to the

missing results, although obviously they will not be exactly the same, owing to the influence of the additional electron in these systems.

In the various curves and surfaces that have been used to display our results, different scales have obviously been used. Generally speaking, the rule that has been followed is that for He, Li⁺, and Be⁺⁺ the ranges of the r_{12} and r_1 axes are the same if multiplied by the atomic number, Z . This has been found to bring the results for these systems into approximate visual coincidence. The H⁻ system does not fit into this scheme, and in this case the ranges will be 4 times that for He. The physical reasons for these scalings will be discussed in section 5.3. It may be seen from table II.1 that the explicitly-correlated Drake wavefunctions are the best, energetically, of the ones which we have examined. This being so, when the ‘total’ correlation effects for each system are examined, we shall use the best Drake wavefunctions. In each part of the analysis, we initially consider the functions and values which are dependent on the position of only one particle, and then proceed to the two-particle properties. The two-particle properties are obviously the most useful for investigating correlation effects, as electron correlation is principally concerned with describing the interparticle interactions realistically.

Before moving on to the analysis we briefly outline the structure of the rest of this chapter. In section 5.2, we examine the total correlation effects for the systems. In section 5.3, the manner in which these effects vary with the atomic number, Z , is considered. In section 5.4, we compare the ways in which the Drake and NA-CI correlated wavefunctions account for different correlation effects. More informatively, the natural orbital analysis of the NA-CI wavefunction will be used in section 5.5 to analyse the way in which the total correlation effects discussed in section 5.2 come about. The entire position space analysis is briefly summarized in section 5.6.

5.2 Total Correlation Effects

As noted above, the best Drake wavefunctions are used for this section of the analysis. Thus when we refer to ‘the correlated values’, etc., we are referring to the values for the energetically best Drake wavefunctions. It will be found that the systems under consideration here fall into two quite distinct groups, as regards correlation effects. On the one hand, one has He, Li⁺ and Be⁺⁺, which are strongly bound, and on the other the H⁻ system, which is very weakly bound [107].

Radial Results

First, we consider the single-particle functions and expectation values. Plots of $D(r_1)$ for the Hartree-Fock (HF) wavefunctions are shown in figure II.2. They have been scaled by Z in the r_1 direction and by Z^{-1} in the direction of the $D(r_1)$ axis. This is to facilitate comparison for different Z -values, a topic which will be discussed in detail in section 5.3. Here, we confine ourselves to noting that these curves possess only one maximum, which would be expected in a state which has identical radial parts at the Hartree-Fock level. The $D(r_1)$ curves for the ground state have the same general shape, although they are rather more compact [126], whilst singly-excited states of He have density distributions with two maxima [127]. The gradient of the functions in figure II.2 is zero at $r_1 = 0$, unlike the ground state, where the corresponding gradient has a finite value. This is because the density of the $2p^2\ ^3P$ state is itself zero at the nucleus, and the effect of the r_1^2 term in the volume element is to make the $D(r_1)$ curve flat in this region. The ground state has a finite density at the nucleus, and the effect of the r_1^2 is simply to force the $D(r_1)$ curve to vanish at the origin.

The $\Delta D(r_1)$ curves for the four systems are shown in figure II.3, illustrating the effect of correlation on the radial distribution function. One sees broadly the same features in each case. The effect of correlation is to move probability from the region of the peak of the $D(r_1)$ Hartree-Fock curve to values of r_1 both closer to, and further away, from the nucleus. This effect is *consistent* with a radial correlation effect, where

the two electrons correlate by assuming different radial positions. Or, in other words, an ‘in-out’ radial correlation effect of the kind seen in the ground state [128]. But, as the $\Delta D(r_1)$ function is a single-particle function, we must seek other evidence to verify this conclusion. The magnitude of the change in the $D(r_1)$ curves due to correlation can be gauged by inspecting the Υ_{r_1} values in table II.3. These show the proportion of the radial distribution function rearranged by correlation effects. The value for H^- is approximately 2 orders of magnitude larger than the values for the other systems, which are small. The differences between the Υ_{r_1} values for these three systems are small compared to this. Figure II.3 also demonstrates that the radial effect in H^- is overwhelmingly biased towards moving distribution *outwards*, whereas in the other systems the proportions moved outwards and inwards are much more comparable. Already we can see that there is a significant difference between H^- and the other systems in the radial correlation effects. The Hartree-Fock representation of the H^- single-particle distribution is much too compact, and an important effect of correlation is to correct this. By contrast, the Hartree-Fock $D(r_1)$ descriptions for the other systems are close to their correlated forms. We calculated values of r_1 at which 98% of the Hartree-Fock $D(r_1)$ is encompassed. For $Z=1,2,3,4$ these are respectively: 21.5, 6.9, 4.2 and 3.0. Most of the changes due to correlation take place within these values, with the exception of H^- where the Drake-84 $\Delta D(r_1)$ still has a significant magnitude at three times the 98% limit.

The expectation values, $\langle r_1^n \rangle$, together with the standard deviation, σ_{r_1} , are displayed in table II.4; these broadly confirm the comments concerning the $\Delta D(r_1)$ curves. In the systems which have a positive charge or are neutral, the effect of correlation is in each system to *increase* the magnitude of each of the expectation values proceeding from the Hartree-Fock wavefunction to the best Drake wavefunction. As each expectation value emphasizes regions either close to, or distant from, the origin, this increase can be seen as corresponding to the inwards and outwards shift of density seen in figure II.3. Not surprisingly, the σ_{r_1} values increase, showing that the distribution becomes more radially diffuse when correlation is introduced, which, again, is consistent with the elec-

trons adopting differing radial positions when correlation is introduced. In particular, it should be noted that $-2Z \langle r_1^{-1} \rangle$ is equal to the electron-nuclear potential energy for the system, where Z is the atomic number. The fact that correlation increases $\langle r_1^{-1} \rangle$ means that the energy for the system will become slightly lower, all other things being equal.

When H^- is considered the situation is somewhat different. The positive n expectation values and σ_{r_1} are increased by correlation, but by a very much larger proportion than in the other systems. The $n = -2$ value is also increased, although by a small proportion. The $n = -1$ value is *reduced* by the introduction of correlation. This is somewhat surprising in view of the fact that this effect will make the energy of the system higher and, by virtue of the variational principle, worse. Because the energy of the correlated wavefunction is obviously better than that for the Hartree-Fock, we expect to find an interparticle correlation effect which will counteract this unfavourable energy effect of correlation.

The two-particle $D(r_1; r_2)$ and $\Delta D(r_1; r_2)$ surfaces show how the radial behaviour of one electron is related to the radial behaviour of the other. The $D(r_1; r_2)$ results are displayed for the Hartree-Fock wavefunctions in figure II.4, and are of course symmetric about the $r_1 = r_2$ diagonal, as is necessary to ensure that the electrons are indistinguishable in their properties. The shape of these surfaces is very similar to that found in the $D(r_1; r_2)$ surfaces for the $1s1s$ shell of Li-like systems [129]. That is, the surfaces possess single peaks, located along the $r_1 = r_2$ diagonal. The corresponding surface for the ground state of He does not appear to have been reported. In surfaces corresponding to systems, or electron pairs in systems, where the two electrons occupy different radial shells the shape is quite different. In these cases, extended features parallel to each horizontal axis are present [127,129].

The $\Delta D(r_1; r_2)$ surfaces are similar for each system and are shown, for the best Drake wavefunctions, in figure II.5. In each instance there is a deep minimum at the approximate location of the peak of the Hartree-Fock $D(r_1; r_2)$ for the system, corresponding to a reduction in the probability of the two electrons being at the same radius. This

diminution in probability is compensated for by an enhancement of the likelihood of the electrons being located so that r_1 and r_2 have *different* values. That is, correlation produces the positive features parallel to the r_1 and r_2 axes. So the effect of correlation is to increase the regions of the $\Delta D(r_1; r_2)$ surfaces where the electrons are at different radii. Hence there is a *negative radial correlation effect*. In other words, the effect of correlation is to make it *less* likely that the electrons have the same radius. Broadly similar effects may be seen in the ground state contours of $\Delta D(r_1; r_2)$ presented by Banyard and Baker [126] for H^- , He and Li^+ . An increase in the average difference between the radii of the electrons would be expected to increase the average interelectronic distance. This, considered in isolation, would then lower the energy of the system. For each system, the values of r_1 and r_2 at which the maxima of the two-particle holes occur are close to the points at which the inner and outer positive regions of the corresponding $\Delta D(r_1)$ curves cross the r_1 axis. In the light of the results for the two-particle holes, we can now conclude that our explanation of the $\Delta D(r_1)$ curves in terms of radial correlation was correct.

Although we have not presented the correlated $D(r_1; r_2)$ surfaces, it is worthy of note that they are qualitatively similar to the Hartree-Fock surfaces, with the exception of H^- . In this system the influence of correlation is so great that the correlated surface has features parallel to each axis somewhat similar to those in the the Hartree-Fock surfaces of the 2^3S , 2^1P and 2^3P singly-excited states of helium generated by Youngman [127]. Thus for the negative ion the effect of radial correlation is of such magnitude that it causes the two-particle radial distribution to have a form typical of two-electron systems where the electrons occupy different orbitals.

We seek corroboration of our conclusions concerning the two-particle surfaces by inspecting table II.5, where the expectation values $\langle r_1^n r_2^n \rangle$ are displayed. The systems other than H^- are considered first. For all n , correlation causes the expectation values to reduce in magnitude. Because the $\langle r_1^n r_2^n \rangle$ values tend to emphasize the $r_1 = r_2$ region of the $D(r_1; r_2)$ surfaces, this reduction due to correlation can therefore be seen as strengthening the conclusion that the effect of correlation is to reduce the probability

of the electrons being at the same radius, as it is clearly reduced for all values of r_1 , not just at the low values corresponding to the deep minima in figure II.5.

In the case of H^- , the $n = -2$ and $n = -1$ values are reduced by correlation, as we would expect from the minimum in figure II.5.a. The $n = +1$ and $n = +2$ values show very large increases, however. This would appear to be because, for the portion of the surface where either r_1 or r_2 is larger than about 20 bohr, there is no appreciable negative region along the $r_1 = r_2$ diagonal. But there are areas where the surface is positive; that is, the positive features running parallel to the axes. Although these are off-diagonal, they will still contribute to the positive n expectation values, and as there is no negative region to compensate for this, we would consequently expect these values to be larger at the correlated level than at the Hartree-Fock level.

The statistical correlation coefficients shown in table II.6 can be used to supplement the conclusions based on the Δ -curves and surfaces. Previously, we have discussed the effects of electron correlation defined as the improvement of the energy of a wavefunction over the energy of the Hartree-Fock wavefunction [6]. Statistical correlation coefficients assess the degree of statistical correlation between two variables. In this case, these variables describe the position of the two electrons in the $2p^2\ ^3P$ state. Statistical correlation is therefore *not* the same as electron correlation, in the sense that we have defined it. Nevertheless, it is to be expected that the two concepts would relate to one another in practice, as an improvement over the Hartree-Fock energy should generally come about by the electrons statistically correlating in order to avoid each other.

Owing to the way in which they are defined, all correlation coefficients lie between -1 and $+1$. A value of $+1$ corresponds to perfect positive correlation, while -1 corresponds to perfect negative correlation. The correlation coefficients are explicitly defined in equation 4.56 and equation 4.57. We have evaluated two kinds of correlation coefficients. The first type are radial correlation coefficients. $\tau_r^{(-1)}$ measures the degree of statistical correlation between the values of the radii of the two electrons in the regions close to the nucleus. $\tau_r^{(+1)}$ measures the same type of correlation, but in regions farther away from the nucleus. All correlation coefficients are equal to zero for the Hartree-Fock

wavefunctions and indeed for any independent-particle representation of this state. The correlation coefficients for the Drake wavefunctions are all negative. This confirms our earlier interpretation of the effect of radial electron correlation as causing the electrons to correlate negatively. In the three systems which are not negatively charged, $\tau_r^{(+1)}$ is significantly larger than $\tau_r^{(-1)}$. This indicates that within these systems radial correlation is most important in regions far from the nucleus. In H^- the situation is reversed.

Angular Results

We now turn to the angular curves and expectation values. In figure II.6 the $P(\theta_{12})$ curve is displayed for the Hartree-Fock wavefunctions. This curve gives the probability that the angle at the nucleus subtended by the two electrons is θ_{12} . In other words, it is the interelectronic angular distribution. The simple angular form of the HF wavefunctions ensures that the $P(\theta_{12})_{HF}$ curve will be identical for each system. The maximum of the curve is at 90° , a result consonant with the relative positions of the lobes in figure II.1. As would be expected from this, inspection of table II.7 shows $\langle \theta_{12} \rangle$ to be equal to 90° for all the Hartree-Fock wavefunctions. The changes to the interelectronic distribution caused by electron correlation are shown in the $\Delta P(\theta_{12})$ curves in figure II.7. For each system, the effect of correlation is to reduce the probability of θ_{12} being less than 90° , and increase the probability of θ_{12} being greater than 90° . A similar effect may be seen in the ground state and singly-excited curves of Banyard and Ellis [34], although these workers employed a slightly different definition of the angular hole. The form of our holes thus leads us to expect that the value of $\langle \theta_{12} \rangle$ will be greater than 90° in the correlated wavefunctions, and table II.7 does indeed show this. The values of $\Upsilon_{\theta_{12}}$ in table II.3 show the magnitude of the changes in $P(\theta_{12})$ due to correlation effects. In the neutral and positive systems, these are large compared with the analogous radial values, Υ_{r_1} , but in H^- , Υ_{r_1} is somewhat larger than $\Upsilon_{\theta_{12}}$. This is consistent with the view that in H^- radial correlation effects are more important relative to the total correlation effects than in the other systems, although it is important to remember that Υ_{r_1} is a single-particle quantity.

The angular holes and the $\langle \theta_{12} \rangle$ values show the effects of correlation averaged over all radial distances. To assess the angular effects of correlation in different radial regions, it is necessary to inspect the angular expectation values $\langle r_1^n r_2^n \cos \theta_{12} \rangle$ displayed in table II.7. In all cases they are zero at the Hartree-Fock level, and are negative for the best Drake wavefunctions. As r_1 and r_2 are always positive, the negative character of the correlated expectation values can only originate from integration over positions of the electrons where θ_{12} is larger than 90° , and hence where $\cos \theta_{12}$ is negative. It is consequently evident that the effect of correlation is to increase the angle between the electrons in all radial regions. As with the radial effects of correlation there is therefore obviously a *negative* angular correlation effect. In a manner analogous to the radial correlation effects, it is clear that an increase in the average value of θ_{12} would be expected to produce an increase in the average interelectronic distance, which would then lower the energy of the system. It is worthy of comment that the correlated value of $\langle r_1^{-1} r_1^{-1} \cos \theta_{12} \rangle$ for H^- is an order of magnitude larger than any of the other $\langle r_1^n r_2^n \cos \theta_{12} \rangle$ values, and $\langle r_1^{-1} r_2^{-1} \cos \theta_{12} \rangle$ is an order of magnitude smaller than any of the other values. This is presumably due to the extremely large positive feature at large r_1 seen in the $\Delta D(r_1)$ curve for H^- .

The angular correlation coefficients measure the degree of correlation between the angular positions of the electrons without being biased by the nature of the radial distribution. $\tau_{\theta_{12}}^{(-1)}$, $\tau_{\theta_{12}}^{(0)}$, and $\tau_{\theta_{12}}^{(+1)}$ assess angular correlation at small, medium and large distances from the nucleus, respectively. We note that in the neutral and positive systems $\tau_{\theta_{12}}^{(+1)}$ and $\tau_{\theta_{12}}^{(0)}$ are always larger than $\tau_{\theta_{12}}^{(-1)}$, whilst in H^- the $\tau_{\theta_{12}}^{(0)}$ value is the largest angular coefficient. In each of the systems, apart from H^- , the radial correlation coefficients are somewhat larger than the angular coefficients, whilst being of a comparable order of magnitude. In H^- , however, the radial coefficients are approximately an order of magnitude larger than the $\tau_{\theta_{12}}^{(-1)}$ and $\tau_{\theta_{12}}^{(+1)}$ values and are more than three times the magnitude of $\tau_{\theta_{12}}^{(0)}$. We conclude from this that radial correlation is very much more important than angular correlation in this system. This is reflected in the extremely large radial effects of correlation which were discussed earlier.

Interparticle Results

The $f(r_{12})$ curves for the Hartree-Fock wavefunctions for the four systems are shown in figure II.8 and are scaled in the same fashion as the $D(r_1)$ curves in figure II.2. It is worth noting that the curve for H^- is much more diffuse than for the other systems, in spite of the Z-scaling. This will be discussed in section 5.3. The $f(r_{12})$ are all flat near to the origin. This is characteristic of Fermi correlation, which is present at the Hartree-Fock level, and prevents the electrons from approaching each other closely. We may view this Fermi effect as a consequence of the requirement that the spatial part of the wavefunction be antisymmetric.

The $\Delta f(r_{12})$, or Coulomb holes, displayed in figure II.9 have a simple form. Probability is removed from regions of small r_{12} , i.e. where the electrons are close together, and placed in regions of higher r_{12} . One can therefore speak of a total *negative* correlation effect in this state. This can be viewed as a combination of the negative radial and angular correlation effects discussed earlier working in unison. It is significant that the shape of these Coulomb holes is remarkably similar to that of the corresponding ground-state holes [7,29,130]. In the curves presented here, however, the Fermi effect ensures that they are flat near the origin. This is not seen in the ground state, where no Fermi correlation is present. The point at which each curve crosses the axis, which may be termed the 'radius' of the hole, is near to the peak of the corresponding $f(r_{12})$ curve.

In table II.8 the expectation values $\langle r_{12}^n \rangle$ and the standard deviation $\sigma_{r_{12}}$ are displayed. For each system the negative n values are reduced by correlation, but the positive n ones are increased. This is clearly a consequence of the outward shift of interparticle distribution due to correlation. In particular, it should be noted that the $n = -1$ expectation value is reduced by correlation. The effect of this is to lower the energy of the state, as this expectation value gives the interelectronic potential energy. In the case of H^- this lowering in energy more than counteracts the surprising increase in electron-nuclear potential energy which was observed earlier. For the other systems the change in interelectronic potential energy due to correlation is approximately twenty

times the change in electron-nuclear potential energy.

Because the virial theorem is obeyed very well by the Hartree-Fock and Drake wavefunctions, the total change in potential energy due to correlation provides an essentially self-contained view of the way in which correlation improves the total energy. In our parallel discussion of correlation effects in momentum space in chapter 8 the changes in $\langle p_1^2 \rangle$ due to correlation effects provide a complementary view of the way in which correlation improves the energy.

It is interesting to see that the effect of correlation is to *reduce* slightly the magnitude of the standard deviation, $\sigma_{r_{12}}$, in the neutral and positive systems. This is surprising in view of the fact that the general effect of correlation is to move the $f(r_{12})$ distribution outwards. It therefore shows that the effect on the $f(r_{12})$ distribution is *localized*, and that there is no general increase in the diffuseness of the function. In the H^- system, the $\sigma_{r_{12}}$ is greatly increased by correlation effects. This fact, together with the very slowly decaying nature of the $\Delta f(r_{12})$ curve for H^- at high r_{12} , demonstrates that correlation effects are, in this case, making the distribution very much more diffuse, as was similarly observed for the $\Delta D(r_1)$ results for this species discussed earlier. In fact, the effects of correlation are so large in H^- that the Hartree-Fock and correlated $f(r_{12})$ are qualitatively different. The values of r_{12} at which 98% of the Hartree-Fock interparticle distribution are enclosed are for H^- , He, Li^+ and Be^{++} 27.6, 9.0, 5.5 and 3.9 respectively. With the exception of H^- the magnitudes of $\Delta f(r_{12})$ beyond these points are small, showing that the effects of correlation are essentially restricted to the most important regions of the Hartree-Fock $f(r_{12})$. But we note that the radii of the Coulomb holes (i.e. the points at which the curves cross the axis) are somewhat larger than the modal values of the corresponding $D(r_1)$ curves for the Hartree-Fock wavefunctions. Thus the interparticle effects of correlation have a long range compared to the radial distributions of the systems.

The $\Upsilon_{r_{12}}$ values shown in table II.3 provide a means of assessing the magnitude of the change in the $f(r_{12})$ distribution caused by correlation effects. The extremely large value for H^- of 27.9% shows that the total effect of correlation in this system is very

large. In the ground state of H^- , this value is approximately 8% [131]. We recall the large values of $\Upsilon_{\theta_{12}}$ and especially Υ_{r_1} for our H^- system. The values of $\Upsilon_{r_{12}}$ for the other systems are comparable to the values of $\Upsilon_{\theta_{12}}$. The value of $\Upsilon_{r_{12}}$ for He, 5.64%, is only slightly larger than the value for the ground state of He, 4.7% [7]. This is somewhat surprising, in view of the arguments presented at the beginning of chapter 2 concerning the importance of electron correlation effects in doubly excited states. One reason for the relatively small difference between the $\Upsilon_{r_{12}}$ values for the 1S ground state and the $2p^2\ ^3P$ state may be the presence of Fermi correlation in the 3P state. The absence of this form of correlation in the ground state means that Coulombic correlation must bear the entire burden of providing a means of keeping the two electrons apart.

It is important that the $\Upsilon_{r_{12}}$ values for He, Li^+ and Be^{++} are very much greater in magnitude than the Υ_{r_1} values, because obviously in these systems the change in $D(r_1)$ due to correlation is small compared to the change in the interelectronic distribution $f(r_{12})$. This is in harmony with the view that single-particle functions (eg $D(r_1)$) should be less sensitive to correlation effects than two-particle functions (eg $f(r_{12})$, $P(\theta_{12})$). The surprising fact is that in H^- the value of Υ_{r_1} is comparable to the value of $\Upsilon_{r_{12}}$. It is evidence that radial correlation in H^- is of a different character to radial correlation in the other systems. This difference originates, no doubt, in the extremely low value of the binding energy, (0.0096 eV), for the $2p^2\ ^3P$ state of H^- [86]. In the other three systems, the principal effect of correlation is to change the interelectronic distribution, whilst leaving the radial description essentially unaltered. This must be borne in mind when the differences in the $\Delta D(r_1)$ curves for different wavefunctions are discussed in section 5.4 and section 5.5.

The $\Delta f(r_{12})$ function presents an overall view of how correlation effects occur. To investigate the effects of correlation at different radii we discuss the $g(r_{12}; r_1)$ functions for the Hartree-Fock wavefunctions in figure II.10, and the $\Delta g(r_{12}; r_1)$ in figure II.11. These surfaces illustrate the behaviour of, and changes to, the interelectronic distribution when a test electron is at different distances, r_1 , from the nucleus. A plane cutting through the $\Delta g(r_{12}; r_1)$ surface corresponding to a fixed value of r_1 can therefore be

regarded as a *partial* Coulomb hole. The entire surface is also referred to as a partial Coulomb hole.

It is apparent from figure II.10 that the maxima of the $g(r_{12}; r_1)$ surfaces lie at a point where $r_{12} > r_1$, and that the surfaces as a whole are biased towards the $r_{12} > r_1$ side of the $r_1=r_{12}$ diagonal. This corresponds to our lobe model of the state at the independent-particle level, (see figure II.1). If we regard one electron as being in the lobe parallel to the z -axis and the second in the perpendicular lobe, it is evident that r_{12} will generally be larger than r_1 . The values of r_1 and r_{12} at the maxima are roughly in accord with what would be expected from applying the theorem of Pythagoras to this interpretation.

We now consider the partial holes in figure II.11. We examine, collectively, the partial holes for the positive and neutral systems. If one looks at how the partial Coulomb hole varies with the value of the radius for a test electron, it can be seen that at each value of r_1 the effect of correlation is to move interelectronic distribution from low r_{12} regions to high r_{12} regions. In other words the form of each partial Coulomb hole is the same as that of the total hole. The zero contour may be regarded as comprising the radii of the different partial holes. We see that the radius increases as r_1 increases. An increased value of r_1 for the test electron will correspond to an average reduction in the momentum of this electron. This would be expected to lead to an enhanced ability of the other electron to avoid the test electron, and thus the observed increase in the radius of the partial Coulomb hole. The equivalent surfaces for the ground state of He and Li^+ show similar features to the ones that we have observed in our 3P state [132].

The partial hole for H^- , displayed in figure II.11.a, has a rather different shape to that of the other systems. The principal difference is the region at $r_{12} > 15$, where the surface has a very small magnitude at values of r_1 which are between the diagonal feature and the feature parallel to the r_{12} axis. One can see a qualitatively similar, but very much smaller, reduction in the corresponding regions of the holes for the other systems. We interpret this feature in the H^- ion as being a manifestation of the extremely large effects of radial correlation seen in the $\Delta D(r_1)$ curve shown in figure II.3.a, and the

$\Delta D(r_1; r_2)$ surface in figure II.5.a. That is, for large r_{12} the radial density is localized in two separate r_1 regions.

We now view the H^- partial hole in the conventional manner described earlier of observing the effect of correlation on the interelectronic distribution for a test electron at fixed r_1 . For $r_1 < 10$, we have qualitatively the same kind of behaviour as in the other systems. That is, a reduction in density at low r_{12} , and an increase at large r_{12} . For r_1 larger than about 15 we see a different form. The effect of correlation is to increase the density at values near to the diagonal, but there is no corresponding reduction at small r_{12} . This lack of any kind of balance between the positive and negative regions in the partial Coulomb holes for H^- manifests itself as the large magnitude of the $\Delta D(r_1)$ curve in figure II.3.a. The partial hole for H^- is relatively much greater in magnitude than those for the other systems, when compared with the corresponding Hartree-Fock distributions. As with the radial functions and the Coulomb hole, the correlated surface for H^- is qualitatively different to the Hartree-Fock distribution.

In conclusion, it should be emphasized that in every case where we have been able to compare our results with the analogous ground state results the same kind of behaviour was observed. We therefore conclude that the way in which electrons correlate in the $2p^2\ ^3P$ state of H^- , He, Li^+ and Be^{++} is the same as in the ground state of these systems, but the total effect here is of a somewhat greater magnitude. This difference in *magnitude* is especially noticeable in H^- . When we have discussed the results for the truncated natural expansion wavefunctions in section 5.5 it will be possible to draw further conclusions about the way in which the total correlation effects are built up.

5.3 Z-Dependent Trends

The variation of the electron correlation effects with the atomic number, Z , will now be discussed. To a certain extent we have already touched on this topic in section 5.2, as some of the differences between the effects for H^- and the other systems were, of necessity, dealt with there. Those differences are extreme manifestations of more general Z -trends.

The gross effects of changing the nuclear charge must first be considered. As we increase Z the state will become more compact, as the additional electron-nuclear Coulombic force manifests itself. In fact, if one inspects the form of the solutions of the Schrödinger equation for the hydrogen-like systems [12], it can be seen that the corresponding $D(r_1)$'s will be identical if divided by Z and plotted against Zr_1 . This is also the case if an independent-particle wavefunction comprising unoptimized hydrogenic radials for the $2p^2\ ^3P$ state is used. The effects of electron shielding and electron correlation would be expected to reduce the extent to which scaling can bring distribution functions into coincidence in wavefunctions which take account of the $\frac{1}{r_{12}}$ interaction. Nevertheless, plotting functions against scaled variables generally produces a reasonable degree of coincidence and thus provides a basis for comparing results for different systems, as the crude effects of increasing the electron-nuclear force have been removed.

Consequently, where we plot results from different systems on the same diagram, we have scaled the abscissae by Z (excepting the curves which are functions of angles). In the case of normalized functions, we have scaled the ordinate by Z^{-1} in order to preserve the normalization and bring the curves into approximate agreement. Where a single diagram comprises results from only one system, we have not actually scaled the abscissae, but in the case of He, Li^+ and Be^{++} the ranges of the abscissae are inversely proportional to Z , as described in section 5.1. Owing to its extreme diffuseness, for H^- the ranges are 4 times the corresponding ranges for He. Again, we consider for the correlated representation the energetically best wavefunctions of Drake because the total correlation effects are being dealt with. We start with the single-particle results, and then move on to the more informative two-particle results.

Radial Results

It is necessary to return to the $D(r_1)$ curves for the four systems at the Hartree-Fock level displayed in figure II.2. They are scaled in the manner just described. It is clear that the effect of scaling has been to bring the positions of the maxima into close agreement. However, as Z increases the scaled $D(r_1)$ become more compact. This

is because the effects of electron shielding present in the Hartree-Fock wavefunction become relatively less important as Z increases. This is what one would forecast, because the larger the electron-nuclear force, the less relatively important the electron-electron repulsion will become. As $Z \rightarrow \infty$ we therefore expect the scaled $D(r_1)_{HF}$ curve to approach a constant form corresponding to hydrogenic radial parts of the wavefunction, as the electron-electron force tends to an infinitesimal perturbation of the electron-nuclear force. The dashed curve in figure II.2 is evaluated from a single-determinant wavefunction containing unoptimized hydrogenic radials. When scaled as in this figure it does not vary with Z , as we noted earlier. It is evident that as Z increases the Hartree-Fock scaled curves tend to this function, a result which verifies our interpretation.

It is clear that the scaled $D(r_1)$ for H^- is very much more diffuse than the other systems. This is comprehensible in terms of the fact that the H^- system is only just bound at the correlated level. At the Hartree-Fock level it is not energetically bound, as the effects of nuclear shielding are not offset by the effects of electron correlation and so the only mechanism preventing one electron from moving out to an infinite distance from the nucleus is the fact that we are dealing with a *restricted* Hartree-Fock wavefunction, where the two radial parts of the wavefunction are required to be identical.

In figure II.12 we see the $\Delta D(r_1)$ curves for He, Li^+ and Be^{++} . They are scaled by Z in the r_1 direction, but there is no scaling of the ordinate. The curve for H^- is not included in this figure, owing to its extremely large magnitude; it can be seen in figure II.3.a. This remarkably large radial effect will be discussed further in section 5.5, in the light of the natural expansion results. We observe that the nodes of the curves in figure II.12 are close together and that the curves have the same general form. This indicates that the *form* of these radial correlation effects is not substantially affected by the change in Z . The fact that the magnitude of the curves, and hence the Υ_{r_1} , get smaller as Z increases indicates that the relative radial effect of correlation gets smaller as Z increases. This corresponds to the fact that the correlation energy for this state remains roughly constant as Z increases, (see table II.9). Because the energy of the systems increases as Z increases, it is readily apparent that the *relative* effect on the

energy of the system decreases as the nuclear charge increases. Interestingly, the Υ_{r_1} values show a greater than linear decrease as one goes up the isoelectronic series. It is possible to improve the agreement of the nodes by plotting the curves against $(Z - k)r_1$ instead of simply Zr_1 . Unfortunately it was found that the value of the parameter k required to produce the narrowest range of inner nodes was quite different from the optimal value of k for the outer nodes—0.28 compared with 0.49.

The expectation values $\langle r_1^n \rangle$ reflect the comments regarding the $D(r_1)$ curves made above. Taking the Hartree-Fock values, as Z increases the positive n values decrease, but the negative n values increase. The σ_{r_1} also decrease with increasing Z . These results correspond to the gross effects that increasing the nuclear charge has on the electronic distribution.

We proceed to the $D(r_1; r_2)_{HF}$ surfaces displayed in figures II.4. On the scales that have been employed, the surfaces for He, Li⁺ and Be⁺⁺ have very similar shapes. This indicates that the gross effects of increasing the nuclear charge have the same approximately Z -scaled effect as on the $D(r_1)$ curves. Note that the extreme diffuseness of the H⁻ surface again violates the Z -scaling, although the general form is the same as in the other cases. These comments are supported by an examination of the values of r_1 at which the maxima occur.

In figure II.5 the $\Delta D(r_1; r_2)$ are displayed and one can see that the surfaces for the systems other than H⁻ are again very similar in shape, although it is interesting to note that the magnitude of the surfaces *increases* with Z , whereas the magnitude of the $D(r_1)$ curves decreases with Z . But this does not indicate any increase in the importance of radial correlation as the scales used for the r_1 and r_2 axes show that the extent of the surfaces becomes more restricted as Z increases. Again, we note that although the general shape of $\Delta D(r_1; r_2)$ for H⁻ is similar to the other systems, it is *very* much more diffuse in terms of the positive features parallel to the r_1 and r_2 axes. The similarity of the $\Delta D(r_1; r_2)$ results for the neutral and positive systems on the scales used demonstrates that the two-particle radial effects of correlation are approximately inversely proportional to Z . The trends for the $\langle r_1^n r_2^n \rangle$ values for the Hartree-Fock

wavefunctions seen in table II.5 are identical to the trends that were noted for $\langle r_1^n \rangle$. That is, the negative n values increase with Z , whilst the positive n results decrease. Broadly similar trends can be seen in the ground state $\Delta D(r_1; r_2)$ surfaces [126].

Angular Results

In figure II.7 the $\Delta P(\theta_{12})$ curves for the four systems are shown. It is evident that the magnitude of the curves, and hence $\Upsilon_{\theta_{12}}$, becomes smaller as Z becomes greater. This reflects the decreasing *absolute* angular effect of correlation as Z increases, corresponding to the overall reduction in the importance of correlation effects as the nuclear charge increases. The values of $\langle \theta_{12} \rangle$ in table II.7 bear this out, decreasing with Z . However, if one plots instead the quantity $Z\Delta P(\theta_{12})$ it can be seen from figure II.13 that the curves for He, Li⁺ and Be⁺⁺ are brought into near-coincidence, at a magnitude substantially greater than H⁻. This demonstrates that angular correlation is less important relative to the total correlation effects in H⁻ than in the other systems. The closeness of the scaled curves, other than for H⁻, corresponds to the $\Upsilon_{\theta_{12}}$ being approximately inversely proportional to Z .

Table II.7 displays the $\langle r_1^n r_2^n \cos \theta_{12} \rangle$ values. The correlated values for $n = 0$ and $n = +1$ get smaller as Z increases, corresponding to the reduction in angular correlation effects seen in figure II.7. Somewhat surprisingly, the $n = -1$ value *increases* with Z . This might be interpreted as showing an increase in the importance of angular correlation close to the nucleus as Z increases. However, as we remarked earlier, as Z increases the magnitude of each $\langle r_1^n \rangle$ value for negative n increases. In other words there is an increase in density in low (r_1, r_2) regions. This may well be responsible for the seemingly anomalous behaviour of $\langle r_1^{-1} r_2^{-1} \cos \theta_{12} \rangle$. We will need to inspect the angular correlation coefficients in table II.6 derived from the angular expectation values to resolve this question.

Interparticle Results

Before the Z dependence of the interparticle correlation effects can be understood it is necessary to consider again the Hartree-Fock $f(r_{12})$ curves for the four systems shown in figure II.8. They are scaled in the same way as the $D(r_1)$ curves discussed earlier. As in those curves, the scaling brings the location of the maxima of He, Li^+ and Be^{++} into very approximate coincidence. However, in this case the H^- curve has a maximum at a value of r_{12} which is substantially larger than the other maxima. The approximate Z -scaling shown for the other three systems seems to indicate that the change in the $f(r_{12})$ curves for these systems when Z varies is principally due to the gross effects of the charge cloud being made more compact. That is, as the $D(r_1)$ function contracts, we would expect the electrons to approach each other more closely, if Coulombic correlation effects are ignored. The correspondence between the extremely diffuse character of the $D(r_1)$ and $f(r_{12})$ curves for H^- suggests a similar interpretation. Curl and Coulson [29] have presented comparable results for the ground state of helium-like systems. In addition to these Hartree-Fock functions, we have also generated an $f(r_{12})$ curve from the unoptimized hydrogenic independent-particle wavefunction described earlier. When scaled as in figure II.8 it does not vary with Z . As expected, the Hartree-Fock curves tend to this function as Z increases.

The variation of correlation-induced changes to the interparticle distribution is demonstrated by figure II.14, where the Coulomb holes for all four systems are shown. The horizontal axis is scaled by Z , but the vertical axis is not scaled. It can be seen that the curves for $Z \geq 2$ are in quite good agreement. In view of the scaling of the r_{12} axis, it is not surprising that the $\Upsilon_{r_{12}}$ values are approximately inversely proportional to Z for these systems. We interpret this as yet another manifestation of the decreasing relative importance of correlation effects as the nuclear charge is increased. The $\text{H}^- \Delta f(r_{12})$ curve is of a much greater extent than the other curves. One can see that the scaled radii of the holes gets slightly larger as Z gets smaller. The extremely large radius of the H^- hole is an exaggerated continuation of this trend. No doubt it reflects the extremely large magnitude of correlation effects in this system. These effects parallel the change in the scaled $f(r_{12})$ Hartree-Fock curves with Z . Similar trends for the helium-like ground

state systems have been reported by Curl and Coulson [29] and by Banyard and Seddon [130]. The only substantial difference is that in the ground state series the H^- hole is not as radically different from the other systems as is the case in the results presented here.

By plotting the curves against a horizontal axis $(Z - k)r_{12}$, the nodes can be brought closer together. We found that $k = 0.60$ brought all four nodes into the range 5.4 to 5.9. If the node for the negative ion was neglected, a value of $k = 0.39$ brought the other three cross-over points into extremely good agreement—between 6.15 and 6.25. It is interesting that when Curl and Coulson [29] sought the same kind of improvement in the ground state Coulomb holes of H^- , He, Li^+ and O^{+6} they found a very similar parameter: $k = 0.38$.

We briefly consider the $g(r_{12}; r_1)$ functions shown in figures II.10. Bearing in mind that for He, Li^+ and Be^{++} the endpoints of r_1 and r_{12} are inversely proportional to Z , the surfaces for these systems are very similar in character. A slight 'drawing-in' with increasing Z , for $Z \geq 2$, is just discernable. This corresponds to the Z -dependent variation in the compactness of the scaled $D(r_1)$ and $f(r_{12})$ curves discussed earlier. Again, the H^- surface is much more diffuse than the other surfaces.

The $\Delta g(r_{12}; r_1)$ surfaces are displayed in figures II.11. The radical difference between the H^- surface and the other surfaces has been discussed in section 5.2. Here, apart from noting the now-expected similarity of the other three surfaces, we comment only on the constant- r_{12} feature at large values of r_{12} dealt with in section 5.2. This attribute, which exhibits a radial effect of correlation, is responsible for the pronounced difference in form of the H^- surface. If we examine the partial holes for the other systems in figures II.11.b-d it is apparent that this feature becomes less important as Z increases. This is compatible with the view that radial correlation effects become less important relative to the total correlation effects as the nuclear charge increases.

Finally, we examine the statistical correlation coefficients shown in table II.6. In almost every case each coefficient becomes smaller in magnitude as Z is increased. This shows, as expected, that statistical correlation effects decrease in importance with in-

creasing atomic number. In particular, we note that $\tau_{\theta_{12}}^{(-1)}$ becomes less negative as Z increases. This confirms our interpretation of the *increase* in the magnitude of $\langle r_1^{-1} r_2^{-1} \cos \theta_{12} \rangle$ with Z discussed earlier. The definition of the statistical correlation coefficients precludes the amount of density in a given radial region from biasing the value of such coefficients. The single exception to the decrease in magnitude of the τ 's with Z occurs with the H^- value of $\tau_{\theta_{12}}^{(+1)}$, which is smaller in magnitude than those of the other systems. We take this as evidence of the very small importance of angular correlation in the outer regions of the H^- system.

Certain trends in the ratios of the coefficients are informative. The ratio of the radial correlation coefficients, $\frac{\tau_r^{(+1)}}{\tau_r^{(-1)}}$, is 0.94, 1.50, 1.49 and 1.49 for H^- , He, Li^+ and Be^{++} respectively, showing that the balance of radial correlation at different distances from the nucleus is similar in the neutral and positive systems. A typical ratio of angular values, $\frac{\tau_{\theta_{12}}^{(0)}}{\tau_{\theta_{12}}^{(-1)}}$, has values of 2.11, 1.68, 1.64 and 1.63 for the four systems in the order above. As with the radial correlation, there is evidently a similarity between the relative strengths of the angular correlation in different radial regions for the systems other than H^- . The other two possible angular ratios were examined and similar properties exist for these. The ratio of a radial τ to an angular τ proves to be more revealing. For the four systems taken with increasing Z , $\frac{\tau_r^{(+1)}}{\tau_{\theta_{12}}^{(0)}}$ is 3.54, 1.87, 1.66 and 1.58 whereas $\frac{\tau_r^{(-1)}}{\tau_{\theta_{12}}^{(0)}}$ is 3.73, 1.25, 1.12 and 1.06. Clearly angular correlation becomes more important *relative* to radial correlation as the atomic number increases.

We end this section by concluding that there is a substantial amount of evidence to show that as Z increases angular correlation effects become relatively more important, compared with radial correlation effects. Additional evidence for this will emerge from the natural orbital analysis results discussed in section 5.5. It is clear that in H^- radial correlation is much more important than angular correlation. Radial, angular and total correlation effects were seen to become less important as the nuclear charge increases.

5.4 The Drake Wavefunctions Compared to the NA-CI Wavefunctions

In the previous sections we discussed the effects of correlation in the $2p^2\ ^3P$ state with reference only to the best Drake wavefunctions. These recover extremely high percentages of the correlation energies and can thus be taken as being good approximations to the exact non-relativistic wavefunctions for the systems under consideration. In this section, and the following section, we shall investigate how the various different correlated wavefunctions account for the total correlation effects discussed earlier.

Here, we discuss how well the Drake explicitly-correlated wavefunctions describe the effects of correlation, especially compared with the full NA-CI wavefunctions. As described in chapter 3, we have analysed two explicitly-correlated Drake wavefunctions for each system. The energetically best function for each system we call the ‘best Drake’; and the shortest we call the ‘short Drake’. For each system, the shortest has the poorest energy of the wavefunctions calculated by Drake.

It is difficult to analyse the difference in correlation effects encompassed by two Hylleraas-type wavefunctions by studying the structure of the wavefunctions. When one goes from the short Drake to the best Drake the principal difference is obviously the increased number of terms. In He, Li^+ and Be^{++} the short Drake wavefunction contains 13 terms, whereas the best contains 70. For H^- the corresponding numbers are 20 and 84. The added terms include higher powers of r_1 , r_2 and r_{12} . As any term containing r_{12} will introduce both radial and angular correlation, it is not easy to assess what *type* of additional correlation is being introduced purely by inspecting the form of the wavefunctions. But it is worth briefly discussing the exponential parameters, α and β , which appear in the Drake wavefunctions (see equation 3.6). These, roughly speaking, indicate the general form of the radial distributions for the two electrons. In the positive and neutral systems these two parameters differ by, at most, 30% , with the relative difference decreasing with increasing Z . But for H^- , α is *three times* β for both the 20-term and 84-term wavefunctions. So the particular values of these parameters

in the Drake wavefunctions reflect the massive ‘in-out’ radial correlation behaviour for H^- discussed earlier. The reduction in the proportional difference between the two exponents as Z becomes larger illustrates the decreasing importance of radial correlation for increasing atomic number discussed in the previous section.

But for the most part our analysis will centre around the differences between the two Drake wavefunctions and the full NA-CI wavefunctions. It is important to note that for all four systems the NA-CI wavefunctions are energetically inferior to *both* Drake wavefunctions. Without any consideration of the forms of the wavefunctions, one might expect properties other than the energy to be more accurately represented by the short Drake wavefunctions than the NA-CI wavefunctions. However, such a simple-minded approach will be seen not to be justified.

Radial Results

We begin by considering the $\Delta D(r_1)$ curves for the four systems displayed in figure II.3 where, for each system, the radial holes produced using both Drake wavefunctions and the NA-CI wavefunction are shown. In figure II.3.a, for H^- , it is obvious that the curves do in fact order in the same way as the energies of the appropriate wavefunctions. The general effect of improvement in the correlation energy recovered is to shift more distribution outwards, or in other words to make the $D(r_1)$ curve more diffuse. It is clear that the NA-CI $\Delta D(r_1)$ curve is considerably less diffuse than the Drake $\Delta D(r_1)$ curves. Jáuregui and Bunge [86] have also presented a $D(r_1)$ curve for H^- produced using their CI wavefunction which has the lowest variational energy so far obtained for this system. Although the Drake-84 wavefunction achieves 99.99% of the correlation energy produced by the wavefunction of Jáuregui and Bunge, the $D(r_1)$ of these workers is significantly more diffuse than that of this highly-accurate explicitly-correlated wavefunction.

The situation with respect to the ordering of the curves is completely different in the other systems. We see that the $\Delta D(r_1)$ for the NA-CI lies *between* the two Drake $\Delta D(r_1)$'s for much of the range of the curves for Li^+ and Be^{++} , and is actually very

much closer to the best Drake than the short Drake. In He the Drake-70 curve lies between the Drake-13 and NA-CI curves. It should also be noted that the principal maxima and minima of the curves for the short Drake functions in these three systems have a greater magnitude than those of the best Drakes. This is reflected in the greater size of the Υ_{r_1} values for the short Drake wavefunctions displayed in table II.3. When we examine the corresponding $\langle r_1^n \rangle$ expectation values, displayed in table II.4, we see that despite this the values for the short Drake are smaller than for the best Drake in these systems, where the values are not actually the same. The same is true for the σ_{r_1} values. This may be understood by noting that at very large and very small values of r_1 the best Drake is somewhat more positive than the short Drake. We note that in these three systems the energy-related $\langle r_1^{-1} \rangle$ value is identical to 5 significant figures for the three classes of wavefunction under consideration. In H^- , these values order in the same fashion as the energy; that is, the electron-nuclear energy actually gets *less* negative and therefore poorer, as the total energy gets more negative.

In a manner similar to the $\Delta D(r_1)$ curves, the expectation values and the standard deviations for the NA-CI wavefunctions for the three systems lie in the range of the two Drake values, with just one exception, and are actually closer to the best Drake, where it is possible to make this distinction. In H^- these values order in the same fashion as the energies. We conclude from the above observations that for He, Li^+ and Be^{++} the NA-CI wavefunction represents the radial density distribution more accurately than the short Drake wavefunction, despite having an inferior energy. But it must be remembered that this has no significant consequences for the energies of these systems, because we have so far only discussed single-particle functions and values.

It is natural to proceed to a discussion of the two-particle radial results. The $\Delta D(r_1; r_2)$ surfaces are, for each system, visually identical for the two Drake and NA-CI wavefunctions, with the exception of the H^- system, where the NA-CI result (see figure II.19.d) is somewhat less diffuse than the explicitly-correlated surfaces, which are indistinguishable. Consequently, these surfaces have not been displayed for the short Drake wavefunctions, although they were calculated for each system. In order to com-

pare the representation of the two-particle radial effects we must have recourse to the $\langle r_1^n r_2^n \rangle$ two-particle expectation values, shown in table II.5. It is found that, with just one exception, the NA-CI values lie within the span of the Drake values for the three positive and neutral systems. The NA-CI values tend to lie closer to the best Drake than the short Drake, but this tendency becomes somewhat less as Z increases. These effects are somewhat surprising as one would expect the behaviour of such two-particle properties to be closely related to the energy of the wavefunction. It therefore seems that the NA-CI wavefunctions represent radial correlation more accurately than the short Drake wavefunctions in these systems. The H^- values order in the same way as the energies.

Angular Results

Analysis of the difference between the representations of angular correlation naturally begins with the angular holes, the $\Delta P(\theta_{12})$, which are displayed in figure II.15. Apart from the results for H^- the curves for the different wavefunctions are not visually distinguishable. In those instances we must refer to the appropriate expectation values, shown in table II.7. In the case of H^- it is readily apparent that the different wavefunctions exhibit differing magnitudes of angular correlation effects. It can be seen that the better the energy of the wavefunction, the *smaller* the size of the angular hole. We thus say that the NA-CI and short Drake functions *over-correlate* angularly. The $\langle r_1^n r_2^n \cos \theta_{12} \rangle$ and $\langle \theta_{12} \rangle$ values for H^- also order like the energies, with the poorest energy wavefunction, (the NA-CI), having values that represent the largest angular separation of the three wavefunctions.

Now we examine these expectation values for the positive and neutral systems. Considering just the two Drake wavefunctions, for these systems the best Drake has values of $\langle r_1^n r_2^n \cos \theta_{12} \rangle$ less negative than the short Drake, and $\langle \theta_{12} \rangle$ closer to 90° than the short Drake. So in these instances there is the same angular over-correlation that was present in H^- , although it is obviously not of a sufficient magnitude to be seen in the angular holes. For the expectation values $\langle r_1^{-1} r_2^{-1} \cos \theta_{12} \rangle$, and $\langle \cos \theta_{12} \rangle$, one

can see that the NA-CI value falls within the bounds of the two Drake values, in all but one case being closer to the best Drake. In these cases the NA-CI wavefunctions reproduce the correlation effects more accurately than the short Drake. This is again unexpected, as these are two-particle expectation values and as such should be sensitive to changes in the correlation energies recovered by each wavefunction.

The case of the $\langle r_1^{-1} r_2^{-1} \cos \theta_{12} \rangle$ expectation value for these three systems is somewhat different. In each case the NA-CI value lies, not *between* the two Drake values, but *beyond* the best Drake. That is, the short Drake is most negative, the best Drake comes next, and the NA-CI is the least negative. Probably the most reasonable interpretation of this behaviour is that for this expectation value the NA-CI wavefunction is actually at least as accurate as that for the best Drake.

Interparticle Results

We now consider the Coulomb holes, displayed in figure II.9, and the $\langle r_{12}^n \rangle$ and $\sigma_{r_{12}}$ values displayed in table II.8. The Coulomb holes for He, Li⁺ and Be⁺⁺ are each visually indistinguishable for the three types of wavefunction under consideration here. For H⁻, however, the three curves can be quite readily distinguished. In this case they order in the same manner as the energies; the more accurate the wavefunction the deeper the hole, and hence the more diffuse the tail of the curve. Because the changes in the angular hole due to increasing electron correlation for H⁻ tend to bring the electrons closer together, we interpret the ordering of the Coulomb holes as reflecting the ordering of the $\Delta D(r_1)$. That is, the increase in the size of the holes with correlation energy is a consequence of the increasing effects of radial correlation.

In order to examine the correlation effects for the interparticle distribution for the other three systems it is necessary to inspect the appropriate expectation values. Considering, initially, the two Drake wavefunctions in isolation, the effect of improving the energy is to make the $\langle r_{12}^{-2} \rangle$ and $\langle r_{12}^{-1} \rangle$ values smaller, and the $\langle r_{12}^{+1} \rangle$ and $\langle r_{12}^{+2} \rangle$ values larger. This continues the trend of changes in the expectation values when one goes from the Hartree-Fock to the short Drake. If we consider how the NA-CI

values fit into this scheme, we see that the positive n values and the $\sigma_{r_{12}}$ lie in the range of the two Drake values and are therefore superior to the short Drake values: another surprising effect. The negative n values do not show this behaviour, being larger than the short Drake values. So the $n = -1$ energy-related expectation values order in the same way as the total energies—a necessary result in view of the effective lack of change in the electron-nuclear energy between the three wavefunctions under consideration and the fulfillment of the virial theorem for these wavefunctions.

These negative n expectation values are therefore the only properties investigated so far where the values for the short Drake wavefunctions are superior to those of the energetically inferior NA-CI wavefunctions—for the systems other than H^- . It seems reasonable therefore, to infer that the short Drakes achieve better energies than those of the NA-CI wavefunctions solely by virtue of their extremely accurate representation of the low- r_{12} regions that the negative n values characterize. This contradicts Gilbert's [26] claim that Hylleraas-type wavefunctions achieve their excellent energies by representing the entire form of the Coulomb hole more accurately than CI wavefunctions. Seddon [131] reached conclusions somewhat similar to ours with respect to the ground state of some helium-like systems, but it should be noted that the explicitly-correlated wavefunctions employed in his study were of a much simpler form than the Drake wavefunctions used here. Clearly, our conclusions cannot apply directly for the H^- system, because no ordering effect was observed, but it seems likely that this is simply due to the poor energetic quality of the NA-CI wavefunction and to the extreme sensitivity of approximate wavefunctions with respect to small improvements to the corresponding energy in this species.

In view of our conclusion that the Drake wavefunctions achieve their excellent energies by representing the interelectronic distribution function, $f(r_{12})$, very accurately as r_{12} tends to low values, it would be intriguing to examine, in a future study, how well our various wavefunctions represent the electron-electron cusp conditions. The cusp condition

$$\lim_{r_{12} \rightarrow 0} \frac{dh(r_{12})}{dr_{12}} = h(r_{12}), \quad (5.1)$$

where $h(r_{12}) = \frac{f(r_{12})}{4\pi r_{12}^2}$, was derived by Thakkar and Smith [133] from the seminal work of Kato [134]. However, it is trivially fulfilled in our 3P state, because $h(r_{12})$ and $\frac{dh(r_{12})}{dr_{12}}$ are both equal to zero at $r_{12} = 0$. But Thakkar's higher-order coalescence condition [135],

$$\lim_{r_{12} \rightarrow 0} \frac{d^3 h(r_{12})}{dr_{12}^3} = \frac{3}{2} \lim_{r_{12} \rightarrow 0} \frac{d^2 h(r_{12})}{dr_{12}^2} \quad (5.2)$$

is applicable to this 3P state. That is, the exact wavefunction for a $2p^2 \ ^3P$ system should fulfil equation 5.2. We predict that both of the Drake wavefunctions would always come closer to obeying this condition than the NA-CI wavefunctions.

We examine, briefly, the statistical correlation coefficients for the wavefunctions that have been discussed in this section. For H^- , all the τ 's order in the same manner as the energies, as would be expected from the other results for H^- . In the case of the angular τ 's, it is evident from an examination of table II.6 that the better the energy of the wavefunction, the *smaller* the magnitude of the correlation coefficients. This exemplifies the difference between electron correlation and statistical correlation. In these cases, the more correlation energy recovered by the wavefunction the *less* statistically correlated are the angular positions of the electrons. For H^- , one of the radial correlation coefficients, $\tau_r^{(+)}$, shows this effect, but the other, $\tau_r^{(-)}$ does increase in magnitude as the energy improves.

The other systems are now considered. When one goes from the short Drake to the best Drake, in all but two cases the τ 's get less negative, as in most of the cases for H^- . In approximately two-thirds of the cases, the NA-CI τ lies between those of the two Drake wavefunctions, or is coincident with one of the Drake values. Where this is not so, the NA-CI value is closer to the best Drake than the short Drake, and so is probably as accurate as the best Drake.

In summary, we have examined various properties and functions for the Drake and NA-CI wavefunctions. We conclude that, although the explicitly-correlated wavefunctions are highly accurate in energetic terms, they are much less effective when assessed on how they reproduce other properties. Although the best Drake wavefunctions are more accurate in most respects than the NA-CI wavefunctions, the short Drake wave-

functions do not perform particularly well, in comparison to their excellent energies. We therefore concur with Beck and Nicolaides [136] in their comment that trial wavefunctions composed of single-particle functions, (i.e. CI wavefunctions), are competitive with explicitly correlated wavefunctions in many respects.

5.5 The Natural Expansions and the NA-CI Wavefunctions

In this section we will investigate how the total correlation effects for the systems are built up, by studying the way that the truncated natural expansions reproduce such correlation effects. These expansions were generated by using the NA-CI wavefunctions, (see appendix C). The nomenclature that we have used for our natural expansions is given in chapter 3. These kinds of expansions have been found useful in examinations of correlation effects in other systems [32,126,132,137,138,139,140,141,142]. This is because a natural expansion truncated to a certain number of configurations has close to the best possible energy for a variationally obtained wavefunction comprising that number of configurations. Combined with the fact that the first natural configuration has an energy close to the Hartree-Fock value, this implies that correlation is being introduced in the most efficient manner possible in a natural configuration. Although we give expectation values for the 1 to 5 natural configuration (NC) wavefunctions, it should be noted that a 3NC wavefunction achieves more than 90% of the correlation energy in all of our systems. This means that the first three configurations encompass most of the correlation effects. We shall therefore concentrate on the results for 1-3 NC wavefunctions in our discussion.

The energies for NC wavefunctions are given in table II.1, and they are also displayed in graphical form in figure II.16. This pictorial representation exhibits the extremely rapid convergence just mentioned in a particularly vivid manner. The natural expansions for the helium-like ground state systems [143] show convergence patterns similar to these, although the rate of convergence is not quite as impressive. Roos [144] has presented a similar diagram for the natural expansion for the H₂O molecule. In this case ten natural orbitals are required to yield 93% of the correlation energy, no doubt

due to the complex nature of correlation effects present in this molecular system.

Each natural configuration contains a particular *type* of natural orbital. Each type of natural orbital has a different radial part, which may be deemed a natural radial, and which comprises a linear combination of the radials in the original NA-CI orbitals of a given angular type. In addition, we will assign a character to the type of correlation introduced by each natural configuration and natural orbital. That is, if a configuration introduces functions with a new type of angular symmetry it will be called an 'angular' configuration. Otherwise, if no new angular function is introduced, it will be called a 'radial' configuration. This characterization is not absolute, because so-called 'angular' configurations also introduce a new type of radial function, and therefore, in principle, allow additional radial correlation. The accuracy and relevance of this assignment of correlation character will be shown by the results that will be presented in this section. It should be pointed out that in the ground state, the first angular natural configuration contains functions of p-symmetry, because the first natural configuration comprises s-type basis functions, whilst in the $2p^2\ ^3P$ state, the first angular configuration is made up of d-type orbitals. So the nature of the correlation introduced by a given configuration in a natural expansion cannot be determined in isolation from the earlier configurations in the expansion.

The kinds of natural orbitals for each system are listed in decreasing order of importance, together with their corresponding configuration coefficients, C_i^{NC} , in table II.10. Some conclusions can be drawn from this table. The first configuration, which should be close to the Hartree-Fock wavefunction, has in each case a large configuration coefficient, which is close to unity. In the case of the He, Li⁺ and Be⁺⁺ systems, the other C_i^{NC} are very small by comparison. This indicates that, for these systems, the Hartree-Fock wavefunction is a good first-order representation of the state. In the case of H⁻, the second natural configuration has a large value of -0.29920, showing that the independent-particle model is fundamentally inadequate for this system. It is also apparent that the C_i^{NC} for the first natural configuration gets larger as Z increases, approaching unity more closely. This demonstrates that as Z increases the Hartree-Fock approximation becomes

a better description of the exact non-relativistic wavefunction—a result in keeping with the discussion in section 5.3. Inspection of the second configuration, that is, the first correlating configuration, is also revealing. In He, Li⁺ and Be⁺⁺ it has an angular character, which shows again that angular correlation is more important than radial correlation in these systems. In H⁻, the second configuration has a radial character, indicating that radial correlation is more important here. We note that for the three systems the third configuration is radial. The ratio $\frac{C_2^{NC}}{C_3^{NC}}$ increases from 1.19 to 1.43 as we go from He to Be⁺⁺. This demonstrates, again, that angular correlation becomes more important relative to radial correlation as Z increases.

The First Natural Configuration and the f-Correction Function

The results that we have obtained for the 1NC wavefunctions are of interest, as they shed light on the relationship between Hartree-Fock wavefunctions and other independent-particle wavefunctions. It is evident from table II.1 and figure II.16 that the energy for the 1NC wavefunction is a very good approximation to the Hartree-Fock energy for He, Li⁺, Be⁺⁺. It is an adequate approximation for H⁻, for the purpose of treating the addition of further configurations as the addition of correlating terms to a Hartree-Fock representation. We note that in all cases the energies of the 1NC representations are actually *worse* than those of the Hartree-Fock wavefunctions. Although the energies of the two types of wavefunction are similar, it will be found that rather more noticeable differences exist between them when one comes to consider some of the correlation difference functions which will be discussed in the succeeding parts of this section. It is therefore important to have an understanding of the nature of the first natural configuration and its relation to the Hartree-Fock wavefunction.

The first point to make is that the Hartree-Fock and 1NC wavefunctions are both independent-particle descriptions, each consisting of a single determinant with the same angular functions. So the 1NC wavefunction for the $2p^2\ ^3P$ state only differs from the Hartree-Fock wavefunction given in equation 3.5 in the radial part.

Larsson [145] has stated that for two-electron systems the natural orbitals are iden-

tical to the Brueckner orbitals. So the first two natural orbitals, which make up the first natural configuration, are the first two Brueckner orbitals. In each case the only difference between the first two orbitals is in the angular part. Now the definition of the Brueckner orbitals is that they are the set of orbitals that produce no singly-substituted configurations when used in a CI wavefunction [146]. Smith and Kutzelnigg [147] have shown that for two-electron systems the single determinant that has the largest overlap with the exact wavefunction is composed of the first two Brueckner (or natural) orbitals. This corresponds to the finding of Coleman [148] that the natural expansion truncated to n configurations and renormalized has the smallest total quadratic deviation from the exact wavefunction for an n configuration wavefunction. The overlaps of our first natural configurations with the NA-CI wavefunctions are, for $Z=1,2,3,4$ respectively, 0.94334, 0.99353, 0.99737, 0.99857.

It is evident that it is possible to view the Hartree-Fock and 1NC levels of description in terms of what property one wishes to optimize. If the best energy for a single-configuration representation is desired, then the Hartree-Fock wavefunction is appropriate. However, if the optimal overlap with the fully-correlated description is required, one must produce the 1NC wavefunction. Löwdin and Shull [149] recognized this in 1956, referring to the close relationship between the two wavefunctions. The degradation in the quality of the energy when one goes from the Hartree-Fock to the 1NC in table II.1 and figure II.16 is now understood.

We can also seek to understand the connection between the two forms of wavefunction by utilizing the many-electron-theory of Sinanoğlu, which was described in chapter 1. In equation 1.7 the exact wavefunction of a system was written as an expansion comprising the Hartree-Fock orbitals, corrections to the Hartree-Fock orbitals—known as f -correction functions, electron pair correlation functions and also higher multi-electron correlation terms. The f -functions represent a single-particle improvement to the Hartree-Fock wavefunction. Sinanoğlu and Tuan [150] showed that these functions make little difference to the energy, but various workers have demonstrated that they can be important when evaluating some single-particle properties [151,152,153,154].

We have evaluated the radial parts of these orbital correction functions for the four systems under consideration, employing the NA-CI wavefunctions. These $f^{rad}(r_1)$ functions are shown in figure II.17. The effect of the orbital correction function is to increase the magnitude of the wavefunction at low- r_1 and high- r_1 and to reduce the magnitude at intermediate values. For the ground state [25], the correction functions are of a broadly similar form, although they are, not surprisingly, rather more compact. Also, they have a non-zero value at $r_1 = 0$, in keeping with the non-zero magnitude of the 1s orbital at the nucleus. The form of the f-functions will become comprehensible presently.

The size of the effect of the f-corrections can be gauged by evaluating their norms, the $\|f(r_1)\|$, which are displayed in table II.11. These decrease very rapidly when Z increases, which one would expect because the deficiency of the $D(r_1)$ for the Hartree-Fock diminishes very quickly as the atomic number increases as was discussed in section 5.3. Revealingly, the norm for H^- is about 36 times larger than for He, thus highlighting the extreme inadequacy of the Hartree-Fock distribution for H^- . The corresponding norms in the ground state are much smaller [25].

The first natural orbital is a good approximation to the Hartree-Fock orbital plus the f-correction function—with appropriate renormalization [155]. We checked the validity of this for our 1NC Hartree-Fock and f-functions. In the light of this, it is possible to regard the f-function as the correction required when going from the optimum energy Hartree-Fock wavefunction to the optimum overlap 1NC wavefunction. Consequently, when correlation difference functions for the 1NC wavefunctions are presented—that is, 1NC distribution functions minus Hartree-Fock distribution functions, it will be possible to attribute their forms solely to the effect of the f-single-particle correction function.

One can judge the relative change in the radial distribution function due to the f-function by inspecting the $\Delta D(r_1)$ curves produced using the 1NC wavefunctions, which are shown in figure II.18. It is clear that the $\Delta D(r_1)_{1NC}$ functions are sizable compared to the full NA-CI results. This is surprising if one regards the first natural configuration as being an approximation to the Hartree-Fock wavefunction. But one must remember that in He, Li^+ and Be^{++} the size of the $\Delta D(r_1)$ curves themselves is

not great, in comparison with the Coulomb holes for example, (see the epsilon values in table II.3). So in these systems one would not expect to see a large difference in the Hartree-Fock and 1NC two-particle functions. In the negative ion the NA-CI $\Delta D(r_1)$ radial hole is extremely large, and the 1NC hole is of a comparable magnitude. Here there is thus reason to expect significant differences in the two-particle behaviour of the two independent-particle wavefunctions.

A similarity between the shape of the 1NC curves and the NA-CI curves can be clearly seen. This shape is the direct consequence of the similar shape of the $f^{rad}(r_1)$ functions shown in the previous figure. In the fully-correlated radial holes this shape was interpreted as a manifestation of the effects of radial correlation—one electron moves in, one electron moves out. It is intriguing that this ‘in-out’ behaviour is seen in the 1NC curves, because the first natural configuration is statistically uncorrelated, (see table II.6) and does not improve on the Hartree-Fock energy. The explanation is that, being a single-particle function, the $\Delta D(r_1)$ radial hole does not show statistical correlation as such. Rather, it shows a one-particle effect of any change to the Hartree-Fock wavefunction, which may or may not be an increase in statistical correlation. In the NA-CI curves this ‘in-out’ feature is indeed a consequence of radial correlation; this can be seen in the two-particle radial holes. But in the 1NC $\Delta D(r_1)$ this effect is purely a result of the Brueckner orbital determinant being a maximal overlap with the exact wavefunction. That is, the 1NC curve achieves its ‘in-out’ character simply because the curve is defined as being similar to the NA-CI curve. So one must be careful when interpreting a one-particle difference curve as demonstrating correlation effects.

Radial Results

Now we consider the radial results in general. Having just discussed the 1NC $\Delta D(r_1)$ results, it is appropriate to commence with the 2NC radial holes. It is clear that in He, Li⁺ and Be⁺⁺ the introduction of the second NC takes the $\Delta D(r_1)$ curves further from the full CI than in the 1NC case. The fact that the second configuration is angular in these cases explains why these radial curves do not get closer to their correct values.

Because there is no appreciable radial correlation in the 'd'-type second configurations, the change in the radial descriptions engendered by their introduction is probably a single-particle effect. In the case of H^- the second NC brings the curve very close to its correct form, in keeping with the radial nature of the second NC in this system and the dominant role of radial correlation here.

The 3NC curves are very close to the full NA-CI curves in all cases. This closeness is in accord with the high proportion of correlation energy recovered by these 3NC wavefunctions. The great similarity between the 3NC, 4NC, 5NC and full NA-CI curves is paralleled by the near identity of the $\langle r_1^n \rangle$ values for these wavefunctions. In particular, the $n = -1$ energy-related value hardly varies at all for these truncations. This demonstrates that after the first three configurations, additional improvements to the wavefunction do not significantly affect the $D(r_1)$ curve. It would thus be expected that the addition of the fourth and fifth configurations will have some other detectable results, because they contribute a small but not insignificant proportion of the correlation energy.

The two-particle radial holes, $\Delta D(r_1; r_2)$, give direct information concerning radial correlation, and are displayed for the NC and NA-CI wavefunctions in figures II.19-22. When these holes are inspected for the systems other than H^- , the most important feature that is seen is the very small magnitude of the surfaces for the 1NC and 2NC wavefunctions. If they were displayed on the same vertical scale as the fully correlated curves they would be barely discernable. In the case of the 1NC wavefunctions, this shows that the large magnitude of the $\Delta D(r_1)_{1NC}$ caused by the orbital correction function does not cause any radial correlation. This is borne out by the fact that the radial correlation coefficients are equal to zero for the 1NC wavefunctions. The small size of the 2NC surfaces indicates that radial correlation here is very small. Such correlation as there is is actually *positive*, as can be seen by the extremely small, positive, $\tau_r^{(n)}$ values. That is, the effect of the second, angular, configuration is to make it marginally more likely that the two radii have the same magnitudes. The fact that the introduction of an 'angular' configuration produces only a miniscule amount of radial correlation

in the wavefunction substantiates our original classification of such configurations as introducing only angular correlation.

If one examines the 1 and 2NC two-particle radial holes for H^- , it is obvious that the 2NC surface is very similar indeed to the fully correlated surface, reflecting the fact that the second configuration introduces radial correlation. Evidently one radial natural configuration is sufficient to produce most of the radial correlation found in the system. The 1NC surface is small in comparison to the other surfaces for this system, but it is still significant when shown on the same vertical scale. Although the radii are not statistically correlated, the $\tau_r^{(n)}$ values being equal to zero, this shows that the addition of the orbital correction function, $f(r_1)$, to the Hartree-Fock wavefunction has a significant effect on the two-particle radial density in this system.

In all cases the 3NC $\Delta D(r_1; r_2)$ surfaces are very similar to the NA-CI surfaces. In the neutral and positive systems the third configuration has a radial character, and again we see that one radial correlating configuration is sufficient to reproduce almost all of the radial correlation. The third natural configuration is of angular character in the case of H^- , and alters the two-particle radial hole only marginally. The surfaces for the 4NC and 5NC wavefunctions have been generated, but are not displayed, because they are visually indistinguishable from the 3NC and NA-CI surfaces

The radial correlation coefficients, τ , for the 2NC wavefunctions for the neutral and positive systems show, as we noted earlier, that the second configuration has only a very small radial correlation effect. The $\tau_r^{(n)}$ values for these wavefunctions are at least 2 orders of magnitude smaller than the corresponding values for the 3NC wavefunctions, and are positive. For H^- , the 2NC wavefunction, which contains only radial correlation, produces radial coefficients close to the NA-CI coefficients, both of which overcorrelate. For all systems the 3NC radial coefficients are close to the NA-CI values, with the $\tau_r^{(+1)}$ values indicating a slight overcorrelation effect.

Angular Results

It is clear that the $\Delta P(\theta_{12})$ curves and angular expectation values will reflect the way

in which the introduction of correlating configurations changes the manner in which the electrons correlate angularly. The 1NC wavefunctions all have angular parts identical to that of the Hartree-Fock representation. This implies that the corresponding $\Delta P(\theta_{12})$ and $\langle r_1^n r_2^n \cos \theta_{12} \rangle$ will be identically equal to zero. The same is true for the 2NC wavefunction for H^- , because the second configuration in this case is of radial character.

The $\Delta P(\theta_{12})$ curves shown in figures II.23 are, for each system, close together. So the introduction of the first angular configuration produces almost all of the angular correlation effects produced by the full NA-CI wavefunction. Additional angular configurations produce a small but definite change in the curve, but the changes produced by radial configurations are extremely small and not discernable in the diagrams. It should be noted that in each diagram the 5NC curve is a significant distance from the NA-CI curve. This is because the NA-CI wavefunction includes configurations of g and h angular character, whereas the 5NC wavefunction only contains p, d and f configurations. One can infer from this result that it is necessary to include natural configurations with high angular momentum orbitals if one wishes to describe the angular correlation effects with high accuracy.

It can be seen that the $\langle r_1^n r_2^n \cos \theta_{12} \rangle$ values for the expansions with one angular configuration included are close to the values for the full NA-CI wavefunctions. For He, Li^+ and Be^{++} the $\langle \cos \theta_{12} \rangle$, $\langle r_1^{+1} r_2^{+1} \cos \theta_{12} \rangle$ and $\langle \theta_{12} \rangle$ values for the 2NC wavefunctions have a greater magnitude than the NA-CI values. Thus there is angular overcorrelation in the medium and large radial regions. Because there is no significant radial correlation in these 2NC wavefunctions, we interpret this overcorrelation as an attempt by the wavefunctions to compensate for their inability to correlate radially. In H^- , all the $\langle r_1^n r_2^n \cos \theta_{12} \rangle$ and $\langle \theta_{12} \rangle$ values for the 3NC wavefunction exhibit overcorrelation. The angular τ values behave in a similar manner to the $\langle r_1^n r_2^n \cos \theta_{12} \rangle$ values. That is, the first non-zero $\tau_{\theta_{12}}^{(0)}$ and $\tau_{\theta_{12}}^{(+1)}$ as we bring in correlation overcorrelate slightly, and in H^- the $\tau_{\theta_{12}}^{(-1)}$ overcorrelates as well. In all cases, the initial angular correlation produces angular correlation coefficients close to the values for the NA-CI wavefunctions.

Interparticle Results

The combined effects of radial and angular correlation for the NC wavefunctions produce the Coulomb holes shown in figures II.24. If we exclude, for the moment, the H^- results, it is clear that the 1NC curves are very small indeed. This shows that the large relative effect of the orbital correction functions on the $D(r_1)$ curves does not change to a significant degree the manner in which the electrons correlate and indicates that the form of the remaining $\Delta f(r_{12})$ curves is dictated by statistical correlation, rather than by the change in the radial distribution function.

Obviously the 2NC holes for these systems are caused by angular correlation, and it can be seen that they are of essentially the same form as the fully-correlated curves, although their radii are slightly larger. The $\Upsilon_{r_{12}}$ values for these curves are between 68% and 74% of the NA-CI values, demonstrating, once again, that angular correlation is more important than radial correlation in these systems. In all four systems the energy-related $\langle r_{12}^{-1} \rangle$ expectation value decreases monotonically from the 1NC wavefunctions to the NA-CI wavefunctions. With the addition of radial correlation, the 3NC holes are close to the NA-CI holes, as was the case with the $\Delta D(r_1)$ and $\Delta P(\theta_{12})$ functions. But the difference between the 3NC and NA-CI curves is noticeable, which was not the case with the $\Delta D(r_1)$ results. Thus the addition of correlation after the third NC produces significant changes only in the interparticle properties, the single-particle ones remaining effectively constant. The radii of the holes become slightly smaller as we go from the 3NC to the NA-CI wavefunctions, ordering in the same manner as the energy of the wavefunctions.

The 1NC hole for H^- is of a substantial magnitude, its $\Upsilon_{r_{12}}$ value being 45% of the NA-CI value. We conclude from this result that much of the extremely large change in the interparticle distribution caused by introducing electron correlation is not due to statistical correlation, but is a manifestation of the very large orbital correction function for this system, the size of which was made necessary by the grossly inadequate description of the radial density at the Hartree-Fock level. In all four systems the shape of the 1NC Coulomb holes is the same as the corresponding $\Delta D(r_1)_{1NC}$: i.e. positive at

small and large values of r_1 and therefore negative in the intermediate regions. Because small values of r_{12} generally correspond to small values of r_1 , this leads us to conclude that the 1NC holes are merely reflections of the change in the radial part of the Hartree-Fock wavefunction engendered by the addition of the Sinanoğlu f-functions.

For H^- , the 2NC hole contains radial correlation and accounts for the shape and magnitude of the NA-CI hole to a somewhat greater extent than do the 2NC wavefunctions for the other systems. The $\Upsilon_{r_{12}}$ value is 79% of the NA-CI value, and the radius is very close to the NA-CI value. This demonstrates the dominant role of the combined radial correlation and orbital correction function in this system. The 3NC hole is extremely close to the NA-CI curve. Although it is not discernable in figure II.24.a the radii of the holes do not order in the same way as the energies, in contrast to the other systems. The ordering with increasing r_{12} is: 5NC, 4NC, 3NC, NA-CI, 2NC.

Finally, we discuss the $\Delta g(r_{12}; r_1)$ surfaces for the NC wavefunctions, shown in figures II.25-28. The partial Coulomb holes for the 1NC wavefunction are all very small compared to the NA-CI surfaces, for the neutral and positive systems. This ties in neatly with the small magnitude of the $\Delta D(r_1; r_2)$ surfaces and the $\Delta f(r_{12})$ curves for the 1NC wavefunctions. The surface for H^- is small, but does have discernable features even if it was to be plotted on the same vertical scale as the other H^- surfaces. We can see in figure II.25.a the beginnings of the positive features along the diagonal and parallel to the r_{12} axis that were interpreted as an effect of radial correlation in figure II.11.a in section 5.2. The fact that these features in the 1NC surface are so small shows that our interpretation was correct, although a small proportion of the fully-correlated features could be ascribed to the effect of the orbital correction function. The positive feature at low r_1 and low r_{12} is caused by the inward movement of density due to the influence of the f-function.

The 2NC surface in H^- is only slightly smaller than the fully correlated function, and has the same shape. This is further confirmation that the 'parallel-diagonal' feature in the H^- partial holes is due to radial correlation. It is now possible to conclude that in H^- the qualitative properties and most of the quantitative properties of the partial

Coulomb hole are determined by the dominant mode of correlation in this system—radial correlation.

He, Li^+ and Be^{++} have, as we discussed in section 5.2, radically different shaped $\Delta g(r_{12}; r_1)$ surfaces compared to that for H^- . It is evident that the 2NC surfaces again reproduce the main features of the fully correlated surfaces, although again with a slightly smaller magnitude. The only qualitative difference between the 2NC surfaces and the NA-CI surfaces is the absence of the fixed- r_{12} radial correlation feature that was discussed in section 5.2. This is because the 2NC wavefunctions contain no significant radial correlation. As with H^- , it is clear that the most important form of correlation, (angular in these systems), determines the general shape of the partial holes and accounts for most of their magnitude. The 3NC surfaces are very close to the full NA-CI surfaces, in keeping with our expectations from the other results. The 4NC and 5NC surfaces were also very similar to the full NA-CI results, and so have not been displayed.

The results for the τ coefficients show that the inclusion of one angular configuration achieves the vast majority of the statistical angular correlation effects and, similarly, that the inclusion of one radial configuration produces a very good representation of the statistical radial correlation effects. This is of some interest, as it might well have been necessary to include more than one configuration of a given correlation type to achieve an adequate representation of the statistical correlation effects. These statistical results correspond to our earlier findings that a wavefunction containing one radial configuration will reproduce the $\Delta D(r_1; r_2)$ surfaces well, and that the inclusion of one angular configuration will reproduce the $\Delta P(\theta_{12})$ curves well. In the case of the Coulomb holes and partial Coulomb holes, both types of correlation are necessary for a faithful representation of the correlation effects in the neutral and positive systems, but in H^- the inclusion of radial correlation alone suffices to produce good approximations to the NA-CI results.

Although we have stressed the overwhelmingly dominant role of radial correlation in the H^- system throughout this chapter, it is important to recognize that angular correlation is essential in this case for the $2p^2\ ^3P$ state to be bound. As we remarked

earlier, the Hartree-Fock wavefunction for H^- is not bound. This is because its energy is less negative than -0.125 —the energy of a single electron in a 2p orbital. Inspection of table II.1 reveals that the 2NC wavefunction, which in this system contains only radial correlation, is not bound either. So it is necessary to include angular correlation to achieve binding, as one can see by the fact that the 3NC wavefunction *is* bound. Jáuregui and C.F.Bunge [86] obtained the same result with their natural expansion for the same system. In an earlier report, C.F.Bunge and A.V.Bunge [156] found that when the radial limit is approached the energy converges to -0.125 as one electron moves out to infinity. Drake [157] has also found this to occur. It is interesting that the critical nature of the third, angular, configuration does not appear to have much impact upon the correlation difference functions we have examined.

5.6 Summary

We have examined electron correlation effects in the $2p^2\ ^3P$ state of H^- , He, Li^+ and Be^{++} by calculating a wide variety of functions and expectation values from a range of correlated and uncorrelated wavefunctions. The principal finding is that the radial and angular correlation effects are both of a negative kind, and combine to form a total negative correlation effect. Correlation effects were seen to become less important as increasing values of the atomic number, Z , were considered, with angular effects becoming more important *relative* to the total effects. Appropriate scaling of axes enabled us to view the positive and neutral systems as members of a single ‘family’. This was not possible for H^- , owing to the extremely large effects of correlation attributable to the very low binding energy [158].

Employing a number of different kinds of correlated wavefunctions was found to be highly fruitful in coming to an understanding of the correlation effects and in evaluating the strengths and weaknesses of the CI and explicitly-correlated approaches. The NA-CI wavefunctions were extremely effective in reproducing various properties accurately, despite being energetically inferior to both of the Hylleraas-type Drake wavefunctions. It would be intriguing to examine the performance of these two kinds of wavefunctions

when assessed on how accurately they reproduce the higher-order coalescence condition of Thakkar [135]. The truncated natural expansions which we generated were especially useful. The highly-ordered manner in which natural configurations introduced the components of the correlation energy made it possible to affirm that the addition of one radial configuration and one angular configuration to the first configuration, (which was energetically similar to the Hartree-Fock wavefunction) produced the overwhelming majority of the overall correlation effects. That is, a 3NC wavefunction is a good approximation to the exact non-relativistic wavefunction. An examination of the f-orbital corrections of Sinanoğlu made comprehensible certain differences between the Hartree-Fock wavefunctions and the first natural configuration.

In particular, the extremely large size of the orbital correction in the H^- system was useful in understanding the very great differences between the Hartree-Fock and correlated descriptions in terms of very large statistical correlation effects, together with a qualitative change in the radial distribution. In this system the radial correlation effects are overwhelmingly dominant, although not in themselves sufficient to bind the state. In the other three systems angular correlation is more important than radial correlation.

Where possible, we have compared our results with the analogous ground state results. We found that the correlation effects presented here were qualitatively identical to the ground state results, although of a somewhat greater magnitude. We attribute this to the doubly-occupied nature of the radial parts of the orbitals in both systems. These results are of interest in view of the contemporary interest in doubly excited states mentioned in chapter 2. Most of this interest has focused on the *differences* between the ground state and doubly excited states, and most workers in this area have used rather different approaches to those employed in this thesis. We shall reserve further comment on these matters until after the examination in Part III of how the ground state and the $2p^2\ ^3P$ state compare in their momentum space correlation properties.

Chapter 6

Position Space Results: Tables and Figures

6.1 Introduction

In order to make the figures and tables presented in this chapter easier to understand we make some comments here regarding the layout and nomenclature. The tables and the figures essentially follow the order in which they are discussed in the text, although naturally it is frequently necessary to refer to an item more than once in the discussion.

Where a variety of different wavefunctions are used to calculate different properties, the wavefunctions are listed vertically in the table, whilst the properties run horizontally. The wavefunctions for each system are collected together in blocks, with the proportion of correlation energy recovered by the wavefunctions increasing as one moves down each block. The only exceptions to this are the 1NC wavefunctions, which have slightly inferior energies to the Hartree-Fock wavefunctions below which they appear.

We briefly reiterate the nomenclature used for the wavefunctions. Where the Froese Fischer numerical Hartree-Fock wavefunction is used it is denoted by 'HF-NUM'. The term 'HF-STO' represents the Hartree-Fock wavefunction with radials fitted by a linear combination of Slater-type orbitals, (see appendix A). This terminology is only employed in the tables—in the figures the Hartree-Fock wavefunctions used are *always* the

HF-STO ones. When the Nicolaides and Asproumallis configuration interaction wavefunction is used it is referred to as : 'NA-CI'. The NA-CI wavefunction when expressed in the natural expansion form may be truncated to a certain number of natural configurations and renormalized. Such a wavefunction containing, say, 3 natural configurations is referred to as a '3NC' wavefunction. For each system two explicitly-correlated wavefunctions generated by Drake were used. A 'Drake-70' wavefunction contains 70 terms, for example. The 'best' Drake wavefunction is the energetically best Drake wavefunction for that system, whilst the 'short' Drake is the one employing the least number of terms.

In some figures curves are displayed which are too close together to be conveniently labelled separately. Usually bracketed labels are used to denote these instances, where the ordering of the labels within each bracket corresponds to the physical ordering of the curves. Examples of this terminology can be seen in figure II.3.c and II.3.d.

Although the 1NC wavefunctions include no correlation whatsoever, either statistical or in the energetic sense of Löwdin [6], it has been found convenient to call them 'correlated descriptions' in captions where a series of natural truncations are referred to.

6.2 Position Space Results: Tables

Wavefunction	Energy	Corr. %
H ⁻ HF-NUM	-0.11588	0.000
1NC	-0.11502	-9.121
2NC	-0.12229	67.65
3NC	-0.12508	97.11
4NC	-0.12513	97.59
5NC	-0.12513	97.62
NA-CI	-0.12516	97.98
Drake-20	-0.12533	99.72
Drake-84	-0.12535	99.99
'Exact' (a)	-0.12535	100.00
He HF-NUM	-0.70141	0.000
1NC	-0.70140	-0.130
2NC	-0.70694	60.78
3NC	-0.70991	93.53
4NC	-0.71017	96.38
5NC	-0.71033	98.15
NA-CI	-0.71049	99.85
Drake-13	-0.71049	99.93
Drake-70	-0.71050	100.00
'Exact' (b)	-0.71050	100.00
Li ⁺ HF-NUM	-1.7873	0.000
1NC	-1.7873	-0.032
2NC	-1.7931	62.48
3NC	-1.7958	91.36
4NC	-1.7962	95.20
5NC	-1.7964	97.46
NA-CI	-1.7966	99.77
Drake-13	-1.7966	99.92
Drake-70	-1.7966	100.00
'Exact' (c)	-1.7966	100.00
Be ⁺⁺ HF-NUM	-3.3732	0.000
1NC	-3.3732	-0.013
2NC	-3.3792	62.93
3NC	-3.3818	90.23
4NC	-3.3822	94.53
5NC	-3.3824	97.09
NA-CI	-3.3827	99.73
Drake-13	-3.3827	99.93
Drake-70	-3.3827	100.00
'Exact' (d)	-3.3827	100.00

Table II.1

The wavefunctions used in this thesis, together with their energies and the percentage of the correlation energy recovered. In each case the 'exact' energy is a theoretical value; for further details see chapter 2.

(a) Taken from Jáuregui and Bunge [86]. (b) Taken from Bhatia [106].
(c) Taken from Drake [110]. (d) Taken from Drake [110].

n	l	p	d	f	g	h
2		x				
3		x	x			
4		x	x	x		
5		x	x	x	x	
6		x	x	x	x	x
7		x	x	x		

Table II.2

The 18-member basis set for the Nicolaidis and Aspromallis Configuration Interaction wavefunction. The presence of an 'x' denotes the existence of basis orbitals with the corresponding 'n' and 'l' values.

Wavefunction	T_{r_1} %	$T_{\theta_{12}}$ %	$T_{r_{12}}$ %	
H^-	1NC	7.40	0.00	9.62
	2NC	10.7	0.00	16.8
	3NC	10.3	10.3	21.3
	4NC	10.3	10.2	21.2
	5NC	10.3	10.2	21.2
	NA-CI	10.3	10.1	21.2
	Drake-20	14.2	9.18	26.5
	Drake-84	15.3	8.84	27.9
He	1NC	0.250	0.00	0.200
	2NC	0.153	6.89	3.87
	3NC	0.370	6.85	5.72
	4NC	0.368	6.80	5.83
	5NC	0.370	6.76	5.75
	NA-CI	0.372	6.64	5.65
	Drake-13	0.404	6.66	5.67
	Drake-70	0.378	6.65	5.64
Li^+	1NC	0.0790	0.00	0.057
	2NC	0.0370	4.61	2.61
	3NC	0.114	4.59	3.65
	4NC	0.112	4.59	3.75
	5NC	0.114	4.58	3.70
	NA-CI	0.115	4.48	3.65
	Drake-13	0.130	4.49	3.64
	Drake-70	0.114	4.49	3.63
Be^{++}	1NC	0.0371	0.00	0.025
	2NC	0.0142	3.45	1.97
	3NC	0.0534	3.45	2.68
	4NC	0.0528	3.45	2.78
	5NC	0.0537	3.45	2.74
	NA-CI	0.0540	3.37	2.68
	Drake-13	0.0691	3.37	2.70
	Drake-70	0.0530	3.38	2.69

Table II.3

The T_{r_1} , $T_{\theta_{12}}$ and $T_{r_{12}}$ values for the various correlated wavefunctions. They are respectively the percentages of the Hartree-Fock $D(r_1)$, $P(\theta_{12})$ and $f(r_{12})$ curves redistributed by the effects of correlation (see the comments in 6.1 regarding the 1NC results).

Wavefunction	$\langle r_1^{-2} \rangle$	$\langle r_1^{-1} \rangle$	$\langle r_1^{+1} \rangle$	$\langle r_1^{+2} \rangle$	σ_{r_1}	
H ⁻	HF-NUM	0.041392	0.16731	8.3220	92.437	4.8147
	HF-STO	0.041388	0.16729	8.3243	92.530	4.8203
	1NC	0.042578	0.16533	9.2241	124.17	6.2522
	2NC	0.043661	0.16530	9.5425	134.73	6.6086
	3NC	0.043244	0.16474	9.5267	133.86	6.5650
	4NC	0.043242	0.16473	9.5265	133.85	6.5647
	5NC	0.043241	0.16473	9.5267	133.86	6.5650
	NA-CI	0.043243	0.16474	9.5266	133.85	6.5649
	Drake-20	0.043008	0.16154	10.804	199.22	9.0830
	Drake-84	0.042999	0.16067	11.481	251.16	10.925
He	HF-NUM	0.24082	0.41790	3.0814	11.691	1.4817
	HF-STO	0.24082	0.41790	3.0814	11.691	1.4817
	1NC	0.24185	0.41849	3.0834	11.731	1.4913
	2NC	0.24112	0.41796	3.0854	11.740	1.4900
	3NC	0.24171	0.41811	3.0898	11.790	1.4977
	4NC	0.24170	0.41809	3.0898	11.790	1.4977
	5NC	0.24170	0.41810	3.0898	11.790	1.4977
	NA-CI	0.24171	0.41810	3.0898	11.790	1.4978
	Drake-13	0.24170	0.41810	3.0895	11.782	1.4958
	Drake-70	0.24172	0.41810	3.0899	11.791	1.4979
Li ⁺	HF-NUM	0.60697	0.66795	1.9043	4.4165	0.88892
	HF-STO	0.60697	0.66795	1.9043	4.4166	0.88893
	1NC	0.60797	0.66834	1.9042	4.4188	0.89035
	2NC	0.60716	0.66797	1.9048	4.4206	0.89007
	3NC	0.60769	0.66806	1.9057	4.4269	0.89169
	4NC	0.60766	0.66804	1.9057	4.4269	0.89167
	5NC	0.60766	0.66804	1.9058	4.4270	0.89169
	NA-CI	0.60768	0.66805	1.9058	4.4271	0.89171
	Drake-13	0.60765	0.66805	1.9057	4.4258	0.89118
	Drake-70	0.60768	0.66805	1.9058	4.4271	0.89174
Be ⁺⁺	HF-NUM	1.1398	0.91796	1.3786	2.3045	0.63560
	HF-STO	1.1398	0.91796	1.3786	2.3045	0.63559
	1NC	1.1408	0.91826	1.3785	2.3047	0.63596
	2NC	1.1399	0.91797	1.3787	2.3053	0.63586
	3NC	1.1404	0.91803	1.3791	2.3069	0.63645
	4NC	1.1404	0.91802	1.3791	2.3069	0.63644
	5NC	1.1404	0.91802	1.3791	2.3069	0.63646
	NA-CI	1.1404	0.91802	1.3791	2.3069	0.63646
	Drake-13	1.1403	0.91802	1.3790	2.3066	0.63627
	Drake-70	1.1403	0.91802	1.3791	2.3071	0.63654

Table II.4

The radial one-particle expectation values, $\langle r_1^n \rangle$, when $n = -2, -1 +1$ and $+2$; and the standard deviations, σ_{r_1} .

Wavefunction	$\langle r_1^{-2} r_2^{-2} \rangle$	$\langle r_1^{-1} r_2^{-1} \rangle$	$\langle r_1^{+1} r_2^{+1} \rangle$	$\langle r_1^{+2} r_2^{+2} \rangle$	
H ⁻	HF-NUM	0.0017133	0.027991	69.256	8544.5
	HF-STO	0.0017129	0.027987	69.294	8561.8
	1NC	0.0018129	0.027333	85.083	15419.0
	2NC	0.00091326	0.022195	72.855	7947.0
	3NC	0.00090562	0.022128	72.937	7956.7
	4NC	0.00090558	0.022128	72.936	7956.3
	5NC	0.00090583	0.022122	72.860	7918.9
	NA-CI	0.00090236	0.022128	72.871	7917.6
	Drake-20	0.00078624	0.020255	85.210	11596
	Drake-84	0.00076624	0.019757	91.951	14727
He	HF-NUM	0.057994	0.17464	9.4952	136.67
	HF-STO	0.057994	0.17464	9.4952	136.67
	1NC	0.058493	0.17513	9.5072	137.62
	2NC	0.058211	0.17473	9.5201	137.82
	3NC	0.050999	0.16889	9.2416	122.95
	4NC	0.050993	0.16888	9.2419	122.96
	5NC	0.051019	0.16892	9.2444	123.09
	NA-CI	0.050564	0.16883	9.2471	123.11
	Drake-13	0.050515	0.16882	9.2444	122.83
	Drake-70	0.050595	0.16883	9.2471	123.08
Li ⁺	HF-NUM	0.36841	0.44615	3.6264	19.506
	HF-STO	0.36841	0.44615	3.6264	19.506
	1NC	0.36963	0.44669	3.6261	19.526
	2NC	0.36885	0.44623	3.6285	19.543
	3NC	0.34206	0.43775	3.5670	18.317
	4NC	0.34204	0.43774	3.5671	18.318
	5NC	0.34212	0.43778	3.5676	18.328
	NA-CI	0.33996	0.43759	3.5680	18.323
	Drake-13	0.33971	0.43758	3.5676	18.303
	Drake-70	0.34002	0.43760	3.5680	18.323
Be ⁺⁺	HF-NUM	1.2991	0.84264	1.9006	5.3109
	HF-STO	1.2991	0.84264	1.9006	5.3109
	1NC	1.3014	0.84321	1.9002	5.3114
	2NC	1.2998	0.84271	1.9010	5.3144
	3NC	1.2330	0.83152	1.8782	5.0791
	4NC	1.2330	0.83150	1.8783	5.0792
	5NC	1.2331	0.83154	1.8784	5.0809
	NA-CI	1.2272	0.83125	1.8785	5.0792
	Drake-13	1.2272	0.83126	1.8785	5.0789
	Drake-70	1.2273	0.83125	1.8786	5.0800

Table II.5

The two-particle radial expectation values, $\langle r_1^n r_2^n \rangle$, when $n = -2, -1, +1$ and $+2$.

Wavefunction	$\tau_r^{(-1)}$	$\tau_r^{(+1)}$	$\tau_{\theta_{12}}^{(-1)}$	$\tau_{\theta_{12}}^{(0)}$	$\tau_{\theta_{12}}^{(+1)}$	
H^-	HF-NUM	0.0	0.0	0.0	0.0	0.0
	HF-STO	0.0	0.0	0.0	0.0	0.0
	1NC	0.0	0.0	0.0	0.0	0.0
	2NC	-0.3140	-0.4168	0.0	0.0	0.0
	3NC	-0.3111	-0.4135	-0.05257	-0.1100	-0.06025
	4NC	-0.3111	-0.4134	-0.05185	-0.1085	-0.05948
	5NC	-0.3114	-0.4153	-0.05186	-0.1085	-0.05950
	NA-CI	-0.3111	-0.4150	-0.05222	-0.1081	-0.05960
	Drake-20	-0.3453	-0.3820	-0.04599	-0.09797	-0.03871
	Drake-84	-0.3524	-0.3340	-0.04460	-0.09434	-0.02940
He	HF-NUM	0.0	0.0	0.0	0.0	0.0
	HF-STO	0.0	0.0	0.0	0.0	0.0
	1NC	0.0	0.0	0.0	0.0	0.0
	2NC	+0.000575	+0.00024	-0.04225	-0.07343	-0.06586
	3NC	-0.08851	-0.1360	-0.04171	-0.07295	-0.06397
	4NC	-0.08849	-0.1360	-0.04121	-0.07191	-0.06299
	5NC	-0.08800	-0.1349	-0.04257	-0.07147	-0.06303
	NA-CI	-0.08936	-0.1337	-0.04264	-0.07140	-0.06292
	Drake-13	-0.08944	-0.1343	-0.04274	-0.07145	-0.06318
	Drake-70	-0.08928	-0.1338	-0.04261	-0.07140	-0.06302
Li^+	HF-NUM	0.0	0.0	0.0	0.0	0.0
	HF-STO	0.0	0.0	0.0	0.0	0.0
	1NC	0.0	0.0	0.0	0.0	0.0
	2NC	+0.000274	+0.000149	-0.02864	-0.04913	-0.04519
	3NC	-0.05295	-0.08149	-0.02849	-0.04900	-0.04451
	4NC	-0.05294	-0.08148	-0.02824	-0.04847	-0.04399
	5NC	-0.05269	-0.08091	-0.02938	-0.04833	-0.04416
	NA-CI	-0.05390	-0.08041	-0.02945	-0.04829	-0.04410
	Drake-13	-0.05396	-0.08060	-0.02951	-0.04831	-0.04427
	Drake-70	-0.05387	-0.08037	-0.02944	-0.04829	-0.04417
Be^{++}	HF-NUM	0.0	0.0	0.0	0.0	0.0
	HF-STO	0.0	0.0	0.0	0.0	0.0
	1NC	0.0	0.0	0.0	0.0	0.0
	2NC	+0.000159	+0.000095	-0.02158	-0.03682	-0.03422
	3NC	-0.03783	-0.05817	-0.02151	-0.03676	-0.03388
	4NC	-0.03782	-0.05816	-0.02136	-0.03644	-0.03356
	5NC	-0.03768	-0.05781	-0.02229	-0.03640	-0.03375
	NA-CI	-0.03868	-0.05755	-0.02236	-0.03638	-0.03371
	Drake-13	-0.03865	-0.05745	-0.02242	-0.03638	-0.03377
	Drake-70	-0.03869	-0.05751	-0.02236	-0.03636	-0.03372

Table II.6

The radial and angular correlation coefficients τ for various wavefunctions. See equations 4.56-57 for their definitions. Note that the Hartree-Fock and 1NC values are each identically equal to zero.

Wavefunction	$\langle r_1^{-1} r_2^{-1} \cos\theta_{12} \rangle$	$\langle \cos\theta_{12} \rangle$	$\langle r_1^{+1} r_2^{+1} \cos\theta_{12} \rangle$	$\langle \theta_{12} \rangle$	
H ⁻	HF-NUM	0.0	0.0	0.0	90.000
	HF-STO	0.0	0.0	0.0	90.000
	1NC	0.0	0.0	0.0	90.000
	2NC	0.0	0.0	0.0	90.000
	3NC	-0.0022734	-0.10999	-8.0643	96.960
	4NC	-0.0022423	-0.10846	-7.9614	96.857
	5NC	-0.0022423	-0.10849	-7.9640	96.859
	NA-CI	-0.0022580	-0.10806	-7.9775	96.838
	Drake-20	-0.0019780	-0.097966	-7.7127	96.200
Drake-84	-0.0019176	-0.094344	-7.3833	95.971	
He	HF-NUM	0.0	0.0	0.0	90.000
	HF-STO	0.0	0.0	0.0	90.000
	1NC	0.0	0.0	0.0	90.000
	2NC	-0.010187	-0.073427	-0.77311	94.647
	3NC	-0.010081	-0.072953	-0.75421	94.617
	4NC	-0.009959	-0.071911	-0.74264	94.546
	5NC	-0.010290	-0.071475	-0.74317	94.518
	NA-CI	-0.010306	-0.071404	-0.74186	94.526
	Drake-13	-0.010331	-0.071449	-0.74438	94.528
Drake-70	-0.010299	-0.071404	-0.74310	94.526	
Li ⁺	HF-NUM	0.0	0.0	0.0	90.000
	HF-STO	0.0	0.0	0.0	90.000
	1NC	0.0	0.0	0.0	90.000
	2NC	-0.017392	-0.049130	-0.19975	93.109
	3NC	-0.017314	-0.048999	-0.19706	93.101
	4NC	-0.017159	-0.048468	-0.19551	93.065
	5NC	-0.017852	-0.048329	-0.19551	93.056
	NA-CI	-0.017897	-0.048292	-0.19524	93.063
	Drake-13	-0.017932	-0.048310	-0.19594	93.065
Drake-70	-0.017890	-0.048287	-0.19554	93.064	
Be ⁺⁺	HF-NUM	0.0	0.0	0.0	90.000
	HF-STO	0.0	0.0	0.0	90.000
	1NC	0.0	0.0	0.0	90.000
	2NC	-0.024594	-0.036818	-0.078886	92.330
	3NC	-0.024528	-0.036759	-0.078150	92.326
	4NC	-0.024356	-0.036444	-0.077411	92.305
	5NC	-0.025421	-0.036395	-0.077852	92.302
	NA-CI	-0.025505	-0.036376	-0.077769	92.308
	Drake-13	-0.025560	-0.036378	-0.077893	92.310
Drake-70	-0.025494	-0.036363	-0.077804	92.308	

Table II.7

Values of $\langle r_1^n r_2^n \cos\theta_{12} \rangle$ when $n = -1, 0$ and $+1$ and values of $\langle \theta_{12} \rangle$. Note that the $\langle r_1^n r_2^n \cos\theta_{12} \rangle$ are each identically equal to zero for the Hartree-Fock and 1NC wavefunctions.

Wavefunction		$\langle r_{12}^{-2} \rangle$	$\langle r_{12}^{-1} \rangle$	$\langle r_{12}^{+1} \rangle$	$\langle r_{12}^{+2} \rangle$	$\sigma_{r_{12}}$
H^-	HF-NUM	0.013956	0.10284	12.277	184.87	5.8443
	HF-STO	0.013953	0.10283	12.281	185.06	5.8517
	1NC	0.013254	0.097324	13.857	248.35	7.5062
	2NC	0.0090840	0.083485	14.946	269.47	6.7874
	3NC	0.0078169	0.078618	15.481	283.84	6.6470
	4NC	0.0077752	0.078539	15.477	283.62	6.6402
	5NC	0.0077768	0.078532	15.479	283.64	6.6370
	NA-CI	0.0077220	0.078471	15.478	283.67	6.6403
	Drake-20	0.0068550	0.072425	17.922	413.87	9.6271
	Drake-84	0.0066372	0.070630	19.237	517.09	12.125
He	HF-NUM	0.090997	0.26879	4.4747	23.381	1.8324
	HF-STO	0.090997	0.26879	4.4748	23.382	1.8325
	1NC	0.091154	0.26885	4.4796	23.462	1.8427
	2NC	0.083989	0.25839	4.6396	25.025	1.8706
	3NC	0.078806	0.25250	4.6757	25.088	1.7961
	4NC	0.078283	0.25201	4.6761	25.065	1.7886
	5NC	0.077842	0.25170	4.6762	25.067	1.7888
	NA-CI	0.077324	0.25141	4.6763	25.065	1.7881
	Drake-13	0.077283	0.25140	4.6757	25.053	1.7862
	Drake-70	0.077270	0.25139	4.6764	25.068	1.7888
Li^+	HF-NUM	0.23462	0.43313	2.7587	8.8331	1.1058
	HF-STO	0.23462	0.43313	2.7587	8.8331	1.1058
	1NC	0.23482	0.43325	2.7589	8.8376	1.1072
	2NC	0.22242	0.42193	2.8257	9.2408	1.1208
	3NC	0.21471	0.41656	2.8375	9.2479	1.0939
	4NC	0.21358	0.41587	2.8381	9.2433	1.0901
	5NC	0.21267	0.41545	2.8384	9.2451	1.0902
	NA-CI	0.21154	0.41502	2.8386	9.2447	1.0896
	Drake-13	0.21144	0.41501	2.8385	9.2434	1.0893
	Drake-70	0.21141	0.41500	2.8386	9.2453	1.0899
Be^{++}	HF-NUM	0.44489	0.59731	1.9951	4.6091	0.79275
	HF-STO	0.44489	0.59731	1.9952	4.6091	0.79274
	1NC	0.44512	0.59742	1.9951	4.6093	0.79309
	2NC	0.42748	0.58572	2.0314	4.7683	0.80099
	3NC	0.41719	0.58054	2.0372	4.7701	0.78725
	4NC	0.41542	0.57974	2.0377	4.7686	0.78507
	5NC	0.41402	0.57926	2.0379	4.7696	0.78509
	NA-CI	0.41225	0.57876	2.0381	4.7694	0.78472
	Drake-13	0.41208	0.57874	2.0380	4.7690	0.78460
	Drake-70	0.41202	0.57872	2.0381	4.7698	0.78485

Table II.8

Values of $\langle r_{12}^n \rangle$ when $n = -2, -1, +1$ and $+2$; and the standard deviations

$\sigma_{r_{12}}$.

	H ⁻	He	Li ⁺	Be ⁺⁺
Corr. Energy	-0.0094707	-0.0090897	-0.0093792	-0.0095398

Table II.9

The correlation energy for each system, using the 'exact' values in Table II.1 for the correlated values of the energy.

i	H ⁻	He	Li ⁺	Be ⁺⁺
1	0.94334 (p)	0.99353 (p)	0.99737 (p)	0.99857 (p)
2	-0.29920 (p)	-0.08579 (d)	-0.05732 (d)	-0.04293 (d)
3	-0.14272 (d)	-0.07226 (p)	-0.04239 (p)	-0.03004 (p)
4	-0.01151 (f)	-0.01267 (f)	-0.00968 (f)	-0.00769 (f)
5	0.00544 (p)	-0.00931 (d)	-0.00695 (d)	-0.00547 (d)
6	-0.00538 (d)	-0.00549 (p)	-0.00391 (p)	-0.00297 (p)
7	0.00318 (d)	-0.00384 (g)	-0.00303 (g)	-0.00245 (g)
8	-0.00317 (g)	-0.00282 (f)	-0.00224 (f)	-0.00180 (f)
9	-0.00293 (p)	-0.00180 (d)	-0.00134 (d)	-0.00108 (d)
10	-0.00189 (f)	-0.00148 (h)	-0.00119 (h)	-0.00096 (h)
11	-0.00123 (h)	-0.00107 (g)	-0.00086 (g)	-0.00070 (g)
12	-0.00081 (g)	-0.00088 (p)	-0.00072 (p)	-0.00056 (p)
13	-0.00045 (f)	-0.00081 (f)	-0.00067 (f)	-0.00053 (f)
14	-0.00042 (d)	-0.00046 (d)	-0.00030 (d)	-0.00023 (d)
15	-0.00017 (p)	-0.00028 (f)	-0.00023 (f)	-0.00017 (f)
16	-0.00010 (f)	-0.00025 (p)	-0.00019 (p)	-0.00015 (p)
17	-0.00006 (d)	-0.00018 (d)	-0.00007 (p)	-0.00004 (p)
18	-0.00005 (p)	-0.00005 (p)	-0.00004 (d)	-0.00003 (d)

Table II.10

The natural configuration coefficients, C_i^{NC} , and the symmetry of the angular functions in each natural configuration, (see equation 3.19).

	H ⁻	He	Li ⁺	Be ⁺⁺
Norm of Orb. Correc.	0.13535	0.0038016	0.0010762	0.00046391

Table II.11

The norms, $||f(\underline{r}_1)||$, of the orbital correction functions $f(\underline{r}_1)$ calculated from the NA-CI wavefunctions.

6.3 Position Space Results: Figures

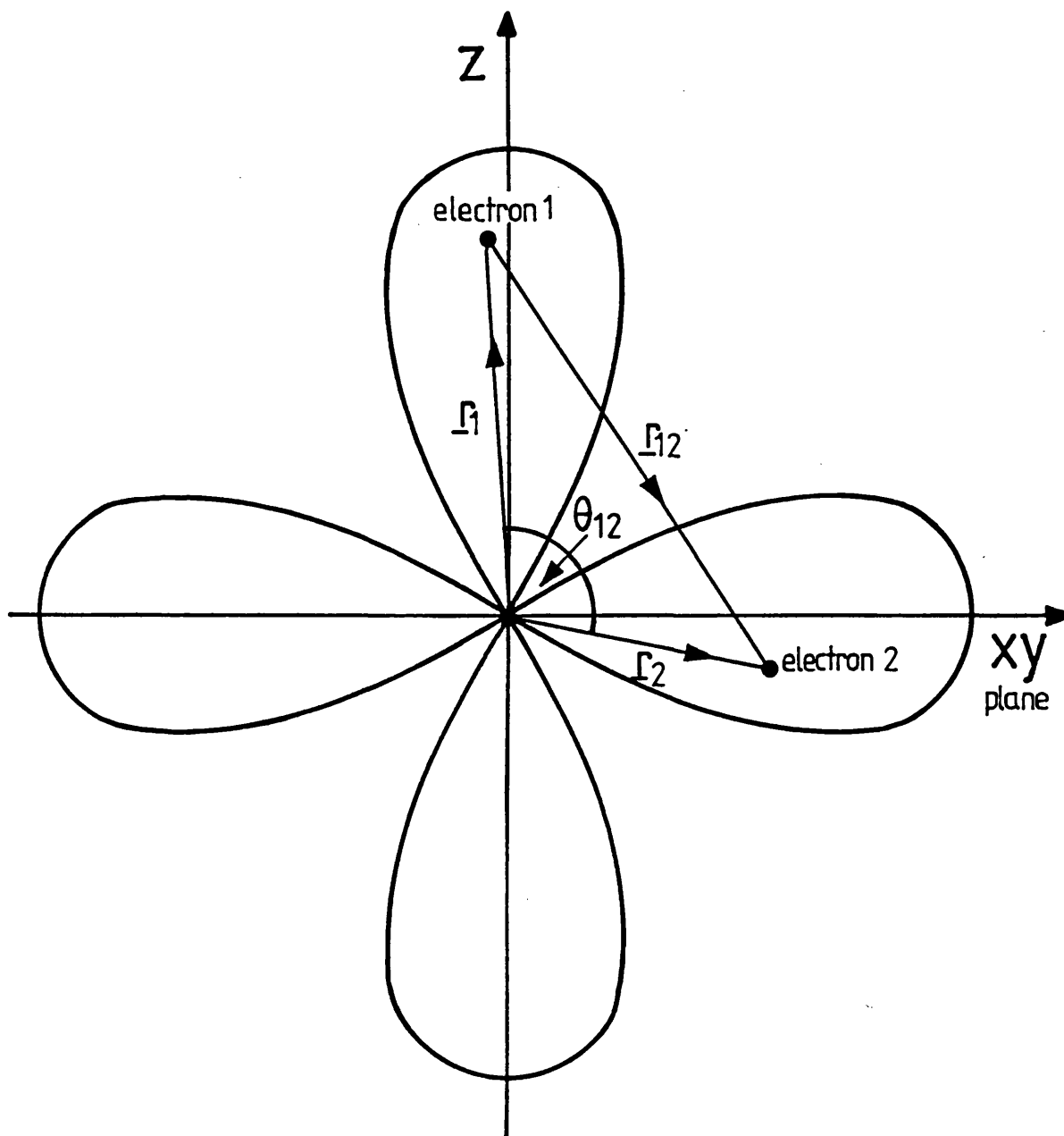


Figure II.1

A schematic orbital representation of the $2p^2 \ ^3P$ state in position space. The two electrons in typical locations are also shown.

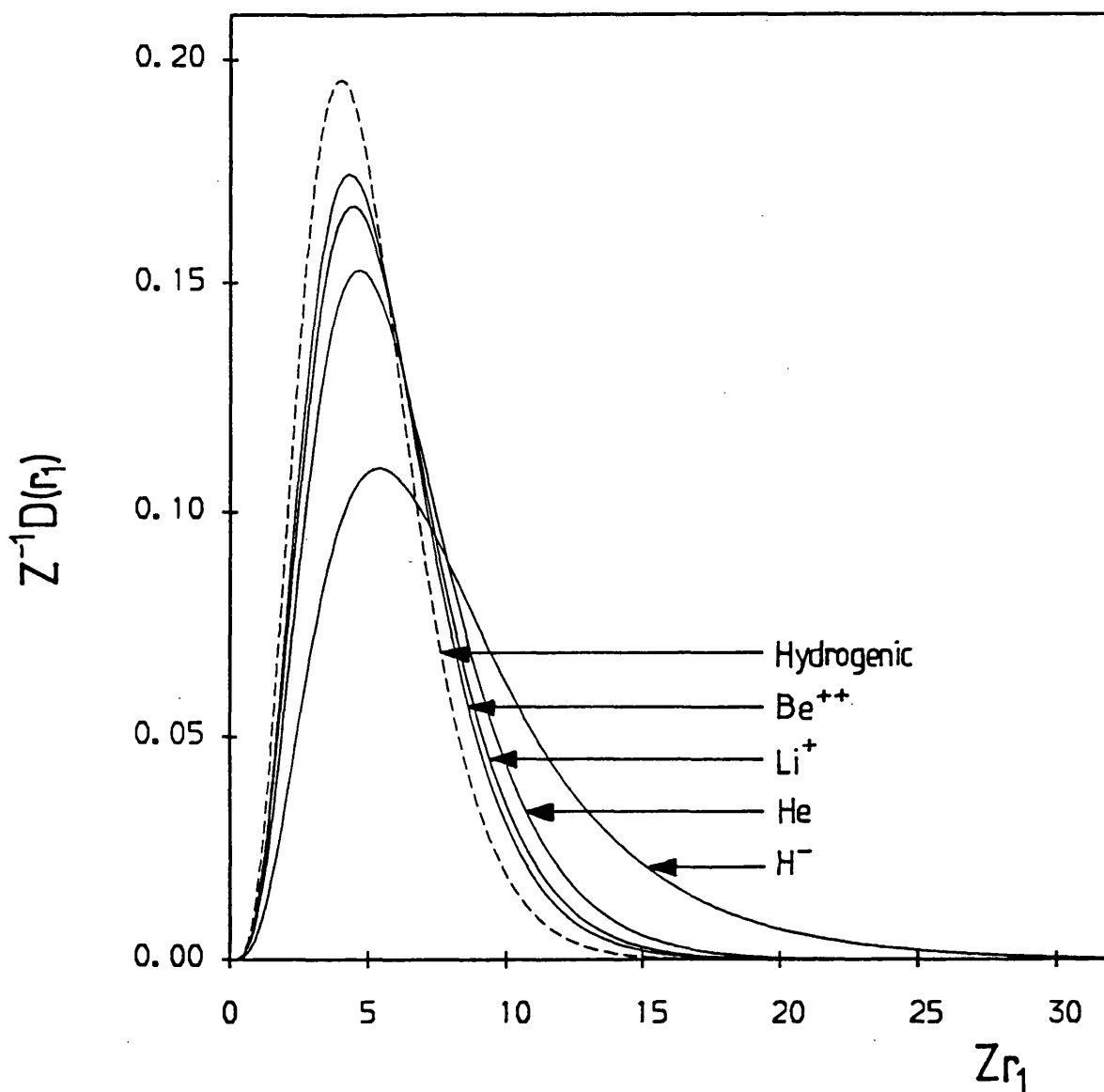


Figure II.2

The $D(r_1)$ distributions for H^- , He, Li^+ and Be^{++} produced using the Hartree-Fock wavefunctions. Also shown as a dashed line is the $D(r_1)$ generated from an independent-particle $2p^2 \ ^3P$ wavefunction comprising unoptimized hydrogenic orbitals. Both axes are scaled.

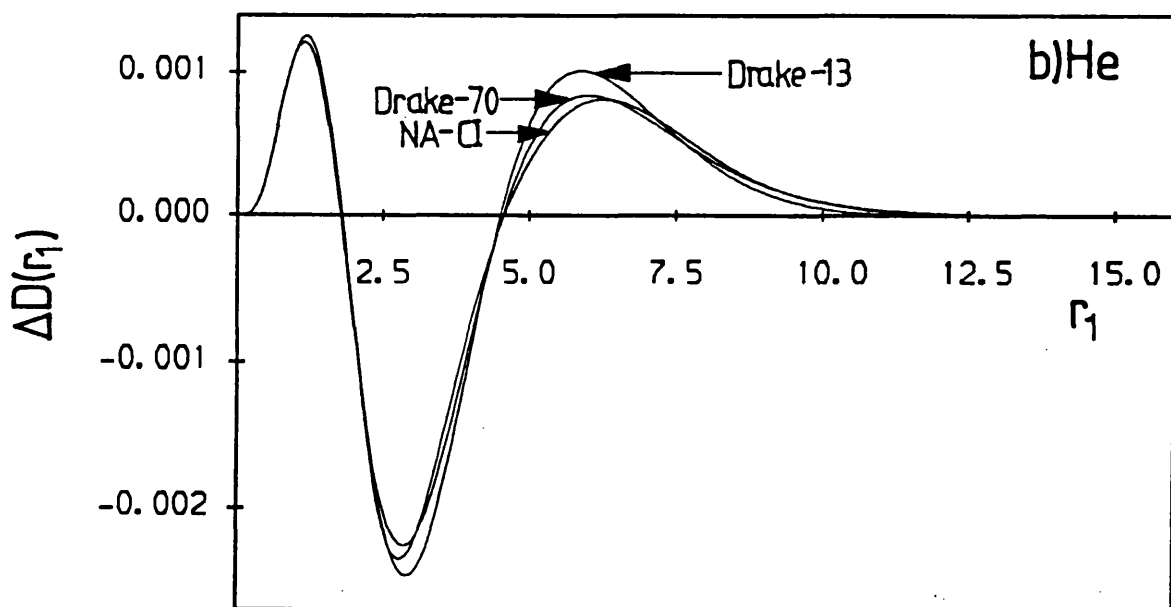
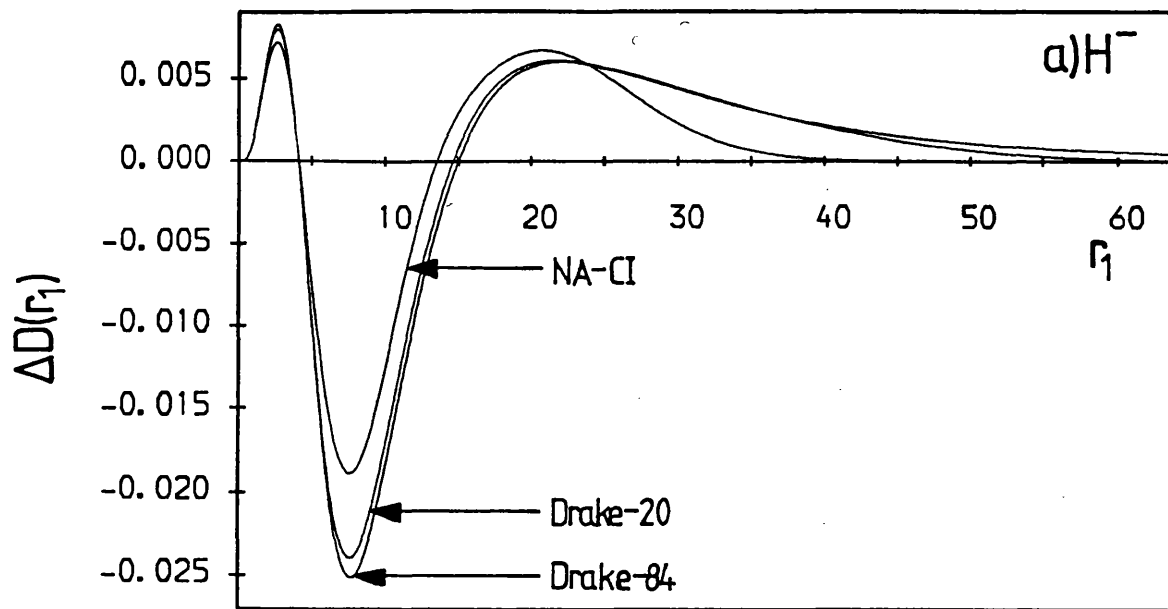


Figure II.3 a) & b)

The one-particle radial holes $\Delta D(r_1)$ for a) H^- and b) He. In each case the 'best' Drake, 'shortest' Drake and NA-CI wavefunctions are used as the correlated descriptions.

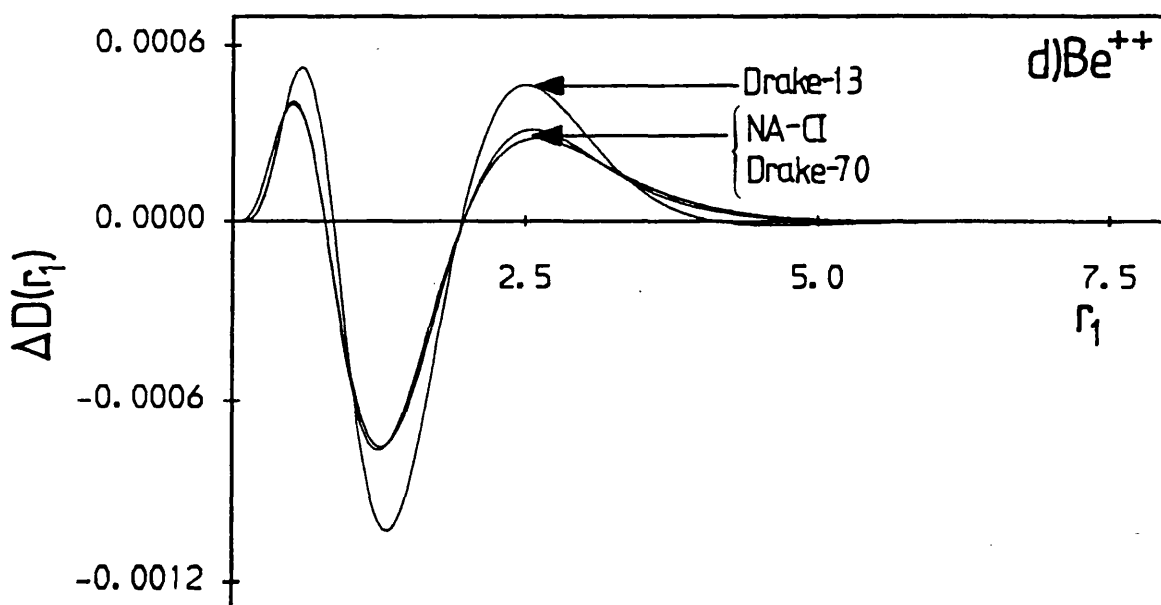
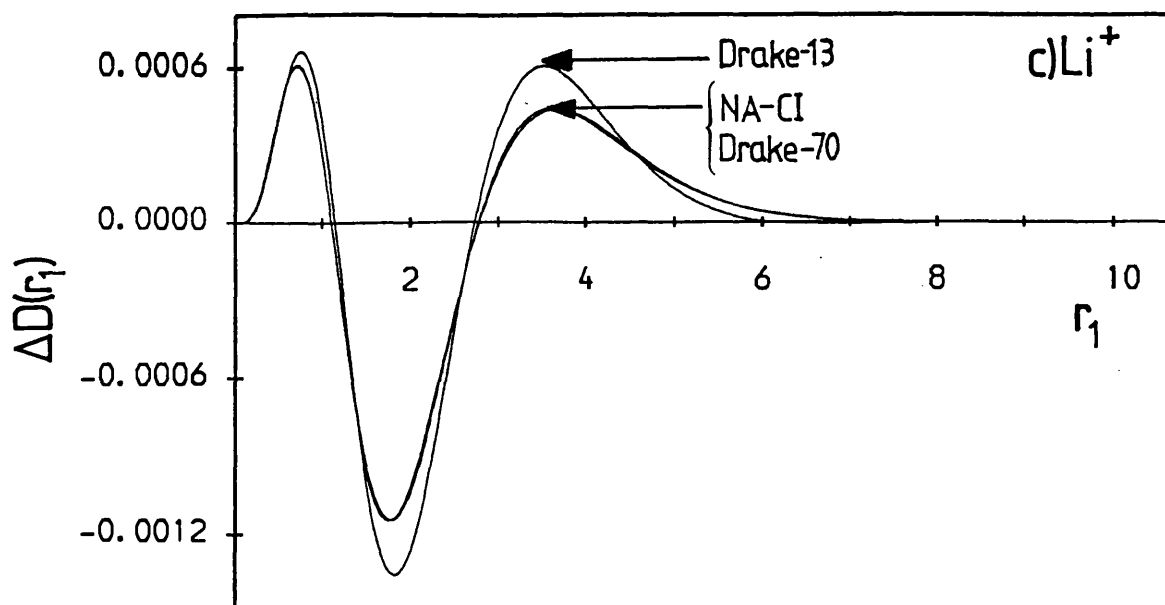


Figure II.3 c) & d)

The one-particle radial holes $\Delta D(r_1)$ for c) Li^+ and d) Be^{++} . In each case the 'best' Drake, 'shortest' Drake and NA-CI wavefunctions are used as the correlated descriptions.

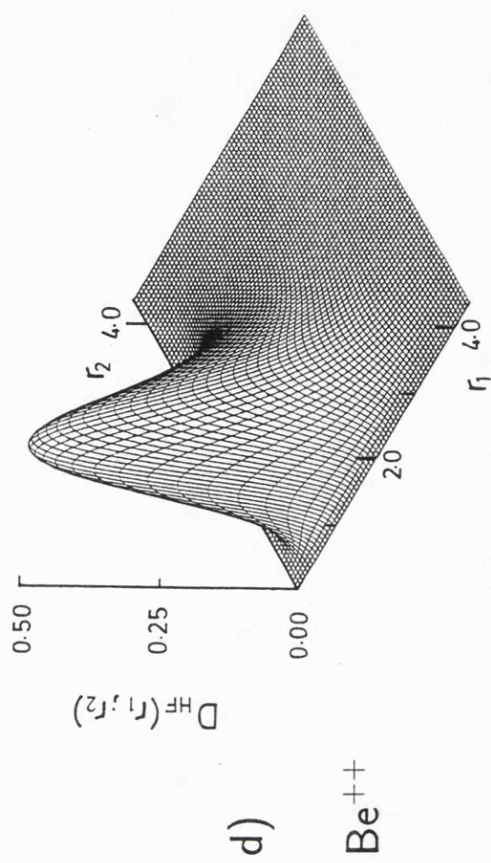
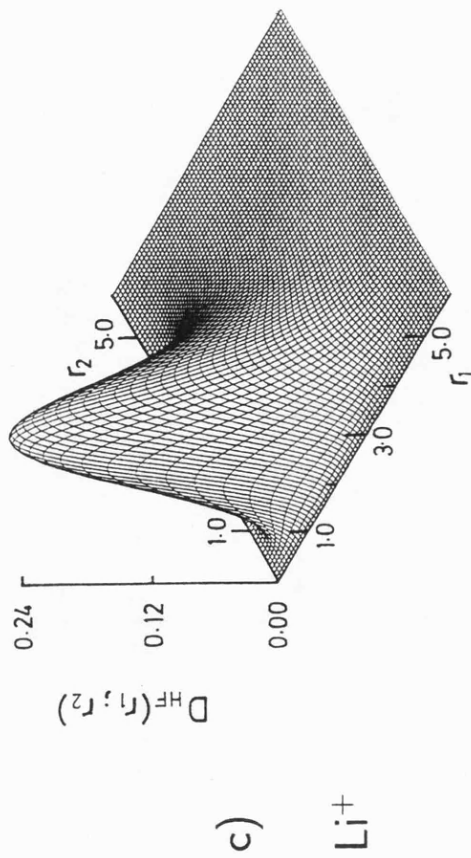
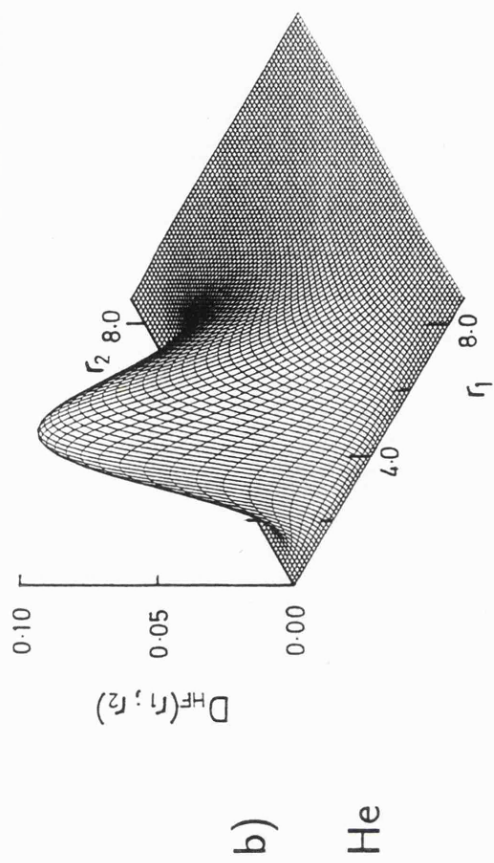
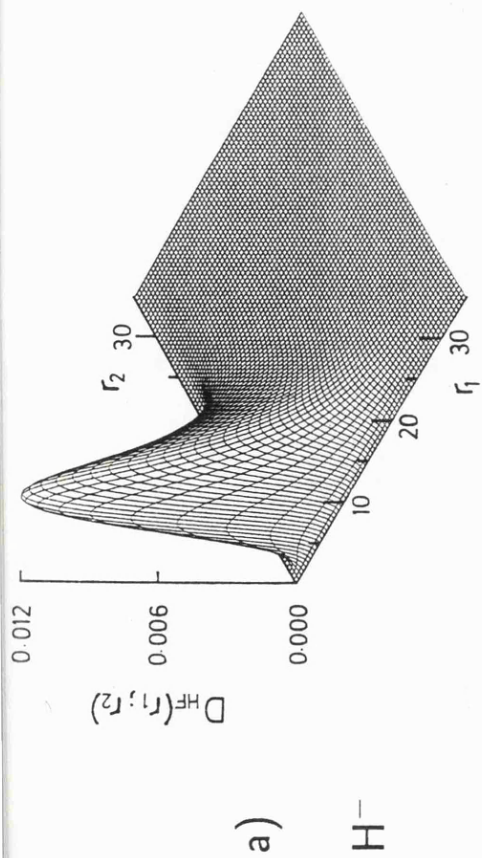


Figure II.4

The two-particle radial surfaces $D(r_1, r_2)$ for the a) H^- , b) He, c) Li^+ , d) Be^{++} systems. The Hartree-Fock wavefunction is used in each case.

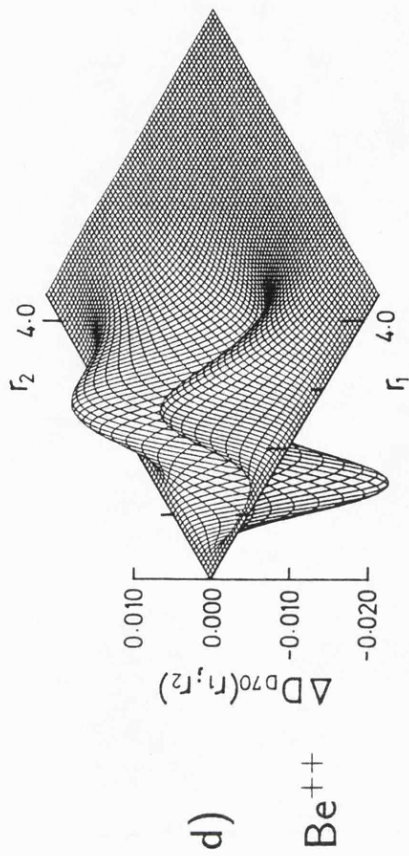
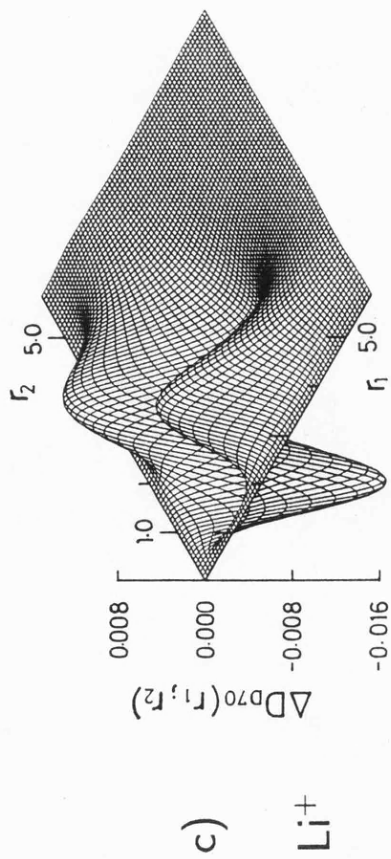
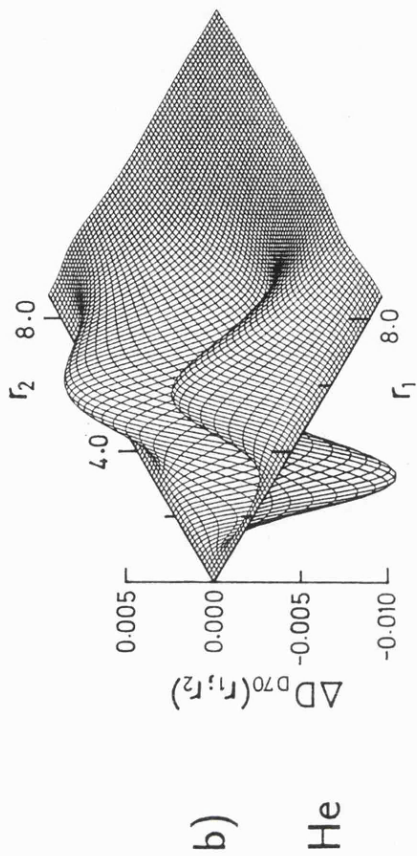
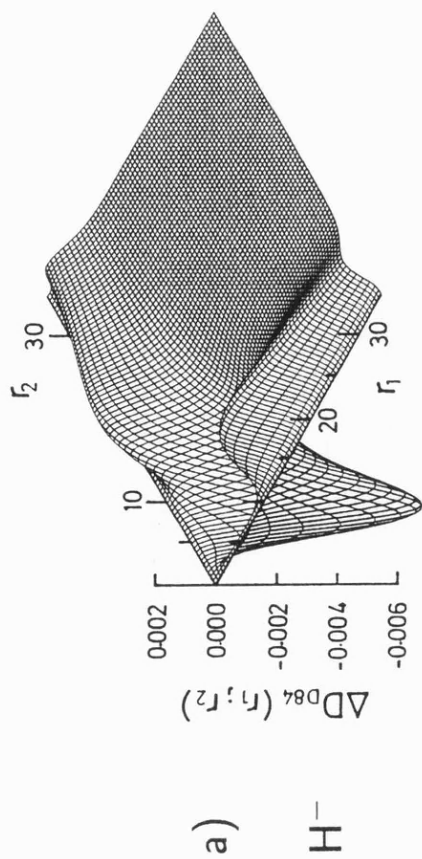


Figure II.5

The two-particle radial holes $\Delta D(r_1; r_2)$ for the a) H^- , b) He , c) Li^+ , d) Be^{++} systems.

The energetically best Drake wavefunction is used as the correlated description in each case.

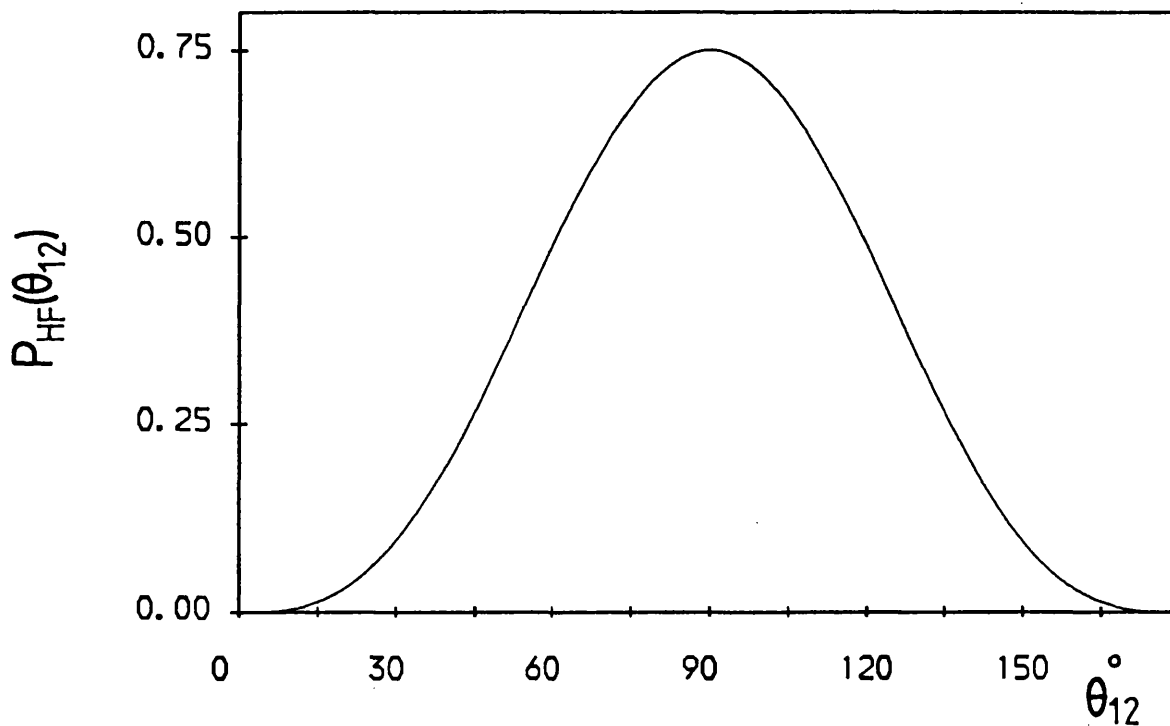


Figure II.6

The $P(\theta_{12})$ distribution for all Hartree-Fock $2p^2 \ ^3P$ wavefunctions.

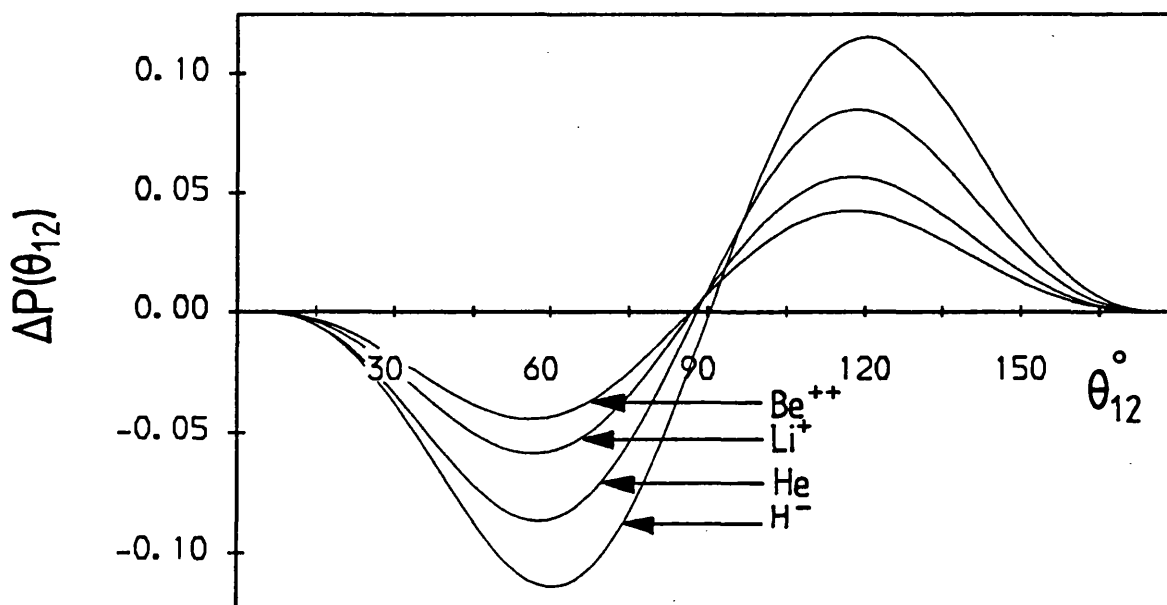


Figure II.7

The angular holes $\Delta P(\theta_{12})$ for H^- , He, Li^+ and Be^{++} . The 'best' Drake wavefunction is employed for each correlated description.

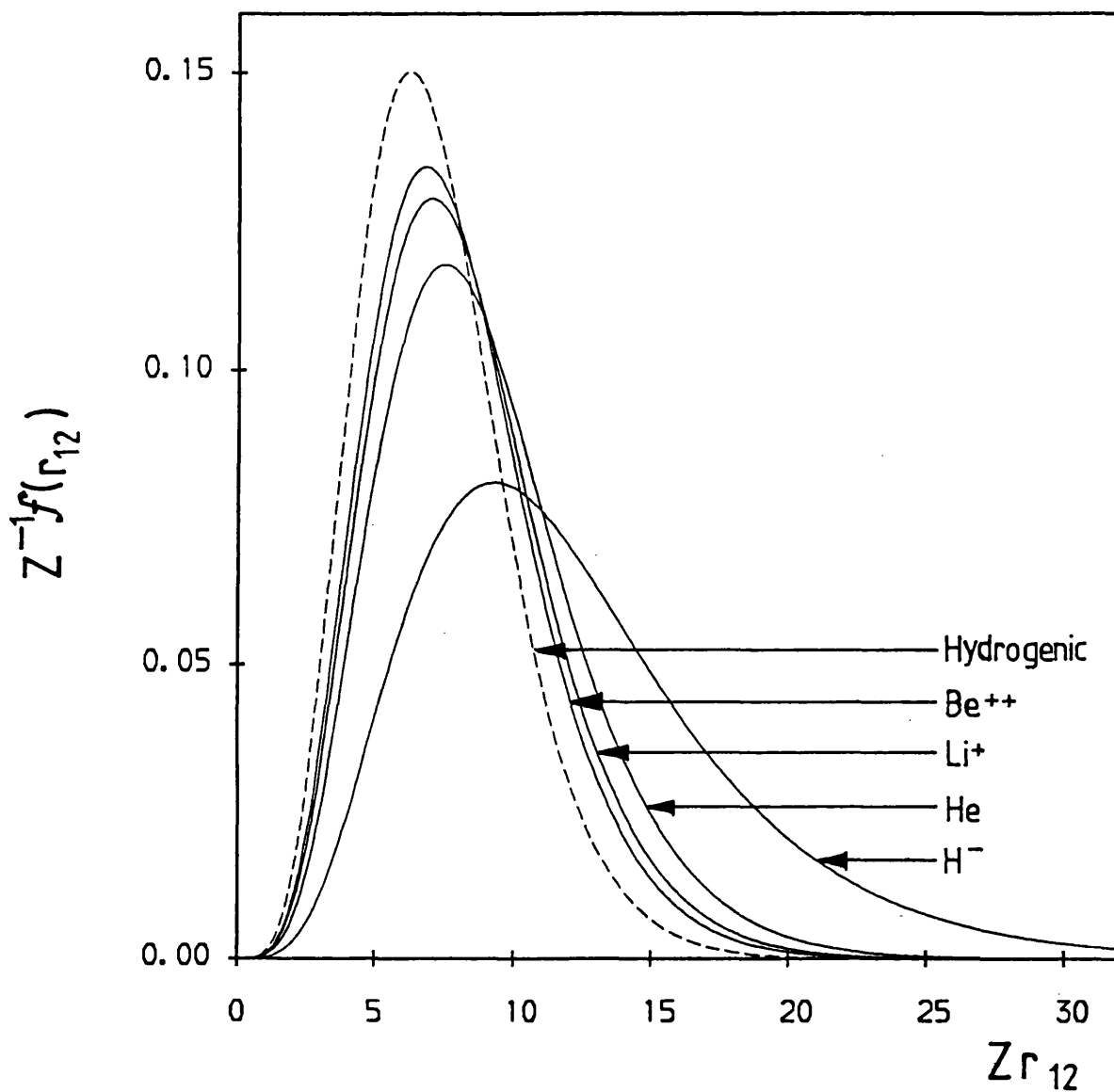


Figure II.8

The $f(r_{12})$ distributions for H^{-} , He, Li^{+} and Be^{++} produced using the Hartree-Fock wavefunctions. Also shown as a dashed line is the $f(r_{12})$ generated from an independent-particle $2p^2\ ^3P$ wavefunction comprising unoptimized hydrogenic orbitals. Both axes are scaled.

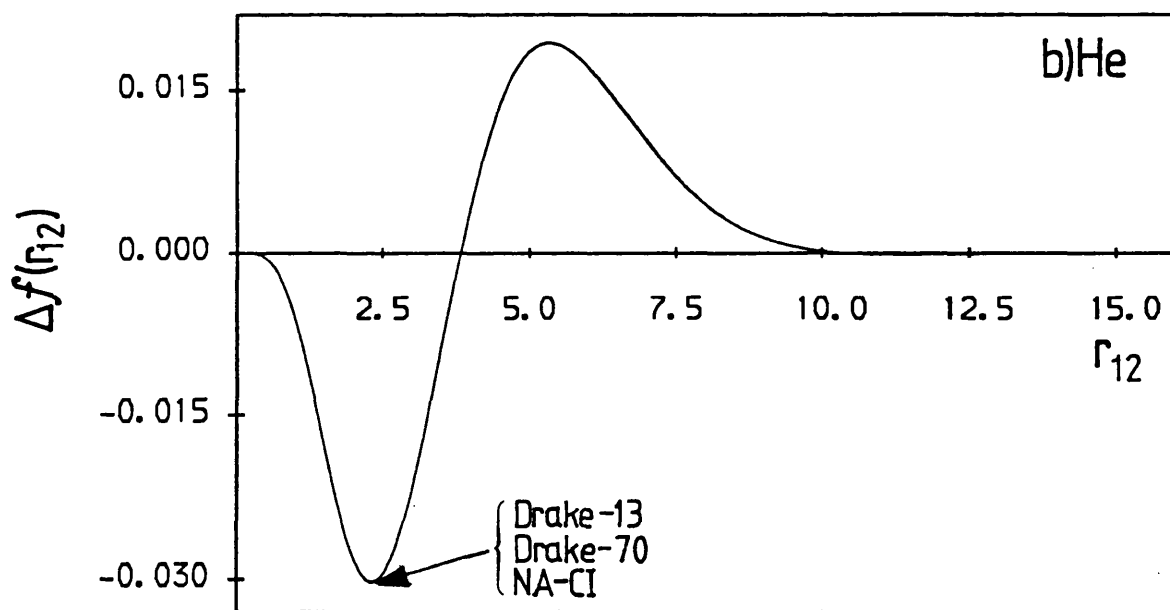
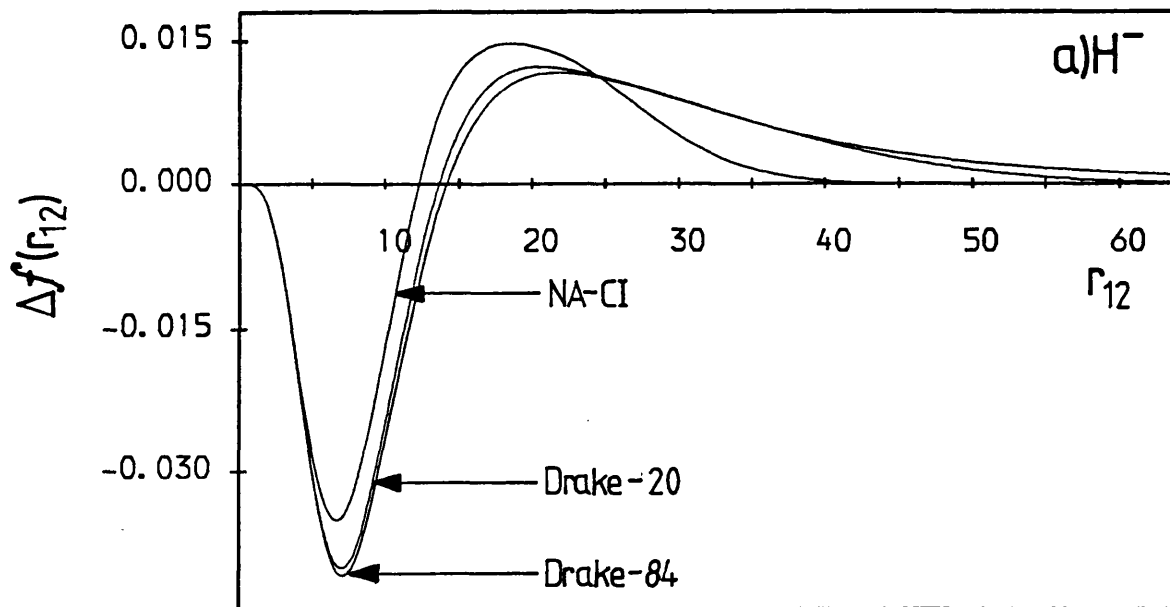


Figure II.9 a) & b)

The Coulomb holes $\Delta f(r_{12})$ for a) H^- and b) He. In each case the 'best' Drake, 'shortest' Drake and NA-CI wavefunctions are used as the correlated descriptions.

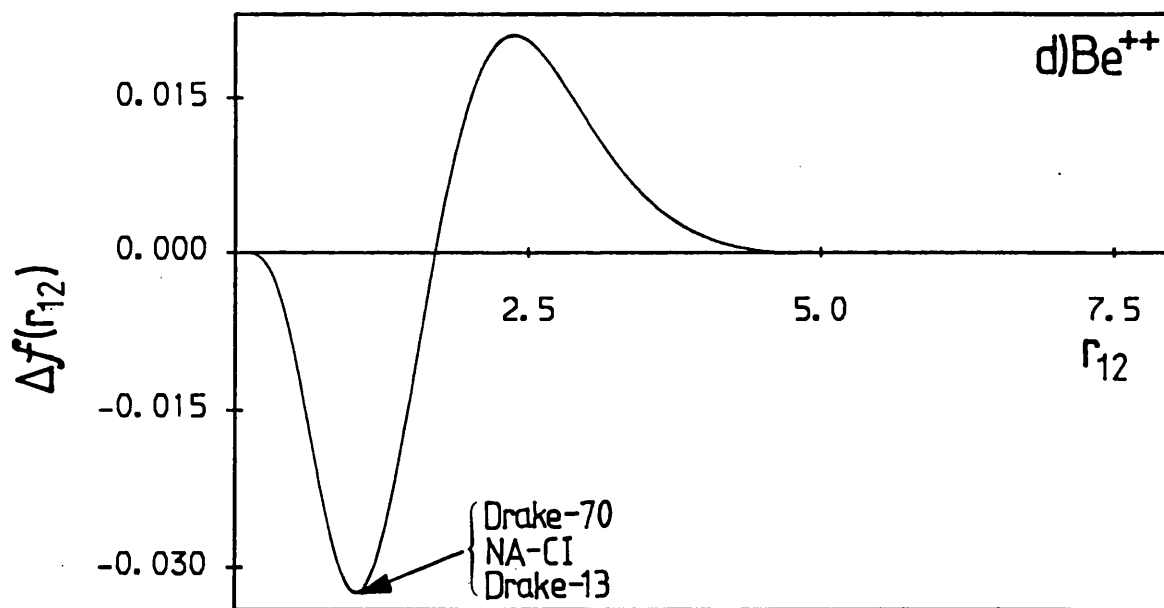
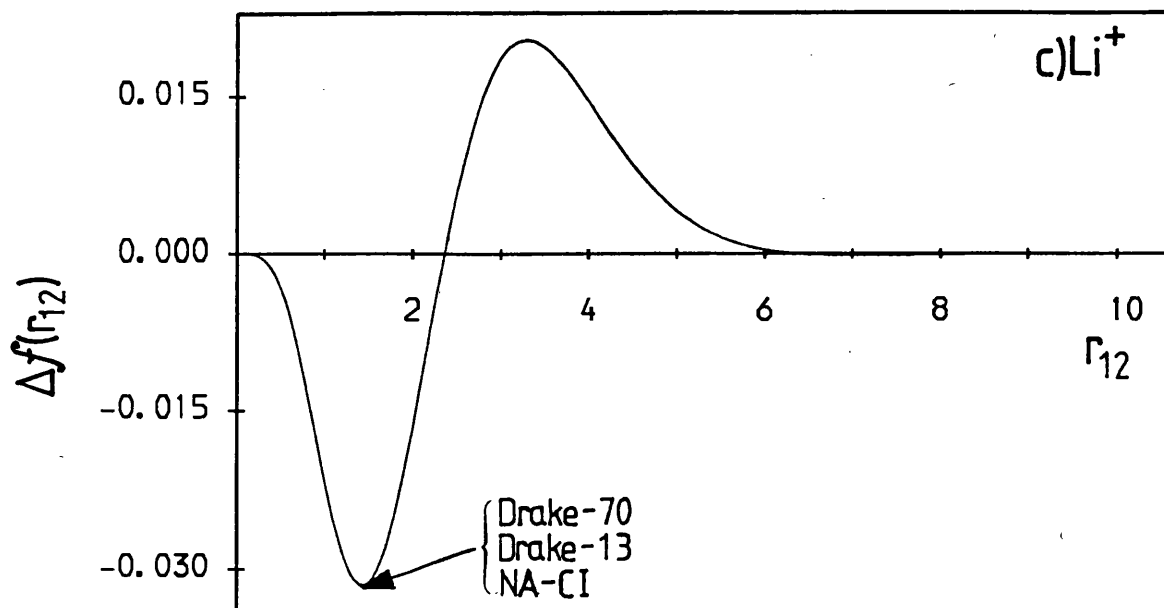


Figure II.9 c) & d)

The Coulomb holes $\Delta f(r_{12})$ for c) Li^+ and d) Be^{++} . In each case the 'best' Drake, 'shortest' Drake and NA-CI wavefunctions are used as the correlated descriptions.

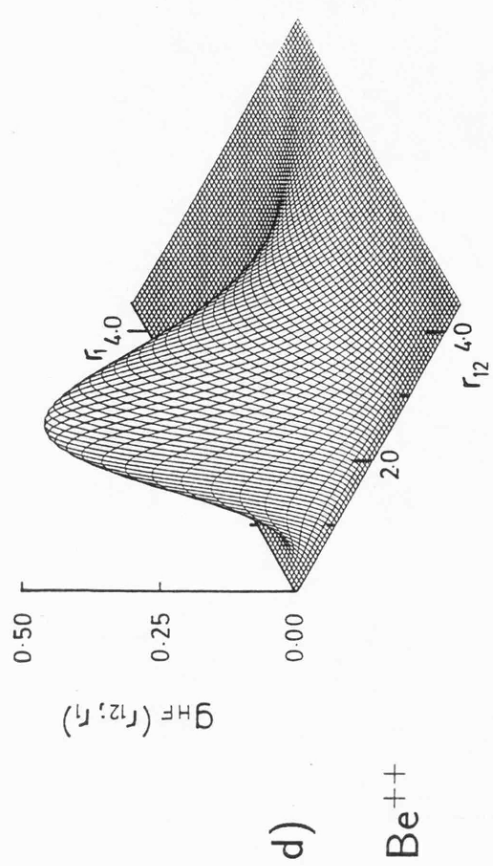
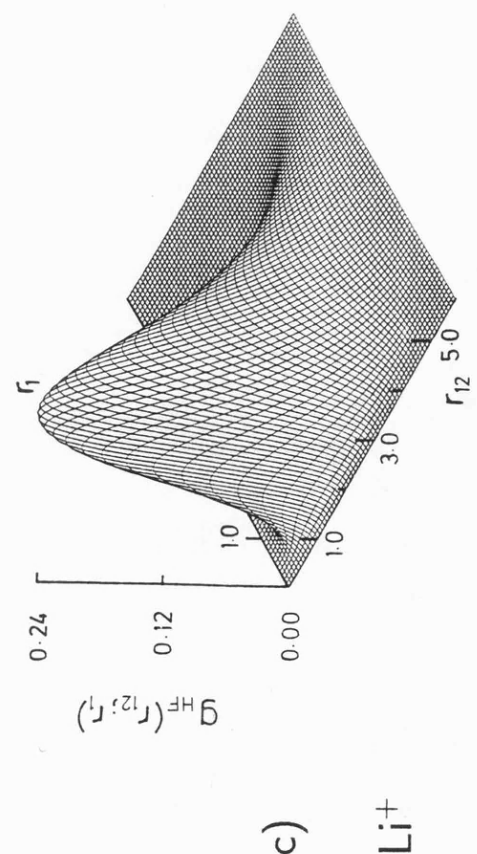
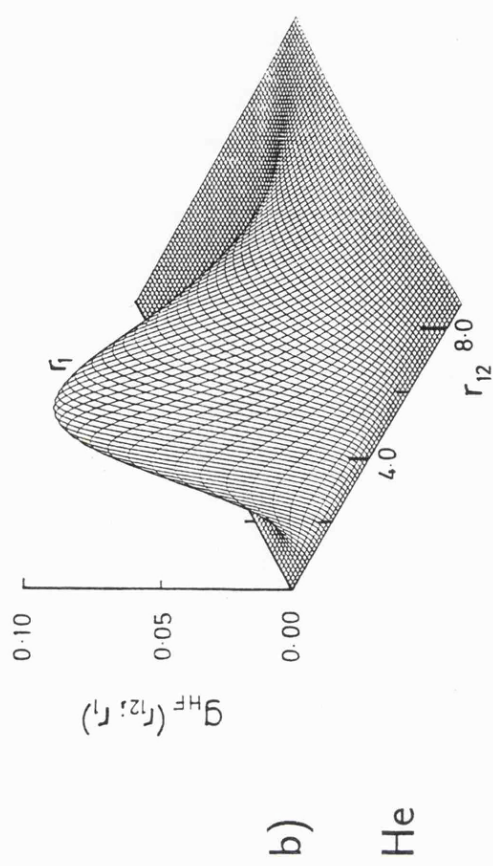
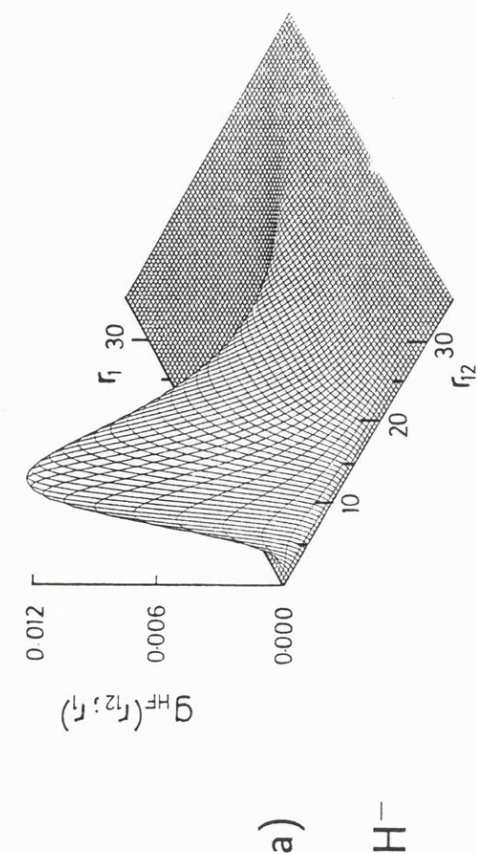


Figure II.10

The partial surfaces $g(r_{12}; r_1)$ for the a) H^- , b) He, c) Li^+ , d) Be^{++} systems. The Hartree-Fock wavefunction is used in each case.

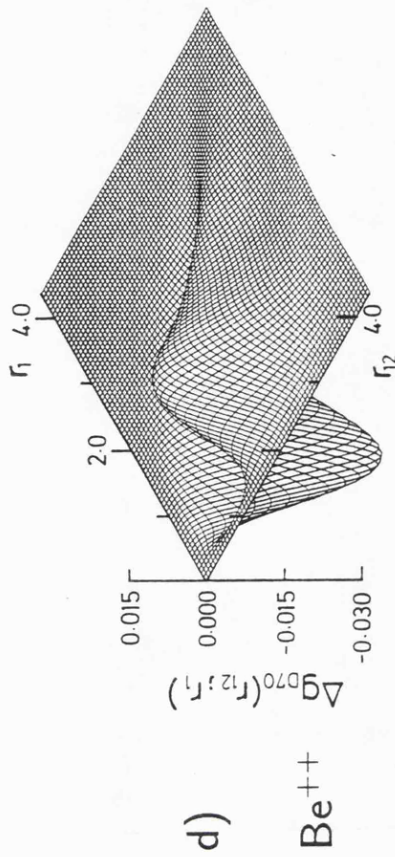
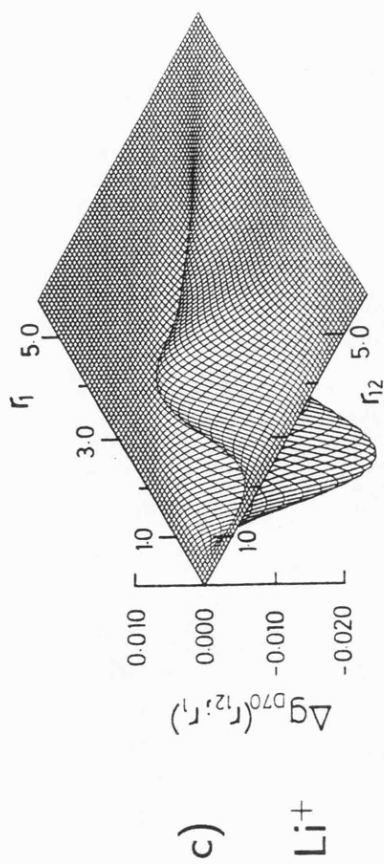
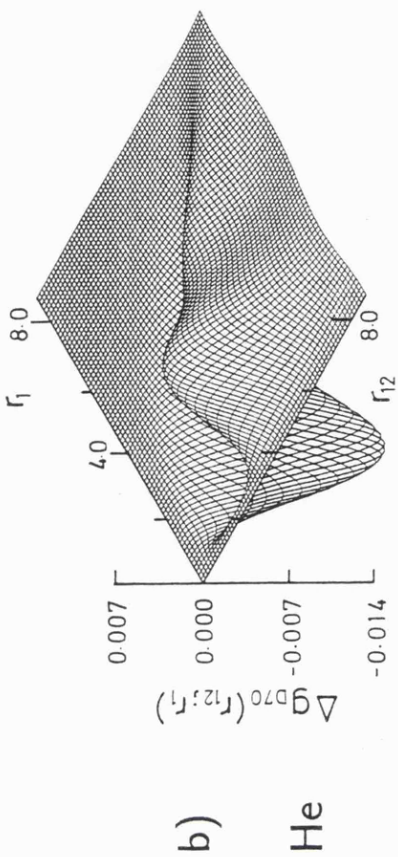
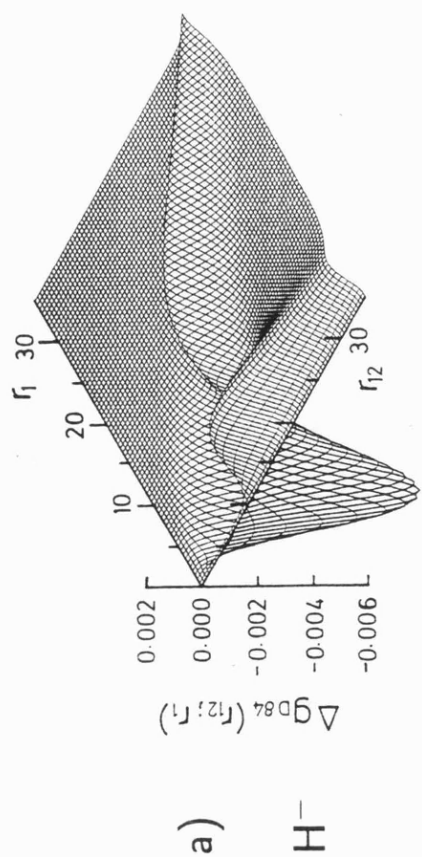


Figure II.11

The partial Coulomb holes $\Delta g(r_{12}; r_1)$ for the a) H^- , b) He, c) Li^+ , d) Be^{++} systems.

The energetically best Drake wavefunction is used as the correlated description in each case.

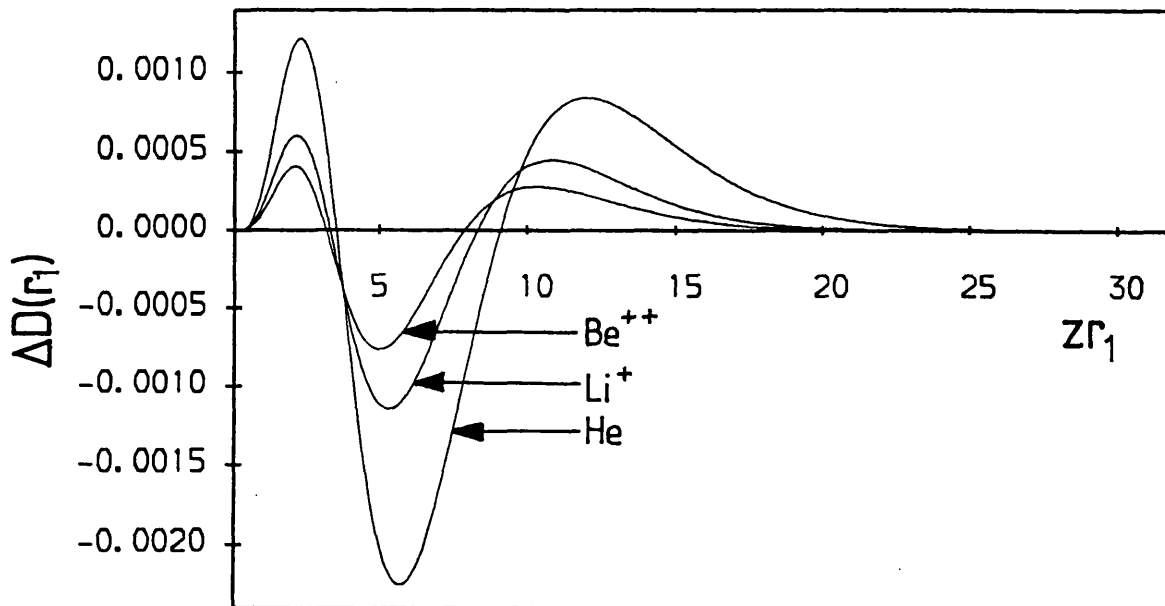


Figure II.12

The one-particle radial holes $\Delta D(r_1)$ for He, Li^+ and Be^{++} plotted against Zr_1 using the 'best' Drake wavefunction as the correlated description for each curve.

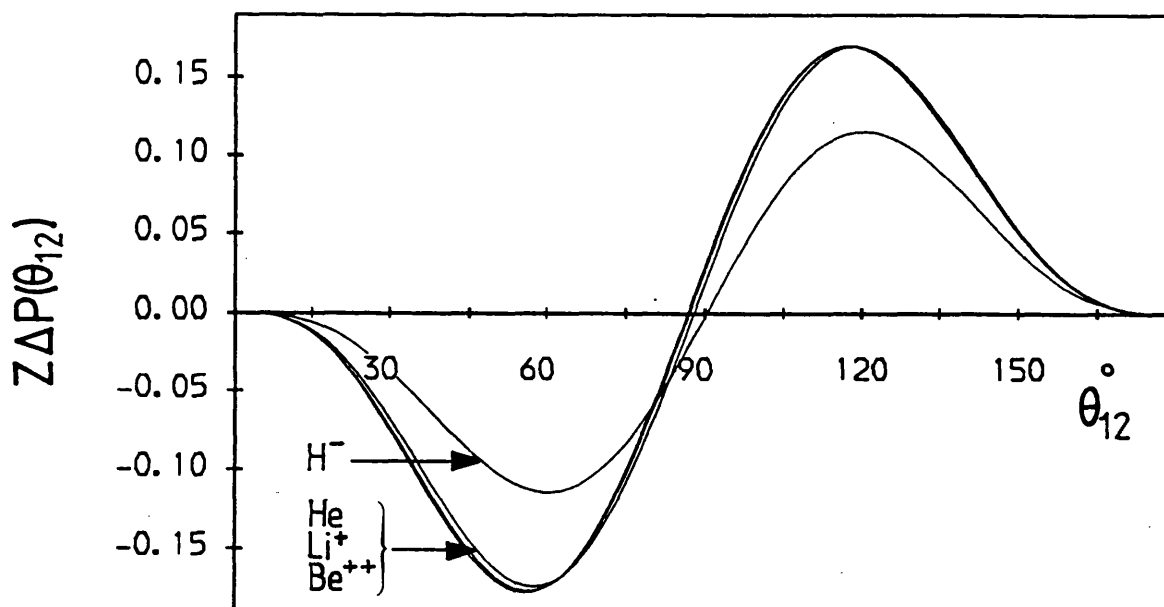


Figure II.13

The angular holes for H^- , He, Li^+ and Be^{++} . The 'best' Drake wavefunction is employed for each correlated description. In this figure the scaled ordinate $Z\Delta P(\theta_{12})$ is used.

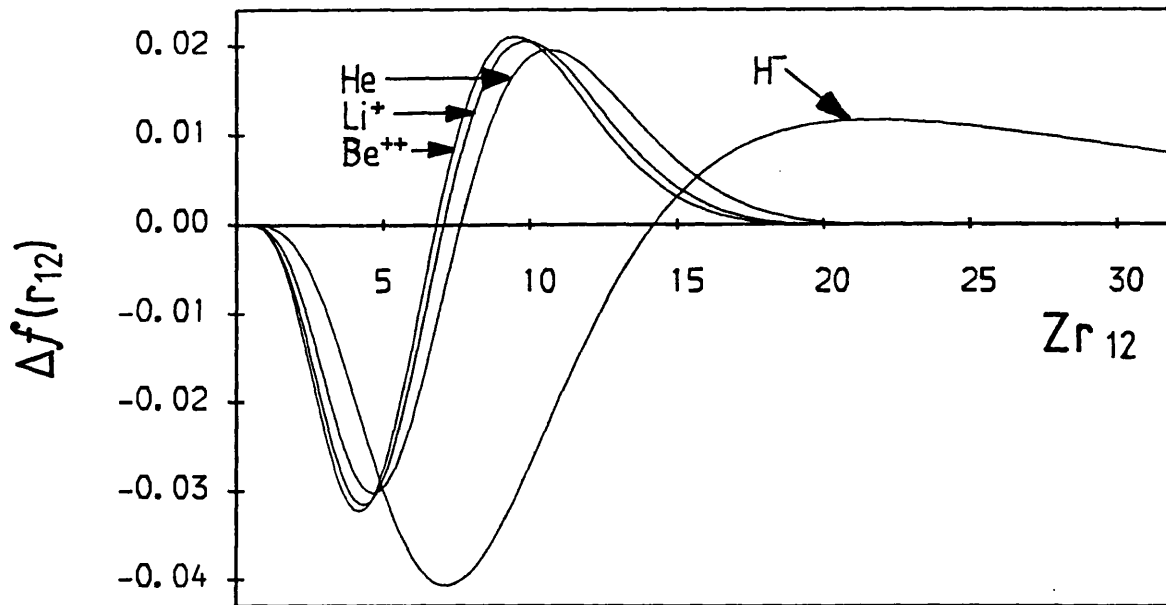


Figure II.14

The Coulomb holes $\Delta f(r_{12})$ for H^- , He, Li^+ and Be^{++} plotted against Zr_{12} using the 'best' Drake wavefunction as the correlated description for each curve.

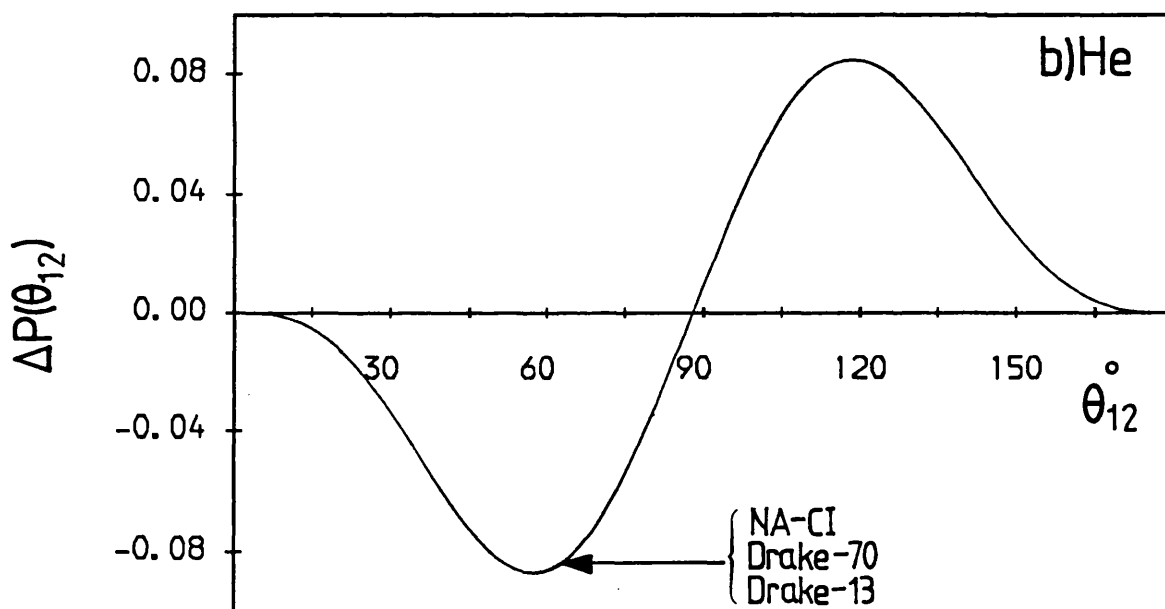
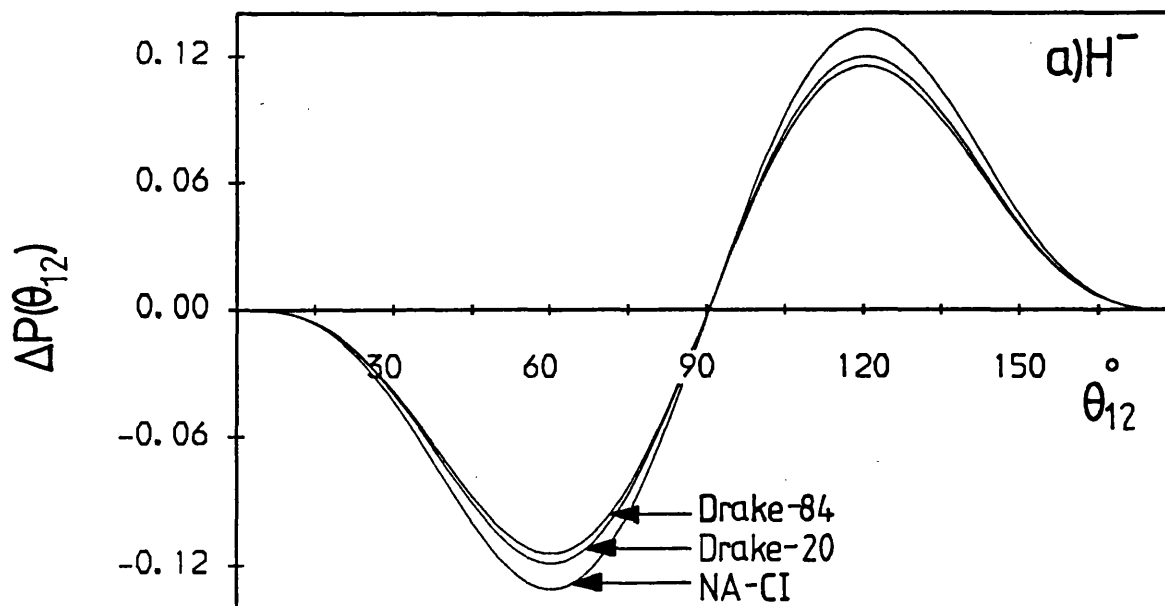


Figure II.15 a) & b)

The angular holes $\Delta P(\theta_{12})$ for a) H^- and b) He. In each case the 'best' Drake, 'shortest' Drake and NA-CI wavefunctions are used as the correlated descriptions.

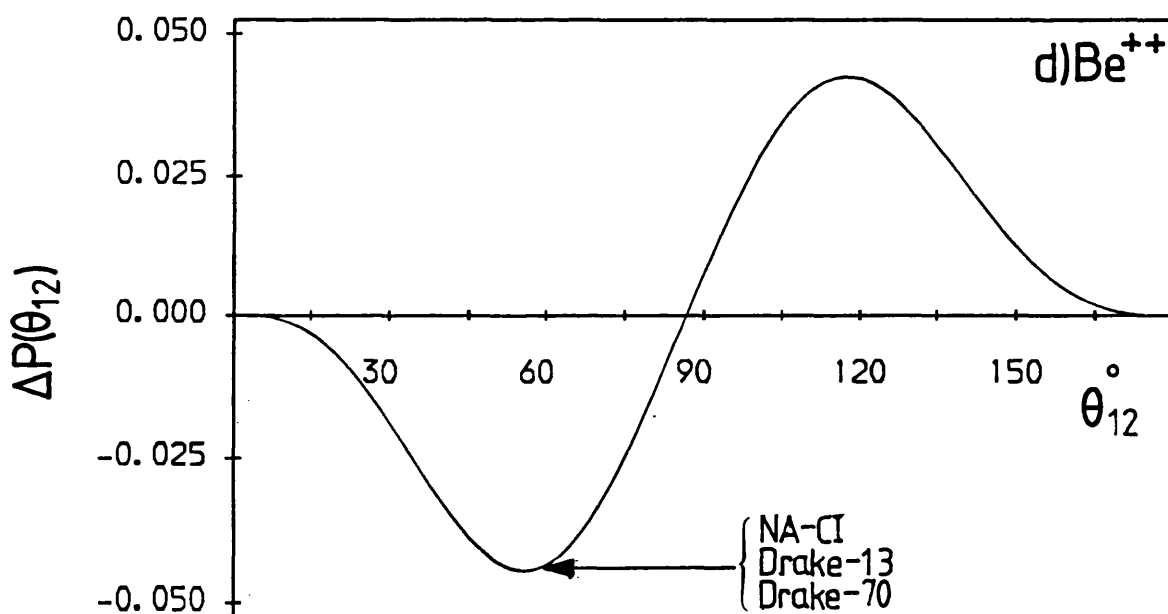
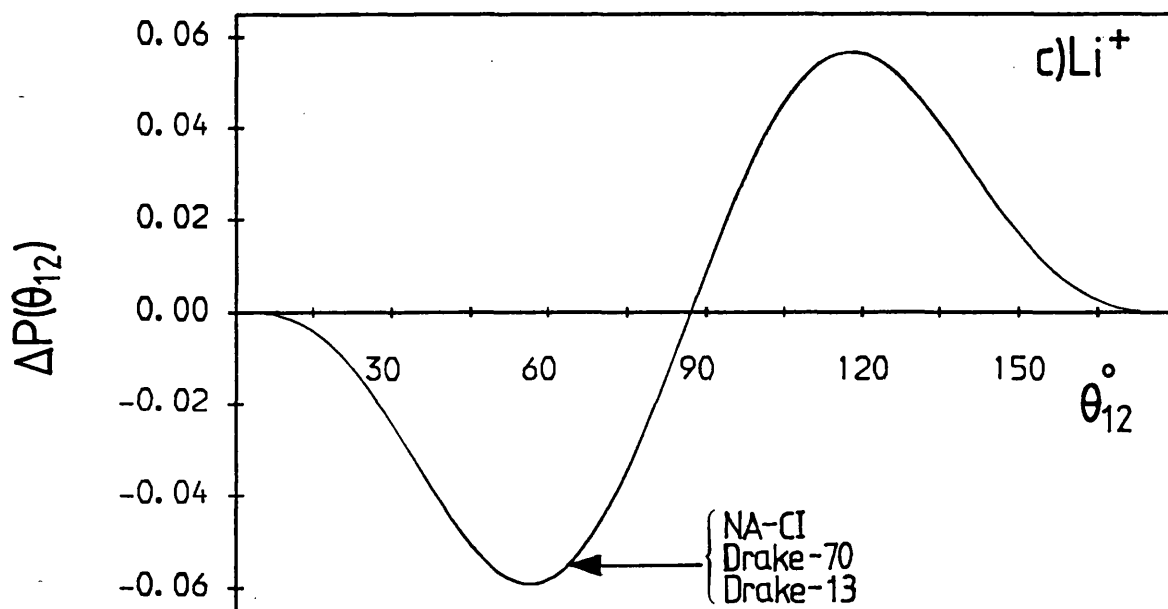


Figure II.15 c) & d)

The angular holes $\Delta P(\theta_{12})$ for c) Li^+ and d) Be^{++} . In each case the 'best' Drake, 'shortest' Drake and NA-CI wavefunctions are used as the correlated descriptions.

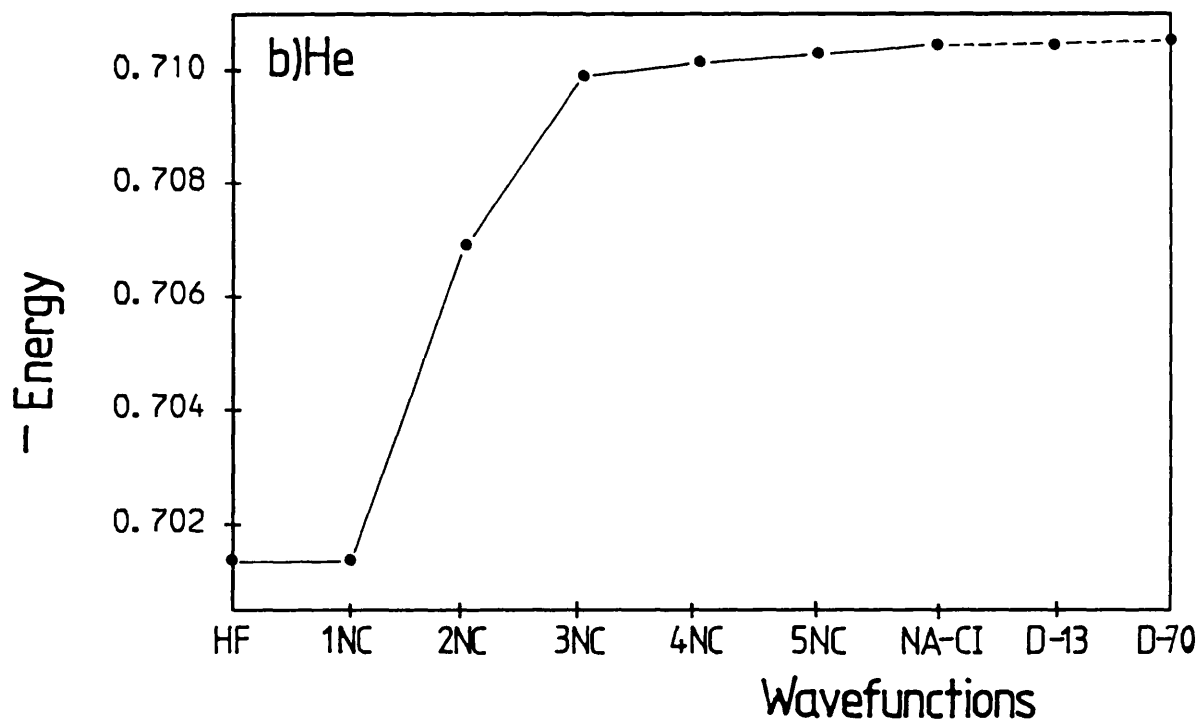
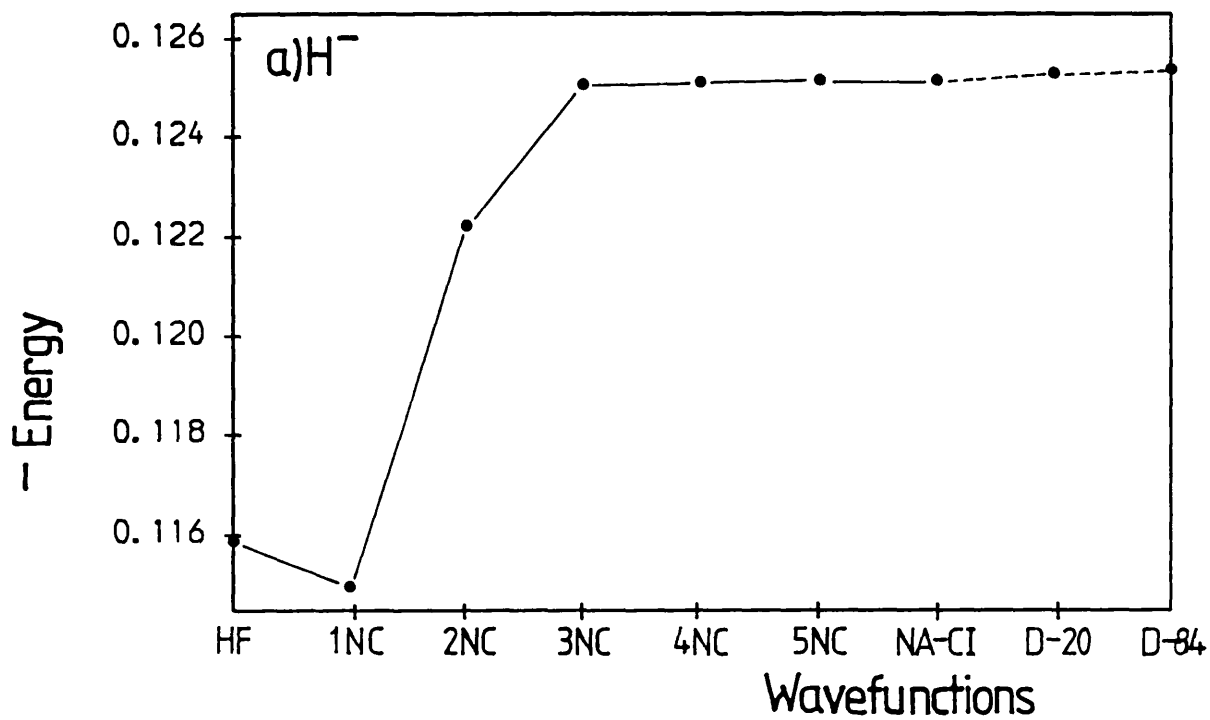


Figure II.16 a) & b)

The energies of the various wavefunctions used in this thesis for a) H^- and b) He. 'D-20' denotes the 20-term Drake wavefunction etc.

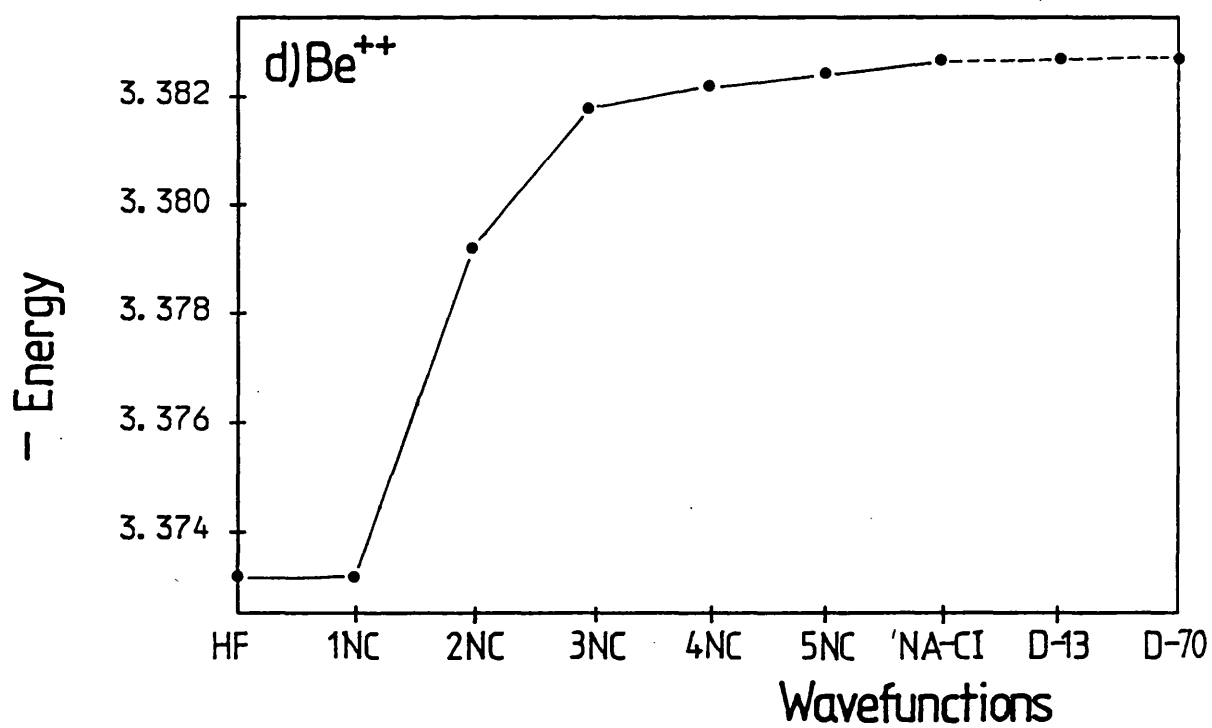
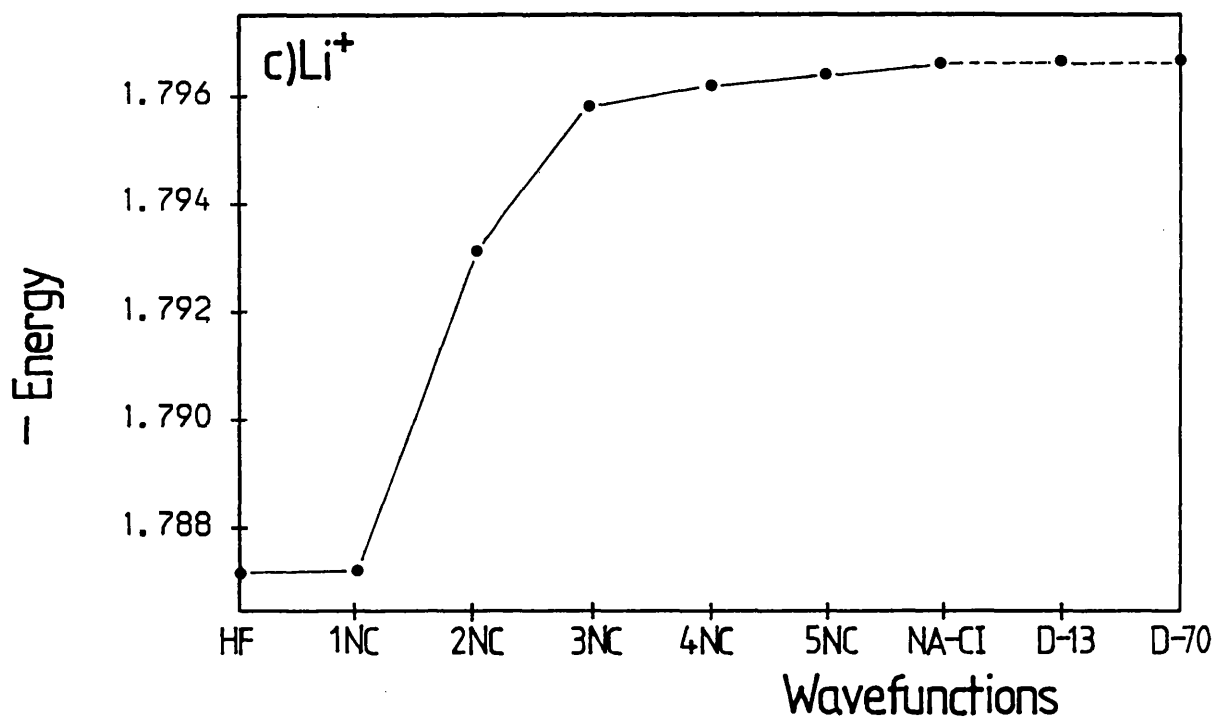


Figure II.16 c) & d)

The energies of the various wavefunctions used in this thesis for c) Li^+ and d) Be^{++} . 'D-13' denotes the 13-term Drake wavefunction etc.

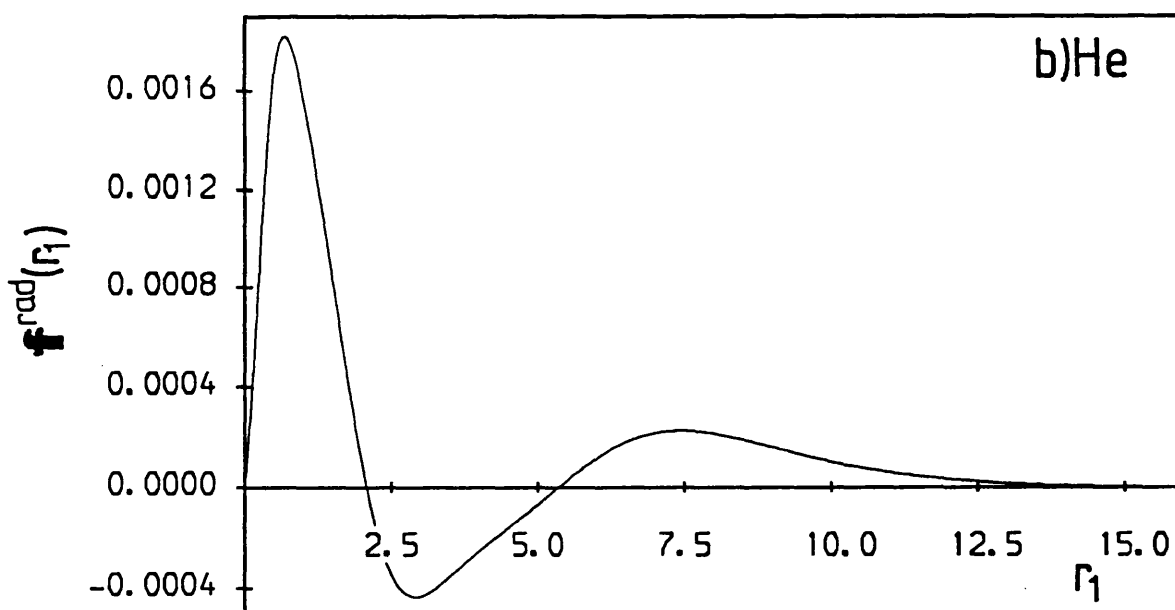
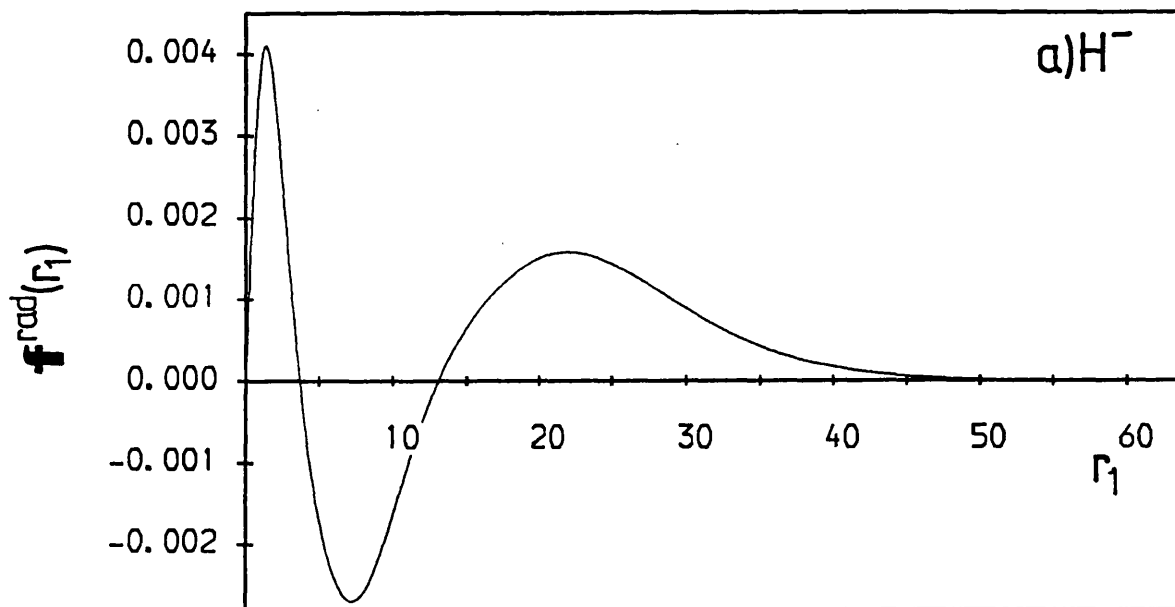


Figure II.17 a) & b)

The radial part $f^{\text{rad}}(r_1)$ of the Sinanoğlu orbital correction function for a) H^- and b) He . They are calculated from the NA-CI wavefunctions.

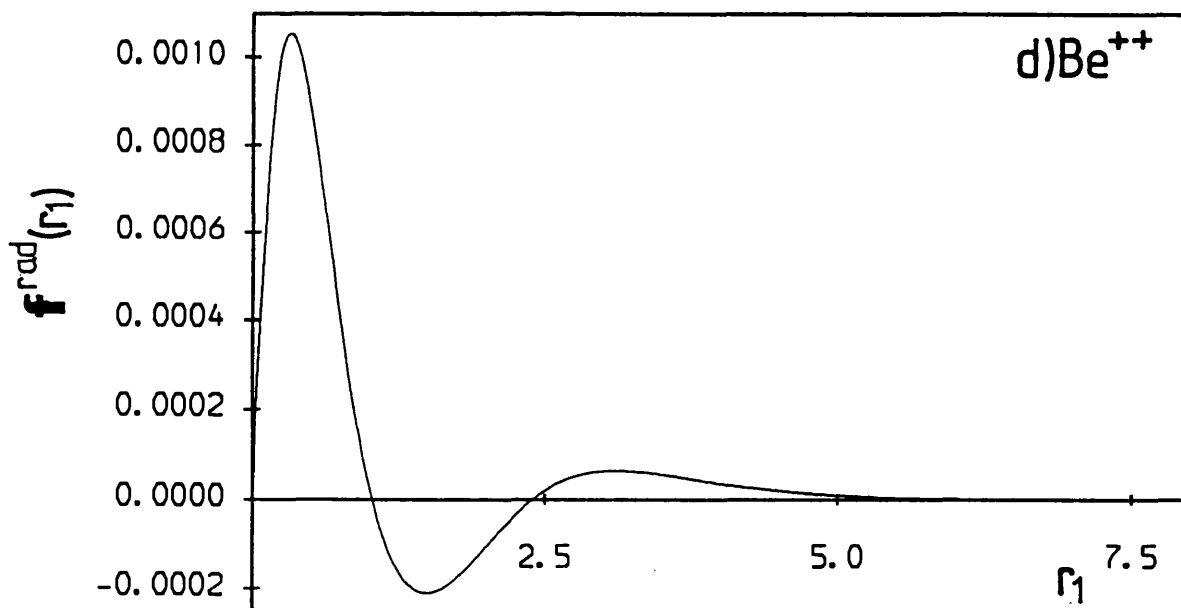
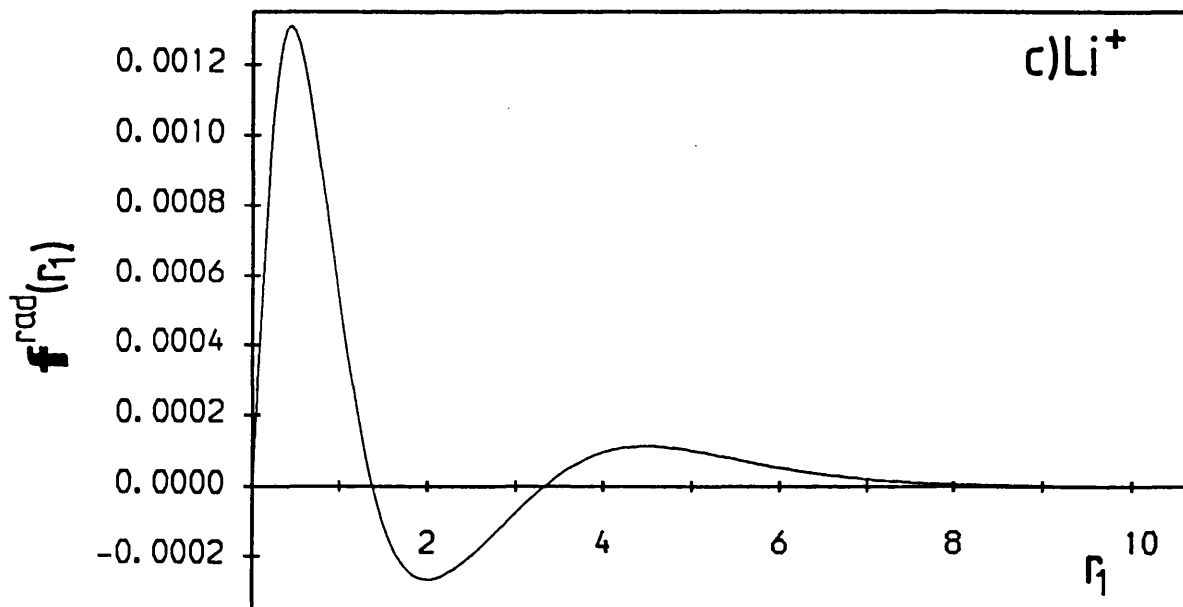


Figure II.17 c) & d)

The radial part $f^{\text{rad}}(r_1)$ of the Sinanoğlu orbital correction function for c) Li^+ and d) Be^{++} . They are calculated from the NA-CI wavefunctions.

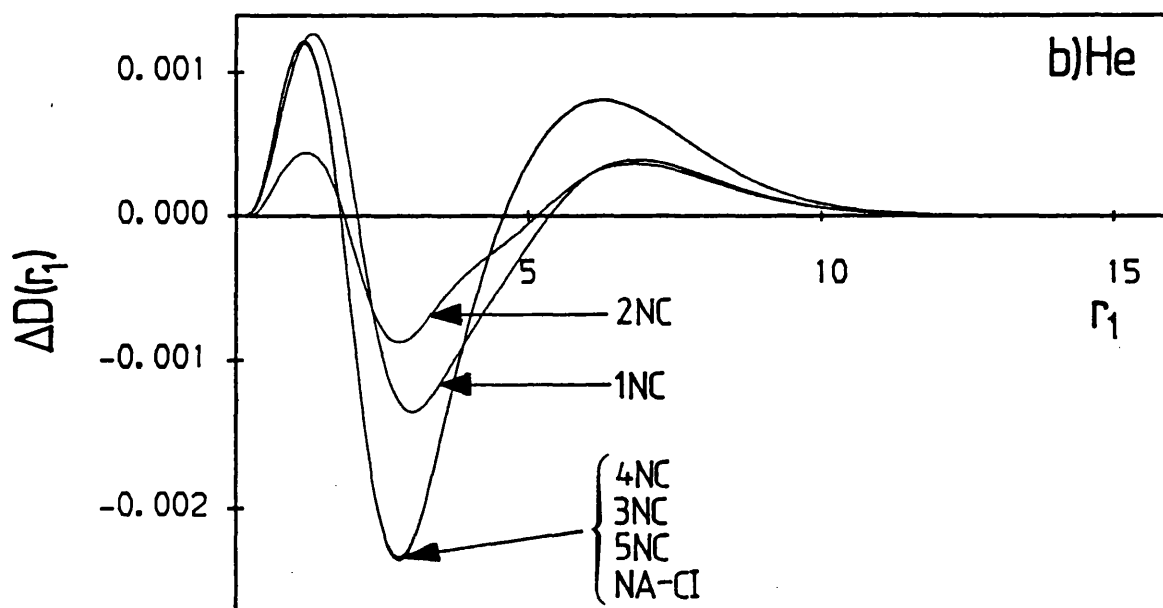
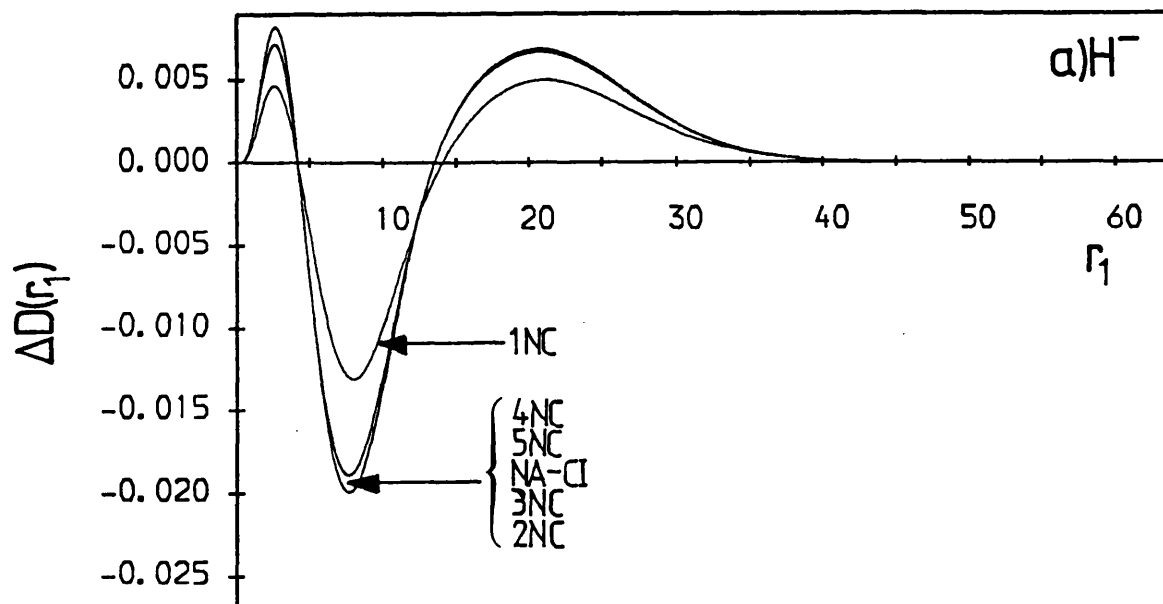


Figure II.18 a) & b)

The one-particle radial holes $\Delta D(r_1)$ for a) H^- and b) He. In each case the 1NC, 2NC, 3NC, 4NC, 5NC and NA-CI wavefunctions are used as the correlated descriptions.

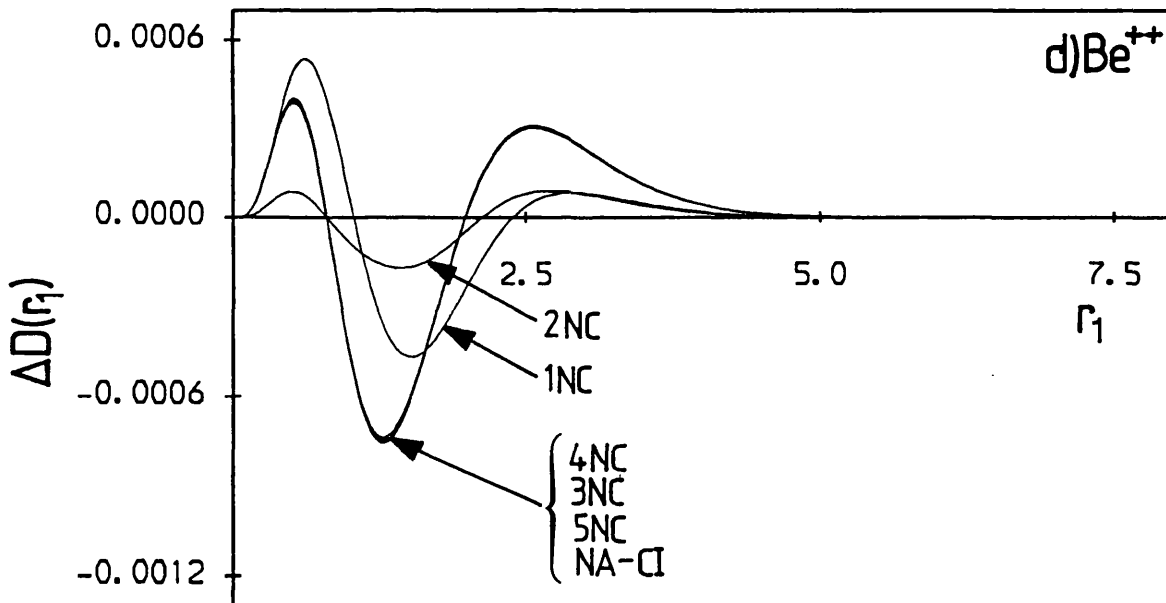
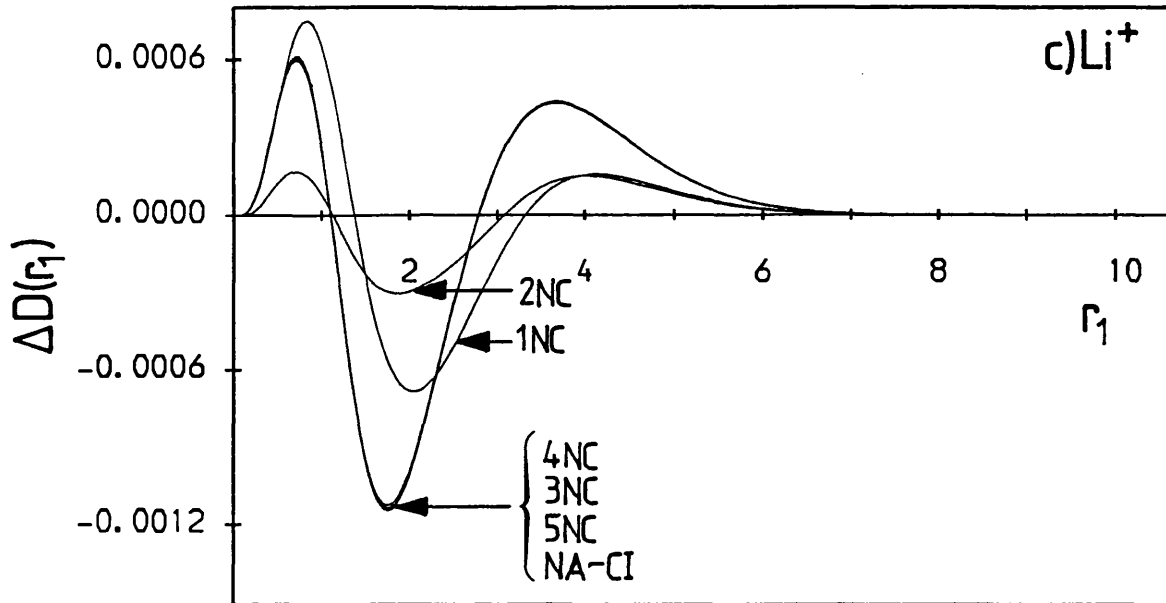


Figure II.18 c) & d)

The one-particle radial holes $\Delta D(r_1)$ for c) Li^+ and d) Be^{++} . In each case the 1NC, 2NC, 3NC, 4NC, 5NC and NA-CI wavefunctions are used as the correlated descriptions.

H^-

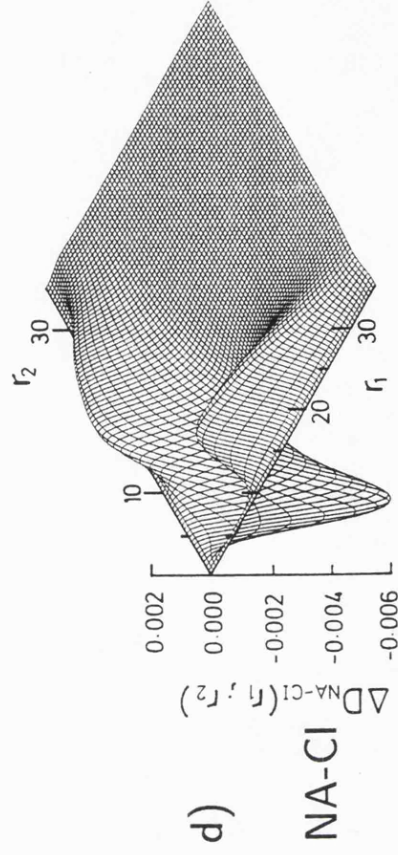
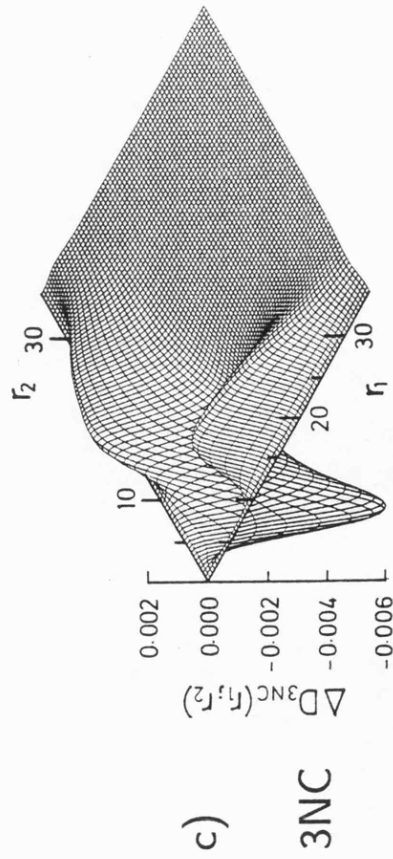
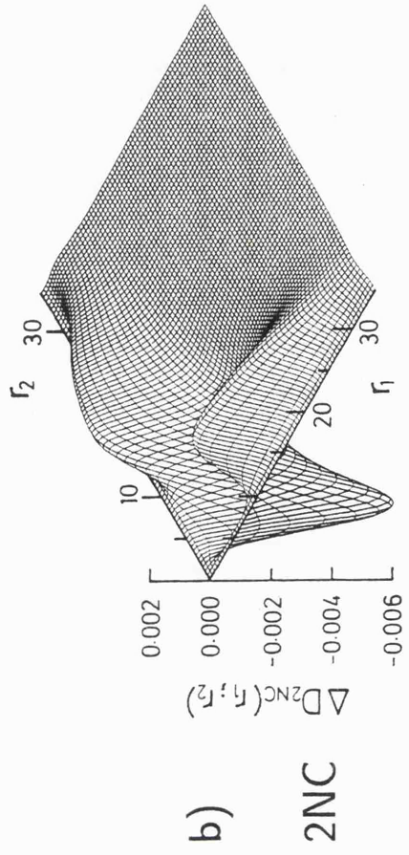
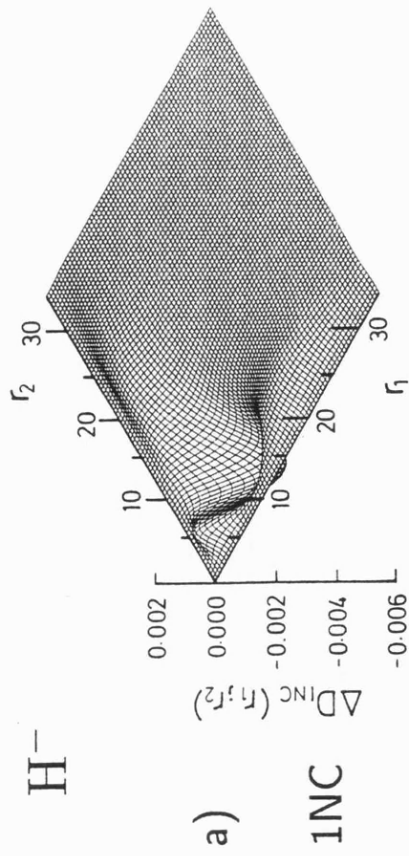


Figure II.19

The two-particle radial holes $\Delta D(r_1; r_2)$ for the H^- system using the a) 1NC, b) 2NC, c) 3NC and d) NA-CI wavefunctions for the correlated descriptions.

He

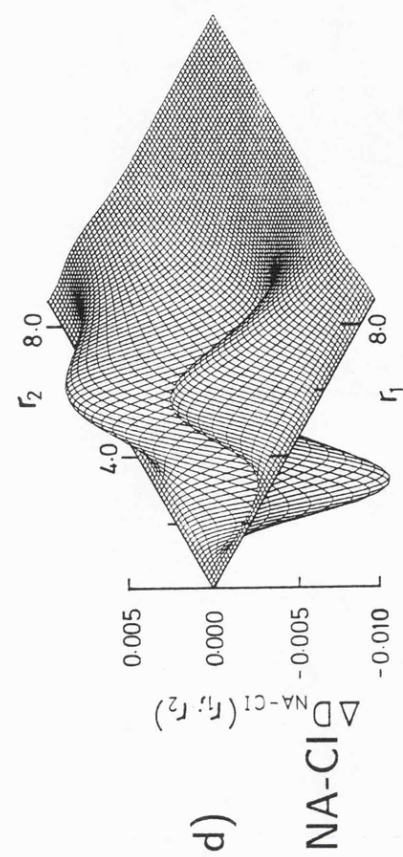
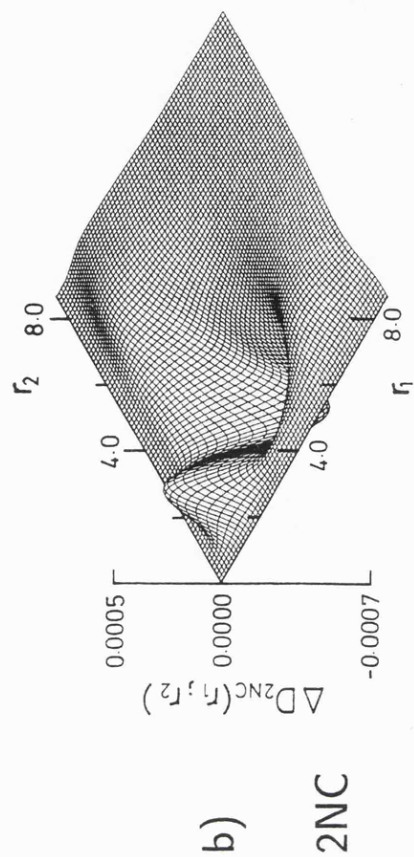


Figure II.20

The two-particle radial holes $\Delta D(r_1; r_2)$ for the He system using the a) 1NC,

b) 2NC, c) 3NC and d) NA-CI wavefunctions for the correlated descriptions.

Note the different vertical scale employed in a) and b).

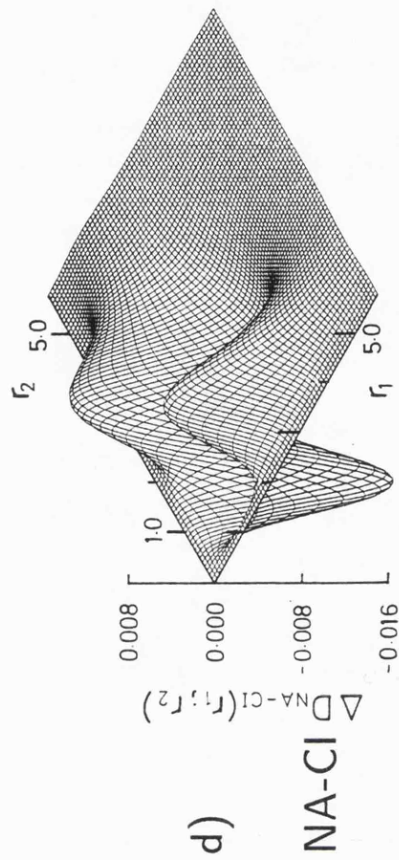
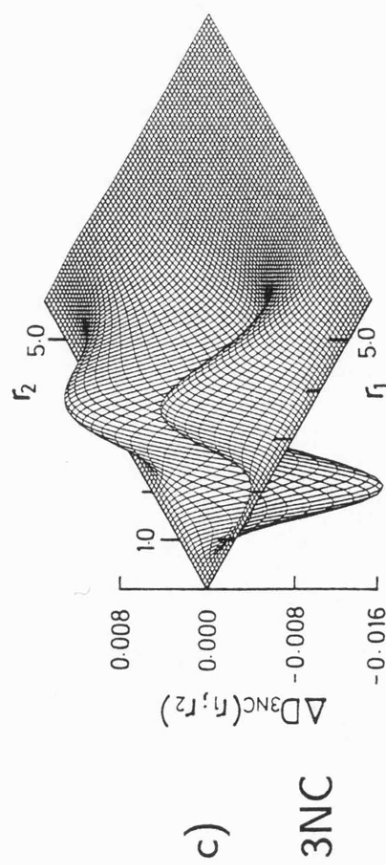
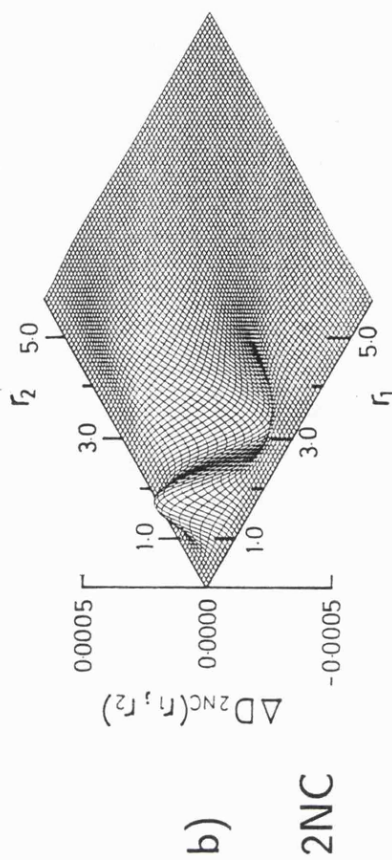
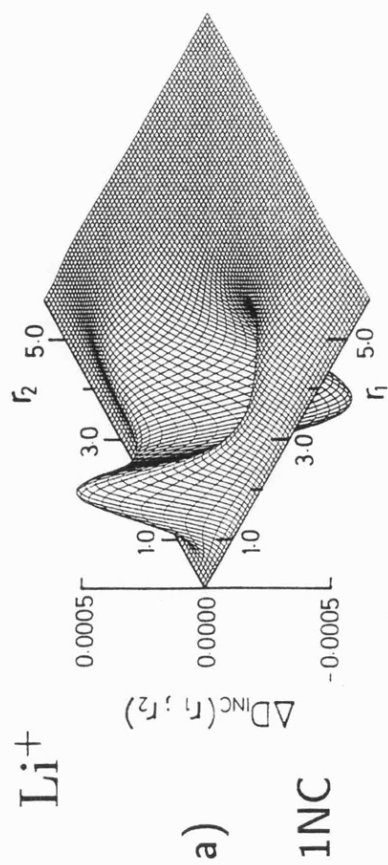


Figure II.21

The two-particle radial holes $\Delta D(r_1; r_2)$ for the Li^+ system using the a) 1NC, b) 2NC, c) 3NC and d) NA-CI wavefunctions for the correlated descriptions. Note the different vertical scale employed in a) and b).

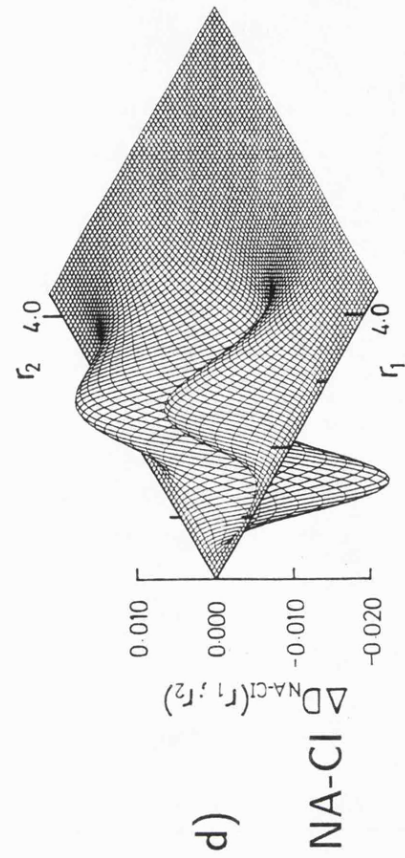
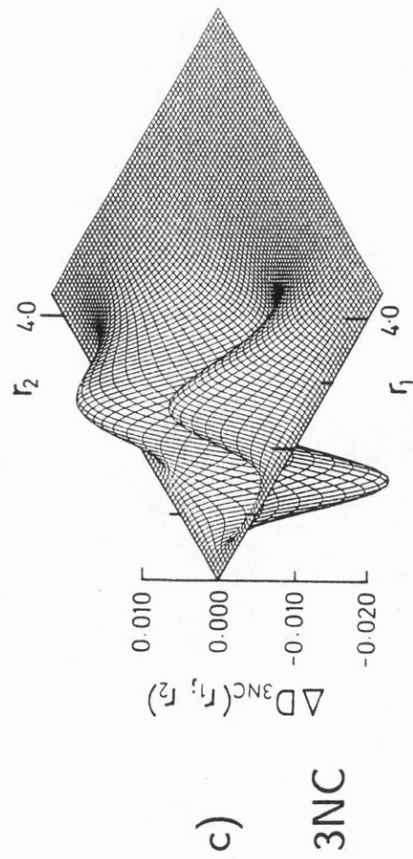
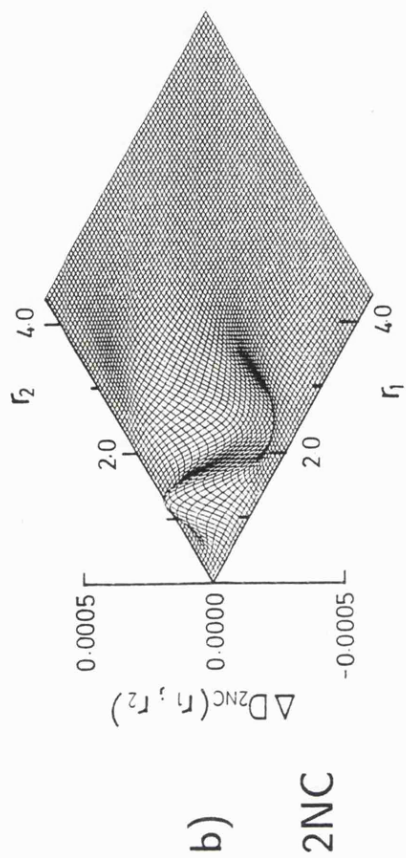
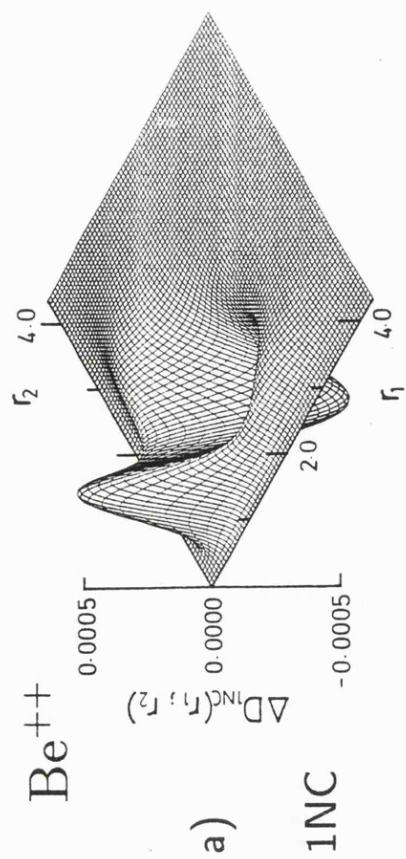


Figure II.22

The two-particle radial holes $\Delta D(r_1, r_2)$ for the Be^{++} system using the a) 1NC,

b) 2NC, c) 3NC and d) NA-CI wavefunctions for the correlated descriptions.

Note the different vertical scale employed in a) and b).

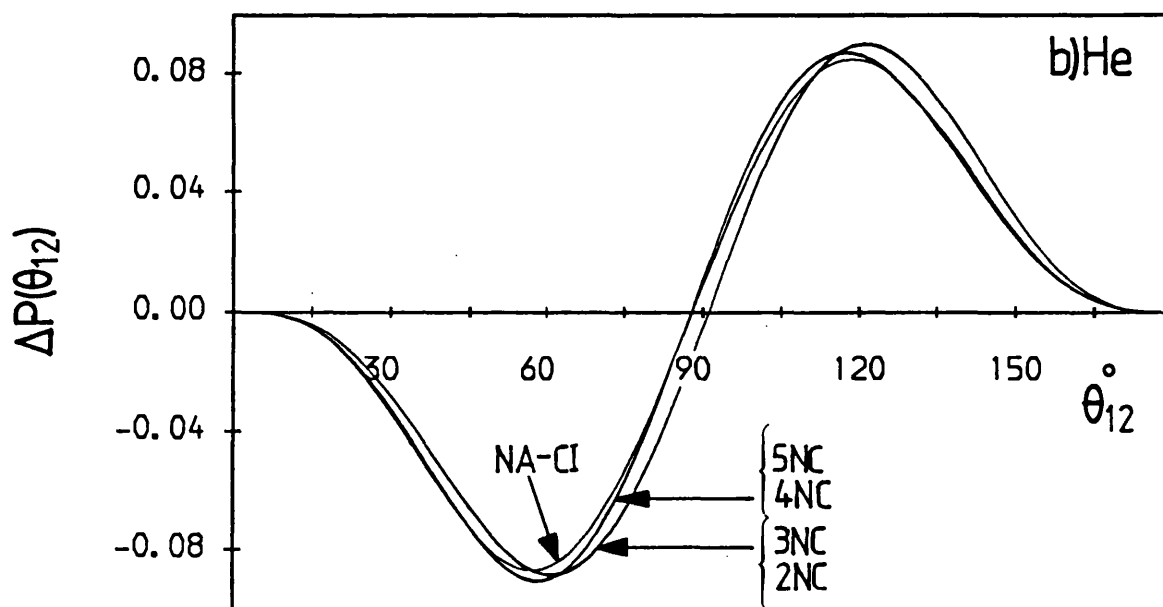
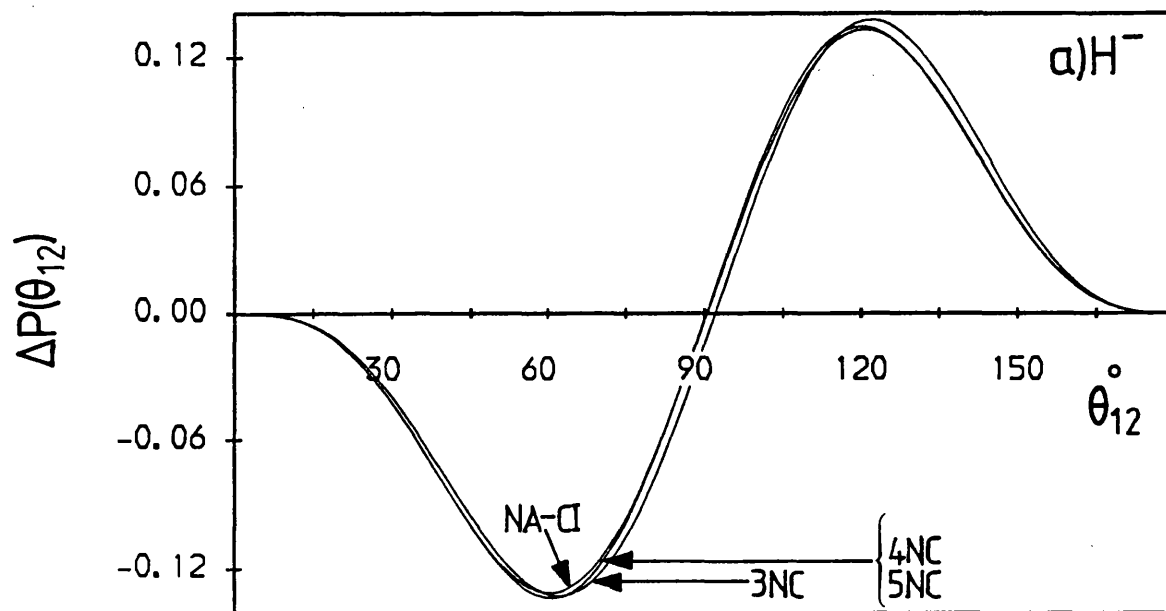


Figure II.23 a) & b)

The angular holes $\Delta P(\theta_{12})$ for a) H^- and b) He. In each case the 3NC, 4NC, 5NC and NA-CI wavefunctions are used as the correlated descriptions. For He the 2NC wavefunction is used as well.

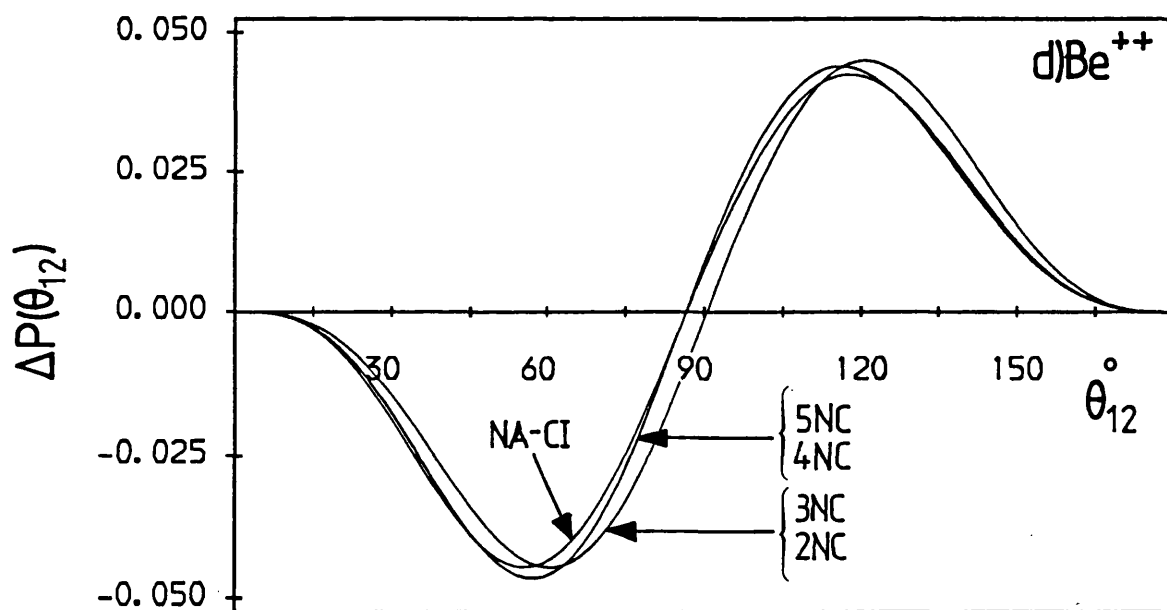
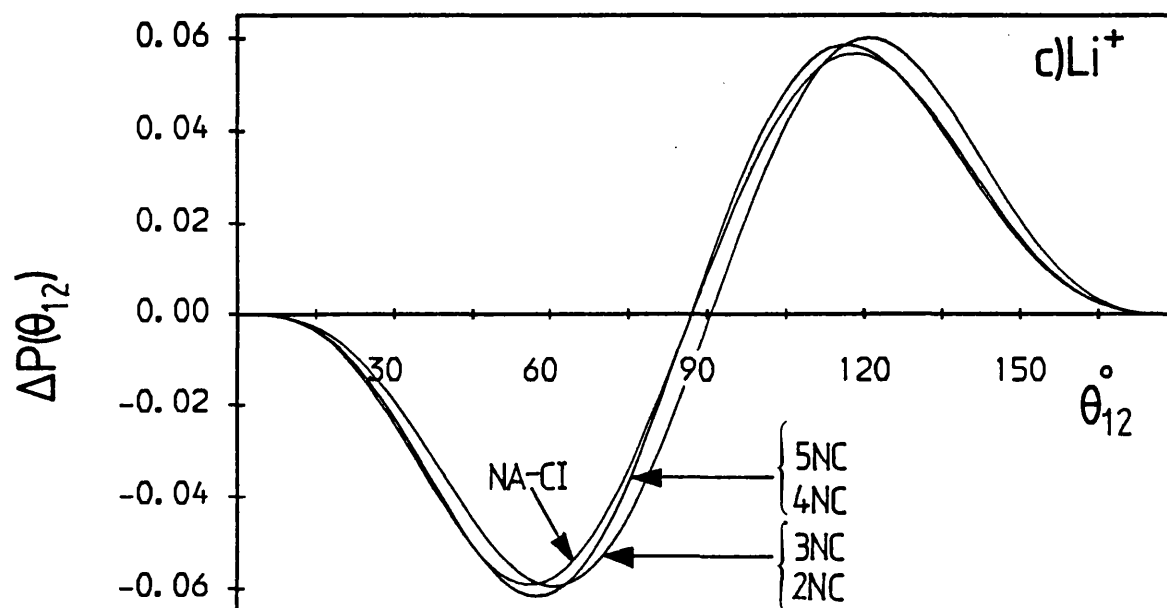


Figure II.23 c) & d)

The angular holes $\Delta P(\theta_{12})$ for c) Li^+ and d) Be^{++} . In each case the 2NC, 3NC, 4NC, 5NC and NA-CI wavefunctions are used as the correlated descriptions.

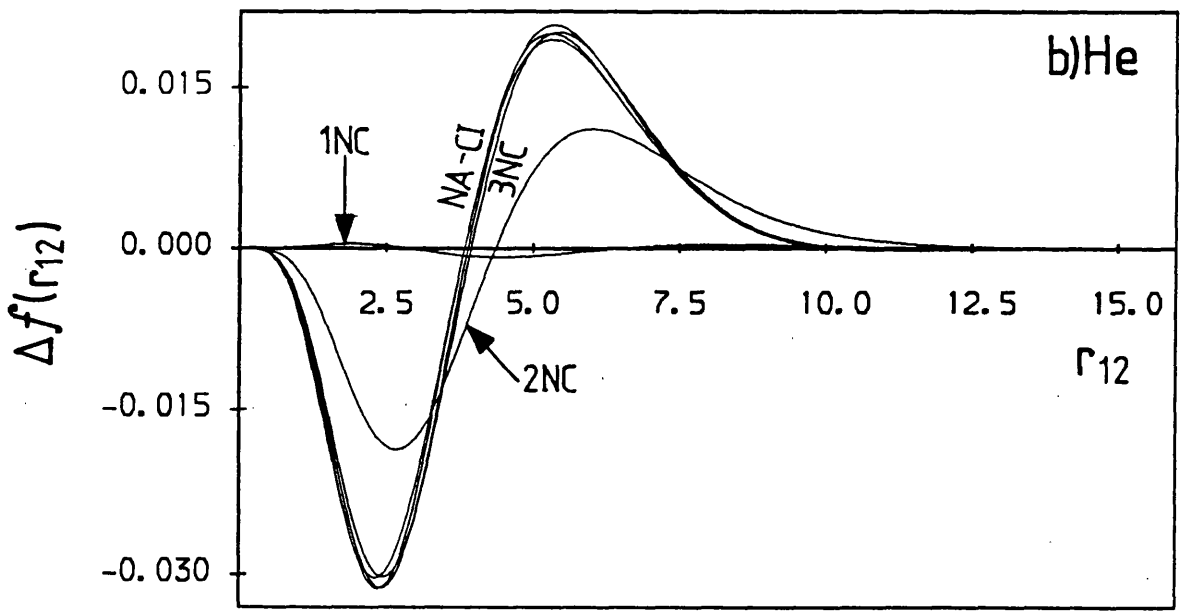
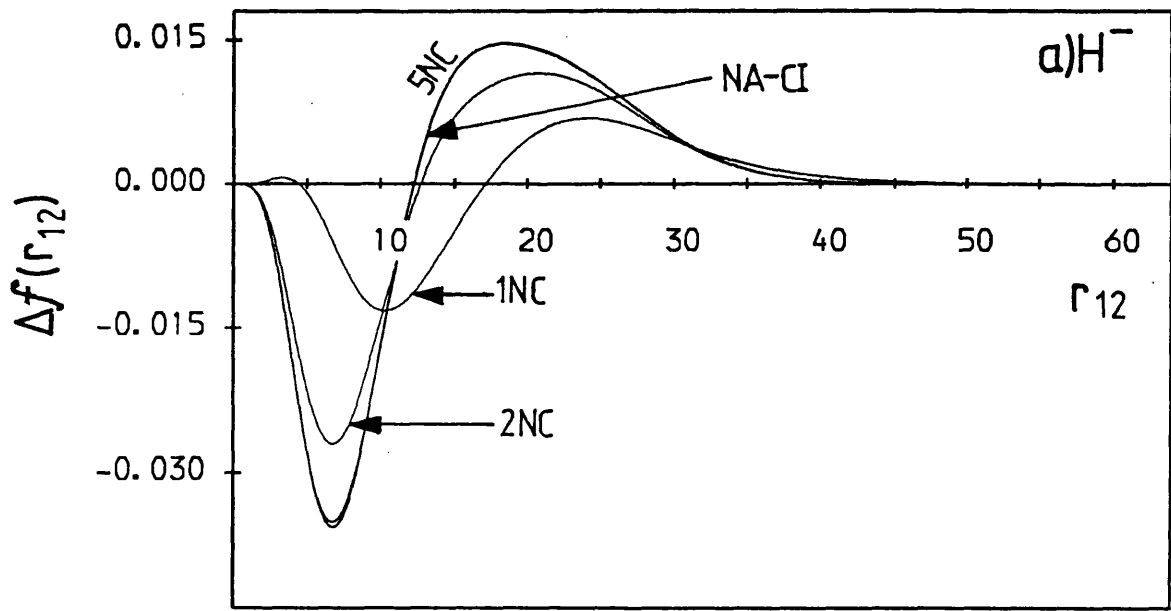


Figure II.24 a) & b)

The Coulomb holes $\Delta f(r_{12})$ for a) H^- and b) He. In each case the 1NC, 2NC, 3NC, 4NC, 5NC and NA-CI wavefunctions are used as the correlated descriptions.

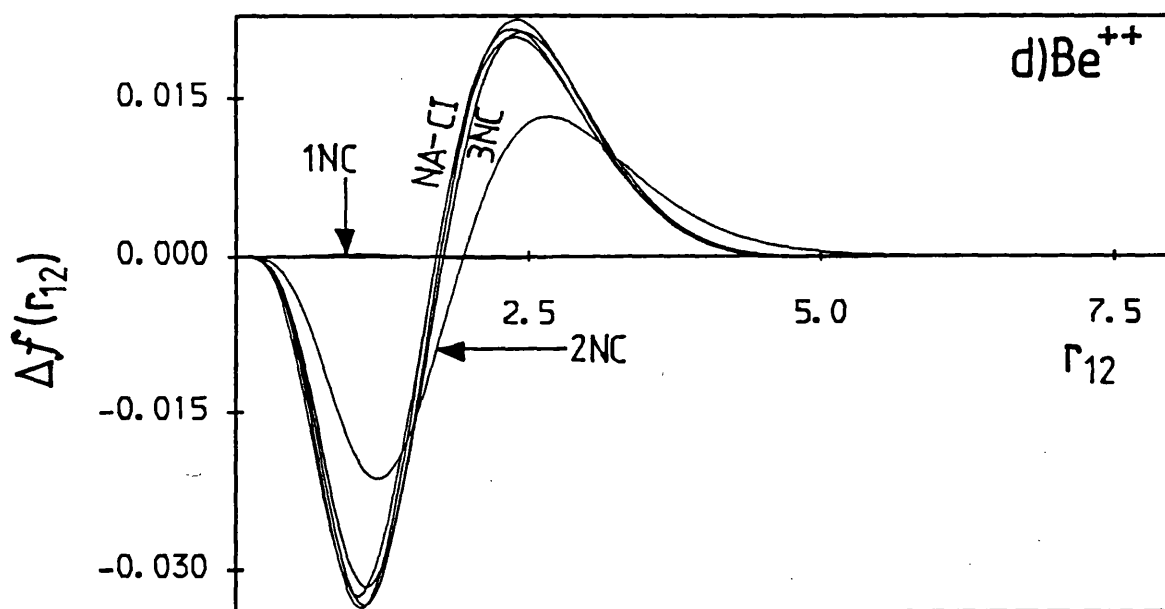
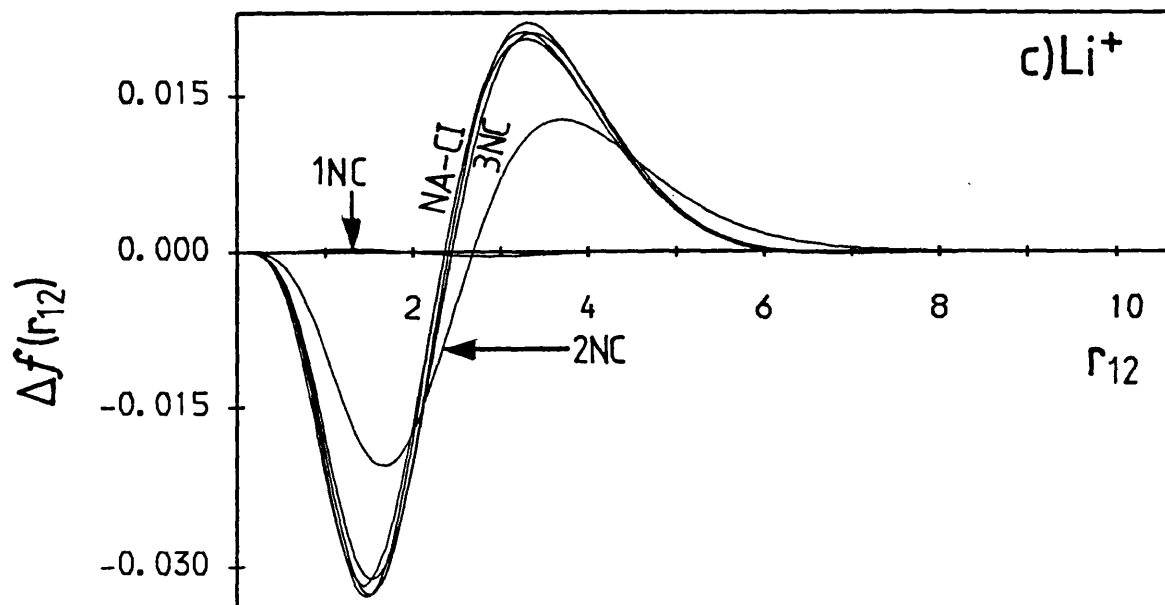


Figure II.24 c) & d)

The Coulomb holes $\Delta f(r_{12})$ for c) Li^+ and d) Be^{++} . In each case the 1NC, 2NC, 3NC, 4NC, 5NC and NA-CI wavefunctions are used as the correlated descriptions.

H^-

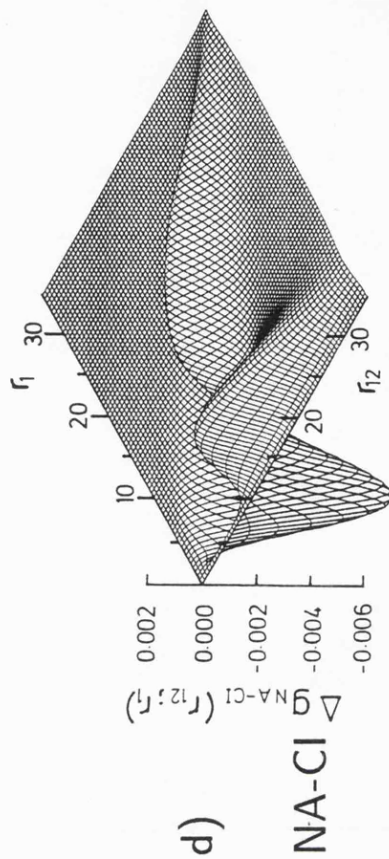
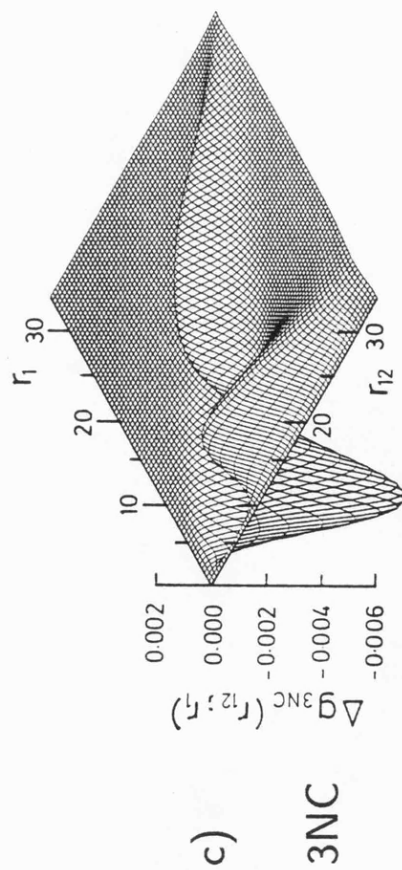
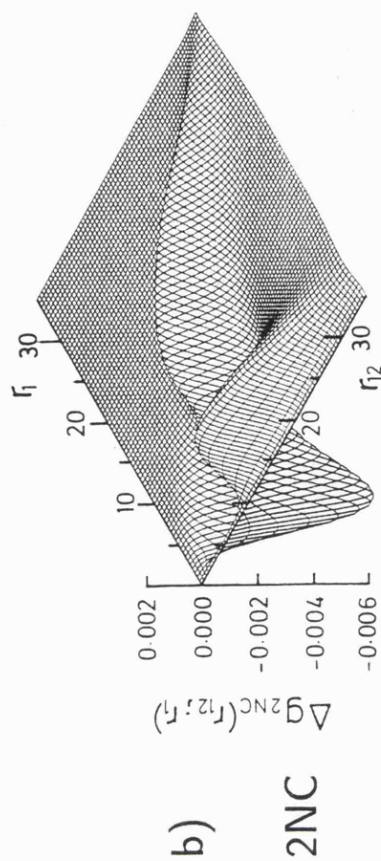
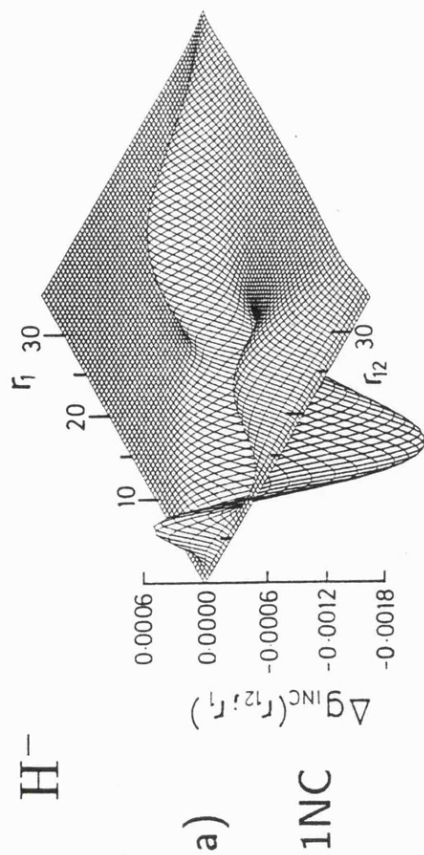


Figure II.25

The partial Coulomb holes $\Delta g(r_{12}; r_1)$ for the H^- system using the a) 1NC, b) 2NC, c) 3NC and d) NA-CI wavefunctions for the correlated descriptions. Note the different vertical scale employed in a).

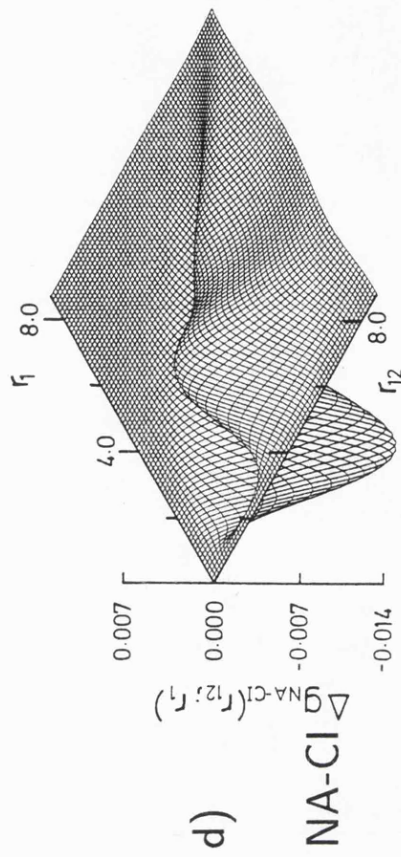
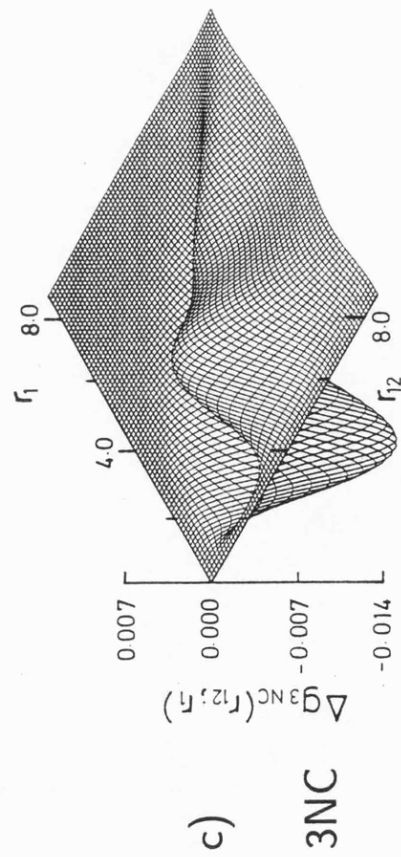
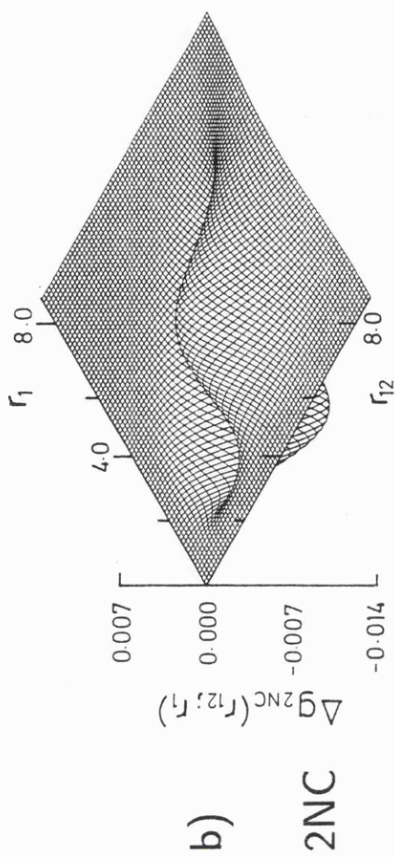
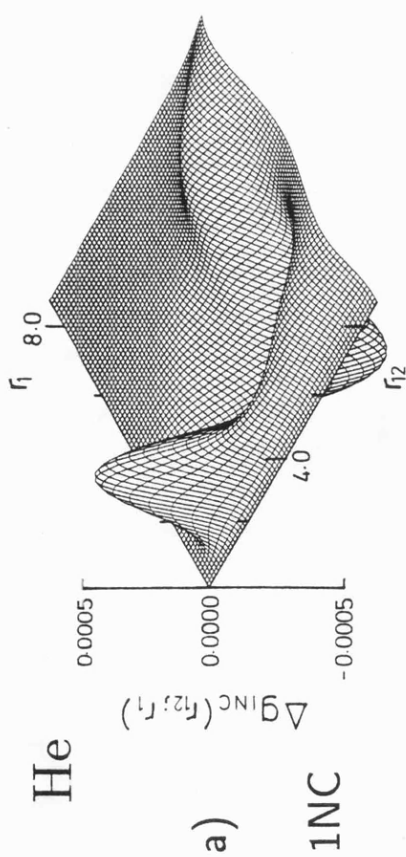


Figure II.26

The partial Coulomb holes $\Delta g(r_{12}, r_1)$ for the He system using the a) 1NC, b) 2NC, c) 3NC and d) NA-CI wavefunctions for the correlated descriptions. Note the different vertical scale employed in a).

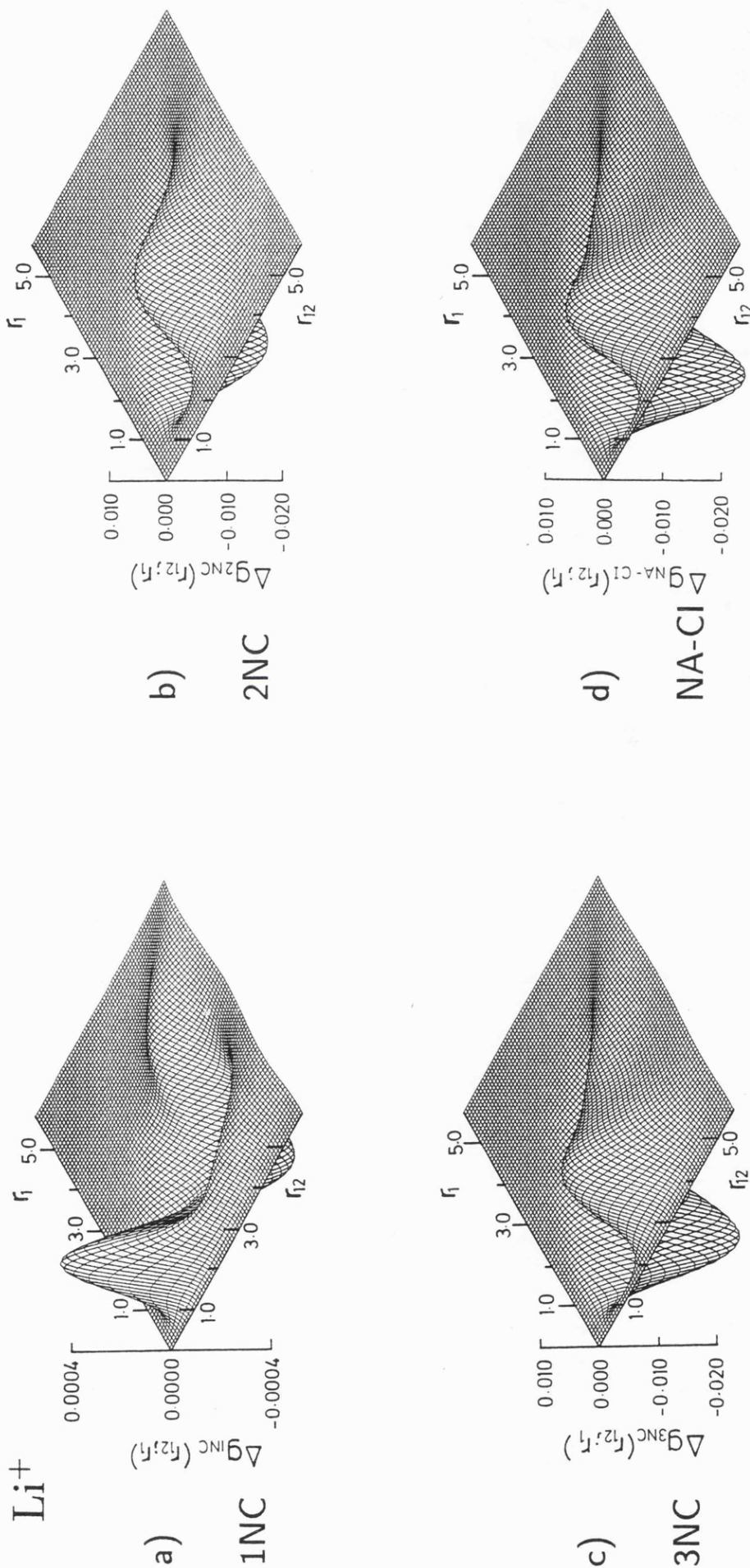


Figure II.27

The partial Coulomb holes $\Delta g(r_{12}; r_1)$ for the Li^+ system using the a) 1NC, b) 2NC, c) 3NC and d) NA-CI wavefunctions for the correlated descriptions. Note the different vertical scale employed in a).

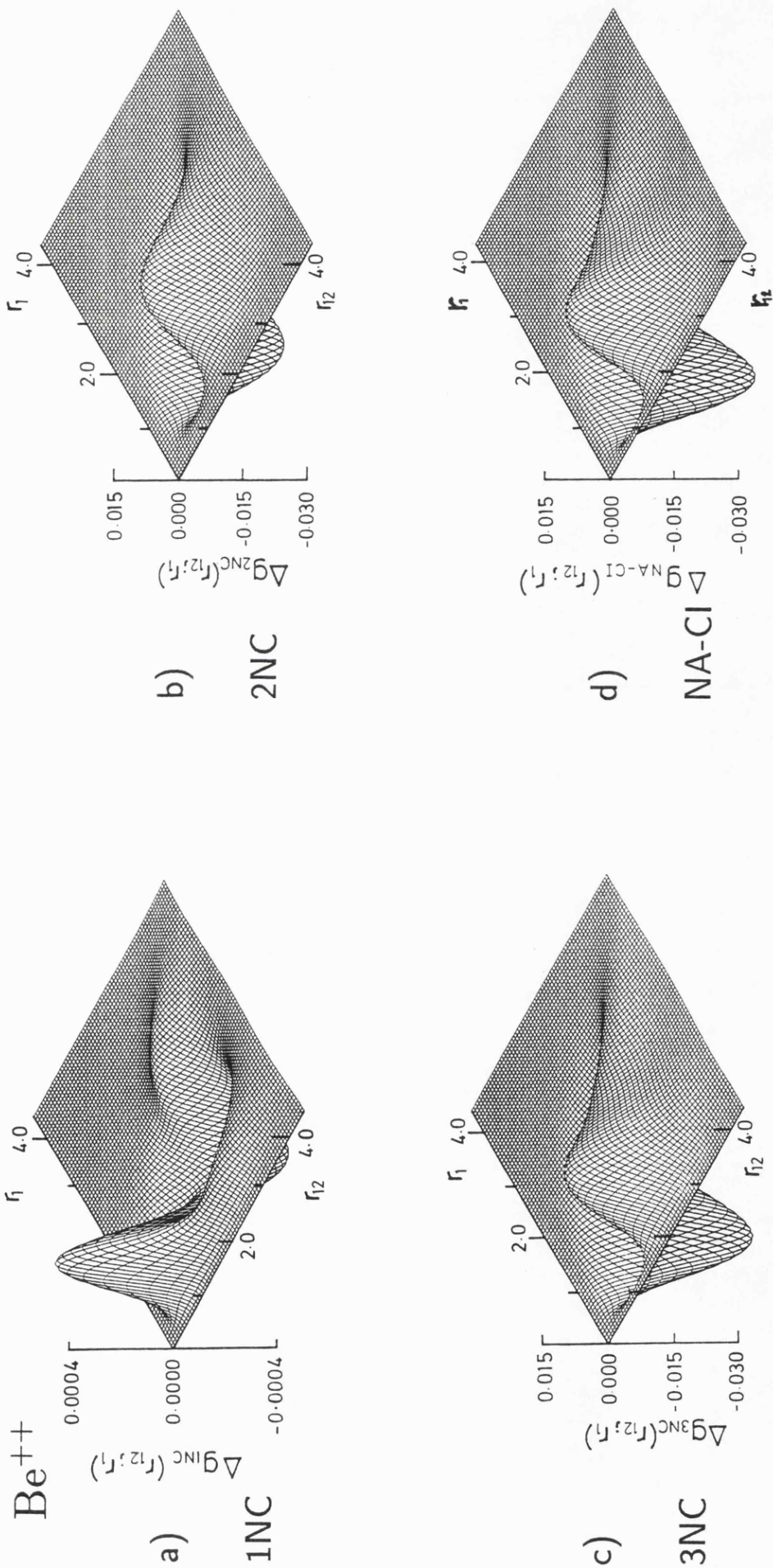


Figure II.28

The partial Coulomb holes $\Delta g(r_{12}; r_1)$ for the Be^{++} system using the a) 1NC, b) 2NC, c) 3NC and d) NA-CI wavefunctions for the correlated descriptions. Note the different vertical scale employed in a).

Part III
Electron Correlation Effects
in Momentum Space

Chapter 7

Momentum Space

7.1 Introduction

In atomic and molecular quantum mechanical calculations it is usual for wavefunctions to be expressed as a function of the positions of the relevant particles. That is, they are evaluated and analysed in position space. However, it is possible to represent a wavefunction in terms of the *momenta* of the particles. In other words, one works in *momentum* space. These two approaches are equally valid. The magnitude and direction of the momentum of an electron are determined by the electron-nuclear and electron-electron forces, and thus an examination of momentum space properties should throw light on these interactions. The position space and momentum space descriptions of a system are linked in quantum mechanics via the Heisenberg uncertainty relations [159]. Although the vast majority of quantum mechanical investigations have been conducted in position space, in recent years there has been much interest in the study of wavefunctions in momentum space [42]. Of course, the concept of momentum space has been used extensively by solid-state physicists for many years [160].

The origin of the consideration of the momentum space properties of atoms and molecules stems from the discovery of the Compton effect, a phenomenon which was first properly understood in the 1920's [161,162]. In the Compton effect, electromagnetic radiation, usually X-rays, is scattered off a system. It is observed that the scattered

radiation is less energetic ('softer') than the incident radiation. This is owing to the exchange of momentum of the incoming photons with the electrons in the system. The reduction in energy of the scattered photons will obviously be reflected in an increase of their wavelength. It was soon noted [163,164] that the wavelength distribution of the scattered radiation was broadened, because the target electrons in an atom or molecule have non-zero momenta. The expression, in atomic units [2], giving the wavelength shift caused by Compton scattering is: [165]

$$\Delta\lambda = \lambda' - \lambda = \frac{4\pi}{c} \sin^2 \frac{\phi}{2} - \frac{2\lambda p_z}{c} \sin \frac{\phi}{2}, \quad (7.1)$$

where λ is the wavelength of the incident radiation, λ' is the wavelength of the scattered radiation, ϕ is the angle of scattering, c is the velocity of light and p_z is the component of the momentum of the electron off which the scattering takes place along the scattering vector. As p_z is not a constant, the second term in equation 7.1 introduces the observed broadening in the Compton-scattered line. Thus the intensity of the scattered radiation of a given wavelength at a given angle should be proportional to the probability that the scattering electron has a component of momentum p_z : this probability is called the directional Compton scattering profile. If the momentum distribution function of the electrons is given by $\rho(\underline{p}) = \rho(p_x, p_y, p_z)$, then the equation for the directional Compton scattering profile is:

$$J(p_z) = \int \int \rho(p_x, p_y, p_z) dp_x dp_y. \quad (7.2)$$

Consequently, observed Compton scattering profiles can give one experimental evidence relating to the momentum space distribution functions of systems.

Clearly it is of interest to compare calculated momentum space distribution functions with those obtained from experiments, and this provided the early impetus for *theoretical* momentum space studies. Momentum space wavefunctions for hydrogen-like systems were produced at a relatively early stage [166]. In 1941 and 1942 Coulson and Duncanson calculated momentum space wavefunctions for various molecular species, and came to various conclusions about the effect of bond formation on momentum distributions [167,168,169,170,171,172].

There are essentially two methods for the production of momentum space wavefunctions. The first is to produce the wavefunction *directly* in momentum space. This approach was followed by various workers in the 1940's and 1950's, in particular by Coulson and McWeeny [173,174,175]. These attempts were not particularly successful, however, and although some workers have persevered with this method [176], most momentum space work in recent years has used the second method.

This second approach consists of taking an already calculated position space wavefunction for the system in question and *transforming* it into a momentum space representation. This technique has obvious attractions, given the profusion of position space wavefunctions available for many atomic and molecular species. The transformation was described by Dirac [177], and is thus usually referred to as the Dirac transformation. It is, in fact, a Fourier transformation, and is given by:

$$\Psi(\underline{P}) = (2\pi)^{-\frac{3N}{2}} \int e^{-i\underline{P}\cdot\underline{R}} \Psi(\underline{R}) d\underline{R}, \quad (7.3)$$

where $\Psi(\underline{R})$ is the position space representation, $\Psi(\underline{P})$ is the momentum space counterpart, and N is the number of electrons.

Although comparison with experimental Compton profiles is an important reason for the study of momentum space wavefunctions, there are other motives for such investigations. In quantum chemistry, the main effort in determining properties and distribution functions is usually directed towards the outer, or valence, electrons, which largely determine the chemical properties of the species under consideration. Momentum space offers definite advantages for investigations of these electrons. This is because the Dirac transformation *inverts* the emphasis of the regions of density. In position space, the valence electron distribution is far from the nucleus, and is usually slowly-varying and diffuse, whereas in momentum space it is close to the origin, and sharply peaked, and is thus emphasized [178].

In molecular studies it is often difficult to decide where the position space origin should most appropriately be situated. In momentum space there is a unique origin, corresponding, naturally, to the electron having no momentum. In other words, a multi-centre distribution is turned into a single-centre distribution [179,142]. Recently, Cooper

has shown that this property makes momentum space ideally suited for examining the question of the similarity of different molecules [180].

Electron correlation effects in momentum space have been examined by various authors. The first was perhaps Weiss [181], who commented that as correlation should cause the electrons to speed up to avoid each other, this would be expected to result in an enhancement of the region of high momentum in the probability distribution. A similar conclusion may be reached by consideration of the virial theorem [182]. Unfortunately, it can also be argued that because a frequent effect of correlation in position space is to move probability *outwards*, the effect of the Dirac transformation should ensure that the inner regions of the momentum distribution are increased in magnitude.

In 1977, Banyard and Moore [123] examined the effect of correlation on momentum space distribution functions for the ground state of helium-like systems. They found that the high momentum region was indeed increased in magnitude. These workers also examined various statistical correlation coefficients, and discovered that although radial correlation effects were negative, as in position space, the angular correlation effects were *positive*. In other words, electron correlation tends to align the momentum vectors of the two electrons. On account of this they predicted that this opposing balance of positive and negative correlation should produce more complicated total correlation effects in momentum space than had been seen in position space.

When Banyard and Reed defined and evaluated the momentum space analogue of the Coulomb hole, (the Coulomb shift) [32], the complex form of the curves vindicated this prediction. A number of studies of correlation effects in momentum space in atoms have, for the most part, confirmed that angular correlation effects are positive [38,43,44,45]. In molecular systems the correlation effects may also be considered in terms of angular and radial correlation, owing to the single-centred nature of the momentum space distribution. Here too the different components tend to act in opposition [179,183].

Given that earlier momentum space correlation studies have proved so fruitful, it seemed natural to conduct such an investigation for the $2p^2\ ^3P$ state. This study will parallel and complement the earlier position space inquiry in Part II of this thesis.

It will clearly be most profitable to transform the position space wavefunctions used in Part II into momentum space. For wavefunctions comprising Slater-type orbitals it is relatively straightforward to apply the Dirac transformation, and hence we have converted the Hartree-Fock and NA-CI wavefunctions into the momentum space representation. But the presence of r_{12} -dependent terms renders the Hylleraas-type Drake wavefunctions extremely difficult to transform. Benesch and Thomas [184] concluded that, for wavefunctions containing odd powers of r_{12} , application of the Dirac transformation involves extensive numerical integration and that consequently explicitly-correlated wavefunctions are not suited to momentum space calculations. We have therefore decided not to conduct an analysis of the Drake wavefunctions in momentum space.

7.2 Wavefunctions

We must now consider how the Hartree-Fock (HF) and the Nicolaides and Aspromalllis configuration interaction (NA-CI) wavefunctions are transformed into momentum space. Both of these may ultimately be reduced to a combination of Slater-type orbitals (STO's), each of which may be written:

$$\phi_{nlm}^{STO}(r, \theta, \phi) = R_{nl}^{STO}(r)Y_l^m(\theta, \phi) = Nr^{n-1}e^{-\zeta r}Y_l^m(\theta, \phi), \quad (7.4)$$

where N is a normalization constant. It may be shown that [143] the Dirac transformation of this orbital is:

$$\phi_{nlm}^{STO}(p, \theta^p, \phi^p) = R_{nl}^{STO}(p)Y_l^m(\theta^p, \phi^p), \quad (7.5)$$

where,

$$R_{nl}^{STO}(p) = \sqrt{\frac{2}{\pi}}(-i)^l \int_0^\infty r^2 R_{nl}^{STO}(r) j_l(pr) dr, \quad (7.6)$$

where $j_l(pr)$ is a spherical Bessel function and p is the *radial* component of the momentum vector $|p\rangle$. The most significant point to be noted about equation 7.5 is that the form of the spherical harmonics is unchanged by the transformation. The super-

script, 'p', on the angular variables indicates that they refer to the orientation of the momentum vector.

In the case of the numerical Hartree-Fock wavefunction, $R_{nl}^{STO}(r)$ is replaced by a numerically-defined function. But equation 7.6 holds for all radial functions, and may be used to transform the numerical Hartree-Fock radial into momentum space. We did in fact carry out this transformation for the numerical functions, in order to assess how well our STO-fitted wavefunctions reproduced the momentum space properties (see Appendix A). Clearly, in this case the integration must be performed numerically; hence the resulting function is numerically defined. But the spherical Bessel function, $j_l(pr)$, can oscillate rapidly, and considerable care must be taken to establish the accuracy of such an integration.

For the STO's which occur in the analytic Hartree-Fock and NA-CI wavefunctions, it may be shown that equation 7.6 reduces to:

$$R_{nl}^{STO}(p) = (-1)^n N(2pa)^l l! \sqrt{\frac{2}{\pi}} \frac{\partial^{n-l}}{\partial \zeta^{n-l}} \left\{ \frac{1}{(\zeta^2 + p^2)^{l+1}} \right\}. \quad (7.7)$$

This expression has been evaluated and tabulated for many STO's [185].

There are several important differences between the position space and momentum space representations of STO's. While all position space STO's are real, it is clear from equation 7.7 that some momentum space STO's will be imaginary. Clearly this must be accounted for in our momentum space analysis. Additionally, this means that a momentum space radial function will *not* generally be equal to its complex conjugate, as is the case in position space.

In position space, the following important integral has a simple analytic solution:

$$\langle R_{nl}^{STO}(r) | r^k | R_{nl}^{STO}(r) \rangle = \int_0^\infty r^{2+k} R_{nl}^{STO*}(r) R_{nl}^{STO}(r) dr, \quad (7.8)$$

where k is an integer. In momentum space, however, the analogous quantity

$\langle R_{nl}^{STO}(p) | p^k | R_{nl}^{STO}(p) \rangle$ is not easy to evaluate analytically. For each system we have therefore evaluated these integrals numerically for all radial functions, and all necessary values of k. As this exercise is computationally time-consuming, and these integrals are required for a number of purposes, the results were calculated once and

stored. Parseval's theorem [186] implies that position space orthonormality properties are preserved when we transform into momentum space. This serves as a valuable check on our numerical integration procedures, if we take $k = 0$ in $\langle R_{nl}^{STO}(p) | p^k | R_{nl}^{STO}(p) \rangle$.

7.3 Evaluation of Correlation Properties

In momentum space we evaluate the same types of functions and quantities as in position space. We shall adopt here the convention that position and momentum space functions will be represented by the same notation, apart from the arguments. The fact that our wavefunctions may be transformed into momentum space orbital by orbital, combined with the invariant nature of the spherical harmonics in the transformation, makes it possible to adapt position space analysis for use in momentum space. In view of these comments, our discussion here will be briefer than was the case in position space. We use the term 'shift' rather than 'hole' to denote momentum space correlation difference functions.

Radial Functions and Properties

A simple momentum space function is the radial distribution function,

$$D(p_1) = \int \Psi^*(\mathbf{p}_1, \mathbf{p}_2) \Psi(\mathbf{p}_1, \mathbf{p}_2) \frac{d\tau_1^p \tau_2^p}{dp_1}, \quad (7.9)$$

where $d\tau_1^p \tau_2^p$ is the volume element of momentum space and \mathbf{p}_1 and \mathbf{p}_2 are the momenta of the two electrons. The corresponding radial shift is given by:

$$\Delta D(p_1) = D(p_1)_{CORR} - D(p_1)_{HF}. \quad (7.10)$$

The subscript, 'CORR', denotes a function produced using a correlated wavefunction and 'HF' denotes a function produced using the Hartree-Fock wavefunction. $D(p_1)$ will normalize to unity, providing a check on our calculations. We have calculated the quantity:

$$\Upsilon_{p_1} = \frac{1}{2} \int_0^\infty |\Delta D(p_1)| dp_1, \quad (7.11)$$

as an aid to the assessment of the magnitude of correlation effects. The expectation values,

$$\langle p_1^n \rangle = \int p_1^n \Psi^*(\underline{p}_1, \underline{p}_2) \Psi(\underline{p}_1, \underline{p}_2) d\tau_1^p \tau_2^p, \quad (7.12)$$

where $n = -2, -1, 0, +1, +2$, together with the standard deviation σ_{p_1} , have been evaluated in order to numerically characterize the shape of the $D(p_1)$ curves.

Some of these expectation values are related to quantities which are, in principle, experimentally measurable. $\langle p_1^2 \rangle$ is equal to the kinetic energy of the system. Taking the calculated value of $\langle p_1^2 \rangle$, together with our earlier position space results, it is possible to check that our results constitute an energy for the system which is the same as that quoted by the workers who originally produced the wavefunction:

$$E = \langle p_1^2 \rangle - 2Z \langle r_1^{-1} \rangle + \langle r_{12}^{-1} \rangle. \quad (7.13)$$

It can be demonstrated that $\langle p_1^{-1} \rangle$ is equal to the height of the spherically-averaged Compton profile [187], and for $0 \leq n \leq 4$ it is possible to show that [188]:

$$\langle p_1^n \rangle = (n+1) \int_0^\infty q^n J(q) dq, \quad (7.14)$$

where $J(q)$ is the spherically-averaged Compton profile.

The two-particle radial density is defined by:

$$D(p_1; p_2) = \int \Psi^*(\underline{p}_1, \underline{p}_2) \Psi(\underline{p}_1, \underline{p}_2) \frac{d\tau_1^p \tau_2^p}{dp_1 dp_2}, \quad (7.15)$$

and we form the related two-particle shift:

$$\Delta D(p_1; p_2) = D(p_1; p_2)_{CORR} - D(p_1; p_2)_{HF}. \quad (7.16)$$

These two-particle functions are related to the one-particle radial functions in the same manner as in position space. To describe these surfaces we have produced the expectation values:

$$\langle p_1^n p_2^n \rangle = \int p_1^n p_2^n \Psi^*(\underline{p}_1, \underline{p}_2) \Psi(\underline{p}_1, \underline{p}_2) d\tau_1^p \tau_2^p, \quad (7.17)$$

for $n = -2, -1, +1, +2$.

The Sinanoğlu expansion that was discussed in chapter 1 may be expressed equally well in momentum space. We will thus have momentum space 'f-functions', which

provide the correction to the momentum space Hartree-Fock orbital description. One of these will be given by:

$${}^{m=1}f(\underline{p}_1) = \frac{\langle \Psi(\underline{p}_1, \underline{p}_2) | {}^{m=0}\phi_{HF}(\underline{p}_2) \rangle}{\langle \Psi(\underline{p}_1, \underline{p}_2) | {}^{m=0}\phi_{HF}(\underline{p}_2) {}^{m=1}\phi_{HF}(\underline{p}_1) \rangle} {}^{m=1}\phi_{HF}(\underline{p}_1), \quad (7.18)$$

where ‘ ${}^{m=1}\phi_{HF}(\underline{p}_1)$ ’ and ‘ ${}^{m=0}\phi_{HF}(\underline{p}_2)$ ’ are the two Hartree-Fock orbitals. The radial part of this orbital correction is denoted by $f^{rad}(p_1)$, and this is the function that we have calculated and presented. In order to quantify the size of the effect of the correction functions, their norms were evaluated. These values are given by:

$$\|f(\underline{p}_1)\| = \sqrt{\langle f(\underline{p}_1) | f(\underline{p}_1) \rangle} = \sqrt{\int_0^\infty f^{rad}(p_1)^* f^{rad}(p_1) p_1^2 dp_1}. \quad (7.19)$$

It should be noted that $f^{rad}(p_1)$ is imaginary for the $2p^2\ ^3P$ state. We have not seen calculations of these kinds of momentum space functions and properties reported in the literature.

$f(p_{12})$ and Related Functions and Properties

As in position space, the interparticle distribution function is expected to be extremely informative concerning correlation effects. This function is defined by:

$$f(p_{12}) = \int \Psi^*(\underline{p}_1, \underline{p}_2) \Psi(\underline{p}_1, \underline{p}_2) \frac{d\tau_1^p \tau_2^p}{dp_{12}}, \quad (7.20)$$

where $p_{12} = |\underline{p}_2 - \underline{p}_1|$. We form the ‘Coulomb shift’ as follows:

$$\Delta f(p_{12}) = f(p_{12})_{CORR} - f(p_{12})_{HF}. \quad (7.21)$$

We employ the term ‘shift’ rather than ‘hole’ for momentum space correlation functions. This phraseology was first introduced by Banyard and Reed [32], when they defined and evaluated the Coulomb shift for the ground state of helium. Their reason for this was that their Coulomb shifts had a more complicated structure than did the corresponding position space Coulomb holes, and it is in fact questionable whether they can be termed ‘holes’. We have adopted this convention for all the momentum space correlation difference functions. The normalization of the $f(p_{12})$ function furnishes a necessary check on the correctness of the $f(p_{12})$ results.

The size of the Coulomb shift may be assessed by evaluating the $\Upsilon_{p_{12}}$ which is given by:

$$\Upsilon_{p_{12}} = \frac{1}{2} \int_0^\infty |\Delta f(p_{12})| dp_{12}. \quad (7.22)$$

We have calculated the expectation values,

$$\langle p_{12}^n \rangle = \int p_{12}^n \Psi^*(\underline{p}_1, \underline{p}_2) \Psi(\underline{p}_1, \underline{p}_2) d\tau_1^p \tau_2^p, \quad (7.23)$$

for $n = -2, -1, 0, +1, +2$, and also the standard deviation of the $f(p_{12})$ curve.

As in position space, it is useful to examine correlation effects at different values of the component of radial momentum, p_1 , and we have therefore evaluated the partial function:

$$g(p_{12}; p_1) = \int \Psi^*(\underline{p}_1, \underline{p}_2) \Psi(\underline{p}_1, \underline{p}_2) \frac{d\tau_1^p \tau_2^p}{dp_1 dp_{12}}, \quad (7.24)$$

from which the partial Coulomb shift is formed,

$$\Delta g(p_{12}; p_1) = g(p_{12}; p_1)_{CORR} - g(p_{12}; p_1)_{HF}. \quad (7.25)$$

Integration of this surface with respect to p_1 alone yields $\Delta f(p_{12})$, and integration with respect to p_{12} alone gives $\Delta D(p_1)$.

Interangular Functions and Properties

We can investigate the angular component of correlation in the same way as in position space. Here, the angle between the momentum vectors is denoted by γ . We define the interangular distribution function $P(\gamma)$ by:

$$P(\gamma) = \int \Psi^*(\underline{p}_1, \underline{p}_2) \Psi(\underline{p}_1, \underline{p}_2) \frac{d\tau_1^p \tau_2^p}{d\gamma}, \quad (7.26)$$

and then define the angular hole by:

$$\Delta P(\gamma) = P(\gamma)_{CORR} - P(\gamma)_{HF}. \quad (7.27)$$

The $P(\gamma)$ functions are normalized, and this provides another test of the correctness of the results. It is interesting to note that the $P(\gamma)$ function for the Hartree-Fock, one

natural configuration (1NC), (and for H^- the 2NC) wavefunctions has the same simple form as the position space function, $P(\theta_{12})$. That is,

$$P(\gamma)_{HF} = \frac{3}{4} \sin^3 \gamma. \quad (7.28)$$

Again, we have assessed the size of the angular shift by evaluating the upslon values,

$$\Upsilon_\gamma = \frac{1}{2} \int_0^\pi |\Delta P(\gamma)| d\gamma. \quad (7.29)$$

It is possible to investigate angular correlation effects in different radial regions by producing angularly-dependent expectation values,

$$\langle p_1^n p_2^n \cos \gamma \rangle = \int p_1^n p_2^n \cos \gamma \Psi^*(\mathbf{p}_1, \mathbf{p}_2) \Psi(\mathbf{p}_1, \mathbf{p}_2) d\tau_1^p \tau_2^p, \quad (7.30)$$

where we take $n = -1, 0, +1$. We have also evaluated the expectation value of γ ,

$$\langle \gamma \rangle = \int \gamma \Psi^*(\mathbf{p}_1, \mathbf{p}_2) \Psi(\mathbf{p}_1, \mathbf{p}_2) d\tau_1^p \tau_2^p. \quad (7.31)$$

Paralleling the position space results, for the wavefunctions where $P(\gamma)$ has the simple form of equation 7.28, the values for $\langle p_1^n p_2^n \cos \gamma \rangle$ are each equal to zero, and $\langle \gamma \rangle$ is equal to 90° . As in position space, it is possible to check the consistency of our results by confirming that they obey the cosine rule:

$$\langle p_{12}^2 \rangle = 2 \langle p_1^2 \rangle - 2 \langle p_1 p_2 \cos \gamma \rangle. \quad (7.32)$$

The $n = +1$ expectation value is of particular interest to us. It may be written in a slightly different form:

$$\langle p_1 p_2 \cos \gamma \rangle = \langle \mathbf{p}_1 \cdot \mathbf{p}_2 \rangle. \quad (7.33)$$

It can be shown [75,189] that $\langle \mathbf{p}_1 \cdot \mathbf{p}_2 \rangle$ is related in a simple manner to the mass-polarization correction for the total energy of the atom:

$$E_M = \frac{m}{M} \langle \mathbf{p}_1 \cdot \mathbf{p}_2 \rangle, \quad (7.34)$$

where m is the mass of the electron and M is the mass of the nucleus. Aashamar [75] and Bhatia [106] presented some theoretically-calculated values of E_M for the systems

under consideration in this thesis, and so we were able to calculate the corresponding values of $\langle p_1 \cdot p_2 \rangle$.

Correlation Coefficients

Statistical correlation coefficients may be defined in the same manner as in position space. The radial coefficients are given by:

$$\tau_p^{(n)} = \frac{\langle p_1^n p_2^n \rangle - \langle p_1^n \rangle^2}{\langle p_1^{2n} \rangle - \langle p_1^n \rangle^2}, \quad (7.35)$$

where we have taken $n = -1, 1$; and the angular coefficients by:

$$\tau_\gamma^{(n)} = \frac{\langle p_1^n p_2^n \cos \gamma \rangle}{\langle p_1^{2n} \rangle}, \quad (7.36)$$

where we have taken $n = -1, 0, +1$. Banyard and co-workers have used a different notation for these five quantities. The two nomenclatures are related as follows:

$$\tau_p^{(-1)} = \tau_{1/p} \quad (7.37)$$

$$\tau_p^{(+1)} = \tau_p \quad (7.38)$$

$$\tau_\gamma^{(-1)} = \tau_{\gamma'} \quad (7.39)$$

$$\tau_\gamma^{(0)} = \tau_{\gamma''} \quad (7.40)$$

$$\tau_\gamma^{(+1)} = \tau_\gamma \quad (7.41)$$

As in position space, the correlation coefficients for the Hartree-Fock and other single-determinant wavefunctions are identically equal to zero.

The results for the quantities and functions described in this chapter can be found in the tables and figures in chapter 9.

Chapter 8

Discussion of Momentum Space

Results

8.1 Introduction

The analysis of momentum space quantum mechanical results is frequently difficult in comparison to the analysis of corresponding position space results. This is because it is generally straightforward to visualize position space quantities and functions, whereas it is much harder to envisage the physical consequences of momentum space effects. It is therefore fortunate that the forms of the Hartree-Fock (HF) and Nicolaides and Aspromallis configuration interaction (NA-CI) wavefunctions are the same in both spaces. That is, in these cases the Dirac transformation is *isomorphic* in that it preserves the structure of the wavefunctions. As was described in chapter 7, the effect of this transformation is simply to change the form of the radial parts of the orbitals in the wavefunctions. This means that the coefficients which give the weight of each configuration in the wavefunction, C_i , are unchanged by the transformation, as are the structures of the configurations themselves. This implies that table II.10, which gives the coefficients and types of configurations for the position space natural expansions, also applies to the natural expansions of the wavefunctions in the momentum space representation.

The momentum space representation of the $2p^2\ ^3P$ state at the independent-particle

level is shown schematically in figure III.1. It has the same lobe form as the corresponding position space representation in figure II.1. This leads us to expect that many of the momentum space Hartree-Fock curves and surfaces will have the same shapes as their position space equivalents. In both spaces, the Hartree-Fock wavefunction has identical radial parts for each electron, the two orbitals differing only in their angular parts. This is the reason that figure II.1 and figure III.1 have the same basic shape.

In position space it was possible to account for correlation effects in relatively straightforward ways relating to the energy. The Coulomb holes clearly improved the energy for each system by reducing the magnitude of $\langle r_{12}^{-1} \rangle$. Subsidiary changes to the electron-nuclear energy could also be used to account for other correlation effects. In momentum space the only quantity directly related to the energy is $\langle p_1^2 \rangle$, which is equal to the total kinetic energy for each system. Because this is a single-particle expectation value, not intrinsically related to statistical correlation, it is to be expected that the Coulomb shifts, $\Delta f(p_{12})$, will be difficult to interpret in energetic terms.

Throughout this chapter we will compare our results to the corresponding position space results in order to further our understanding of how position space and momentum space correlation effects complement each other. Comparisons will also be made between these momentum space results for the $2p^2 \ ^3P$ state and previous momentum space results for the ground state of helium-like systems [32,123]. It will be of interest to discover whether the same parallels are found to occur in momentum space as were seen to occur in position space in chapter 5.

Because the explicitly-correlated Drake wavefunctions have not been transformed into momentum space, the full NA-CI wavefunctions are the best approximations to the exact non-relativistic momentum space representations for the systems under consideration available to us. Judging by the high percentage of the correlation energy recovered, the NA-CI wavefunctions should represent the momentum space properties well. However, we note that in position space the NA-CI wavefunction for H^- showed small but noticeable deviations from the energetically superior Drake wavefunctions for most curves and properties. But these deviations were never large enough to cause us

to interpret the correlation effects in H^- differently if the Drake wavefunctions had not been available. Thus the general form of the momentum space NA-CI properties for H^- should be accurate enough for our purposes.

Owing to the inverting effect of the Dirac transformation remarked upon in chapter 7, the Z -scaling convention used in position space is not appropriate here. Instead, where the horizontal axis is scaled, it is scaled by Z^{-1} . Where horizontal axes are not scaled, the ranges for the neutral and positive systems are the same when divided by Z . The range for H^- is half of this value.

In section 8.2 the total momentum space correlation effects are discussed. Z -dependent trends are analysed in section 8.3. The means by which the total correlation effects are built up are investigated by use of the natural expansion in section 8.4. It should be noted that this natural expansion analysis is indispensable for a full understanding of the total momentum space correlation effects. The main conclusions are briefly summarized in section 8.5.

8.2 Total Correlation Effects

Radial Results

The $D(p_1)$ curves for the Hartree-Fock wavefunctions, displayed in figure III.2, are similar in general form to the $D(r_1)$ curves. They possess a single maximum and are flat at small p_1 . Scaling by Z^{-1} in the horizontal direction and by Z in the vertical direction brings the curves into rough coincidence. The dashed curve denotes the limiting value of the curve given by an independent-particle $2p^2 \ ^3P$ wavefunction containing unoptimized hydrogenic radials. We note that the ordering of the curves is the reverse of that of the $D(r_1)$ curves. These features will be discussed in detail in section 8.3.

It can be seen that the radial shifts displayed in figure III.3 are also similar in form to the position space radial holes. In this section only the shifts for the full NA-CI wavefunctions are commented upon. In each case the effect of correlation is to depress the Hartree-Fock $D(p_1)$ curve in the vicinity of its peak, and increase the magnitude of the curve in the low- p_1 and high- p_1 regions. A consequence of the enhanced magnitude

at high- p_1 is an increase due to correlation in the magnitude in the energy-related $\langle p_1^2 \rangle$ expectation values shown in table III.1. As the Hartree-Fock and NA-CI wavefunctions each obey the virial theorem to a high level of accuracy, the change in this expectation value may be regarded as complementing the change in potential energy, calculated from position space expectation values. Because the Dirac transformation converts position space radial functions into momentum space radial functions, and $D(r_1)$ and $D(p_1)$ each comprise simple combinations of radial functions, it is not surprising that the $\Delta D(r_1)$ and $\Delta D(p_1)$ curves have a similar shape.

The H^- radial shift is much greater in magnitude than those for the other systems. The extremely large value of Υ_{p_1} for H^- displayed in table II.2 shows this. It is 12.9%, slightly larger than the corresponding NA-CI position space value of 10.3%. This large magnitude is an indication that momentum space radial correlation is much more important for H^- than the other systems. For the other systems Υ_{p_1} is between 1.58 and 1.89 times larger than the Υ_{r_1} value. The larger value of the momentum space correlation effect can be thought of as being due to the important role that the $\langle p_1^2 \rangle$ expectation value has in making up the total correlation energy. The change in the energy-related $\langle r_1^{-1} \rangle$ value due to correlation is, by comparison, much less important.

With only one exception, for the neutral and positive systems the $\langle p_1^n \rangle$ get larger for positive n and smaller for negative n when correlation is introduced—the same result has been reported for the ground state of He and Li^+ [143]. This is in contrast to position space, where *all* the expectation values $\langle r_1^n \rangle$ are larger at the correlated level than at the Hartree-Fock level. So it can be seen that the inward shift of density is less important in momentum space than in position space; this, again, is presumably because of the energetic importance of enhancing the high- p_1 regions. For H^- all the values increase in magnitude. The introduction of correlation causes every σ_{p_1} to become larger, as the form of the $\Delta D(p_1)$ curves would suggest. We expect the inward and outward movement of density to be a manifestation of statistical radial correlation, but to verify this it is necessary to consider the two-particle radial functions.

The Hartree-Fock $D(p_1; p_2)$ surfaces displayed in figure III.4 have the same shape

as the equivalent position space $D(r_1; r_2)$ surfaces. Figure III.5 shows the two-particle radial shifts, $\Delta D(p_1; p_2)$, calculated by using the NA-CI as the correlated wavefunctions. They also have the same shape as the corresponding $\Delta D(r_1; r_2)$ surfaces. In each of these diagrams probability is being moved from the region of the peak of the $D(p_1; p_2)$ surface, where $p_1 \sim p_2$, to areas where p_1 and p_2 have different values. Hence negative radial correlation is taking place, just as in position space. The ground state two-particle radial shifts for H^- He and Li^+ presented by Banyard and Reed [32] have the same shape as those just described, although they are somewhat more extensive in the p_1 and p_2 directions, in keeping with the greater compactness of the ground state in position space.

In addition, one can see that the introduction of correlation causes the expectation values $\langle p_1^n p_2^n \rangle$ shown in table III.3 to become smaller, with only one exception. This shows that radial correlation takes place at all values of the momentum, not just in the proximity of the deep minimum. The exception is the $\langle p_1^{-1} p_2^{-1} \rangle$ value for H^- , which shows an increase. In position space the $\langle r_1^n r_2^n \rangle$ values become smaller due to correlation, with the exception of $\langle r_1^{+1} r_2^{+1} \rangle$ and $\langle r_2^{+1} r_2^{+2} \rangle$ for H^- . Thus we can see that anomalous high- r_1 results correspond to anomalous low- p_1 results, in accordance with the previously discussed properties of the Dirac transformation. The $\langle p_1^n p_2^n \rangle$ values for the ground state of H^- He and Li^+ decrease in magnitude without exception as correlation is introduced [143].

The $\tau_p^{(n)}$ values provide a means of assessing the statistical correlation of the radial components of the momenta in a wavefunction. They can be seen in table III.4. For the Hartree-Fock wavefunction both $\tau_p^{(-1)}$ and $\tau_p^{(+1)}$ are identically equal to zero, as in the analogous position space cases. As one would expect from the form of the $\Delta D(p_1; p_2)$ surfaces, the coefficients for the NA-CI wavefunctions are all negative, just like the position space τ 's. In each system $\tau_p^{(-1)}$ is close to $\tau_r^{(-1)}$, and $\tau_p^{(+1)}$ is close to $\tau_r^{(+1)}$, the difference being typically $\sim 10\%$. So radial correlation is quantitatively as well as qualitatively similar in the two spaces. The radial coefficients for H^- are much larger than for the other systems— another indication of the great importance of radial

correlation in the negative ion. In both spaces radial correlation is generally greater in the high radial value region than in the low radial value region. It is interesting that the Dirac transformation does not invert this ordering. Banyard and Moore [123] have presented $\tau_p^{(-1)}$ and $\tau_p^{(+1)}$ values for the ground state of H^- , He and Li^+ . They are negative, but of a smaller magnitude than our $2p^2\ ^3P$ results. The ground state $\tau_p^{(+1)}$ values are only slightly smaller than the $\ ^3P$ results, but the $\tau_p^{(-1)}$ are less than half the magnitude of our coefficients. Therefore, momentum space radial correlation is larger in this doubly excited state than in the ground state.

Angular Results

With the nature of the radial correlation having been established, it is necessary to investigate angular correlation. We note again that $P(\gamma)$ for the Hartree-Fock wavefunctions is identical to the position space function $P(\theta_{12})$ for the Hartree-Fock wavefunctions (see figure II.6 and figure III.6). This corresponds to the fact that the independent-particle wavefunctions have the same form in both spaces. The angular shifts for the NA-CI wavefunctions displayed in figure III.7 are the reverse of the position space angular holes discussed in chapter 5. That is, electron correlation is decreasing the probability of γ being greater than 90° , and increasing the probability of it being less than 90° . Clearly the effect of angular correlation is to tend to *align* the momentum vectors of the two electrons, in contrast to position space where the effect is to increase the angle, θ_{12} , between the position vectors. This positive angular correlation effect has also been observed in momentum space correlation studies of the ground state of H^- , He and Li^+ and in some singly excited states of He [43,123].

The $\langle p_1^n p_2^n \cos \gamma \rangle$ and $\langle \gamma \rangle$ values in table III.5 give more detailed information regarding the angular correlation effects. The enhanced alignment of the momentum vectors causes $\langle \gamma \rangle$ to become *less* than 90° . All $\langle p_1^n p_2^n \cos \gamma \rangle$ at the NA-CI level are positive, demonstrating that the positive correlation occurs in all radial regions of momentum. Naturally, these results are unlike those in position space, where the angular correlation is of a negative character. For H^- and He, $\langle p_1^{-1} p_2^{-1} \cos \gamma \rangle$ is larger than

$\langle \cos \gamma \rangle$ which is larger than $\langle p_1^{+1} p_2^{+1} \cos \gamma \rangle$, whereas for Li^+ and Be^{++} this ordering is reversed. This can be attributed to the increased diffuseness of the momentum space representation as Z increases. A similar change in ordering exists for the ground state results [123]. The values of $\langle p_1^{+1} p_2^{+1} \cos \gamma \rangle$ derived from Aashamar's [75] and Bhatia's [106] mass-polarization correction results will be discussed in section 8.4.

In table III.4 the angular statistical correlation coefficients, $\tau_\gamma^{(n)}$, give a measure of angular correlation unbiased by the amount of distribution present in each radial momentum region. With the exception of H^- , $\tau_\gamma^{-1} < \tau_\gamma^0 < \tau_\gamma^{+1}$. The ratios between the three angular coefficients for each system, apart from H^- , are remarkably similar in value: $\frac{\tau_\gamma^{(+1)}}{\tau_\gamma^{(-1)}}$ is equal to 1.90 in each case; $\frac{\tau_\gamma^{(+1)}}{\tau_\gamma^{(0)}}$ ranges from 1.01 for He to 1.06 for Be^{++} . Similar regularities may be observed in the ground state τ 's, although they are not so striking. The $\tau_\gamma^{(n)}$ themselves are smaller in the ground state than in the $2p^2 \ ^3P$ state, showing that electron correlation is indeed more important in this doubly excited state. The ratio $\frac{\tau_\gamma^{(+1)}}{\tau_\gamma^{(0)}}$ is 4.26 in H^- , 1.85 in He, 1.66 in Li^+ and 1.59 in Be^{++} , indicating that radial correlation becomes relatively less important as Z increases.

We have in table III.4 also presented a result for He due to Krause, Morgan and Berry [64]. They quote the quantity $\frac{\langle \underline{p}_1 \cdot \underline{p}_2 \rangle}{\langle T \rangle}$, where T is the kinetic energy of the system. This is the same quantity as our statistical correlation coefficient $\tau_\gamma^{(+1)}$, although these authors do not refer to it as such. Its value is quite similar to our result for the NA-CI wavefunction.

Krause et al. use their 'floppy molecule' model of doubly excited atomic states (mentioned in chapter 2) to predict the sign of $\langle \underline{p}_1 \cdot \underline{p}_2 \rangle$ for various doubly excited two-electron states. This model assigns one unit of 'quantum bending vibration' to the $2p^2 \ ^3P$ state of He. In the 'floppy molecule' scheme the two-electron atom is thought of as being similar to a linear triatomic molecule. Krause and co-workers present a pictorial classical representation of the $2p^2 \ ^3P$ of the He atom, which we reproduce in figure III.8. The two electrons and the nucleus are collinear, with the nucleus in the middle. The unit of bending vibration is represented as the electrons moving in phase perpendicular to the line of the 'molecule', and it is on this basis that the positive value

of $\langle \underline{p}_1 \cdot \underline{p}_2 \rangle$ is predicted. The correctness of this prediction for the $2p^2 \ ^3P$ state, and indeed for seven other doubly excited states mentioned in reference [64], is an impressive achievement of the molecular model. However, the collinear representation of the $2p^2 \ ^3P$ state does not sit easily with our finding that the average angle between the electrons is only slightly greater than 90° (see table II.7 in the position space results). This result was also noted by Ezra and Berry [65] in an earlier paper.

The positive angular correlation and the negative radial correlation in momentum space act in opposition to each other, in contrast to position space where the correlation effects worked in unison. As a consequence of this it is to be expected that the total momentum space correlation effects will be more complex than the corresponding total position space effects.

Interparticle Results

Scaled $f(p_{12})$ curves generated using the Hartree-Fock wavefunctions for the four systems, together with the $Z \rightarrow \infty$ limiting $f(p_{12})$ curve produced using an unoptimized hydrogenic independent-particle wavefunction, are shown in figure III.9. The flatness of the curves at small p_{12} is a consequence of the Fermi effect, which in momentum space prevents the momenta of the electrons, which have parallel spins, from being the same. The Z -dependent trends of these functions will be discussed in section 8.3. However, it is pertinent to note that although the general shape of the $f(p_{12})$ curves is similar to that of the $f(r_{12})$ curves, the extreme diffuseness of the $H^- f(r_{12})$ is not paralleled by any of the $f(p_{12})$ curves. The order of these scaled momentum space curves is reversed compared with the order of the position space curves.

As we predicted, the NA-CI Coulomb shifts do indeed have complex structures, which can be seen in figures III.10. The intricate nature of the correlation effects explains why we refer to Coulomb 'shifts' in momentum space, instead of the position space term, 'holes'. The shifts for the natural configuration wavefunctions, also displayed in these figures, will be found to provide additional interpretation of the total shifts in section 8.4. In each NA-CI shift there are negative regions at low- p_{12} and high- p_{12} and,

as is necessary to provide a total normalization of zero, a positive region at intermediate values of p_{12} . The negative radial correlation which was established by analysis of the $\Delta D(p_1; p_2)$ curves and the $\tau_p^{(n)}$ correlation coefficients would be expected to *decrease* the probability of the difference between the momenta having low values. On that account we attribute the small- p_{12} negative feature to the effect of radial correlation. Similarly, the reduction in probability at high- p_{12} due to correlation is explicable by the action of positive angular correlation in decreasing the magnitude of $P(\gamma)$ for $\gamma \geq 90^\circ$.

It is noticeable that the inner negative area in H^- is much larger than the outer negative area, whereas in the other systems this order is reversed. This distinction is reflected in the expectation values, $\langle p_{12}^n \rangle$, which can be seen in table III.6. For the neutral and positive systems the negative n values increase in magnitude under the influence of correlation, but the positive n values decrease. The reverse holds for H^- . This variation is, no doubt, due to the extremely large radial correlation effects present in H^- . In each case the standard deviation of the $f(p_{12})$ curve, $\sigma_{p_{12}}$, is reduced by the effect of correlation, indicating an overall 'sharpening-up' of the distribution.

Interestingly, the $\Upsilon_{p_{12}}$ values for each system are much less than the Υ_γ values. The $\frac{\Upsilon_\gamma}{\Upsilon_{p_{12}}}$ ratio is equal to 1.88 for H^- , and is more than 2.0 for the other systems. This presumably reflects the opposing nature of the two components of electron correlation in momentum space. An additional consequence of this opposition is seen in the fact that the $\Upsilon_{p_{12}}$ value is always less than the corresponding $\Upsilon_{r_{12}}$ value. For H^- , $\frac{\Upsilon_{p_{12}}}{\Upsilon_{r_{12}}} = 0.22$ and for the other systems lies in the range 0.4 – 0.5. A similar observation was made for the ground state [32], although in this case the fraction was about one-third.

The Coulomb shifts for the $2p^2 \ ^3P$ state are of a very similar shape to those for the ground state of H^- , He and Li^+ [32], apart from the absence in the $1s^2 \ ^1S$ state of the flatness of the curves at very small p_{12} values. This difference is because the spins of the electrons in the 1S ground state are anti-parallel and there is consequently no Fermi correlation. As expected, the $2p^2 \ ^3P$ shifts are more compact than those of the corresponding ground state systems. However, the ground state systems have somewhat smaller $\Upsilon_{p_{12}}$ values, being only about a third of the 3P values for He and Li^+ , and about

90% for H^- . In the position space discussion it was seen that the ground state $\Upsilon_{r_{12}}$ value for He was about 83% of the $2p^2\ ^3P$ value. The greater effects of electron correlation in this doubly excited state, compared to the ground state, are therefore seen to be more noticeable in momentum space than in position space.

The $g(p_{12}; p_1)$ Hartree-Fock surfaces seen in figure III.11 are very similar in shape to the position space Hartree-Fock $g(r_{12}; r_1)$ surfaces which are displayed in figure II.10. The distribution lies predominantly on the $p_{12} \geq p_1$ side of each diagram. As in position space, this shape can be explained in terms of the 'lobe' diagram shown in figure III.1. That is, if each lobe is considered to contain one electron, then the electron-origin-electron triangle will usually be approximately right-angled. Hence p_{12} will generally be larger than p_1 (or p_2). As in the analogous position space cases, Pythagoras' theorem was found to be approximately fulfilled by the peak values of p_{12} and p_1 . No $g(p_{12}; p_1)$ results have been reported for the ground state of helium-like systems, but for the lithium-like series the K-shell partial surfaces have been presented by Al-Bayati [129]. These surfaces describe the momentum space characteristics of two electrons each in the 1s state and should thus be similar to the missing ground state results. They have the same form as our results.

In contrast to the Hartree-Fock surfaces, the $\Delta g(p_{12}; p_1)$ surfaces, or 'partial shifts', are completely different from the position space $\Delta g(r_{12}; r_1)$ surfaces discussed in chapter 5. The $\Delta g(p_{12}; p_1)$ produced using the NA-CI wavefunctions are presented in figure III.12. In a similar manner to the $\Delta f(p_{12})$ curves, the complex shape of these surfaces illustrates the opposing effects of angular and radial correlation. We primarily use the partial Coulomb shifts to assess the characteristics of the change in the interelectronic distribution due to correlation at different magnitudes of the electronic momentum, p_1 . This is done by inspecting the variation of the surface with p_{12} for fixed p_1 .

At small values of p_1 the correlation is negative in character. That is, the cross-section is negative for small p_{12} and positive for large p_{12} . We consequently ascribe the correlation effects at low- p_1 principally to radial correlation. As p_1 increases the form

of the cross-section changes dramatically, so that the effect of correlation is positive. In other words, the probability at small p_{12} is increased, and the probability at large p_{12} is decreased. This effect is quite small in H^- , reflecting the dominant role of radial correlation in that system. Thus the balance has moved in favour of angular correlation at high- p_1 . The ground state surfaces of Banyard and Reed [32] for H^- , He and Li^+ are very similar in shape to our partial shifts, although they are somewhat more extended in the p_1 and p_{12} directions, as would be expected from the more diffuse nature of the ground state $\Delta f(p_{12})$ curves and $\Delta D(p_1; p_2)$ surfaces.

Support for our interpretation in terms of radial and angular correlation can be found by returning to the correlation coefficients in table III.4. As one moves from the $\tau_\gamma^{(-1)}$ value, which assesses angular correlation in the inner radial region to $\tau_\gamma^{(0)}$, and to $\tau_\gamma^{(+1)}$, which gauges angular correlation in the outer radial region, one finds a steady increase in magnitude for the neutral and positive systems. For H^- , $\tau_\gamma^{(+1)}$ is larger than $\tau_\gamma^{(-1)}$, although $\tau_\gamma^{(0)}$ is larger than either of these. Even though $\tau_p^{(+1)}$ is greater than $\tau_p^{(-1)}$ in each case, the increase is much smaller than for the angular τ values. Thus it is evident that the balance of the components of statistical correlation changes with the momentum in the manner that the partial Coulomb shifts indicate.

In spite of the fact that the surface for H^- is clearly of a different shape compared with those of the other three systems, it is interesting to note that this difference is of a quantitative rather than a qualitative nature. That is, the H^- surface is recognizably part of the same 'family' as the other three surfaces. This could not be said of the $\Delta g(r_{12}; r_1)$ surfaces discussed in chapter 5. It should be noted that the large magnitude of the $\Delta D(p_1)$ curve for H^- implies that for most fixed- p_1 slices of the partial shift there will be a large imbalance between the areas of the positive and negative parts of the cross-section. In the ground state the H^- shift also stands out from He and Li^+ .

It is also interesting that for H^- the position space partial Coulomb hole is quite similar in shape to the momentum space partial Coulomb shift. Doubtless this is attributable to the dominant role of radial correlation in both spaces. This means that the reversal of the nature of angular correlation has a much smaller effect in this system.

In this section it has been seen that whilst the radial component of correlation is negative, as is the case in position space, the angular component is positive, as opposed to the negative position space angular effect. The conflict between these two forms of correlation produced complicated total correlation effects, quite unlike those seen in position space, but which were nevertheless found to be quite comprehensible in terms of our understanding of the components of correlation themselves. Apart from the different *sign* of angular correlation in momentum space, the individual components of correlation in momentum space were found to be similar to their position space counterparts.

Where possible, the $2p^2\ ^3P$ results were compared with corresponding ground state momentum space results. In all cases the qualitative similarity was very great, although the 1S results were of a lower magnitude. We therefore conclude that the mechanisms of momentum space electron correlation are the same in both states, thus paralleling the position space findings. As in position space, we attribute the striking resemblance between the correlation effects in the two states to the double occupancy of the radial part of the independent-particle wavefunction—in this case the momentum space representation of the wavefunction. We note that the analysis of the truncated natural expansion Coulomb shifts and partial Coulomb shifts will prove to be extremely useful in the further interpretation of the NA-CI shifts discussed in section 8.4.

8.3 Z-Dependent Trends

The most important influence on the manner in which the Hartree-Fock properties, the correlation effects and hence the correlated description vary with the atomic number, Z , is the effect of the Dirac transformation. We commented upon this in chapter 7. The form of the Dirac transformation implies that a compact position space wavefunction will correspond to a diffuse momentum space representation and *vice versa*. In particular, this means that the ordering scheme in position space, whereby the higher the value of Z is in the $2p^2\ ^3P$ series, the more localized each function is, becomes reversed in momentum space. Consequently, where we have explicitly scaled curves the function has been plotted against the independent variable multiplied by Z^{-1} , in contrast to

position space where it was multiplied by Z . Where no overt scaling is employed, the ranges of the horizontal axes for a given function for He, Li^+ and Be^{++} , (excepting where these represent angular variables), multiplied by Z^{-1} are equal to a common value. The range for H^- is equal to one half of this common value, in keeping with the differing properties of the negative ion. We are dealing with total correlation effects in this section and so, again, all correlation properties and functions refer to those generated when using the NA-CI wavefunctions.

Radial Results

The momentum space radial distribution function, $D(p_1)$, for the Hartree-Fock wavefunctions is shown in figure III.2 and exemplifies the preceding comments concerning the relationship between the position space and momentum space representations. As well as being scaled by Z^{-1} in the horizontal direction, they are scaled by Z in the vertical direction, in order to bring the curves into rough coincidence and to preserve normalization. This approximate comparability between the scaled curves evinces the character of the Dirac transformation, in view of the corresponding similarity between the Z -scaled $D(r_1)$ functions. As Z increases from 1 to 4 the scaled curves become more diffuse, as opposed to the scaled position space Hartree-Fock curves, $D(r_1)$, which become more compact. The fact that the scaling used does not bring the $D(p_1)$ curves into exact coincidence illustrates the effects of electronic shielding of the nucleus. As one would expect, the $\langle p_1^n \rangle$ expectation values for the Hartree-Fock wavefunctions decrease with Z for negative n , but increase for positive n . Similarly, it is seen that σ_{p_1} increases with Z . The same is true for the correlated expectation values.

For comparison, a $D(p_1)$ curve generated by using an unoptimized hydrogenic-basis single-determinant $2p^2\ ^3P$ wavefunction is also included in figure III.2. Because the function $ZD(Z^{-1}p_1)$ is found not to vary with Z for this wavefunction, this curve represents a limiting value where no interelectronic interaction of any kind is present. It is evident that as $Z \rightarrow \infty$ the $D(p_1)$ curve, scaled as in figure III.2, will tend to this limiting value as the interelectronic force becomes a negligible addition to the electron-nuclear force.

The beginnings of this process can be seen here: the curve for Li^+ is closer to the curve for Be^{++} than the curve for He. These trends are similar, although in the opposite direction, to those in position space.

The nodes of the $\Delta D(p_1)$ curves for He, Li^+ and Be^{++} almost coincide when plotted against Z^{-1} , as is evident from figure III.13. This agreement is rather better than was seen for the nodes of the scaled position space $\Delta D(r_1)$ curves for these systems. The H^- curve has not been included in this plot, owing to its extremely large magnitude. But it can be seen from figure III.3.a that the nodes of the $\Delta D(p_1)$ for H^- are reasonably close to those for the other systems, in contrast to position space where the outer node of the $\text{H}^- \Delta D(r_1)$ curve bears no relation to the outer nodes for the other systems. Therefore, although the radial shift for H^- is quantitatively quite different from the other shifts, due to the dominant nature of radial correlation and the large size of the f-orbital correction in H^- , (to be discussed in section 8.4), it is qualitatively somewhat similar. The Υ_{p_1} values decrease extremely rapidly as Z increases. This rapidity prevents a Z^2 scaling of the vertical axis from bringing the curves for the systems other than H^- into approximate coincidence, which would be the case if Υ_{p_1} was inversely proportional to Z .

It should be noted that the positive portion of these curves at low p_1 decreases relative to the size of the other positive region situated at large p_1 . This feature is not present in the analogous position space curves and we attribute it to a Z -dependent decrease in the importance of radial correlation at low values of the momenta compared to radial correlation at high momenta. The statistical correlation coefficients bear this out. The ratio of the 'outer' coefficient to the 'inner' coefficient, $\frac{r_p^{(+1)}}{r_p^{(-1)}}$ increases with the atomic number, and takes the values: 1.09, 1.25, 1.30 and 1.32 for H^- , He, Li^+ and Be^{++} respectively.

The $D(p_1; p_2)$ surfaces in figure III.4 scale in the expected fashion. The $p_1 (= p_2)$ values at the maxima are quite similar for the systems other than H^- , if they are multiplied by Z^{-1} . These numbers are 0.19, 0.28, 0.30 and 0.32 respectively for H^- , He, Li^+ and Be^{++} . Naturally the magnitudes of the maxima of the surfaces decrease

with Z . The variation in the two-particle holes is one of magnitude, rather than shape as is clear from figure III.5. The Z^{-1} scaled values of p_1 for the principal minima are for H^- , He, Li^+ and Be^{++} respectively, 0.20, 0.21, 0.23, and 0.24. Interestingly, the H^- surface fits well into the Z^{-1} scaling scheme, in contrast to position space, where the $H^- \Delta D(r_1; r_2)$ does not relate easily to the other surfaces. This is despite the difference between the $H^- D(p_1; p_2)$ and other $D(p_1; p_2)$ surfaces at the Hartree-Fock level that has just been noted. The actual magnitudes of the extrema of the two-particle shifts decrease particularly quickly with Z , corresponding to the reduction in radial correlation with increasing Z . In passing, we note that for both the Hartree-Fock and the NA-CI wavefunctions the $\langle p_1^n p_2^n \rangle$ for negative n values diminish with increasing Z , but there is an increase for positive n .

The radial correlation coefficients, $\tau_p^{(n)}$, become smaller as Z increases, thereby reflecting the reduction in the importance of correlation effects as the electron-nuclear force is increased. The $\tau_p^{(+1)}$ value is always somewhat larger than the $\tau_p^{(-1)}$. As we commented above, the ratio $\frac{\tau_p^{(+1)}}{\tau_p^{(-1)}}$ increases somewhat as Z goes from 1 to 4, indicating a shift in the region in which the radial correlation is most important.

Angular Results

Except that, of course, angular correlation effects are positive in momentum space in this state though they are negative in position space, the Z -trends of the angular shifts in figure III.7 are quite similar to those of the position space angular holes discussed in Part II, and displayed in figure II.7. When Z increases the magnitude of the $\Delta P(\gamma)$ curves and the Υ_γ values become smaller, thus manifesting the general decrease in the importance of correlation as Z increases. If the ordinate is scaled by Z , as in figure III.14, then the shifts for the neutral and positive systems are seen to be extremely close together, and of a substantially greater magnitude than the H^- curve. This demonstrates that angular correlation is relatively much less important in H^- than in the other systems. The near coincidence of these three curves corresponds to the Υ_γ values being almost exactly inversely proportional to Z . Similar effects were observed in

position space.

In table III.4 the angular correlation coefficients are seen to diminish in magnitude as Z increases, with one interesting exception. The H^- value of $\tau_\gamma^{(-1)}$ is slightly smaller than the value for He: this is an example of the secondary role that angular correlation plays in this system. The ratio $\frac{\tau_\gamma^{(+1)}}{\tau_\gamma^{(-1)}}$ is virtually constant for He, Li^+ and Be^{++} , being equal to 1.90, while for H^- it is 2.18. The ratio $\frac{\tau_\gamma^{(+1)}}{\tau_\gamma^{(0)}}$ is equal to 0.78, 1.01, 1.04 and 1.06 for H^- , He, Li^+ and Be^{++} respectively. The balance of angular correlation between the different momentum regions is therefore fairly stable for the systems other than H^- .

Interparticle Results

The $f(p_{12})$ curves produced using the Hartree-Fock wavefunctions are displayed in figure III.9 and are scaled in both directions in the manner of the $D(p_1)$ curves considered earlier in this section. The scaling brings the curves into very approximate coincidence, although the location of the maxima do not coincide. The fact that the curves are brought into rough and ready agreement shows that the gross Z -dependence of the interparticle momentum distribution is governed by the nature of Dirac transformation. That is, the unscaled $f(p_{12})$ functions become more diffuse as Z increases, whereas, in position space, the unscaled $f(r_{12})$ functions become more compact. As Z becomes bigger, the scaled $f(p_{12})$ curves become more expansive, again reversing the parallel scaled $f(r_{12})$ trend. Also included in the figure is the $f(p_{12})$ function produced using the same hydrogenic wavefunction mentioned with regard to the scaled $D(p_1)$ curves. Again, we regard this as a bare-nucleus limit: i.e. it represents the interelectronic distribution in the absence of any electron-electron interaction whatsoever. In view of this, the scaled Hartree-Fock $f(p_{12})$ should tend to this function as Z tends to infinity. This feature is illustrated in figure III.9. The two-particle expectation values exhibit trends in keeping with the gross effects of changing Z . For negative n , $\langle p_{12}^n \rangle$ becomes smaller as one goes up the isoelectronic series; positive n values and $\sigma_{p_{12}}$ increase.

Moving on to the Coulomb shifts, it can be seen that the scaling employed in figure III.15 produces a good agreement for the position of the nodes and for much of the

functions. The usual Z^{-1} scaling is employed for the horizontal axis, but the ordinate is scaled by the novel Z^2 factor. The combination of these scalings means that the areas of the curves, and hence the $\Upsilon_{p_{12}}$ values, are scaled by Z . The success of this scaling scheme corresponds to the $\Upsilon_{p_{12}}$ values being inversely proportional to Z . In position space the Coulomb holes were plotted against Zr_{12} , and this succeeded in bringing the curves into coincidence, with the exception of the H^- hole, which was much more extensive than the other scaled holes. The $\Upsilon_{r_{12}}$ value for H^- did not fit in with the results for the other systems, being very much larger than an inverse linear extrapolation from the three other upilon values would suggest. Once again, momentum space is found to be more appropriate than position space for the inclusion of the negative H^- ion in a scaled Z -series. The ground state Coulomb shifts were presented on a Z^{-1} scaled basis by Banyard and Reed [32] and this succeeded in bringing the nodes into good agreement. Although they plotted the function without any scaling of the vertical axis, it seems from the magnitude of the maxima of the reported curves that a Z^2 scaling of the same kind as that used here for the 3P state would produce a similar agreement in the 1S ground state.

It is apparent that the small- p_{12} negative region displays considerable variation with Z . Recalling that this feature is caused by radial correlation, it is to be expected that it would be large in the H^- system, where radial correlation is predominant. In fact, it dwarfs the large- p_{12} negative region in magnitude. As we proceed up the isoelectronic series, it is clear that the inner negative region becomes steadily smaller in relation to the rest of the curve. This demonstrates that radial correlation becomes less important relative to angular correlation as Z increases. This can also be seen in the typical ratio of angular and radial correlation coefficients, $\frac{\tau_p^{(+1)}}{\tau_r^{(0)}}$, which takes the values: 4.26, 1.85, 1.66 and 1.59 for H^- , He, Li^+ and Be^{++} respectively. A similar trend can be observed in the coefficients for the ground state shifts. It would be interesting to discover whether the trend whereby the relative importance of radial correlation decreases with Z is strong enough to eliminate completely the inner negative portion of the curve in the $Z=5$ system, B^{3+} .

This small- p_{12} Z -dependent trait can be used to explain the reduction in the relative magnitude of the small- p_1 positive region of the $\Delta D(p_1)$ curves. A small value of p_{12} will generally correspond to small values of p_1 , (and indeed p_2). It is therefore not surprising that a relative reduction in the effects of correlation at small- p_{12} should be accompanied by a reduction in the effects of correlation at small- p_1 .

The partial surfaces for the Hartree-Fock wavefunctions, which are shown in figure III.11 exhibit the kind of Z dependence which is now familiar. The values of $Z^{-1}p_{12}$ at which the maximum of $g(r_{12}; r_1)$ is found for H^- , He, Li^+ and Be^{++} are respectively: 0.26, 0.39, 0.43 and 0.45. At the maxima the values of $Z^{-1}p_1$ are 0.19, 0.28, 0.30 and 0.32—the numbers applying to the systems as before. It is obvious that H^- stands apart from the other species.

As expected, the partial shifts in figure III.12 display more Z -variation than the correlation surfaces that have been dealt with previously; that is, the $\Delta D(p_1; p_2)$ functions. The surfaces for the neutral and positive systems have a very similar shape on the scales used, although the two minima become more distinct as Z increases. The H^- surface is rather different from the others, with the low- p_1 positive feature being larger than the diagonal positive region—in contrast to the other systems. This is, no doubt, due to the greater relative importance of radial correlation, which determines the form of the partial shift at low momenta in the negative ion. In H^- the two minima present in the neutral and positive ions have merged into one minimum. It did not prove possible to connect the scaled location of the global maxima and minima to the variation in Z . Despite the substantial difference between the partial shifts for the negative ion and the other systems, all four surfaces recognizably belong to the same 'family'. This is in contrast to position space, where the partial Coulomb hole for H^- was not found to be comprehensible in the same terms as the results for the other systems.

In this section it has been evident that the H^- system stands apart from the other members of the $2p^2 \ ^3P$ series—an effect also present in position space. But in a variety of correlation difference functions it has emerged that the effects of correlation in the H^- ion can be encompassed within the general trends for the other systems in a manner

not possible in position space. The inability of the position space correlation study to do this was due to the extremely diffuse nature of the position space representation of the $2p^2 \ ^3P$ state of H^- . The effect of the Dirac transformation is to make the momentum space description of this system highly compact, but in a manner that clearly still allows Z-scaling to occur.

8.4 The Natural Expansions and the NA-CI Wavefunctions

At the beginning of this chapter it was noted that the isomorphic nature of the Dirac transformation results in the NA-CI wavefunctions having essentially the same structure in momentum space as they had in position space. Of course, this also applies to these wavefunctions when they are expressed as natural expansions. Specifically, the C_i^{NC} configuration coefficients and the spherical harmonics in each configuration are the same in each representation. As a consequence of this, table II.10, presented in the position space results section, chapter 6, applies to the momentum space natural expansions as well.

The properties of this particular natural expansion were discussed in some detail in section 5.5, but it is useful to recapitulate them briefly here. The wavefunction obtained by truncating the expansion to one natural configuration, (the '1NC' wavefunction), has an energy similar to the Hartree-Fock energy. The addition of subsequent configurations introduces the correlation energy in a well-ordered, highly convergent manner. The 3NC wavefunctions recover over 90% of the correlation energy in all cases. Each configuration has a specific angular character— 'p', 'd', 'h' etc. and also contains a different type of radial function. A configuration is termed 'angular', if a new type of angular function is introduced to the natural expansion on account of its inclusion, and 'radial' otherwise. As in position space, a so-called angular configuration may allow a small degree of radial correlation. For details of the energies for each truncation table II.1 and figure II.16 in the position space results section may be consulted.

In H^- , the second natural configuration (that is, the first correlating configuration) is radial in character, and has a large C_2^{NC} coefficient, whereas the third natural con-

figuration is angular. Thus, in *both* spaces the correlation effects in H^- are very large and radial effects are dominant. In the other systems, the second natural configuration is angular in nature, having a relatively small C_2^{NC} value, and the third configuration is radial. The ratio $\frac{C_2^{NC}}{C_3^{NC}}$ increases, proceeding from He to Be^{++} , thus demonstrating that angular correlation becomes more important with increasing atomic number in each representation.

Although, for each system, the first natural configuration has an associated energy quite close to the corresponding Hartree-Fock energy, some properties and functions in position space were found to show marked differences for the 1NC and Hartree-Fock wavefunctions. This was understood in terms of the Sinanoğlu f-corrections and the Brueckner orbitals. We now discuss the corresponding momentum space topics.

The f-Corrections and the First Natural Configuration

The $\Delta D(p_1)$ curves, using the truncated natural expansion wavefunctions and the full NA-CI wavefunctions, are shown in figure III.3. It is immediately evident that the $\Delta D(p_1)_{1NC}$ curves have a substantial magnitude relative to the curves for the NA-CI wavefunctions. In other words the $D(p_1)$ curves for the 1NC wavefunctions are somewhat different from those for the Hartree-Fock wavefunctions. A similar state of affairs held for the position space $\Delta D(r_1)_{1NC}$ functions.

Naturally, the Hartree-Fock and the 1NC wavefunctions each comprise only one determinant and the angular parts are the same for both cases. Therefore the disparity must lie in the radial parts of the wavefunctions. In fact, the first two momentum space natural orbitals are really the first two momentum space Brueckner orbitals. The radial part of the first Brueckner orbital is a good approximation to the Hartree-Fock radial function with the radial part of the Sinanoğlu f-correction added on and renormalized. Consequently, to explain the non-trivial magnitude of the $\Delta D(p_1)$ curves for the 1NC wavefunctions it is necessary to investigate the f-corrections in momentum space.

The Sinanoğlu expansion is customarily used to represent the position space wavefunction, in the manner described in chapter 1. Although the functions contained within

it are generally regarded as being functions of the *positions* of the particles there is no reason why they should not be taken as being functions of *momenta*. The radial part, $f^{rad}(p_1)$, of the momentum space orbital correction functions which appear in this expression is presented for each system in figure III.16. It is interesting that they are pure imaginary functions, whilst the $f^{rad}(r_1)$ functions were real. This is appropriate, because the momentum space Hartree-Fock radial function (of 2p character) is also pure imaginary. The $f^{rad}(p_1)$ functions are negative at small and large values of p_1 , and this might be thought strange, considering that the f-function represents the difference between the 1NC radial function and the Hartree-Fock radial function and that the $\Delta D(p_1)_{1NC}$ is positive in these regions. But there is no contradiction, because the momentum space representation of the Hartree-Fock radial function is in fact always negative.

We have evaluated the norms of the $f(p_1)$ functions, $\|f(p_1)\|$, and as anticipated they were found to be equal to the position space $\|f(r_1)\|$ values shown in table II.11. So the inadequacies of the Hartree-Fock radial description are of the same magnitude in both spaces from the point of view of the orbital correction functions. The size of the $\|f(p_1)\|$ decreases rapidly as Z increases, a result which is in keeping with our earlier finding that the Hartree-Fock wavefunction tends to the correct wavefunction as one moves up the isoelectronic series.

The first Brueckner configuration (i.e. the 1NC wavefunction) constitutes the best single-determinant approximation to the exact wavefunction in terms of the overlap values. This explains the form of the $\Delta D(p_1)_{1NC}$ curves; their defining characteristic is their closeness to the $\Delta D(p_1)$ for the NA-CI wavefunctions. The overlaps between the 1NC wavefunctions and the NA-CI wavefunctions are the same in both representations and were given in section 5.5.

It is important to emphasize that the large relative magnitudes of the 1NC $\Delta D(p_1)$ curves are not in any sense effects of correlation in a direct way. The energy of the 1NC wavefunctions is inferior to those of the Hartree-Fock wavefunctions, so there is no *electron* correlation (i.e. in the sense of Löwdin [6]). All the 1NC statistical τ values presented in table III.4 are identically equal to zero, as is the case for the Hartree-

Fock wavefunctions. Therefore the addition of the orbital correction functions to the Hartree-Fock orbitals does not provide any *statistical* correlation either.

We can see why the form of the radial shifts for these uncorrelated wavefunctions is so similar to the form of the NA-CI radial shifts, especially in H^- . The NA-CI radial shift is the single-particle consequence of the radial correlation effects seen in the two-particle radial shifts, but is not in itself actually exhibiting statistical correlation effects. Thus the best overlap condition causes the $\Delta D(p_1)$ curves for the 1NC wavefunctions to *mimic* the single-particle side effects of electron correlation. We would therefore expect the two-particle correlation functions generally to have small magnitudes for the 1NC wavefunctions. In position space this was found to be so, with the exception of the $\Delta f(r_{12})$ for the H^- system.

Radial Results

The 2NC radial shifts lie somewhat closer to the NA-CI curves than do the 1NC shifts for most values of p_1 . This is especially true for the high- p_1 regions for each system. In H^- , the 2NC $\Delta D(p_1)$ curve is very close to the NA-CI shift, an understandable result in view of the radial nature of the second configuration in H^- . For He, Li^+ and Be^{++} the improvement in the radial description by the second configuration, which is of an angular nature, is less easy to comprehend. The $\langle p_1^n \rangle$ and σ_{p_1} values for the 2NC wavefunctions for these systems are all closer to the NA-CI values than the 1NC values are. In position space the analogous 2NC curves tended to be further away from the NA-CI result than were the 1NC functions. But in position space, the only energy-related expectation value associated with these curves was the $\langle r_1^{-1} \rangle$ value—which provided only a small proportion of the total potential energy. In momentum space, the $\langle p_1^2 \rangle$ expectation value is equal to the total kinetic energy and is almost equal in magnitude to the total energy, by virtue of the near fulfillment of the virial theorem for the 2NC wavefunctions. Consequently, it is very important in the composition of the total energy for these wavefunctions. So the chief effect in all four systems of the improvement of the 2NC $\Delta D(p_1)$ over the 1NC $\Delta D(p_1)$ is greatly to improve the description of the kinetic

energy—a result in keeping with the $\sim 60 - 70\%$ of the correlation energy recovered by these wavefunctions.

From the point of view of statistical correlation the introduction of the second, angular, configuration in the neutral and positive systems produces very small, positive $\tau_p^{(n)}$ values, as in position space. In H^- the radial effect provided by the second configuration results in $\tau_p^{(n)}$ values of a slightly greater magnitude than the NA-CI coefficients. Clearly it is difficult to evaluate to what extent a radial shift is due to electron correlation or orbital correction.

Not surprisingly, the radial shifts for the 3NC wavefunctions are all very close to the NA-CI curves, an outcome similar to the corresponding position space results. This is because the 3NC wavefunctions recover over 90% of the correlation energy. It is important to remember that, with the exception of H^- , the magnitudes of the radial shifts are small compared with the Coulomb shifts, as illustrated by the relative size of the Υ_{p_1} and $\Upsilon_{p_{12}}$ values. Therefore, quite large changes in the $\Delta D(p_1)$ relative to the *total* NA-CI shift may have only a very small effect on the $\Delta f(p_{12})$.

The two-particle radial shifts displayed using various truncations of the natural expansions for the four systems in figures III.17-20 are more directly related to correlation effects than the functions that have just been discussed. We begin with the results for He, Li^+ and Be^{++} . The $\Delta D(p_1; p_2)$ surfaces for the 1NC wavefunctions represent the effect of the f-correction functions on the Hartree-Fock $D(p_1; p_2)$ results, and are, of course, statistically uncorrelated as well as being lacking in electron correlation. The 1NC shifts for these systems each have very small magnitudes compared to the NA-CI surfaces. This accords with the $\tau_p^{(n)} = 0$ results for these wavefunctions which were noted earlier. But, obviously, this lack of statistical correlation does not mean that changes in the radial parts of an independent-particle wavefunction, (e.g. from Hartree-Fock to Brueckner), will have no effect on the joint probability of the two electrons having particular values of p_1 and p_2 . Otherwise these surfaces would be identically equal to zero at all points.

In the systems other than the negative ion the second natural configuration provides

an angular effect and consequently would not be expected to change the two-particle radial distribution appreciably. Therefore it is not surprising that the $\Delta D(p_1; p_2)_{2NC}$ surfaces are small in size, their extrema being of the same order of magnitude as those of the corresponding 1NC results. A similar finding was reported by Banyard and Reed [32] for the ground state momentum space results. This result verifies that the earlier attribution of an angular character to these configurations is essentially correct. It will be recalled that the introduction of the second configuration, of d character, does, in fact, allow a degree of additional radial correlation, because the radial part of a d orbital is different in character from the radial part of a p orbital, (the character of the first natural configuration). The small magnitude of these 2NC surfaces and the small positive radial τ values show that the effect of the d configuration is overwhelmingly angular. In position space the magnitudes of the $\Delta D(r_1; r_2)$ distributions for the 1NC and 2NC wavefunctions for these systems were also small.

It is evident that the 3NC surfaces are very close to the NA-CI surfaces in both magnitude and shape. This is due to the radial character of the third configuration in these systems. It has p character, and thus introduces no new angular function. The $\tau_p^{(n)}$ coefficients for the 3NC are very close to the NA-CI values. So, in these systems, one radial configuration (within the *natural expansion* representation) suffices to introduce almost all the radial correlation effects, as in position space.

The $\Delta D(p_1; p_2)$ surface for the 1NC wavefunction for the H^- ion is extremely large and has a shape completely different from the NA-CI shift. The large discrepancy between the 1NC and Hartree-Fock $D(p_1; p_2)$ surfaces reflects the extremely large difference between the $D(p_1)$ curves for these two single-determinant wavefunctions: the Υ_{p_1} value for the $\Delta D(p_1)_{1NC}$ radial shift is 10.3%. In particular, this discrepancy is due to the large size of the inner positive region of the $\Delta D(p_1)_{1NC}$ function. It must be remembered that, for the 1NC wavefunction, the $\tau_p^{(n)}$ correlation coefficients are equal to zero and that therefore the large magnitude of the $\Delta D(p_1; p_2)_{1NC}$ surface is a consequence of the single-particle radial properties of the HF and 1NC wavefunctions.

It is interesting that for H^- the position space two-particle hole, $\Delta D(r_1; r_2)$ for 1NC

(seen in figure II.19.a) is quite small compared with the corresponding NA-CI surface, despite the large size of the $\Delta D(r_1)_{1NC}$ curve. This may be understood by considering the relevant $\langle p_1^n p_2^n \rangle$ and $\langle r_1^n r_2^n \rangle$ expectation values. For the 1NC wavefunction, the $\langle p_1^{-2} p_2^{-2} \rangle$ and $\langle p_1^{-1} p_2^{-1} \rangle$ are gigantic compared with the Hartree-Fock and indeed even the NA-CI wavefunctions. This effect corresponds to the large positive region at low- p_1 and low- p_2 present in the $\Delta D(p_1; p_2)$ surface. In position space, the $\langle r_1^{+2} r_2^{+2} \rangle$ and $\langle r_1^{+1} r_2^{+1} \rangle$ values are similarly huge for the 1NC wavefunction. However, there are no large features at high- r_1 , high- r_2 on the $\Delta D(r_1; r_2)_{1NC}$ surface, and the massive expectation values must be caused by the surface having small positive values over extremely large regions of r_1 and r_2 . Examination of a contour plot for this surface reveals the existence of this spatially extensive positive region. The effect of the Dirac transformation is evidently to enfold this region into the massive positive feature seen in momentum space. It is interesting to note that for the $D(p_1; p_2)$ function the 1NC representation is in fact appreciably inferior to that of the Hartree-Fock wavefunction at many points. That is, the 1NC $D(p_1; p_2)$ surface is frequently further from the correlated NA-CI surface than is the Hartree-Fock surface.

The second natural configuration is radial for H^- , and as with the first introduction of radial correlation in the other systems it produces a $\Delta D(p_1; p_2)$ surface extremely similar to the NA-CI result. The same phenomenon was observed for the ground state. The third configuration is of an angular character, and so the 3NC $\Delta D(p_1; p_2)$ is very close to both the 2NC and NA-CI results. In all four systems $\Delta D(p_1; p_2)$ surfaces were generated using the 4NC and 5NC wavefunctions as the correlated descriptions, but these have not been displayed owing to their similarity to the NA-CI results.

Angular Results

Earlier in this section the comment was made that the angular part of every 1NC wavefunction is identical to that of the Hartree-Fock wavefunctions. The angular part of the 2NC representation of H^- is also of this common form, owing to the radial nature of this second natural configuration. This means that the corresponding $\tau_\gamma^{(n)}$ coefficients

are all identically equal to zero, as are the $\langle p_1^n p_2^n \cos \gamma \rangle$ expectation values. The $P(\gamma)$ functions for these wavefunctions are identical to the Hartree-Fock curve, with the consequence that there are no angular shifts in these cases.

As we observed in section 8.2, the total momentum space angular shifts, $\Delta P(\theta_{12})$, and the position space angular holes, $\Delta P(\gamma)$, have very similar appearances, apart, obviously, from the fact that the angular effect is negative in position space, but positive in momentum space. Different truncations of the natural expansion expressed in momentum space introduce differing amounts of angular correlation, as can be seen by inspecting figure III.21. The first angular configuration (the second NC in He, Li⁺ and Be⁺⁺, but the third in H⁻), reproduces the shape of the full angular shift very well. Similarly, the $\langle p_1^n p_2^n \cos \gamma \rangle$ and $\tau_\gamma^{(n)}$ values in these cases are close to the NA-CI values. Some overcorrelation can be observed in the τ 's corresponding to high values of the radial component of momentum. These phenomena were all seen in the analogous position space instances. It is interesting that in *both* spaces the overcorrelation occurs in the outer regions of the radial variable, (r_1 or p_1). This should caution us against an indiscriminate use of the Dirac transformation to predict behaviour in one space from known behaviour in the other.

The convergence properties of the angular shifts, $\Delta P(\gamma)$, subsequent to the addition of the first angular configuration, are broadly similar to the position space manner of convergence. The addition of a natural configuration conferring further angular correlation produces a small but significant change in the angular shift. A radial configuration produces only a miniscule change, as we would expect. But the NA-CI $\Delta P(\gamma)$ is barely distinguishable from the 5NC (or 4NC) shift, despite the inclusion of configurations of angular character, (g and h), not present in the 5NC wavefunction. So in momentum space the inclusion of three types of angular correlation, (p, d and f), is sufficient to represent the angular shift very accurately. In *position* space the additional angular correlation in the NA-CI wavefunction produced a noticeable difference between the NA-CI and 5NC angular holes.

The extremely small changes in the angular shifts due to the addition of radial con-

figurations tend to move the description closer to the original 2NC curve, whereas in position space the curves moved from the 2NC level to the NA-CI $\Delta P(\theta_{12})$ monotonically, except in H^- . This phenomenon is so small that it cannot be seen in the figures. Incidentally, it should be noted that the angular correlation coefficients do not converge in a monotonic fashion either. This demonstrates, again, that statistical correlation and electron correlation are different, and do not always order in the same way: this is a result that has been observed for many of the τ values dealt with in this thesis.

We have calculated values of $\langle p_1^{+1} p_2^{+1} \cos \gamma \rangle$ from the mass-polarization results of Aashamar [75], and Bhatia [106], and these are included in table III.5. Aashamar's results were calculated from wavefunctions obtained by means of perturbation theory, and the energies appear to be of the same level of accuracy as the NA-CI energies, with the exception of the H^- result, which is significantly more accurate than the NA-CI value. The mass-polarization values given by Bhatia were produced using highly accurate explicitly-correlated Hylleraas-type wavefunctions. His energy for H^- is second only in calibre to the result of Jáuregui and Bunge [86] for variational results, and the energy for He is the lowest variational result to date. The Aashamar results for the neutral and positive ions are extremely close to our NA-CI expectation values, while the result for H^- shows a significant deviation from our value, presumably owing to the relatively poor quality of the NA-CI energy for this system. The Bhatia results are roughly in accord with these values.

Interparticle Results

The ways in which the truncated natural expansions approach the full NA-CI level for the properties and functions that we have discussed so far in this section were comparable to the corresponding position space convergence properties. But these results were either single-particle or only measured one component of correlation. These behave in quite similar ways to their position space analogues, bearing in mind, of course, the *positive* effect of angular correlation in momentum space. The topics that will now be discussed concern the result of the interplay between radial and angular correlation. It

was seen in section 8.2 that these *total* effects of correlation, which are embodied in the total and partial Coulomb shifts, are radically different from the corresponding position space functions. Thus it might be expected that the natural expansion convergence will show some novel features for these interparticle curves and surfaces.

We return to figures III.10, where the Coulomb shifts for the NA-CI and NC wavefunctions are shown. Previously, the negative regions at high and low- p_{12} were attributed to the effects of positive angular and negative radial correlation respectively. The correlation character of each natural configuration allows the form of the $\Delta f(p_{12})$ functions to be investigated in more detail. The 1NC curves have very small magnitudes and Υ_{p_1} values, apart from the aberrant H^- shift which will be discussed presently. In the neutral and positive systems the effect of the f-corrections on the interparticle distribution is clearly small, in accord with the small magnitude of the $\Delta D(p_1; p_2)_{1NC}$ surfaces and the identically zero value of the $\Delta P(\gamma)_{1NC}$ functions. This is to be expected, as the 1NC functions contain no allowance for electron correlation in a direct manner.

We know that the second natural configuration, which bestows the initial correlation in each system, is radial in nature in H^- , but angular for the other systems. Each 2NC $\Delta f(p_{12})$ in these three cases is positive at small p_{12} , and negative for large p_{12} . In this way it may be seen that the angular configuration has the effect of reducing the difference between the momentum vectors: in these systems the $\langle p_{12}^n \rangle$ values are larger for 2NC wavefunctions than at the Hartree-Fock level for negative n , but smaller for positive n . Clearly, these results are a consequence of the augmented alignment of the momentum vectors caused by angular correlation and shown by the angular shifts and expectation values. It is apparent that the 2NC curves are very similar to the NA-CI curves for $Z^{-1}p_{12} \gtrsim 1.0$, showing that our earlier explanation of the negative outer regions in the NA-CI Coulomb shifts in terms of angular correlation was correct. The 2NC $\Delta f(p_{12})$ curve for H^- is different in form. The addition of negative radial correlation by the second natural configuration causes the Coulomb shift to have the shape of a typical position space Coulomb hole: negative at small- p_{12} and positive at large- p_{12} .

It is evident that the $\Delta f(p_{12})$ curves for the 3NC wavefunctions are all quite close to

the final NA-CI result—a consequence of the similar closeness of the functions considered earlier in this section which were evaluated by using these two types of wavefunctions. In the case of the He, Li⁺ and Be⁺⁺ systems the third natural configuration has a radial nature, whereas in H⁻ it introduces an angular type of correlation. In all four cases the kind of correlation associated with the third natural configuration *opposes* the correlation previously added by the second natural configuration. The primary effect in the positive and neutral systems, where this additional correlation is radial, is sharply to reduce the low- p_{12} positive region in size and to create the small negative feature in this region. This is a result in keeping with our earlier analysis of this depression in terms of a radial effect. As we commented in section 8.3, the declining relative size of this inner area as Z becomes larger demonstrates the increasing dominance of angular correlation over radial correlation. The angular effect of the third natural configuration for the H⁻ natural expansion introduces the small negative region at high- p_{12} . We note that the conflict between the first and second correlating configurations means that the Υ_{p_1} values for the 3NC wavefunctions are less than those for the 2NC level of description. In the ground state the results of Banyard and Reed [32] for the 2NC and 3NC Coulomb shifts for H⁻, He and Li⁺ are similar to those just discussed.

Interestingly, the convergence of the Coulomb shifts from 3NC to the NA-CI result is extremely erratic, with the exception of H⁻ where the magnitude of the depth of the large minimum orders in the same way as the energy. In contrast, the radii of the position space Coulomb holes converged monotonically, with the exception of H⁻.

The anomalous 1NC $\Delta f(p_{12})$ for H⁻ must now be discussed. It is clearly the result of the changes in the Hartree-Fock radial function engendered by the addition of the Sinanoğlu f -correction function. It was seen that the 1NC radial correlation difference functions for H⁻, $\Delta D(p_1)$ and $\Delta D(p_1; p_2)$, were also extremely large compared with the NA-CI results. The effect of the orbital correction in the single-particle radial shift is greatly to increase the magnitude at small values of p_1 . The consequence of this will obviously be to enhance the probability of small p_{12} . Indeed, the shape of the 1NC Coulomb shift is very similar to that of the radial shift for H⁻. As we increase either p_1

or p_{12} there is a large positive region, then a large negative region, then a small positive region. In fact, the same ordering holds for the other systems, but in these cases the 1NC Coulomb shifts are extremely small relative to the NA-CI curves. The reason that the H^- 1NC $\Delta f(p_{12})$ is so large in relation to the other 1NC $\Delta f(p_{12})$ functions is that the f-correction is so large in this system. This can be seen by inspecting the values of the norms of these functions, which are the same in both spaces, in table II.11. Also, the value of Υ_{p_1} for 1NC H^- is between 30 and 290 times the magnitude of the other 1NC epsilon values. An interesting perspective is gained by realising that the addition of the f-function to the H^- Hartree-Fock wavefunction actually makes the interparticle distribution much *worse* over almost the entire range of p_{12} —a similar phenomenon was observed with the two-particle radial shift, whereas in *position* space it made the Coulomb hole substantially closer to the NA-CI form. Hence, although the Brueckner wavefunctions are superior to the Hartree-Fock wavefunctions with respect to single-particle properties, they can be markedly inferior for some two-particle properties. In other words, the 1NC functions are further away from the NA-CI values than are the Hartree-Fock values.

In view of the previous discussion it is not surprising that the representation of the partial Coulomb shifts, $\Delta g(p_{12}; p_1)$, by the truncated natural expansion wavefunctions is also informative. These can be seen in figures III.22-25. The 1NC surfaces are very small for He, Li^+ and Be^{++} , in accordance with the small effect of the orbital corrections on interparticle properties in these systems. The very large size of this surface for the 1NC wavefunction for H^- and its gross inferiority to the Hartree-Fock description in the low (p_{12}, p_1) region are explicable on the same basis as the similar phenomena in the 1NC Coulomb shift and two-particle radial shift were understood.

The 2NC $\Delta g(p_{12}; p_1)$ for H^- is very similar to the NA-CI surface in both magnitude and form. This is because radial correlation is dominant in this system; the partial shift is thus essentially determined by radial effects, the majority of which are provided by the second configuration. The $\Delta g(p_{12}; p_1)_{2NC}$ functions for the other three systems are radically different in behaviour from the NA-CI surfaces. If we consider the shape of the

shift at a fixed value of p_1 we find that it is always positive in character, as one would expect from the angular nature of the second natural configuration. Thus the negative correlation feature at small p_1 , parallel to the p_{12} axis, seen in each of the NA-CI surfaces is indeed due to radial correlation, as we asserted in section 8.2. The comparison of the 2NC and NA-CI partial shifts shows particularly clearly that the balance between the two components of correlation is strongly dependent on the magnitude of p_1 . At low values of p_1 , the radial component of momentum of the test electron, radial correlation is dominant, whilst at large- p_1 regions the angular effects take precedence.

It is interesting that the minima of the 2NC surfaces are close to the positions of the outer minima in the $\Delta g(p_{12}; p_1)$ surfaces for the NA-CI descriptions. The two minima in the NA-CI surfaces for these three systems can thus be regarded as a superposition of the minimum arising from the angular effect, seen in the 2NC surfaces, and a minimum due to the effect of radial correlation. For all the systems the 3NC surfaces are very similar to the fully correlated NA-CI results, as one would expect from all the previous 3NC curves and surfaces. The 4NC and 5NC partial shifts are not visually distinguishable from the NA-CI surfaces, so we have not presented them.

In momentum space both forms of correlation are required to produce the qualitative features of the Coulomb and partial Coulomb shifts for He, Li⁺ and Be⁺⁺, whereas in position space the angular correlation effect of the second natural configuration was sufficient to produce most of the essential attributes of the $\Delta f(r_{12})$ curves and $\Delta g(r_{12}; r_1)$ surfaces. In this respect, therefore, radial correlation is more important in momentum space than in position space. For H⁻, only radial correlation is required—in either space. The ground state results of Banyard and Reed [32] for the 2NC and 3NC and fully-correlated surfaces for the first three members of the helium series are similar to the results just discussed.

8.5 Summary

Momentum space electron correlation effects in the $2p^2\ ^3P$ isoelectronic series for $Z=1-4$ were investigated by examining a wide variety of momentum space functions and ex-

pectation values for a range of correlated and uncorrelated wavefunctions. We found that, for these systems, the effects of radial correlation are negative in character, as in position space, whereas angular correlation effects are *positive* in nature, in contrast to position space, where they are negative. The conflict between the two components of correlation produced total effects which were both complex and informative. In particular, the partial Coulomb shifts enabled us to assess how the balance between radial and angular correlation was dependent on the value of p_1 for a test electron. It was found that radial correlation was more important at small values of p_1 , while angular effects became dominant at larger values. With the exception of the opposite natures of angular correlation in the two spaces, the forms of behaviour of the *individual* components of the correlation effects were found to be very similar in both representations.

As expected, the effect of the Dirac transformation was to reverse the way in which the range of the Hartree-Fock and correlation difference functions varied with the atomic number. As Z increased, the functions always become more extensive in the p_1 or p_{12} direction, in contrast to position space, where they become more compact. Owing to this phenomenon, it was found that scaling the non-angular abscissae by Z^{-1} was highly successful in bringing the results for different systems into approximate coincidence. Naturally, the magnitude of the correlation effects decreased with Z . In a similar manner to position space, it was evident that angular effects became more important relative to radial effects as the atomic number increased. The correlation effects for H^- were found to be extremely large and overwhelmingly radial in nature, again, as in position space. This meant that the curves and surfaces for the negative ion were rather different from those for the other systems. Interestingly, however, it was found that the enfolding nature of the Dirac transformation allowed the H^- results to be included within the isoelectronic series in a manner that was not possible for the extremely diffuse position space representation. It may therefore be that momentum space correlation studies will be found to be a valuable tool for the understanding of negative ions in general—especially with regard to their inclusion in isoelectronic ‘families’.

The truncated natural expansions were found to be particularly useful in under-

standing how the radial and angular components of correlation combine to produce the total effects. Without the natural expansion results it would have been difficult to comprehend the Coulomb shifts and partial Coulomb shifts for the NA-CI wavefunctions. It was found that the inclusion of one configuration of a radial character in a truncation produced the vast majority of the radial results and the same was found for angular-type configurations and angular effects. Thus, in the same way that was found in position space, the 3NC wavefunction provided an excellent approximation to the full NA-CI representation when judged on momentum space results. The properties of the momentum space Sinanoğlu f-correction were useful in coming to an understanding of the difference between certain facets of the Hartree-Fock and 1NC independent-particle approximations. This was particularly so for H^- , where the differences were sizable.

Throughout this chapter we have compared our results with those available for the ground state helium-like systems. In each case we found that the correlation effects in the two states were qualitatively identical. But the magnitude of the effects in the doubly excited state studied here was significantly larger than in the $1s^2 \ ^1S$ state: this effect was also seen in the position space study, but to a somewhat smaller degree. As in position space, we attribute this similarity between the ground state and doubly excited state to the fact that in both cases the radial parts of the momentum space representations of the orbitals are the same.

The current interest in doubly excited atomic states has generally concentrated on their highly correlated nature and emphasized the disparity between them and the ground state [56,64,65]. We have found, however, that the correlation behaviour of the $2p^2 \ ^3P$ state is comprehensible in the same terms as the ground state. Indeed, there is far more variation between the correlation effects in H^- and the effects in the neutral and positive systems studied in this thesis than between any of these 3P systems and its $1s^2 \ ^1S$ counterpart. However, it should be recognized that the correlation difference functions presented here assess only *Coulombic* correlation, because the Hartree-Fock functions which we used as the basis of our study contain Fermi correlation. In the light of this, it would be most interesting to examine the correlation effects in doubly

excited systems where where such Fermi correlation is not present. In particular, an investigation of the $2p^2 \ ^1S$ and $2p^2 \ ^1D$ states might prove to be especially illuminating. Because these are singlet states, the only correlation present is Coulombic in nature and so a study of the kind presented in this thesis would encompass the *entire* correlation effects.

Chapter 9

Momentum Space Results: Tables and Figures

9.1 Introduction

The presentation of the momentum space results is similar to that for the position space tables and figures. The Froese Fischer numerical Hartree-Fock wavefunction is abbreviated to 'HF-NUM', while the Hartree-Fock function with radial parts represented by a summation of Slater-type orbitals is referred to as: 'HF-STO'. It should be noted that *all* the graphical results where the Hartree-Fock wavefunctions are employed use the fitted functions. The Nicolaides and Aspromallis configuration interaction wavefunctions are denoted by the abbreviation, 'NA-CI'. A natural expansion truncated to, say, two configurations is called a '2NC' wavefunction.

Although, for each system, the 1NC wavefunctions include no correlation whatever, either statistical or in the energetic sense of Löwdin [6], it has been found convenient to call them 'correlated descriptions' in captions where a series of natural truncations are referred to.

There are some instances where curves are displayed which are too close together to be conveniently labelled individually. In these cases bracketed labels are used, with the ordering of the labels within each bracket denoting the physical ordering of the curves. Some examples of this usage may be seen in figure III.3.

9.2 Momentum Space Results: Tables

Wavefunction		$\langle p_1^{-2} \rangle$	$\langle p_1^{-1} \rangle$	$\langle p_1^{+1} \rangle$	$\langle p_1^{+2} \rangle$	σ_{p_1}
H ⁻	HF-NUM	31.710	4.7401	0.29109	0.11588	0.17650
	HF-STO	31.729	4.7417	0.29106	0.11587	0.17651
	1NC	42.338	5.3136	0.28434	0.11831	0.19354
	2NC	43.741	5.3624	0.28961	0.12483	0.20237
	3NC	43.104	5.3180	0.29144	0.12578	0.20208
	4NC	43.099	5.3175	0.29148	0.12580	0.20210
	5NC	43.099	5.3175	0.29147	0.12580	0.20210
	NA-CI	43.097	5.3173	0.29150	0.12584	0.20215
He	HF-NUM	3.7378	1.6982	0.74543	0.70141	0.38176
	HF-STO	3.7391	1.6983	0.74543	0.70141	0.38177
	1NC	3.7597	1.7013	0.74585	0.70371	0.38395
	2NC	3.7441	1.6975	0.74751	0.70650	0.38435
	3NC	3.7491	1.6974	0.74879	0.71002	0.38644
	4NC	3.7487	1.6973	0.74887	0.71019	0.38651
	5NC	3.7485	1.6973	0.74893	0.71035	0.38659
	NA-CI	3.7484	1.6972	0.74898	0.71051	0.38670
Li ⁺	HF-NUM	1.3964	1.0434	1.1983	1.7873	0.59265
	HF-STO	1.3964	1.0434	1.1983	1.7873	0.59266
	1NC	1.3980	1.0437	1.1988	1.7896	0.59378
	2NC	1.3955	1.0427	1.1999	1.7927	0.59410
	3NC	1.3960	1.0427	1.2006	1.7959	0.59531
	4NC	1.3959	1.0426	1.2007	1.7962	0.59537
	5NC	1.3959	1.0426	1.2008	1.7964	0.59544
	NA-CI	1.3959	1.0426	1.2008	1.7966	0.59553
Be ⁺⁺	HF-NUM	0.72526	0.75353	1.6511	3.3731	0.80431
	HF-STO	0.72525	0.75353	1.6511	3.3732	0.80433
	1NC	0.72545	0.75356	1.6515	3.3755	0.80506
	2NC	0.72473	0.75316	1.6524	3.3788	0.80531
	3NC	0.72487	0.75314	1.6529	3.3819	0.80616
	4NC	0.72484	0.75312	1.6530	3.3822	0.80621
	5NC	0.72483	0.75311	1.6530	3.3825	0.80627
	NA-CI	0.72482	0.75311	1.6530	3.3827	0.80635

Table III.1

The radial one-particle expectation values, $\langle p_1^n \rangle$, when $n = -2, -1, +1$ and $+2$; and the standard deviations, σ_{p_1} .

Wavefunction	T_{P_1} %	T_{γ} %	$T_{P_{12}}$ %
H ⁻ 1NC	10.1	0.00	5.91
2NC	13.2	0.00	6.92
3NC	12.9	8.74	4.52
4NC	12.9	8.65	4.55
5NC	12.9	8.65	4.61
NA-CI	12.9	8.62	4.58
He 1NC	0.316	0.00	0.197
2NC	0.361	6.19	3.22
3NC	0.575	6.09	2.52
4NC	0.582	6.04	2.47
5NC	0.585	6.05	2.31
NA-CI	0.587	6.01	2.35
Li ⁺ 1NC	0.0870	0.00	0.0607
2NC	0.126	4.16	2.26
3NC	0.195	4.13	1.80
4NC	0.199	4.11	1.74
5NC	0.201	4.11	1.66
NA-CI	0.203	4.09	1.69
Be ⁺⁺ 1NC	0.0343	0.00	0.0029
2NC	0.0665	3.13	1.73
3NC	0.0963	3.12	1.39
4NC	0.0992	3.11	1.35
5NC	0.100	3.12	1.29
NA-CI	0.102	3.10	1.31

Table III.2

The T_{P_1} , T_{γ} and $T_{P_{12}}$ values for the various correlated wavefunctions. They are respectively the percentages of the Hartree-Fock $D(p_1)$, $P(\gamma)$ and $f(p_{12})$ curves redistributed by the effects of correlation (see the comments in section 9.1 concerning the 1NC results).

Wavefunction	$\langle p_1^{-2} p_2^{-2} \rangle$	$\langle p_1^{-1} p_2^{-1} \rangle$	$\langle p_1^{+1} p_2^{+1} \rangle$	$\langle p_1^{+2} p_2^{+2} \rangle$	
H ⁻	HF-NUM	1005.5	22.468	0.084732	0.013429
	HF-STO	1006.7	22.484	0.084714	0.013426
	1NC	1792.5	28.235	0.080849	0.013997
	2NC	915.66	23.254	0.067425	0.0070479
	3NC	900.18	22.986	0.068983	0.0075014
	4NC	900.06	22.984	0.069013	0.0075156
	5NC	901.58	22.972	0.068972	0.0075094
	NA-CI	901.41	22.971	0.069044	0.0075801
He	HF-NUM	13.971	2.8839	0.55566	0.49197
	HF-STO	13.981	2.8843	0.55566	0.48235
	1NC	14.136	2.8943	0.55630	0.49521
	2NC	14.051	2.8834	0.55915	0.50019
	3NC	12.646	2.7992	0.54254	0.44017
	4NC	12.644	2.7989	0.54272	0.44064
	5NC	12.644	2.7990	0.54306	0.44236
	NA-CI	12.613	2.7985	0.54332	0.44243
Li ⁺	HF-NUM	1.9500	1.0888	1.4360	3.1943
	HF-STO	1.9500	1.0888	1.4360	3.1943
	1NC	1.9543	1.0894	1.4370	3.2026
	2NC	1.9493	1.0876	1.4402	3.2170
	3NC	1.8389	1.0700	1.4152	2.9873
	4NC	1.8387	1.0699	1.4155	2.9890
	5NC	1.8388	1.0700	1.4159	2.9944
	NA-CI	1.8351	1.0698	1.4162	2.9927
Be ⁺⁺	HF-NUM	0.52600	0.56781	2.7262	11.378
	HF-STO	0.52599	0.56781	2.7262	11.378
	1NC	0.52627	0.56785	2.7274	11.394
	2NC	0.52551	0.56734	2.7307	11.423
	3NC	0.50468	0.56099	2.6972	10.841
	4NC	0.50466	0.56097	2.6975	10.845
	5NC	0.50466	0.56097	2.6980	10.856
	NA-CI	0.50391	0.56089	2.6983	10.848

Table III.3

The two-particle radial expectation values, $\langle p_1^n p_2^n \rangle$, when $n = -2, -1, +1$ and $+2$.

Wavefunction	$\tau_p^{(-1)}$	$\tau_p^{(+1)}$	$\tau_\gamma^{(-1)}$	$\tau_\gamma^{(0)}$	$\tau_\gamma^{(+1)}$	
H ⁻	HF-NUM	0.0	0.0	0.0	0.0	0.0
	HF-STO	0.0	0.0	0.0	0.0	0.0
	1NC	0.0	0.0	0.0	0.0	0.0
	2NC	-0.3671	-0.4017	0.0	0.0	0.0
	3NC	-0.3572	-0.3907	+0.03302	+0.09286	+0.07366
	4NC	-0.3570	-0.3904	+0.03284	+0.09163	+0.07151
	5NC	-0.3578	-0.3914	+0.03285	+0.09163	+0.07153
	NA-CI	-0.3577	-0.3898	+0.03252	+0.09146	+0.07091
He	HF-NUM	0.0	0.0	0.0	0.0	0.0
	HF-STO	0.0	0.0	0.0	0.0	0.0
	1NC	0.0	0.0	0.0	0.0	0.0
	2NC	+0.00223	+0.00251	+0.03332	+0.06598	+0.07132
	3NC	-0.09460	-0.1214	+0.03310	+0.06492	+0.06740
	4NC	-0.09446	-0.1211	+0.03287	+0.06404	+0.06580
	5NC	-0.09412	-0.1193	+0.03397	+0.06408	+0.06517
	NA-CI Krause et al.	-	-	-	+0.06401	+0.06480
Li ⁺	HF-NUM	0.0	0.0	0.0	0.0	0.0
	HF-STO	0.0	0.0	0.0	0.0	0.0
	1NC	0.0	0.0	0.0	0.0	0.0
	2NC	+0.000976	+0.00116	+0.02320	+0.04440	+0.04832
	3NC	-0.05567	-0.07424	+0.02315	+0.04405	+0.04690
	4NC	-0.05559	-0.07405	+0.02302	+0.04360	+0.04608
	5NC	-0.05541	-0.07312	+0.02392	+0.04375	+0.04583
	NA-CI	-0.05592	-0.07261	+0.02397	+0.04371	+0.04563
Be ⁺⁺	HF-NUM	0.0	0.0	0.0	0.0	0.0
	HF-STO	0.0	0.0	0.0	0.0	0.0
	1NC	0.0	0.0	0.0	0.0	0.0
	2NC	+0.000539	+0.000655	+0.01770	+0.03340	+0.03639
	3NC	-0.03954	-0.05356	+0.01768	+0.03323	+0.03567
	4NC	-0.03949	-0.05344	+0.01761	+0.03295	+0.03519
	5NC	-0.03938	-0.05289	+0.01835	+0.03312	+0.03507
	NA-CI	-0.03984	-0.05265	+0.01840	+0.03310	+0.03495

Table III.4

The radial and angular correlation coefficients τ for various wavefunctions. See equations 7.35-36 for their definitions. Note that the Hartree-Fock and 1NC values are each identically equal to zero. The result for 'Krause et al' is taken from reference [64].

Wavefunction	$\langle p_1^{-1} p_2^{-1} \cos\gamma \rangle$	$\langle \cos\gamma \rangle$	$\langle p_1^{+1} p_2^{+1} \cos\gamma \rangle$	$\langle \gamma \rangle$	
H ⁻	HF-NUM	0.0	0.0	0.0	90.000
	HF-STO	0.0	0.0	0.0	90.000
	1NC	0.0	0.0	0.0	90.000
	2NC	0.0	0.0	0.0	90.000
	3NC	+1.4231	+0.092859	+0.0092641	84.124
	4NC	+1.4154	+0.091631	+0.0089969	84.207
	5NC	+1.4157	+0.091634	+0.0089987	84.207
	NA-CI	+1.4017	+0.091456	+0.0089228	84.217
	Aashamar	-	-	+0.00808	-
	Bhatia	-	-	+0.0074996	-
He	HF-NUM	0.0	0.0	0.0	90.000
	HF-STO	0.0	0.0	0.0	90.000
	1NC	0.0	0.0	0.0	90.000
	2NC	+0.12477	+0.065980	+0.050385	85.825
	3NC	+0.12411	+0.064920	+0.047856	85.892
	4NC	+0.12321	+0.064037	+0.046732	85.952
	5NC	+0.12733	+0.064085	+0.046293	85.949
	NA-CI	+0.12766	+0.064014	+0.046044	85.950
	Aashamar	-	-	+0.046046	-
	Bhatia	-	-	+0.045699	-
Li ⁺	HF-NUM	0.0	0.0	0.0	90.000
	HF-STO	0.0	0.0	0.0	90.000
	1NC	0.0	0.0	0.0	90.000
	2NC	+0.032377	+0.044401	+0.086627	87.190
	3NC	+0.032318	+0.044051	+0.084237	87.212
	4NC	+0.032135	+0.043595	+0.082778	87.243
	5NC	+0.033390	+0.043750	+0.082336	87.233
	NA-CI	+0.033461	+0.043715	+0.081987	87.233
	Aashamar	-	-	+0.081980	-
	Be ⁺⁺	HF-NUM	0.0	0.0	0.0
HF-STO		0.0	0.0	0.0	90.000
1NC		0.0	0.0	0.0	90.000
2NC		+0.012831	+0.033395	+0.12297	87.887
3NC		+0.012819	+0.033226	+0.12064	87.897
4NC		+0.012761	+0.032953	+0.11901	87.916
5NC		+0.013303	+0.033120	+0.11862	87.905
NA-CI		+0.013339	+0.033105	+0.11822	87.904
Aashamar		-	-	+0.11818	-

Table III.5

Values of $\langle p_1^n p_2^n \cos\gamma \rangle$ when $n = -1, 0$ and $+1$ and values of $\langle \gamma \rangle$. Note that for all systems the $\langle p_1^n p_2^n \cos\gamma \rangle$ are identically equal to zero for the Hartree-Fock and 1NC wavefunctions. The 'Aashamar' and 'Bhatia' values have been calculated from the mass-polarization corrections in reference [75] and reference [106].

Wavefunction	$\langle p_{12}^{-2} \rangle$	$\langle p_{12}^{-1} \rangle$	$\langle p_{12}^{+1} \rangle$	$\langle p_{12}^{+2} \rangle$	$\sigma_{p_{12}}$
H ⁻ HF-STO	0.013953	0.10283	12.281	185.06	5.8517
1NC	0.013254	0.097324	13.857	248.35	7.5062
2NC	0.0090840	0.083485	14.946	269.47	6.7874
3NC	0.0078169	0.078618	15.481	283.84	6.6470
4NC	0.0077752	0.078539	15.477	283.62	6.6402
5NC	0.0077768	0.078532	15.479	283.64	6.6370
NA-CI	0.0077220	0.078471	15.478	283.67	6.6403
He HF-STO	0.090997	0.26879	4.4748	23.382	1.8325
1NC	0.091154	0.26885	4.4796	23.462	1.8427
2NC	0.083989	0.25839	4.6396	25.025	1.8706
3NC	0.078806	0.25250	4.6757	25.088	1.7961
4NC	0.078283	0.25201	4.6761	25.065	1.7886
5NC	0.077842	0.25170	4.6762	25.067	1.7888
NA-CI	0.077324	0.25141	4.6763	25.065	1.7881
Li ⁺ HF-STO	0.23462	0.43313	2.7587	8.8331	1.1058
1NC	0.23482	0.43325	2.7589	8.8376	1.1072
2NC	0.22242	0.42193	2.8257	9.2408	1.1208
3NC	0.21471	0.41656	2.8375	9.2479	1.0939
4NC	0.21358	0.41587	2.8381	9.2433	1.0901
5NC	0.21267	0.41545	2.8384	9.2451	1.0902
NA-CI	0.21154	0.41502	2.8386	9.2447	1.0896
Be ⁺⁺ HF-STO	0.44489	0.59731	1.9952	4.6091	0.79274
1NC	0.44512	0.59742	1.9951	4.6093	0.79309
2NC	0.42748	0.58572	2.0314	4.7683	0.80099
3NC	0.41719	0.58054	2.0372	4.7701	0.78725
4NC	0.41542	0.57974	2.0377	4.7686	0.78507
5NC	0.41402	0.57926	2.0379	4.7696	0.78509
NA-CI	0.41225	0.57876	2.0381	4.7694	0.78472

Table III.6

Values of $\langle p_{12}^n \rangle$ when $n = -2, -1, +1$ and $+2$; and the standard deviations $\sigma_{p_{12}}$.

9.3 Momentum Space Results: Figures

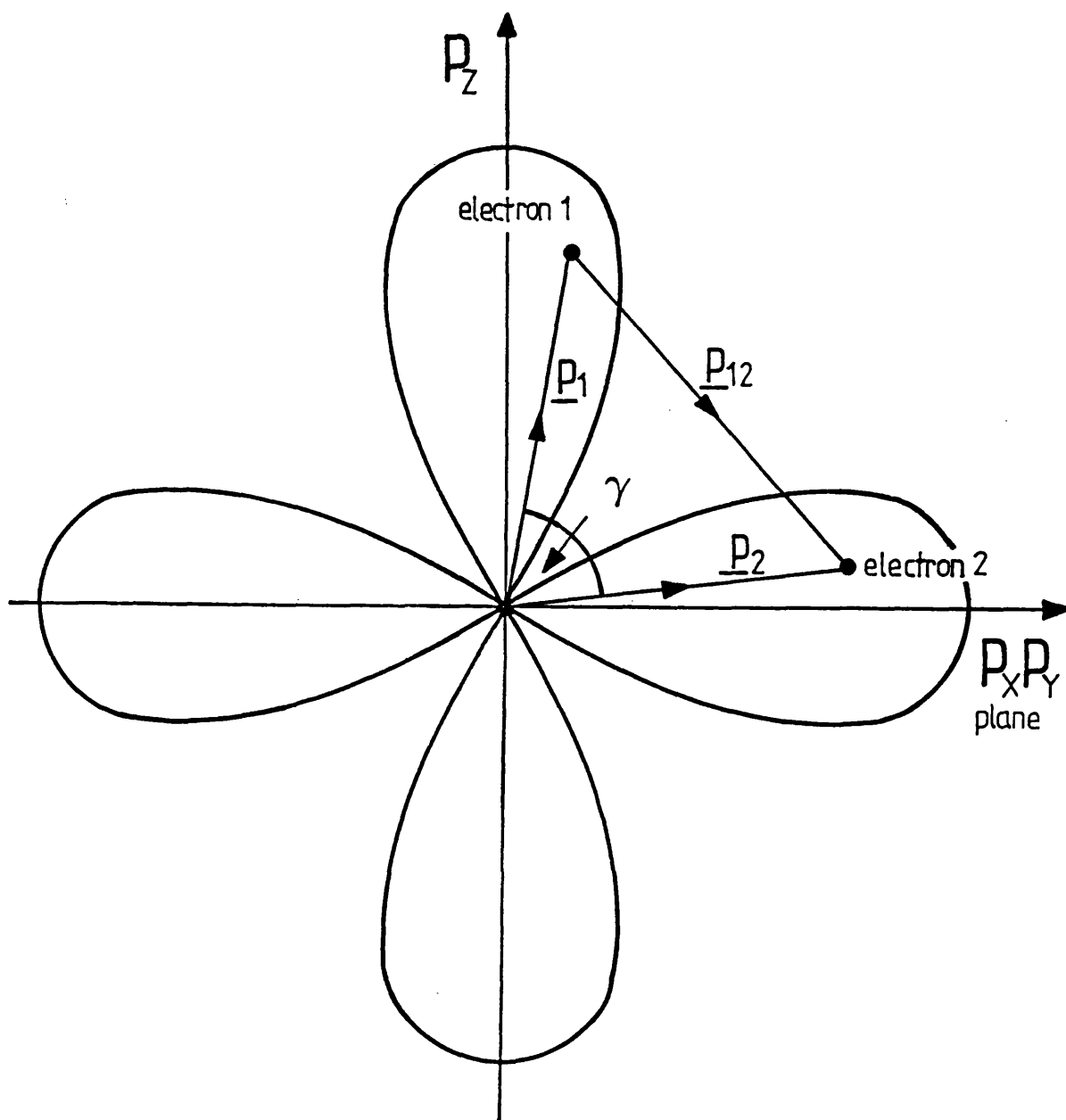


Figure III.1

A schematic orbital representation of the $2p^2 \ ^3P$ state in momentum space. The two electrons with typical momenta are also shown.

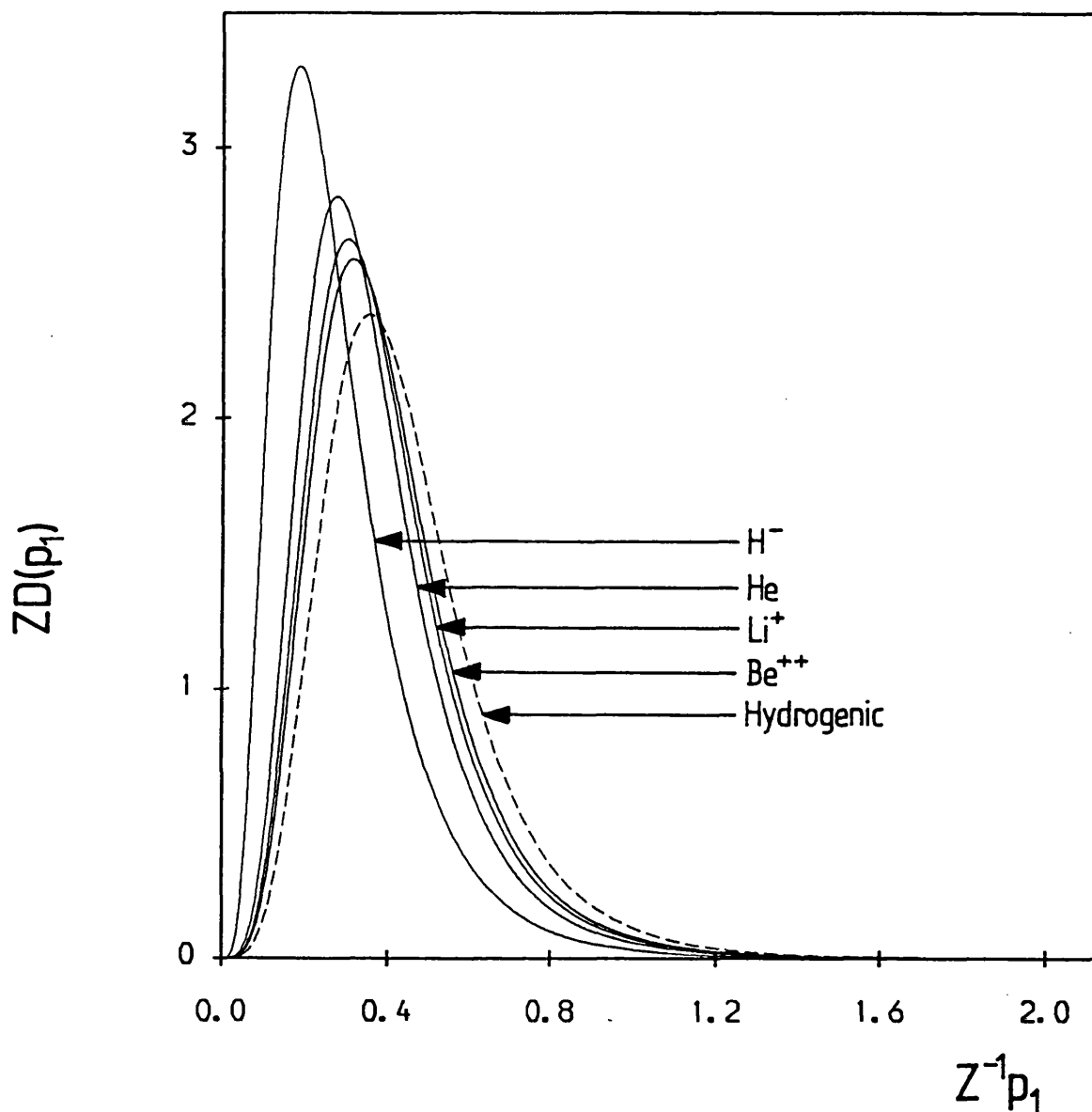


Figure III.2

The $D(p_1)$ distributions for H^- , He, Li^+ and Be^{++} produced using the Hartree-Fock wavefunctions. Also shown as a dashed line is the $D(p_1)$ generated from an independent-particle $2p^2\ ^3P$ wavefunction comprising unoptimized hydrogenic orbitals. Both axes are scaled.

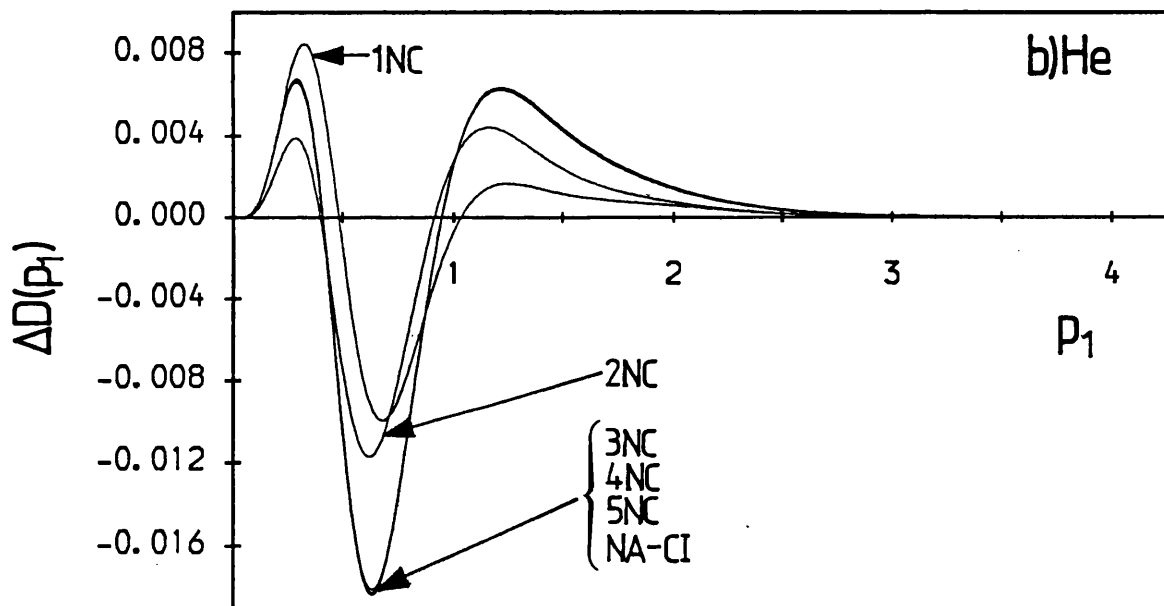
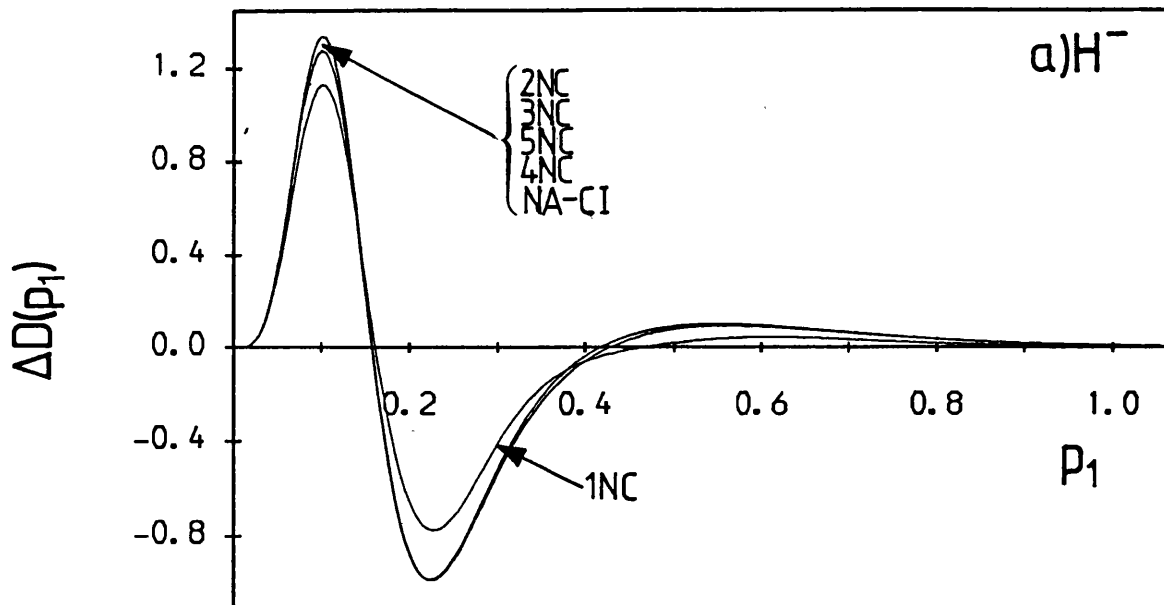


Figure III.3 a) & b)

The one-particle radial shifts $\Delta D(p_1)$ for a) H^- and b) He. In each case the 1NC, 2NC, 3NC, 4NC, 5NC and NA-CI wavefunctions are used as the correlated descriptions.

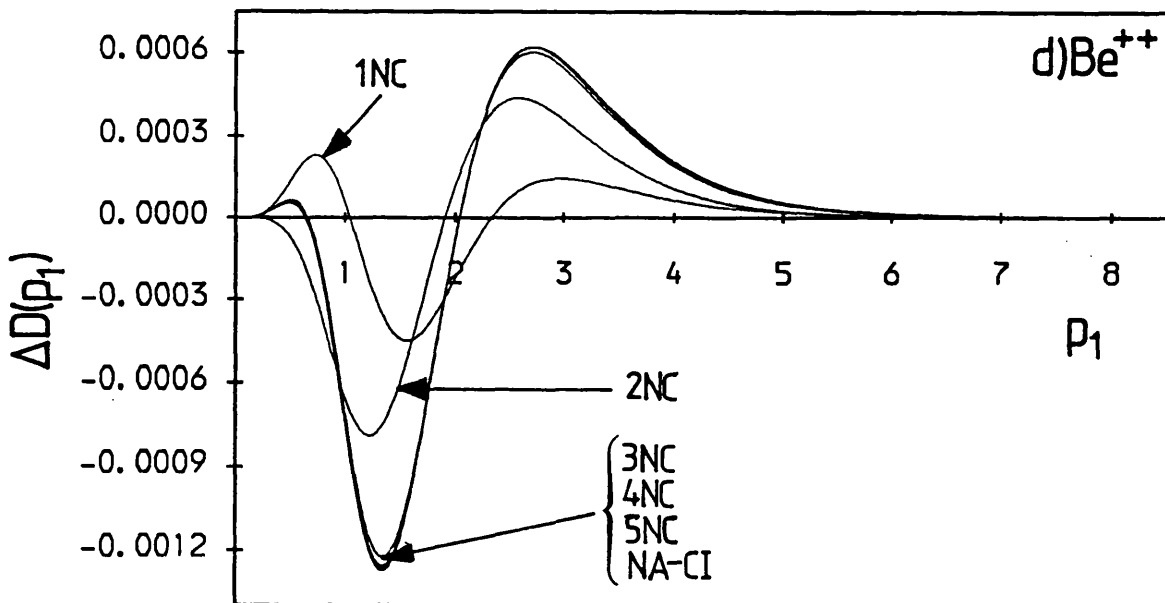
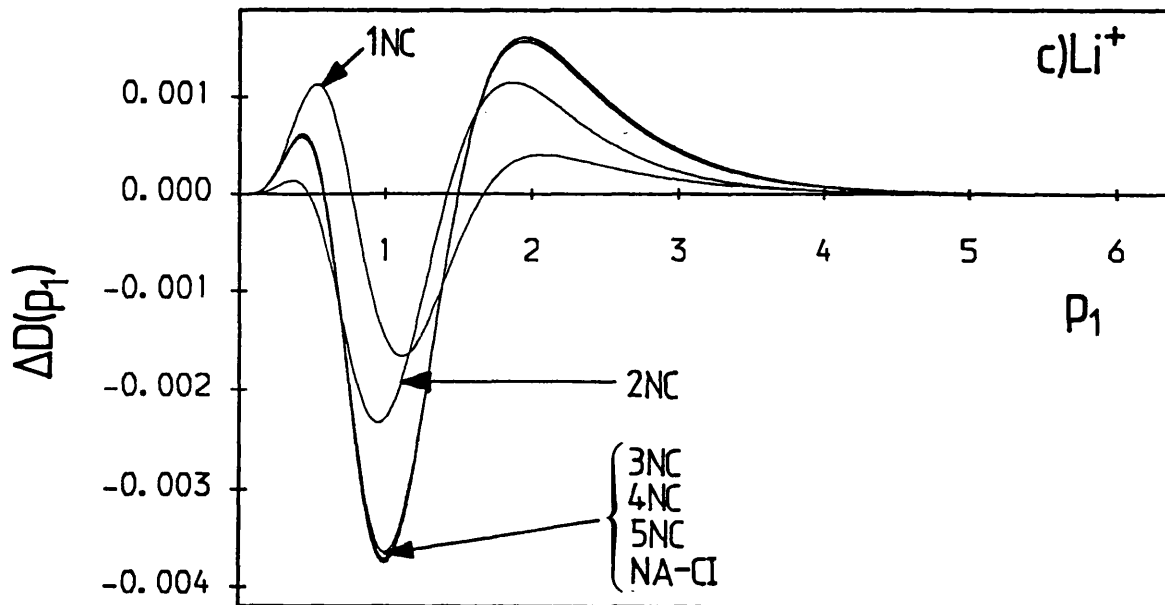


Figure III.3 c) & d)

The one-particle radial shifts $\Delta D(p_1)$ for c) Li^+ and d) Be^{++} . In each case the 1NC, 2NC, 3NC, 4NC, 5NC and NA-CI wavefunctions are used as the correlated descriptions.

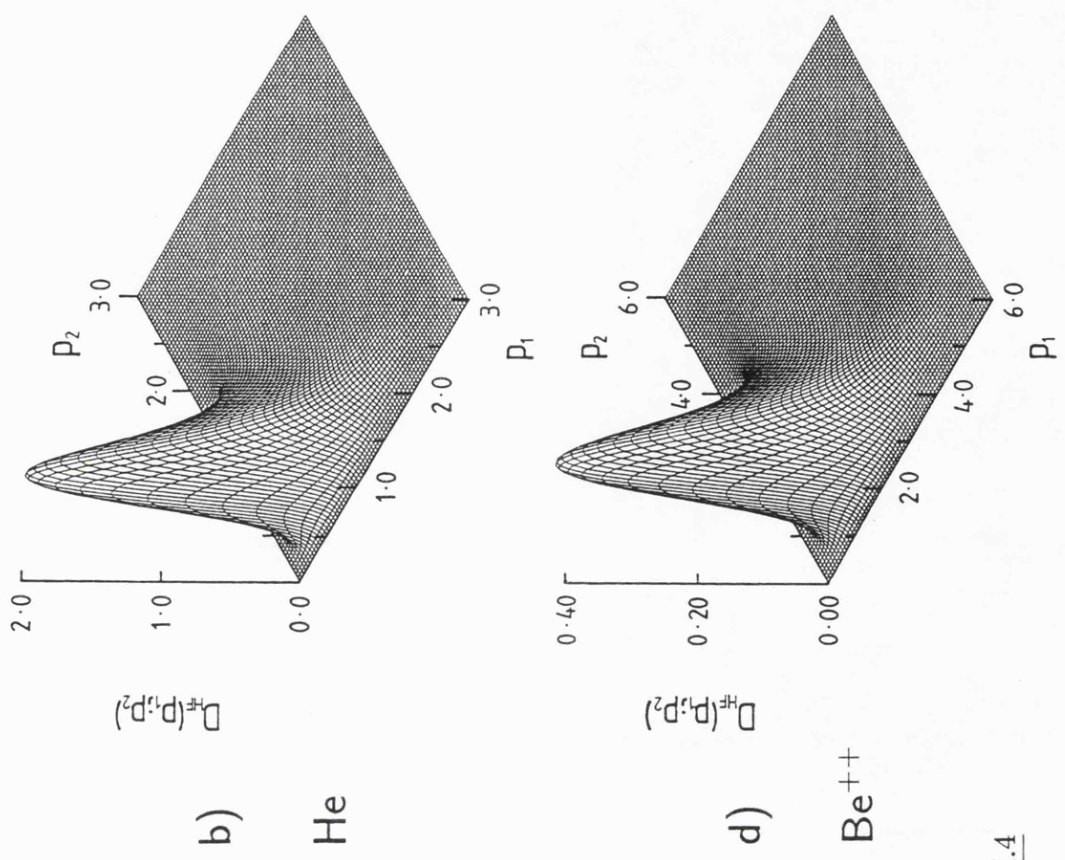
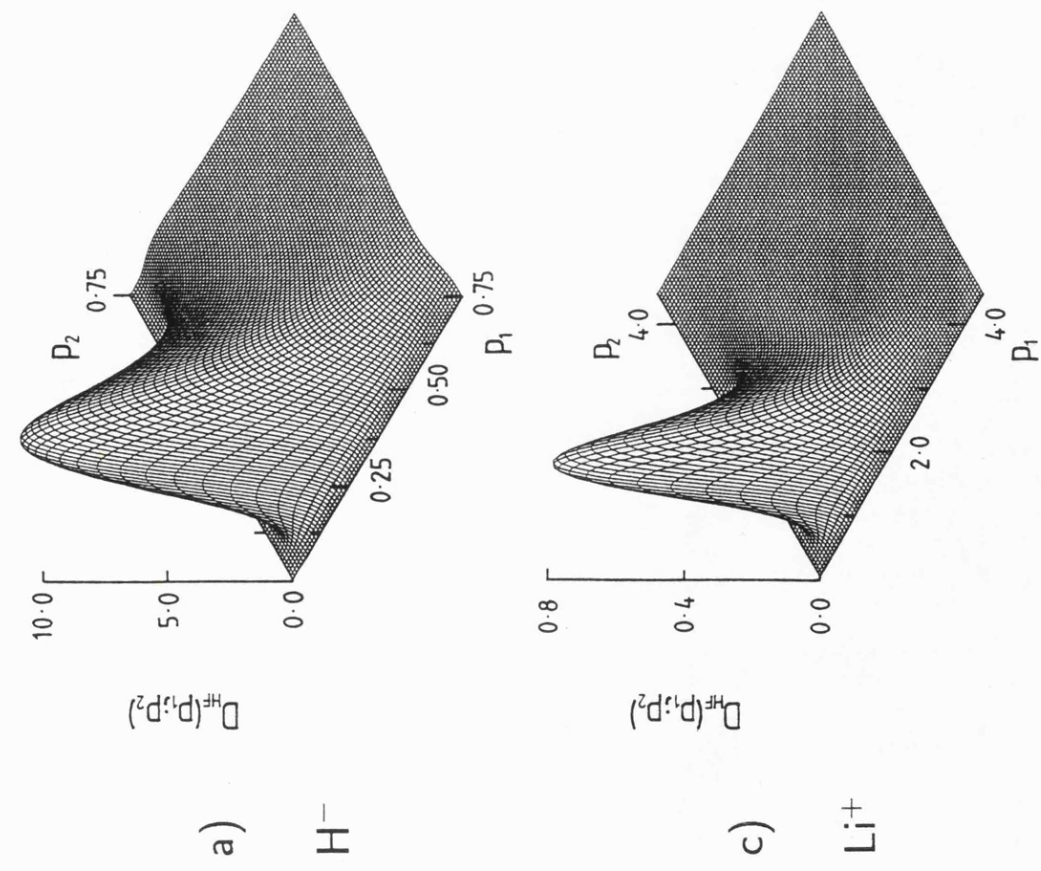


Figure III.4

The two-particle radial surfaces $D(p_1; p_2)$ for the a) H^- , b) He , c) Li^+ , d) Be^{++} systems. The Hartree-Fock wavefunction is used in each case.

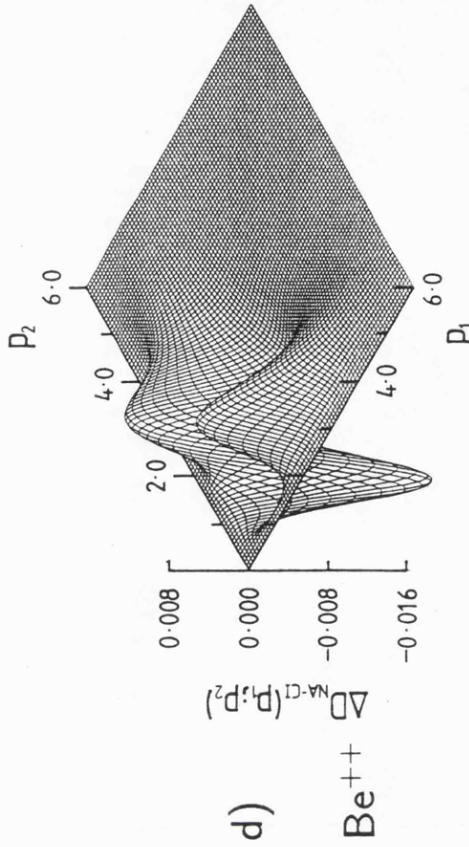
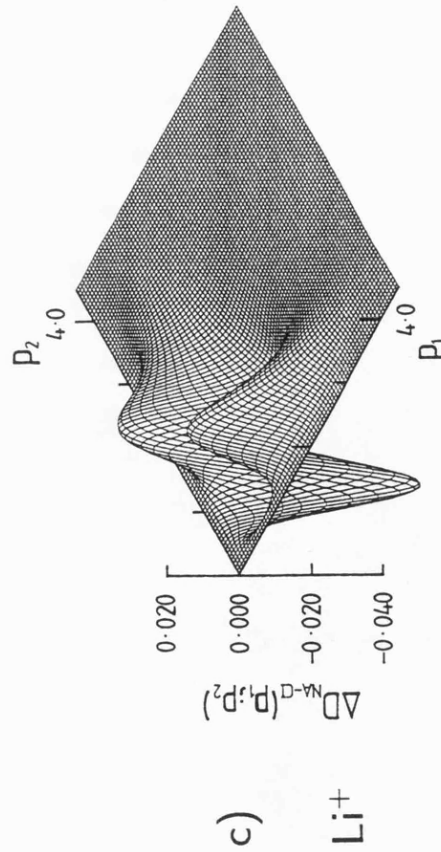
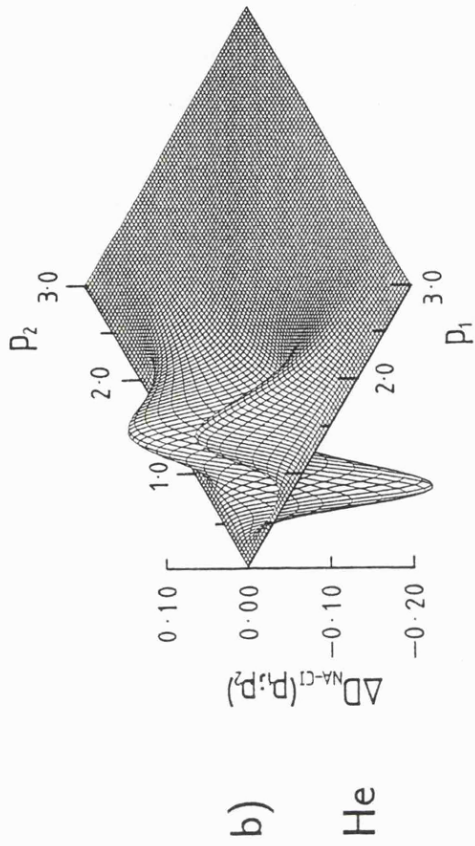
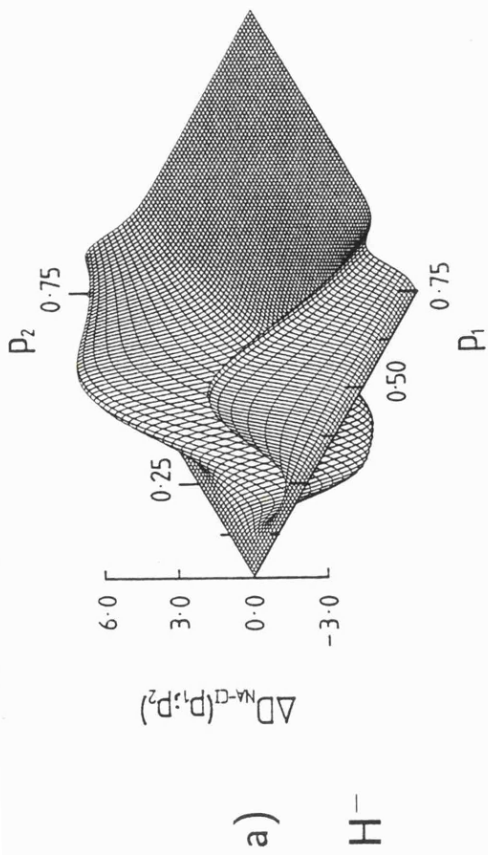


Figure III.5

The two-particle radial shifts $\Delta D(p_1; p_2)$ for the a) H^- , b) He , c) Li^+ , d) Be^{++} systems. The NA-CI wavefunction is used as the correlated description in each case.

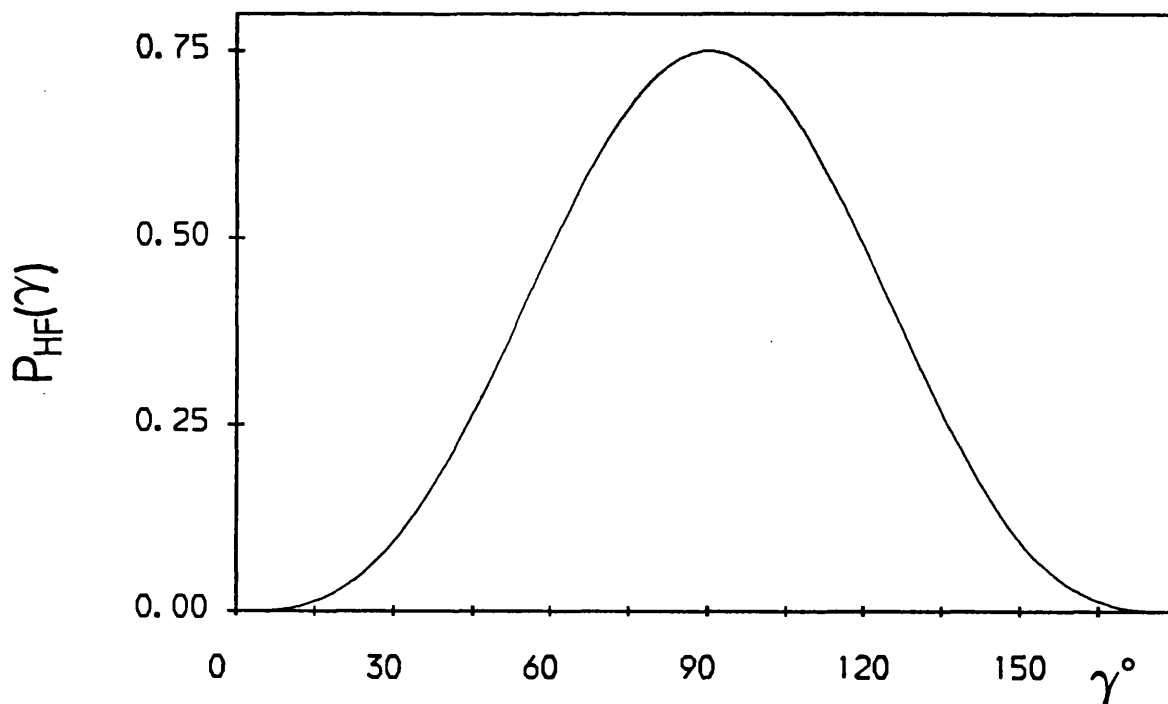


Figure III.6

The $P(\gamma)$ distribution for all Hartree-Fock $2p^2\ ^3P$ wavefunctions.

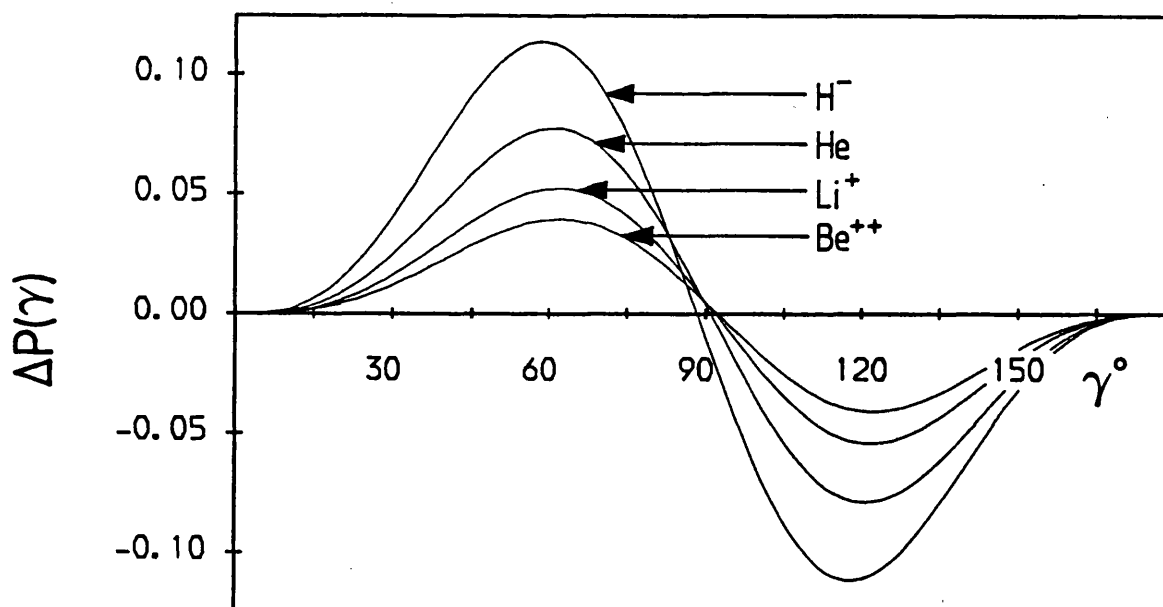


Figure III.7

The angular shifts $\Delta P(\gamma)$ for H^- , He, Li^+ and Be^{++} . The NA-CI wavefunction is employed for each correlated description.

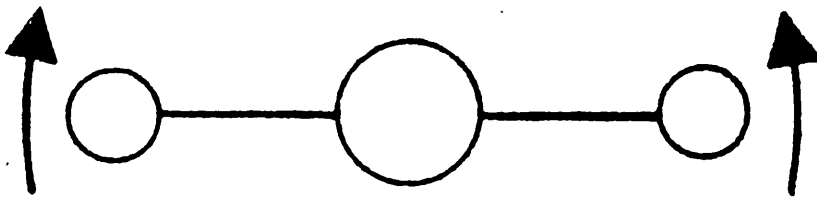


Figure III.8

The $2p^2 \ ^3P$ state for He according to Krause, Morgan and Berry [64]. The circle in the centre represents the nucleus, whilst the other two circles denote the electrons. The arrows denote collective bending vibrational motions of the electrons.

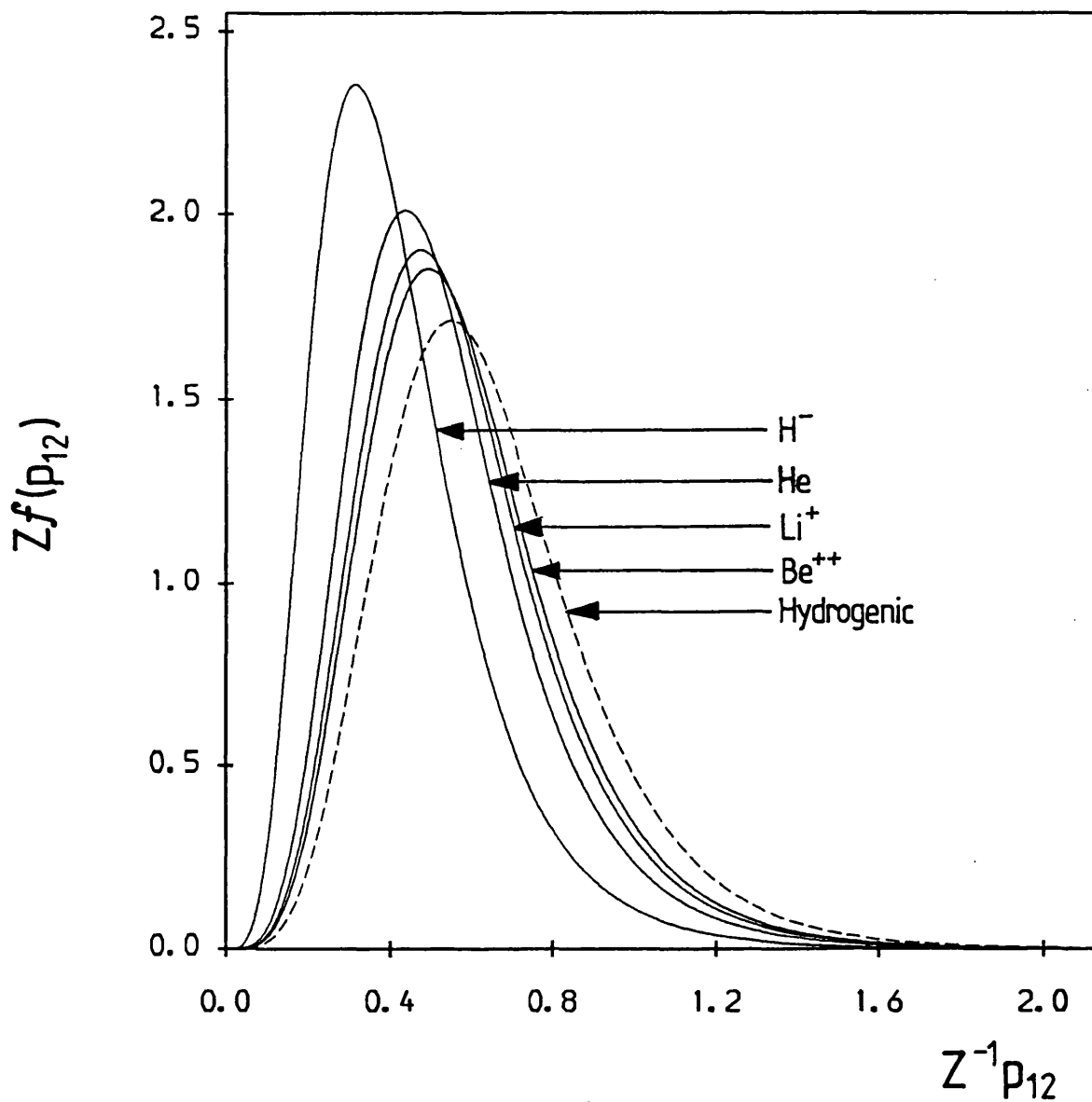


Figure III.9

The $f(p_{12})$ distributions for H^- , He, Li^+ and Be^{++} produced using the Hartree-Fock wavefunctions. Also shown as a dashed line is the $f(p_{12})$ generated from an independent-particle $2p^2 \ ^3P$ wavefunction comprising unoptimized hydrogenic orbitals. Both axes are scaled.

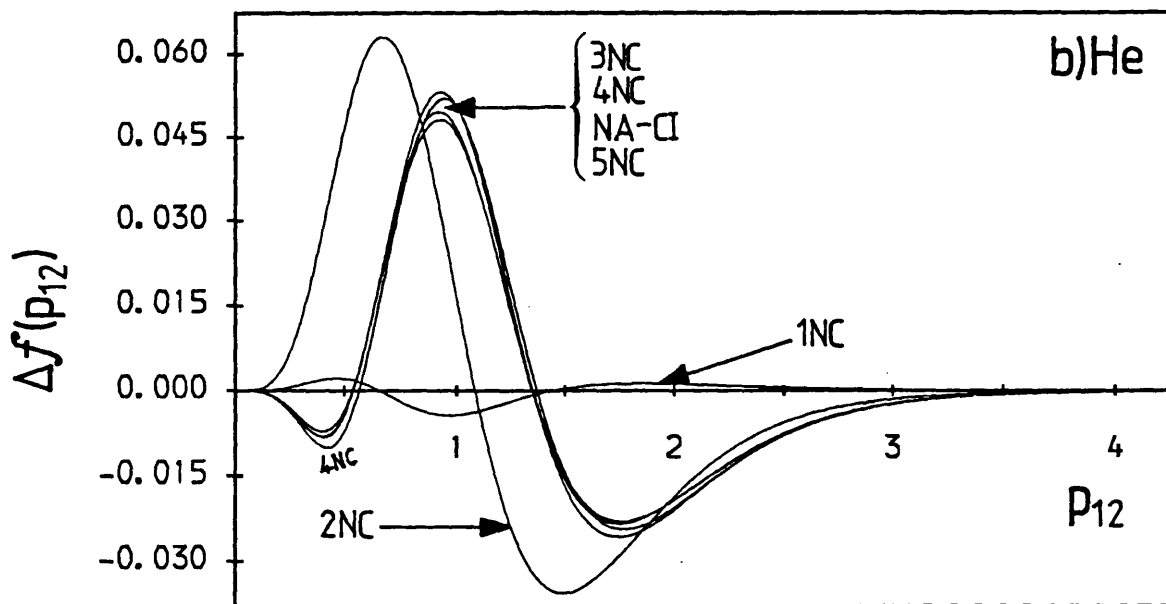
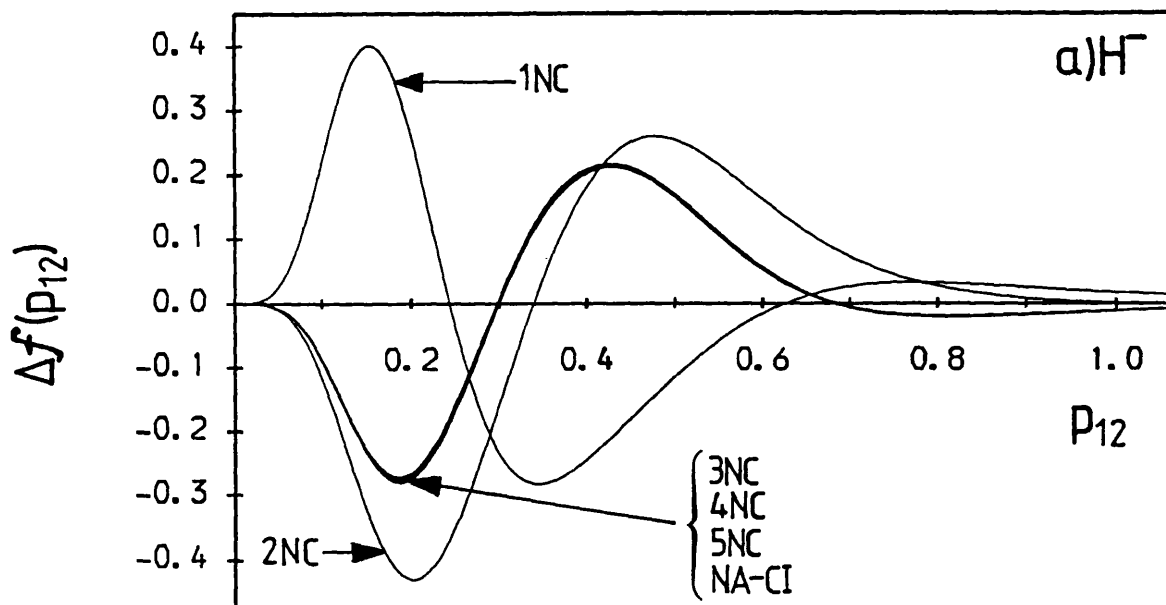


Figure III.10 a) & b)

The Coulomb shifts $\Delta f(p_{12})$ for a) H^- and b) He. In each case the 1NC, 2NC, 3NC, 4NC, 5NC and NA-CI wavefunctions are used as the correlated descriptions.

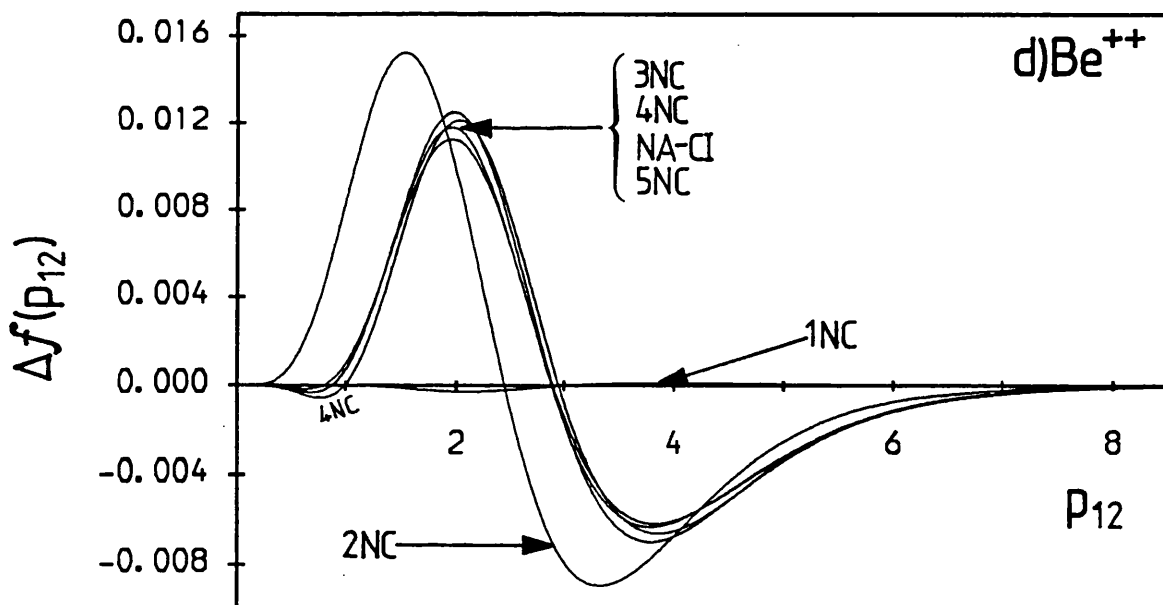
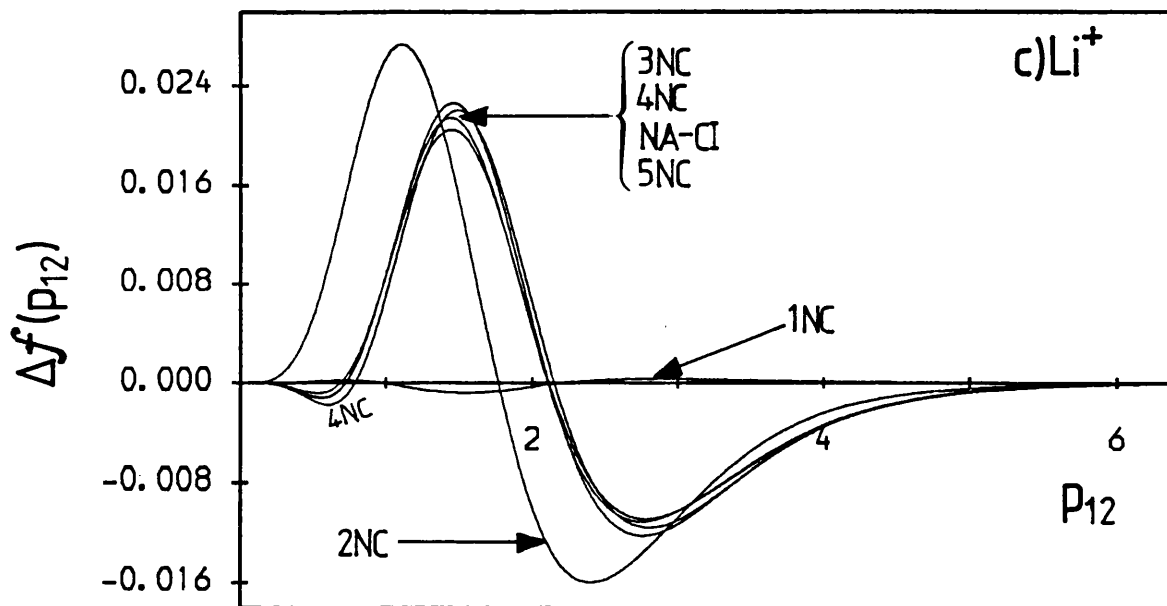


Figure III.10 c) & d)

The Coulomb shifts $\Delta f(p_{12})$ for c) Li^+ and d) Be^{++} . In each case the 1NC, 2NC, 3NC, 4NC, 5NC and NA-CI wavefunctions are used as the correlated descriptions.

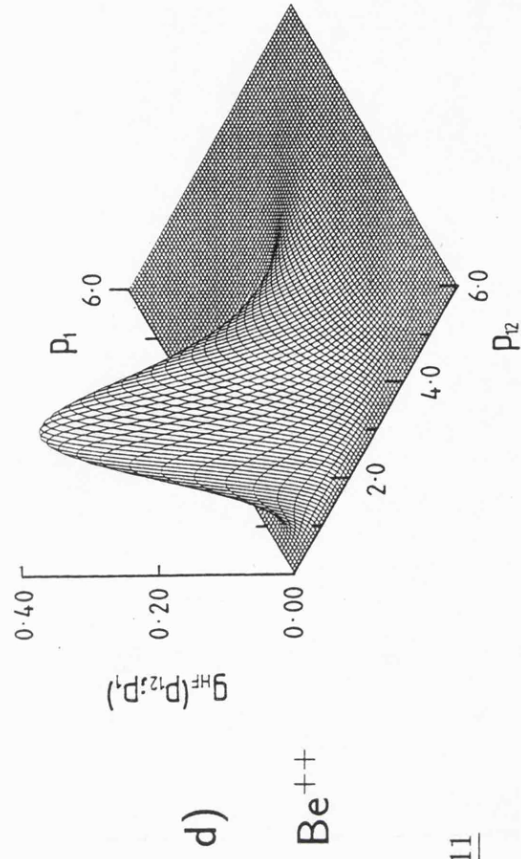
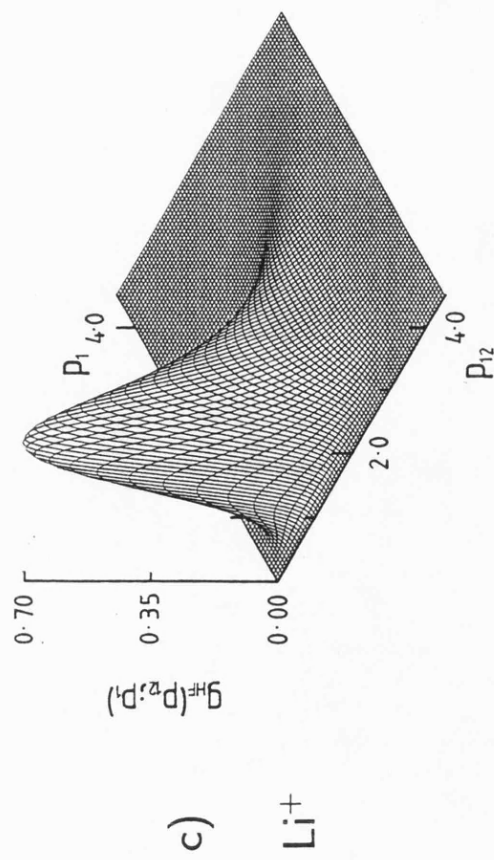
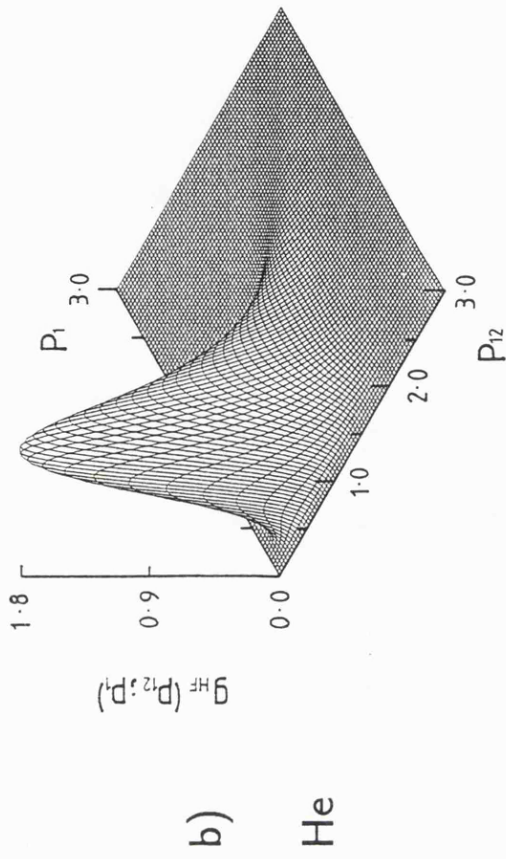
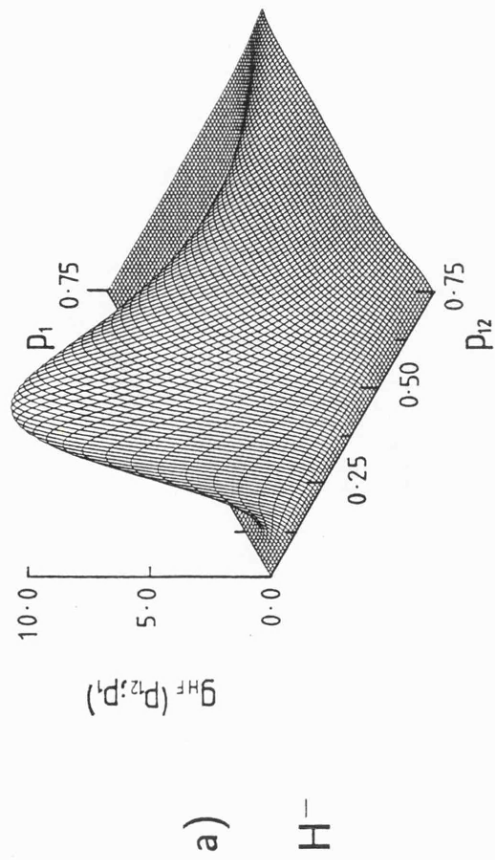


Figure II.11

The partial surfaces $g(p_2; p_1)$ for the a) H^- , b) He, c) Li^+ , d) Be^{++} systems. The Hartree-Fock wavefunction is used in each case.

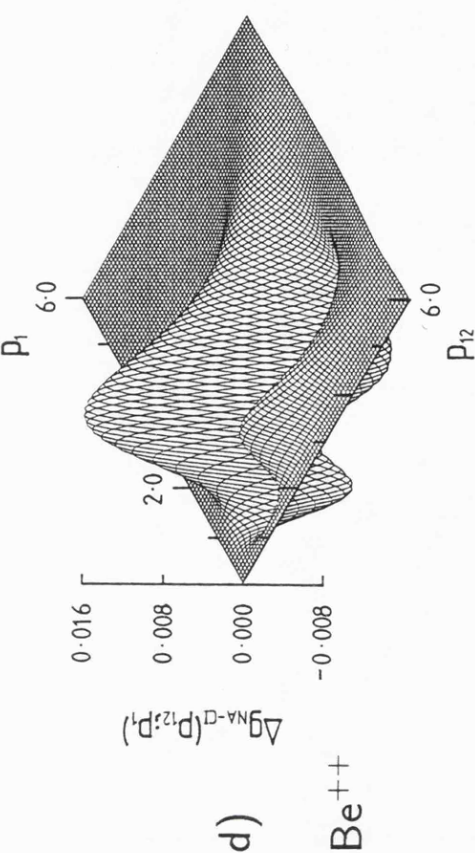
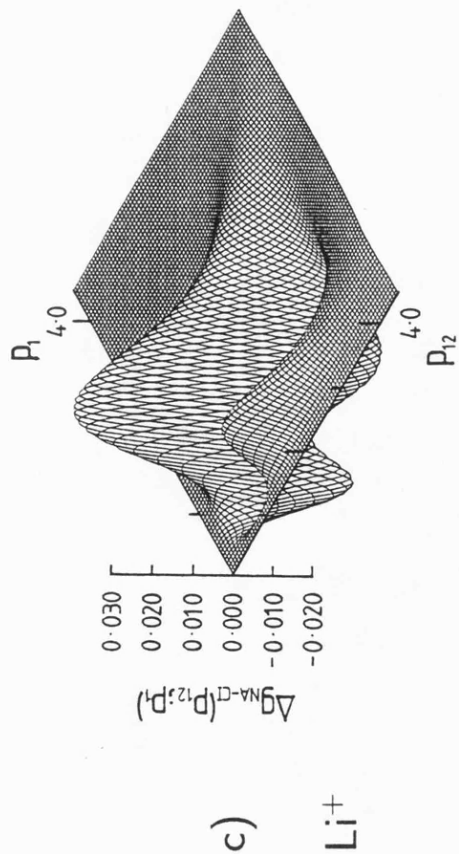
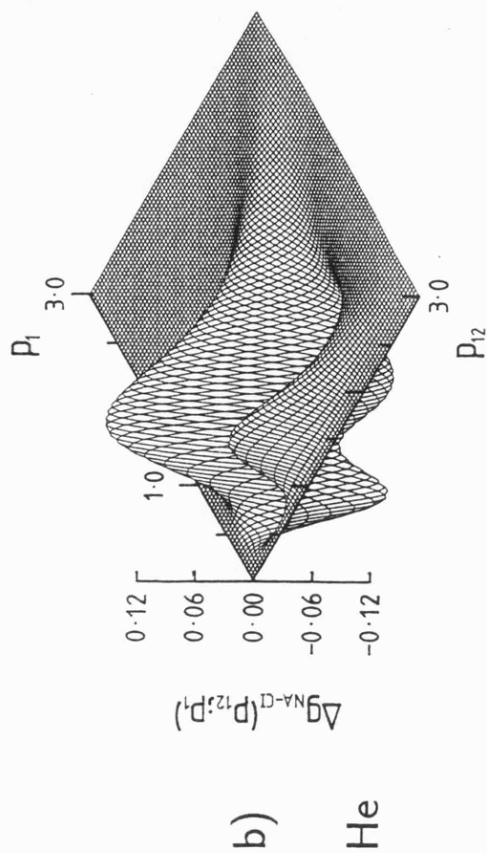
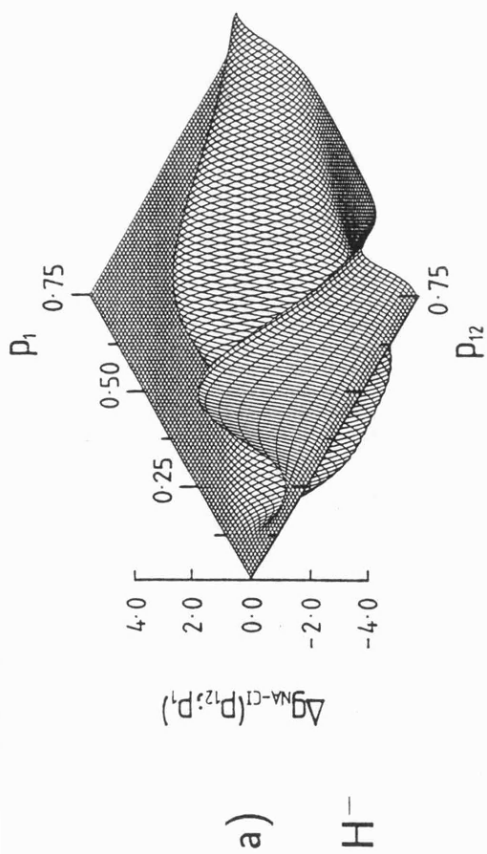


Figure III.12

The partial Coulomb shifts $\Delta g(p_{12}; p_1)$ for the a) H^- , b) He, c) Li^+ , d) Be^{++} systems.

The NA-CI wavefunction is used as the correlated description in each case.

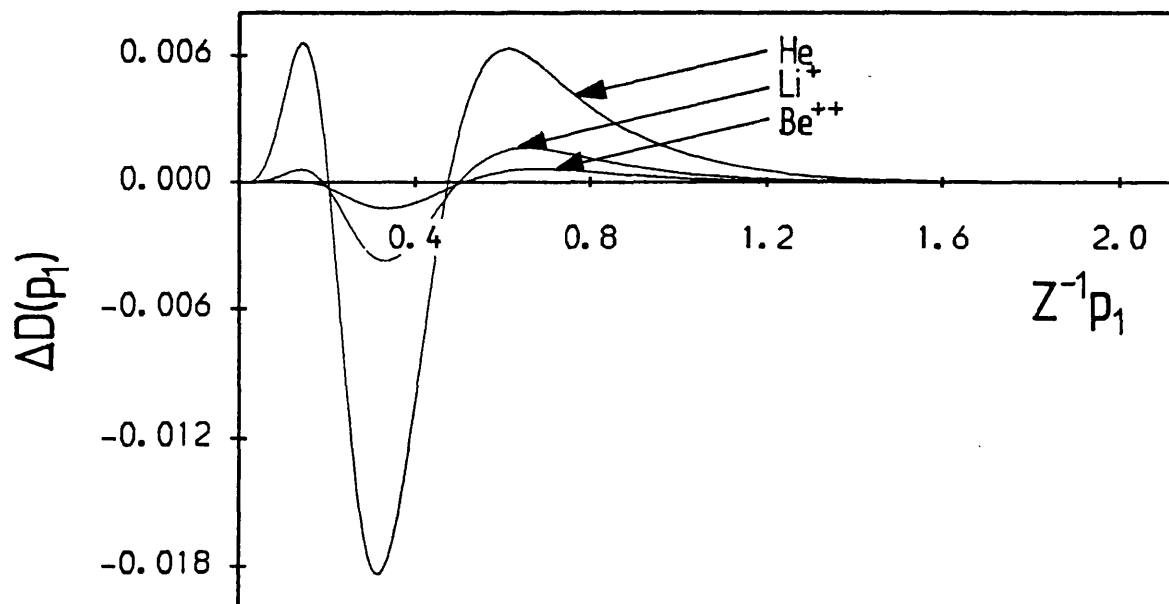


Figure III.13

The one-particle radial shifts $\Delta D(p_1)$ for He, Li^+ and Be^{++} plotted against $Z^{-1}p_1$ using the NA-CI wavefunction as the correlated description for each curve.

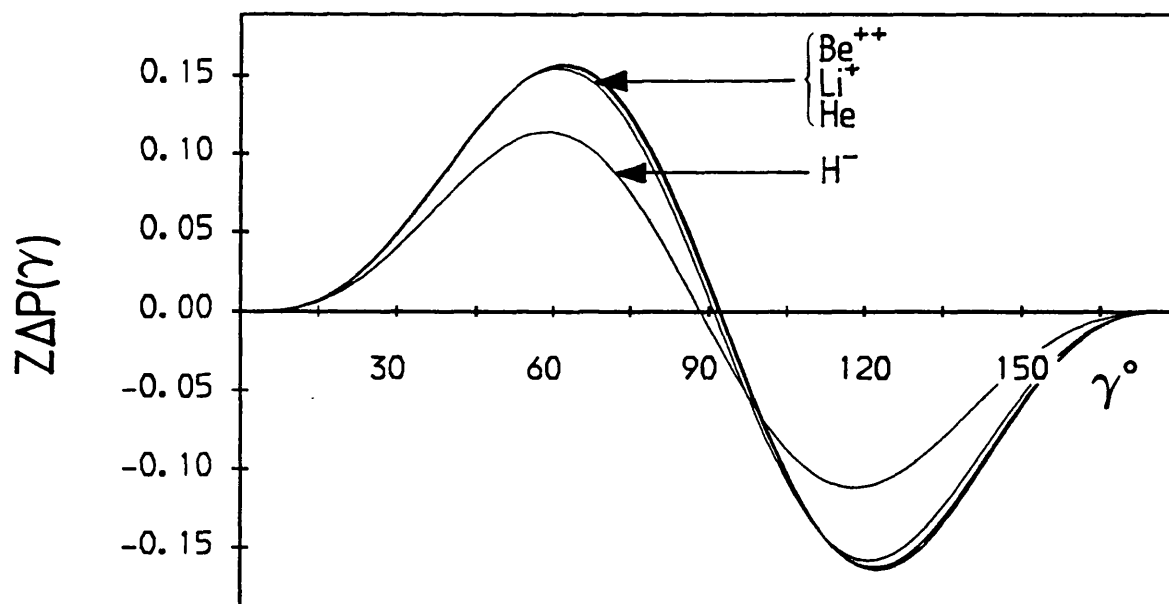


Figure III.14

The angular shifts for H^- , He, Li^+ and Be^{++} . The NA-CI wavefunction is employed for each correlated description. In this figure the scaled ordinate $Z\Delta P(\gamma)$ is used.

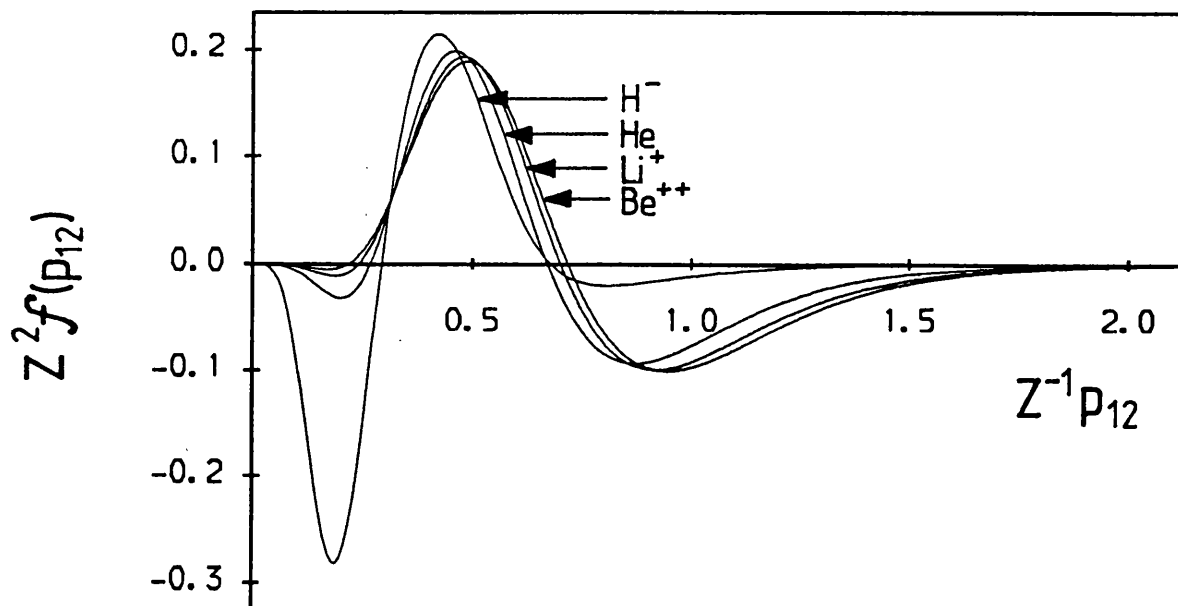


Figure III.15

The Coulomb shifts $\Delta f(p_{12})$ for H^- , He , Li^+ and Be^{++} plotted against $Z^{-1} p_{12}$ using the NA-CI wavefunction as the correlated description for each curve.

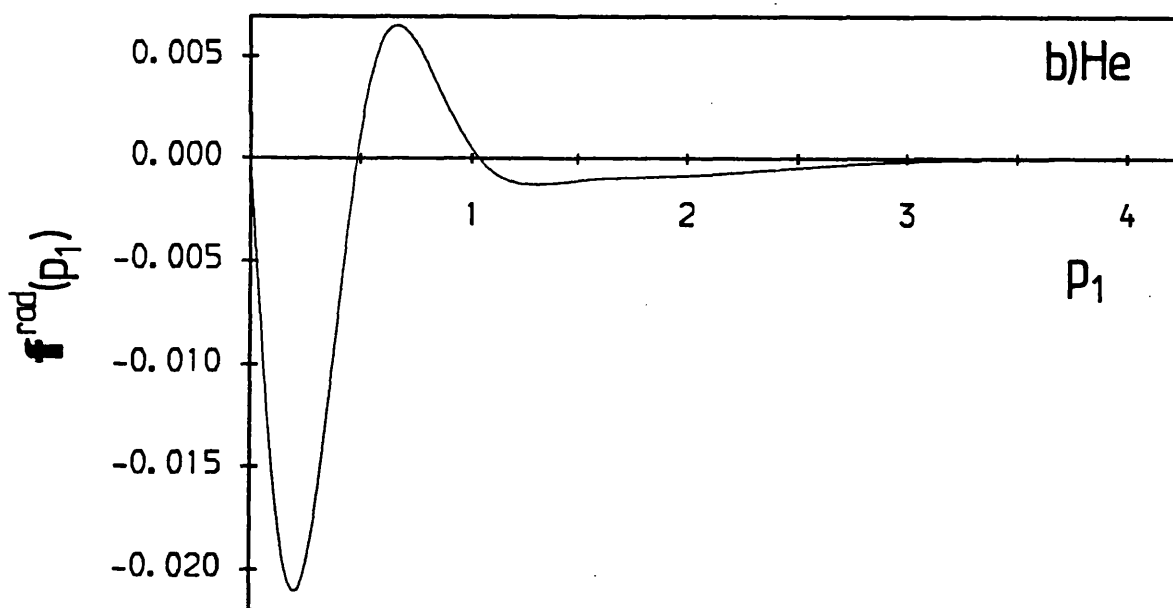
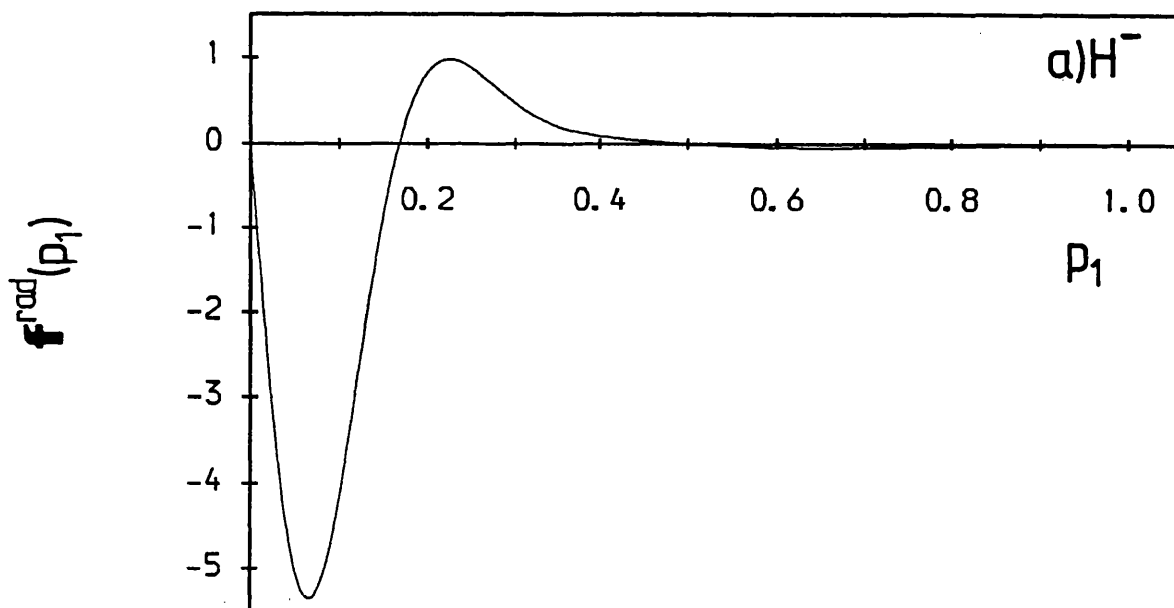


Figure III.16 a) & b)

The imaginary part of the radial part $f^{rad}(p_1)$ of the Sinanoğlu orbital correction function for a) H^- and b) He. They are calculated from the NA-CI wavefunctions.

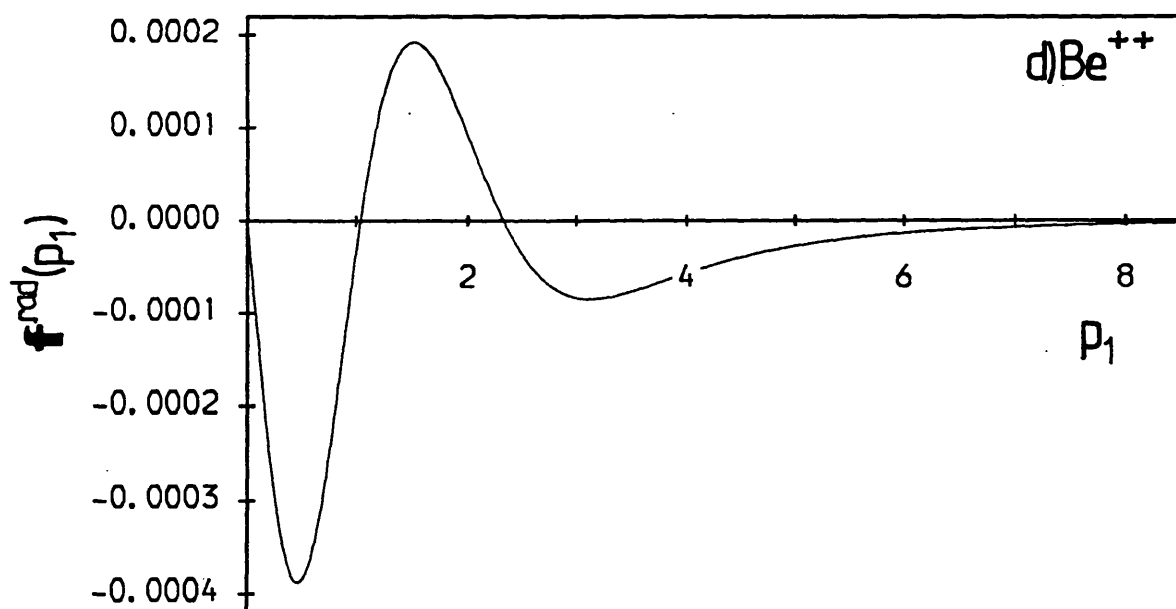
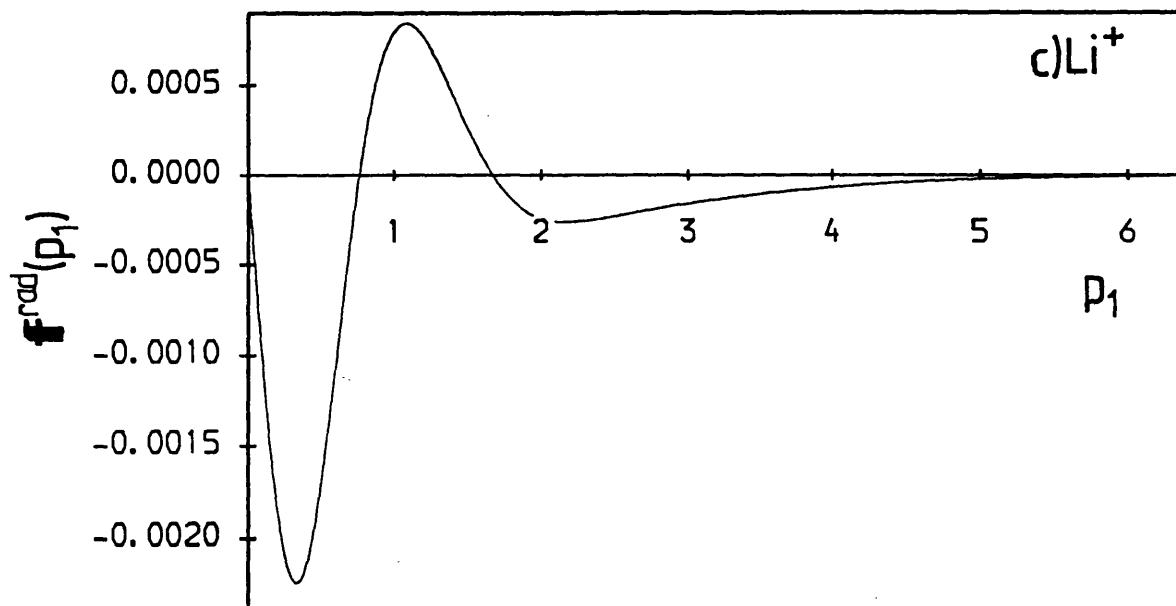


Figure III.16 c) & d)

The imaginary part of the radial part $f^{rad}(p_1)$ of the Sinanoğlu orbital correction function for c) Li^+ and d) Be^{++} . They are calculated from the NA-CI wavefunctions.

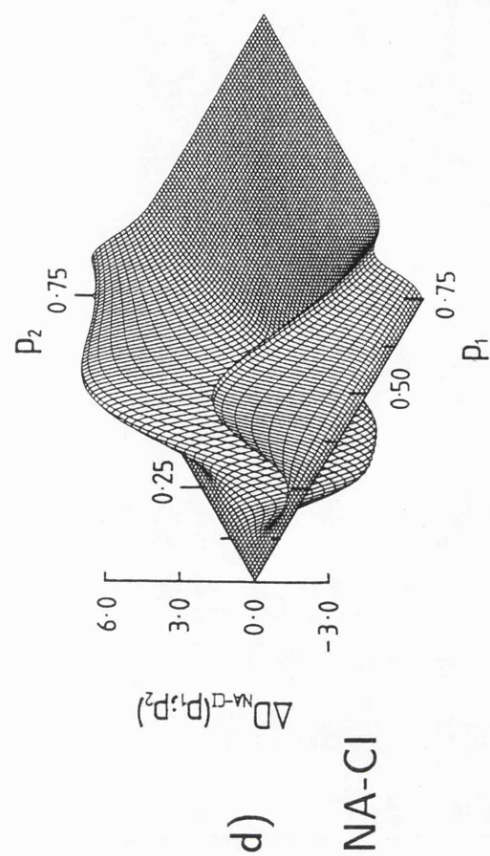
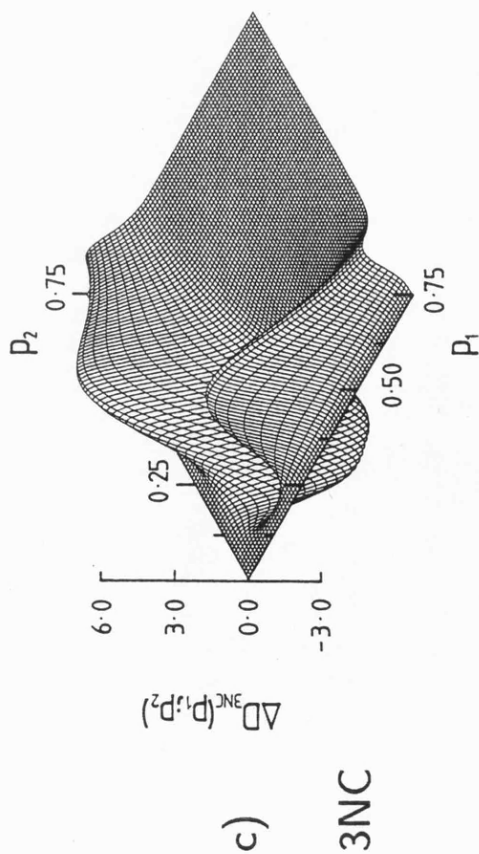
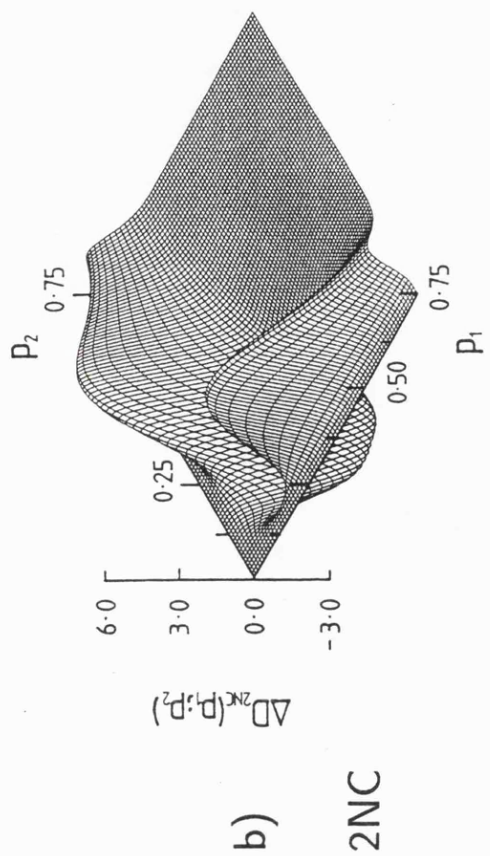
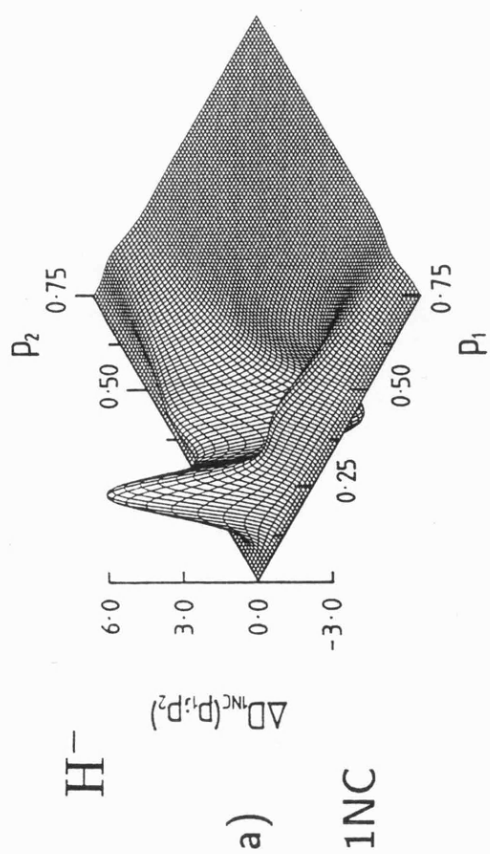


Figure III.17

The two-particle radial shifts $\Delta D(p_1, p_2)$ for the H^- system using the a) 1NC, b) 2NC, c) 3NC and d) NA-CI wavefunctions for the correlated descriptions.

He

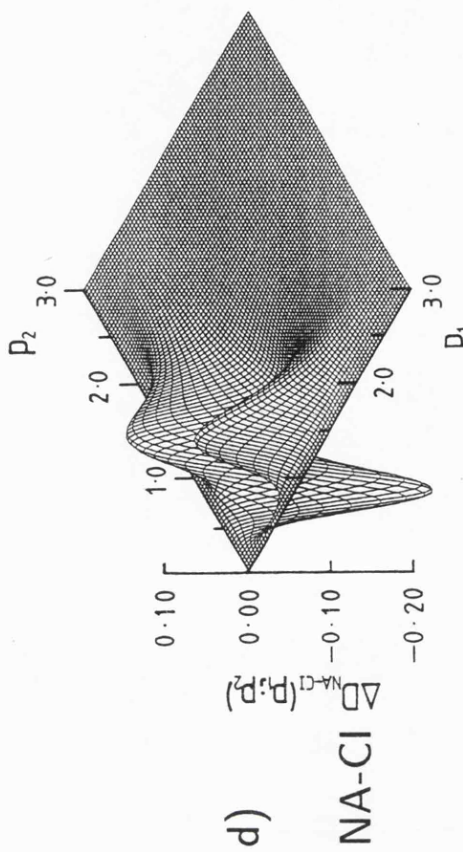
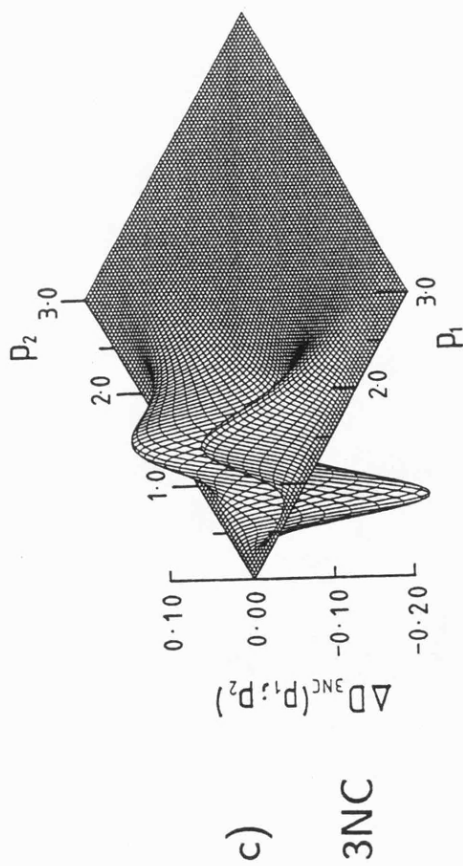
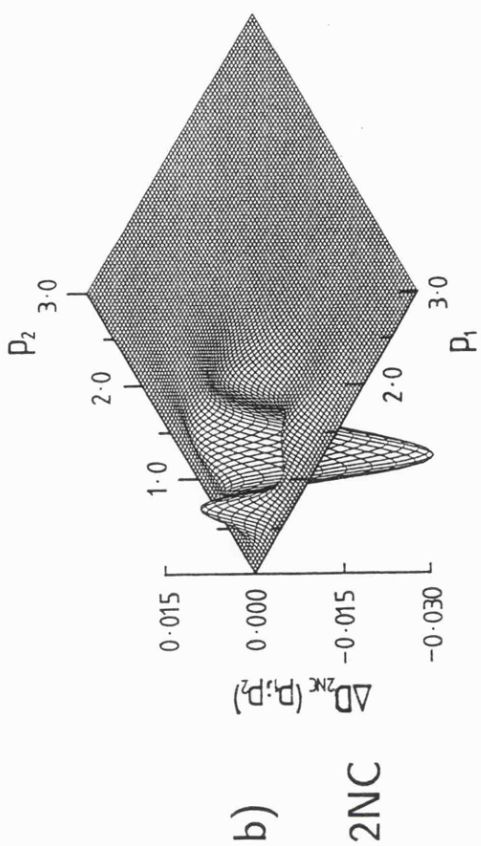
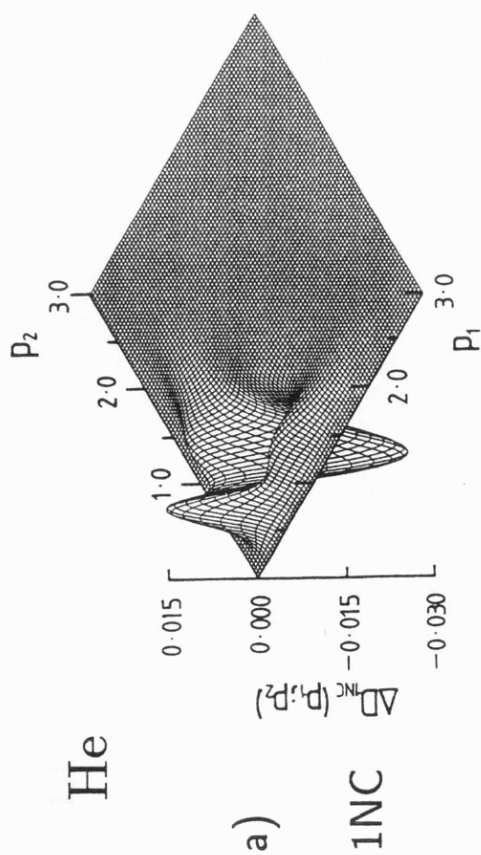


Figure III.18

The two-particle radial shifts $\Delta D(p_1, p_2)$ for the He system using the a) 1NC, b) 2NC, c) 3NC and d) NA-CI wavefunctions for the correlated descriptions.

Note the different vertical scale employed in a) and b).

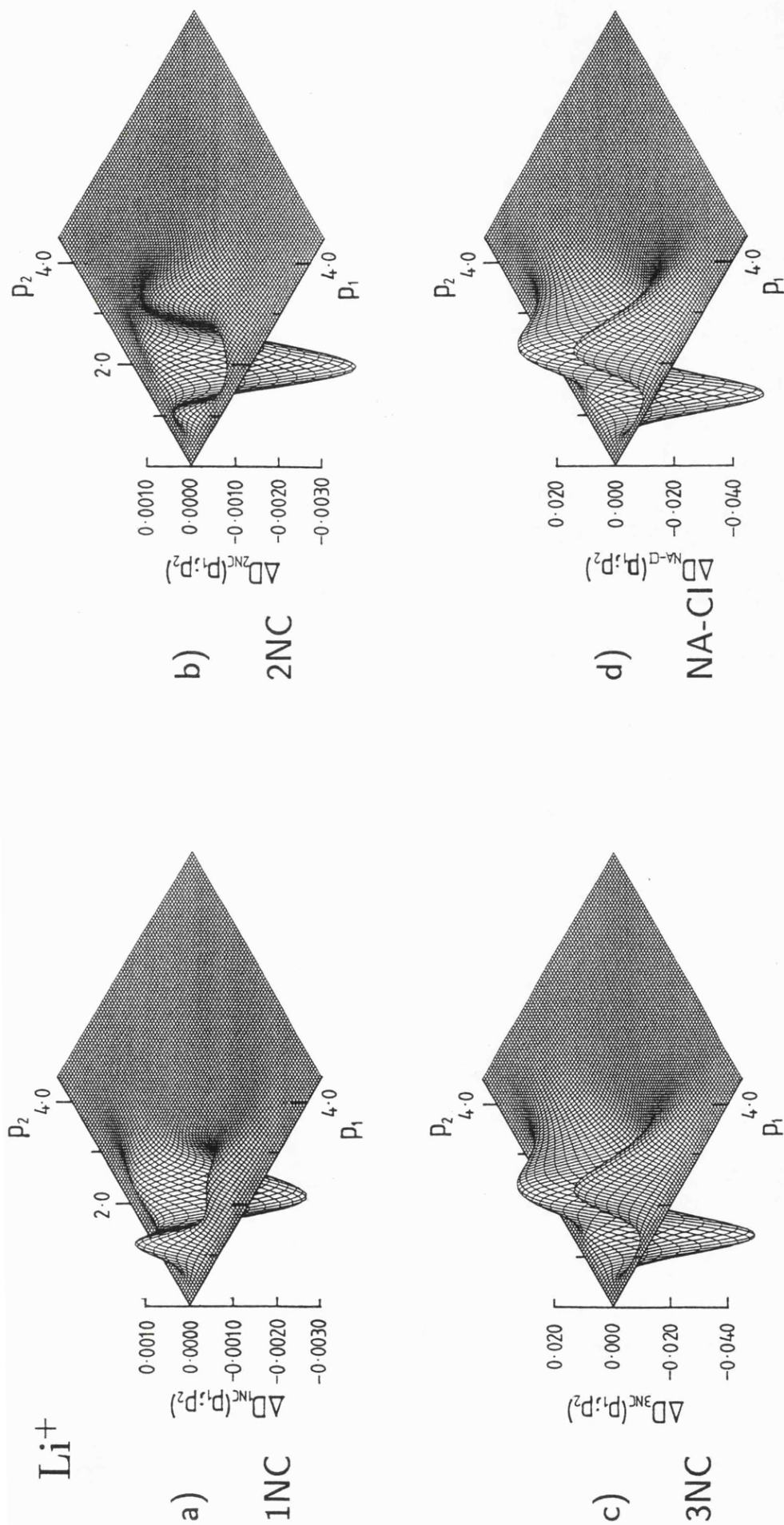


Figure III.19

The two-particle radial shifts $\Delta D(p_1, p_2)$ for the Li^+ system using the a) 1NC,

b) 2NC, c) 3NC and d) NA-CI wavefunctions for the correlated descriptions.

Note the different vertical scale employed in a) and b).

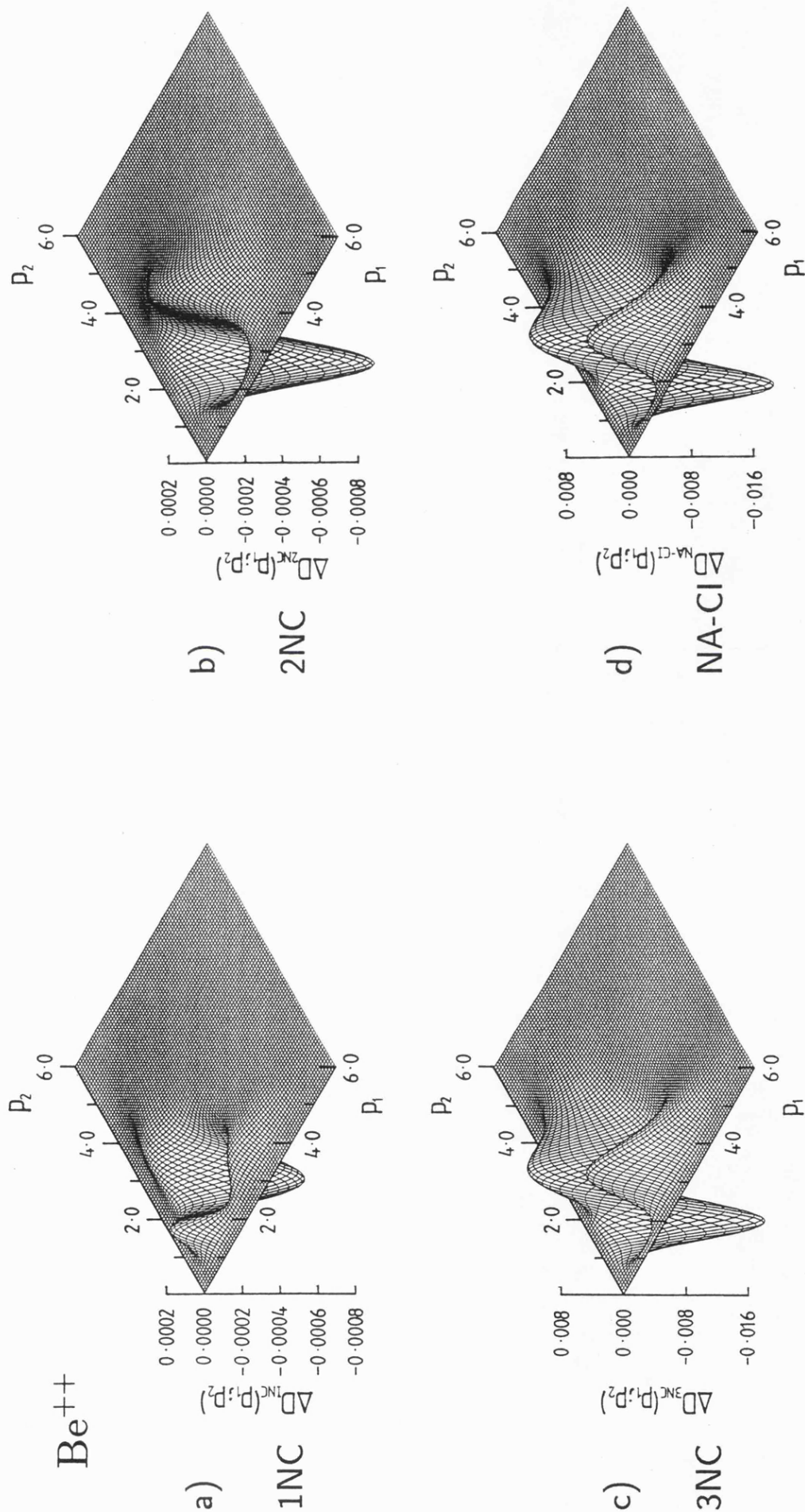


Figure III.20

The two-particle radial shifts $\Delta D(p_1; p_2)$ for the Be^{++} system using the a) 1NC,

b) 2NC, c) 3NC and d) NA-CI wavefunctions for the correlated descriptions.

Note the different vertical scale employed in a) and b).

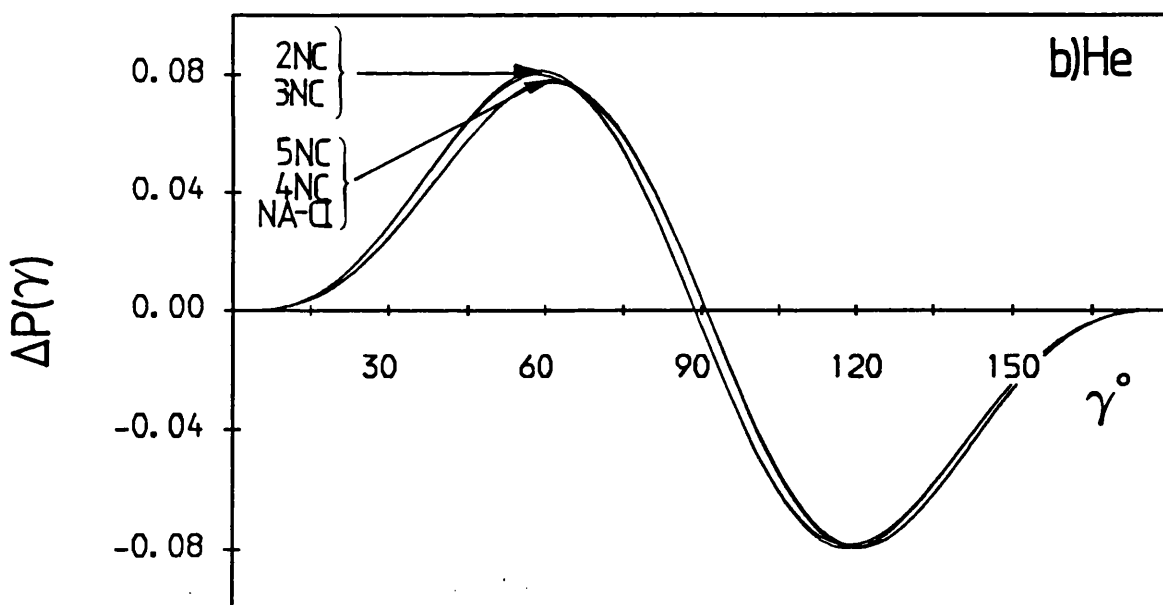
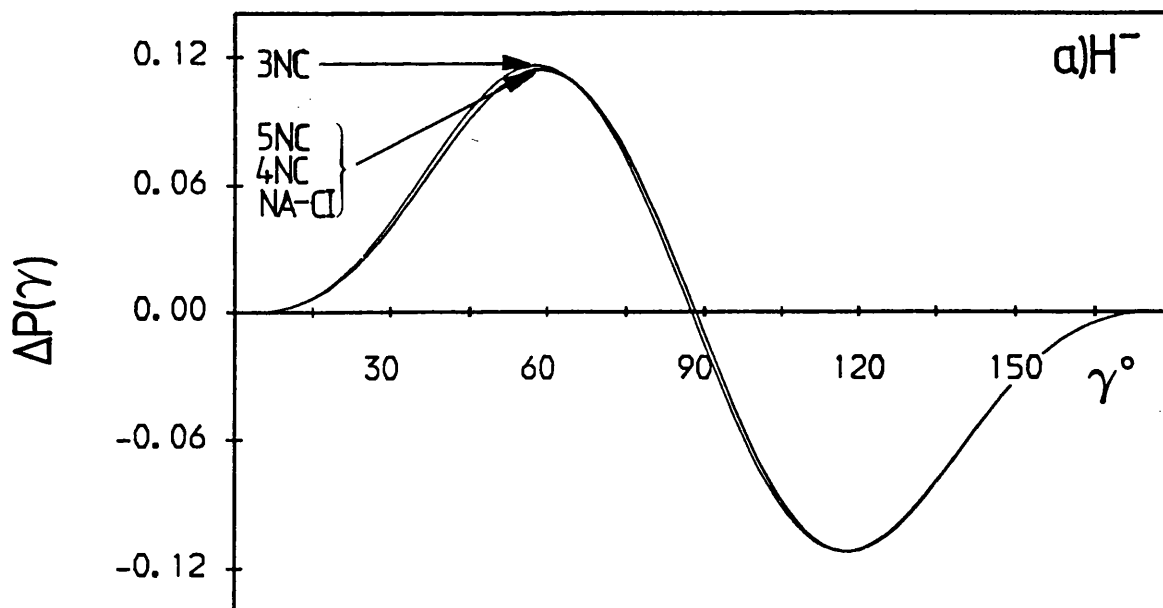


Figure III.21 a) & b)

The angular shifts $\Delta P(\gamma)$ for a) H^- and b) He. In each case the 3NC, 4NC, 5NC and NA-CI wavefunctions are used as the correlated descriptions. For He the 2NC wavefunction is used as well.

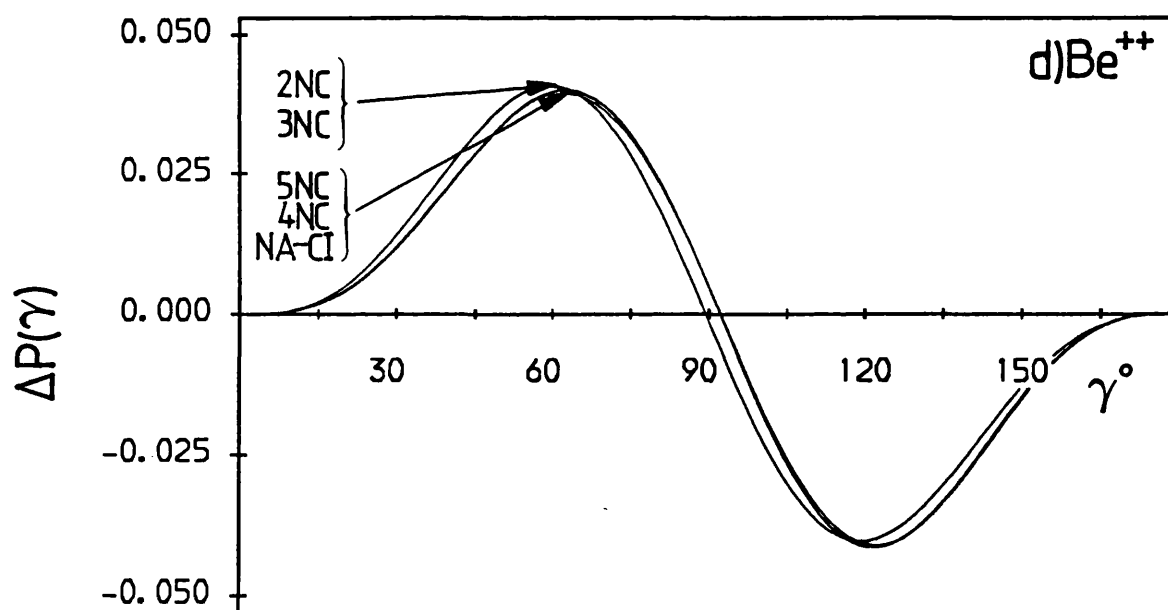
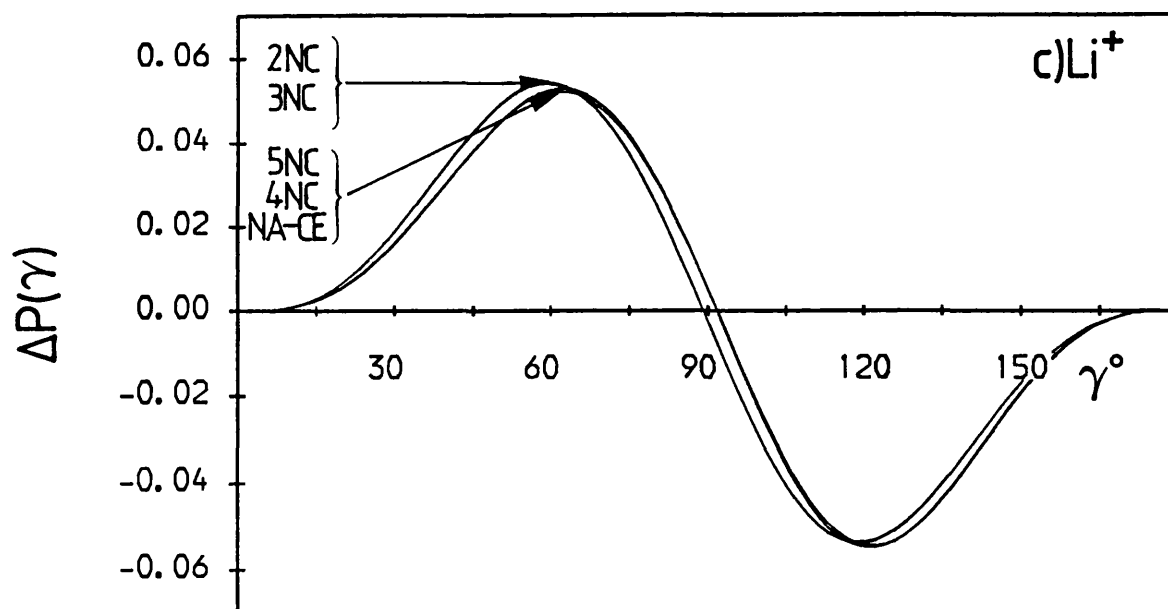


Figure III.21 c) & d)

The angular shifts $\Delta P(\gamma)$ for c) Li^+ and d) Be^{++} . In each case the 2NC, 3NC, 4NC, 5NC and NA-CI wavefunctions are used as the correlated descriptions.

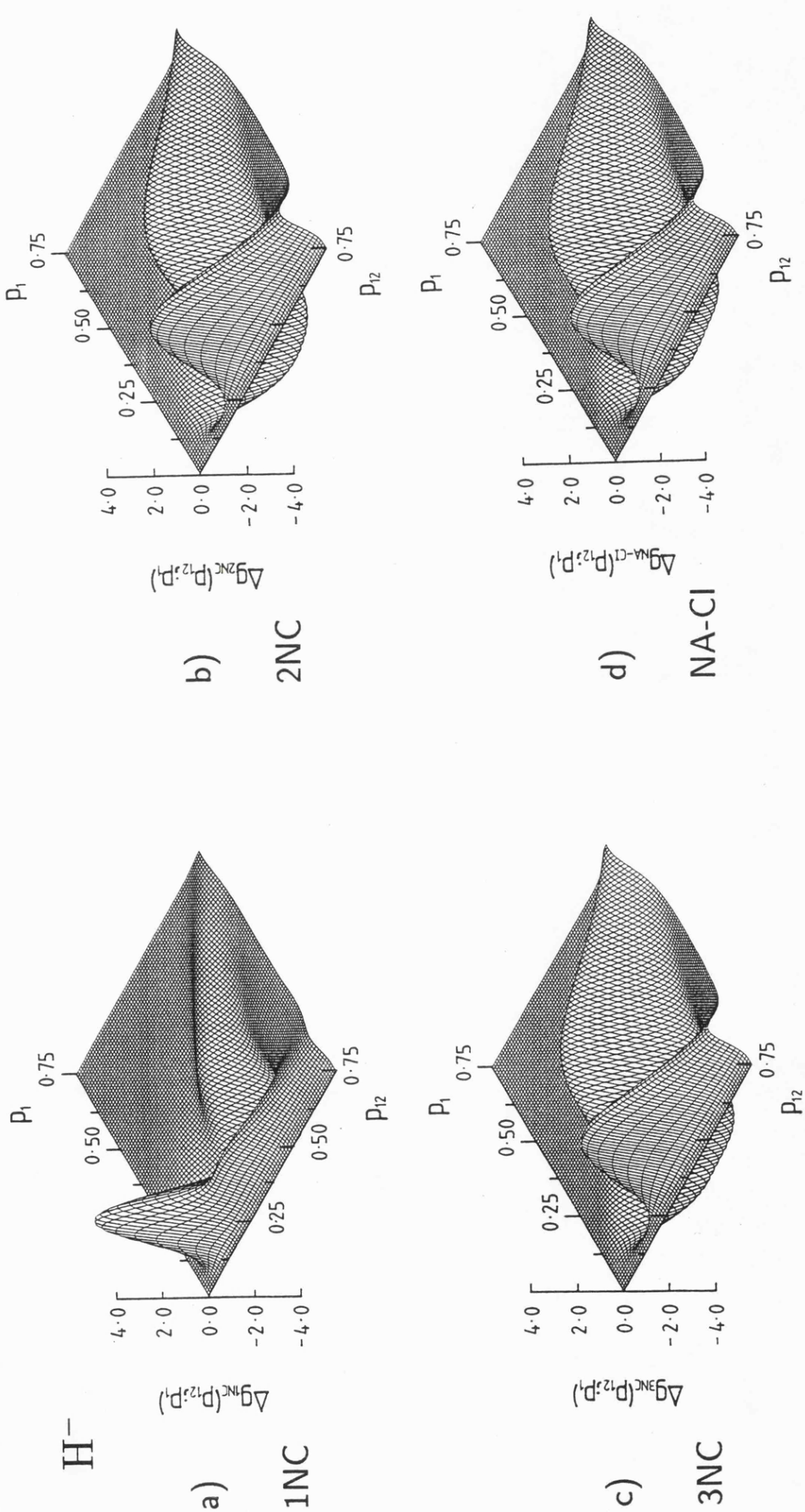


Figure III.22

The partial Coulomb shifts $\Delta g(p_{12}; p_1)$ for the H^- system using the a) 1NC, b) 2NC, c) 3NC and d) NA-CI wavefunctions for the correlated descriptions.

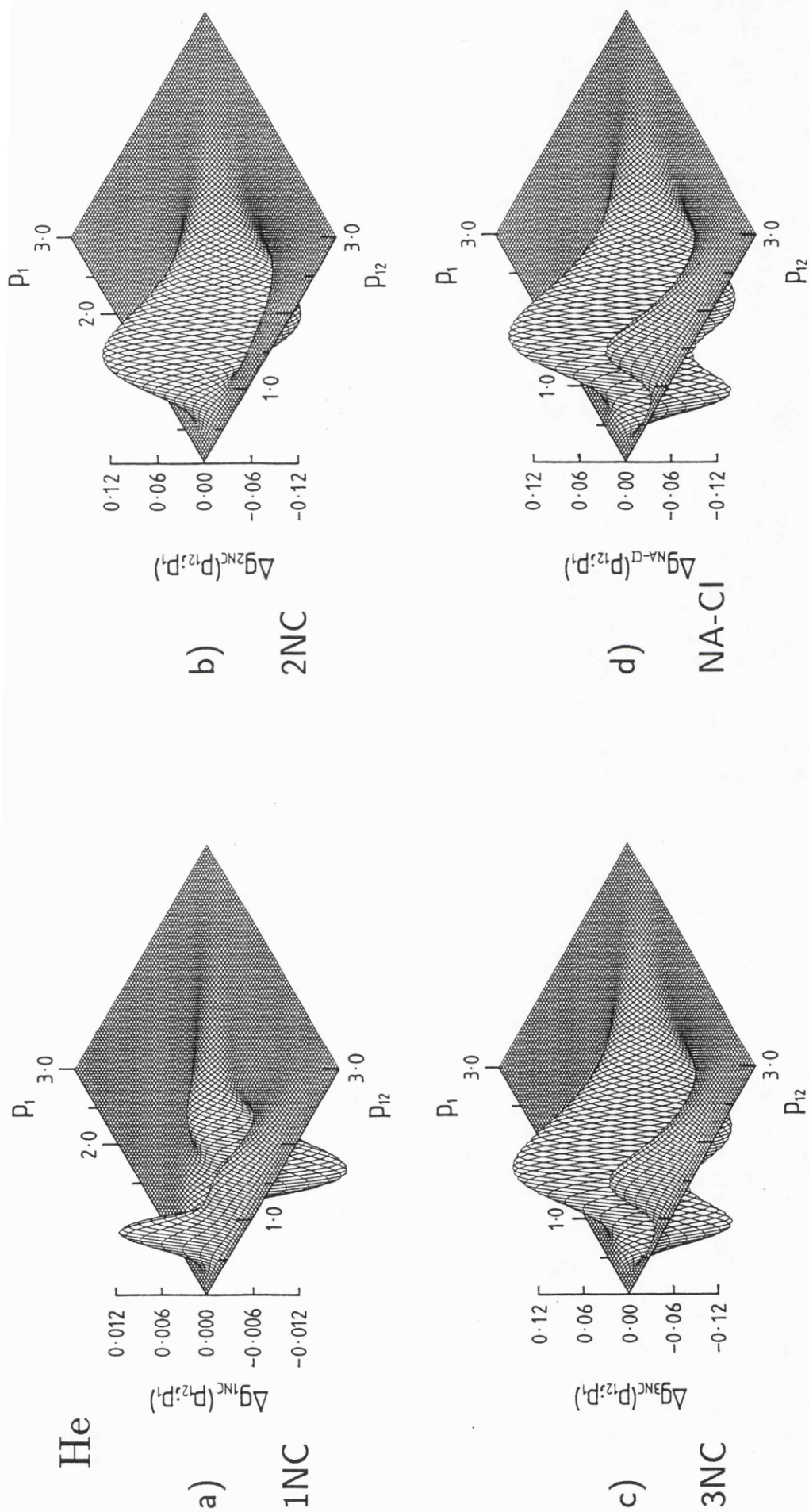


Figure III.23

The partial Coulomb shifts $\Delta g(p_{12}; p_1)$ for the He system using the a) 1NC, b) 2NC, c) 3NC and d) NA-CI wavefunctions for the correlated descriptions. Note the different vertical scale employed in a).

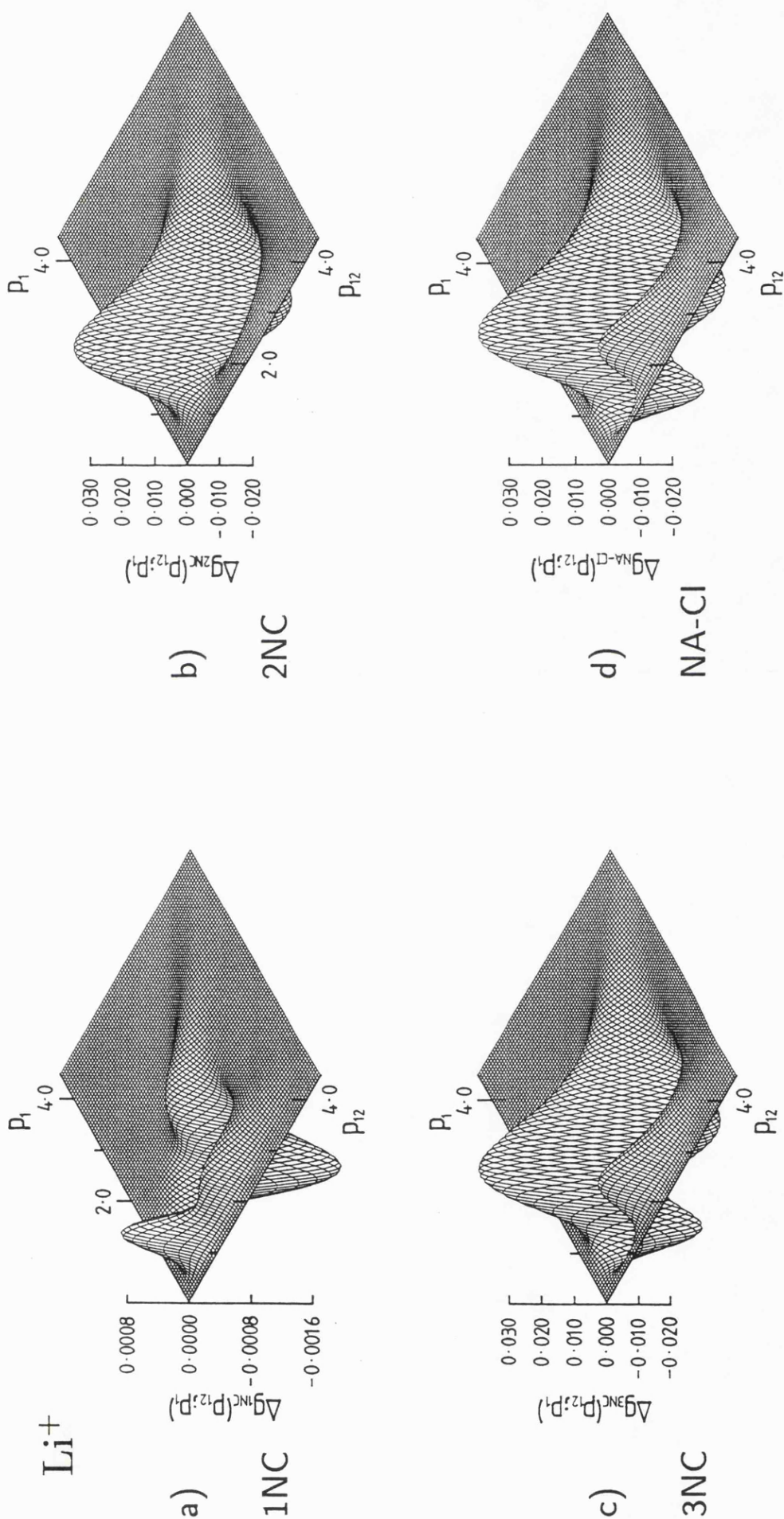


Figure III.24

The partial Coulomb shifts $\Delta g(p_{12}; p_1)$ for the Li^+ system using the a) 1NC, b) 2NC, c) 3NC and d) NA-CI wavefunctions for the correlated descriptions. Note the different vertical scale employed in a).

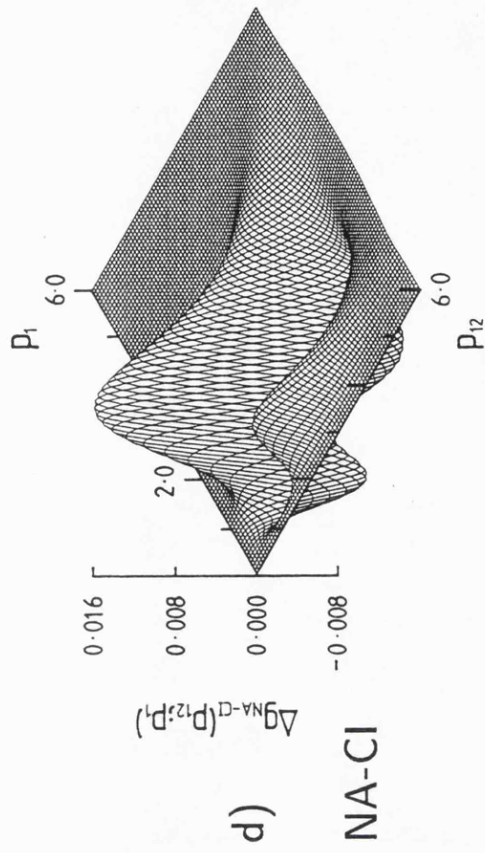
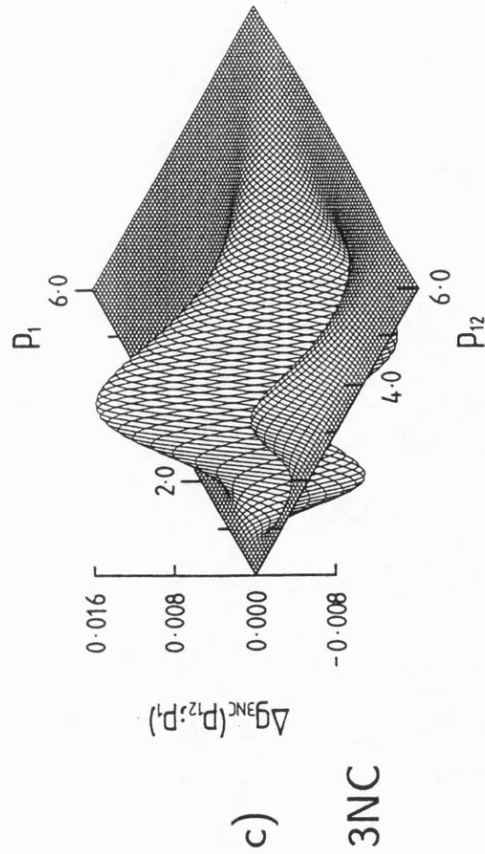
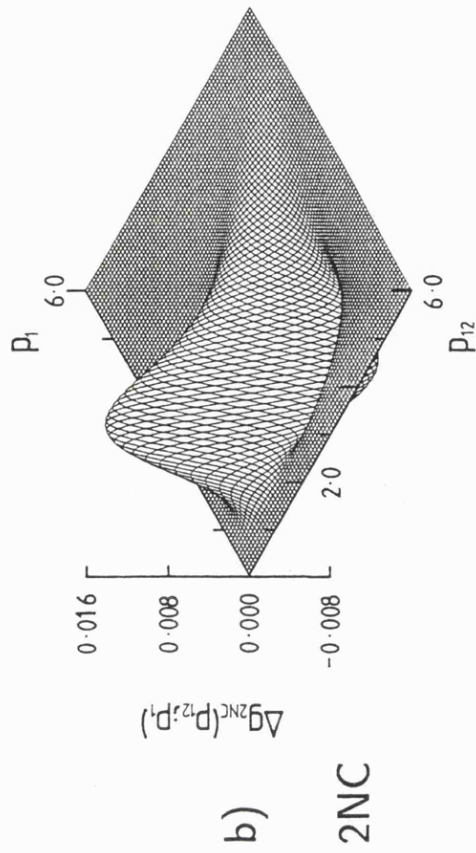
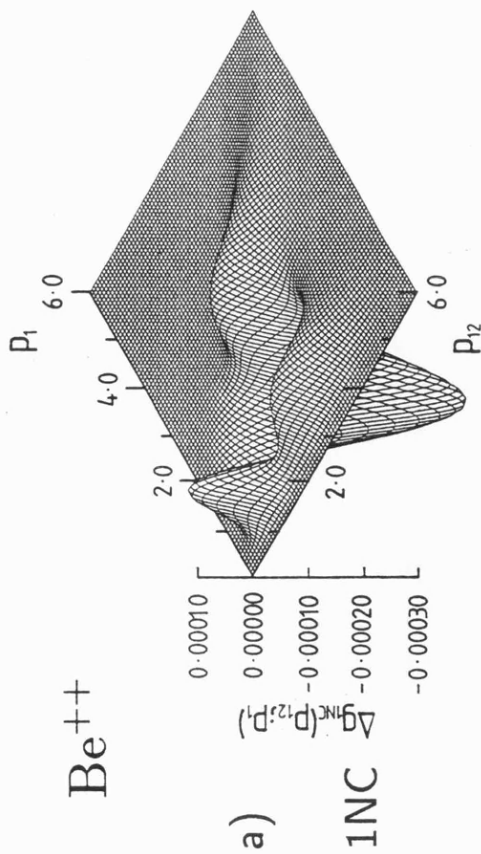


Figure III.25

The partial Coulomb shifts $\Delta g(p_{12}; p_1)$ for the Be^{++} system using the a) 1NC, b) 2NC, c) 3NC and d) NA-CI wavefunctions for the correlated descriptions. Note the different vertical scale employed in a).

Part IV
Appendices

Appendix A

Curve-Fitting

A.1 Introduction

Two of the wavefunctions which we have used for our analysis, as originally calculated, contained some numerically-defined radial functions. We have fitted these functions with linear combinations of the radial parts of Slater-type orbitals (STO's). This was done to make our analysis more tractable. Each Froese Fisher Hartree-Fock (HF) wavefunction contains a numerical radial function $R(r)_{HF}^{NUM}$. This function is also used in the first configuration of the Nicolaidis and Aspromallis configuration interaction (NA-CI) wavefunctions. It would be feasible, though difficult, to carry out the analysis described in chapter 4 for the HF wavefunctions using the numerical functions, but such an approach would be impracticable for the NA-CI wavefunction, owing to the large number of analytically-defined radial functions also present. A further reason for using the fitted radial functions in this work was our desire to conduct a correlation study in momentum space as well as in position space. Although it is possible to transform a numerically-defined radial function into a numerically-defined momentum space radial function via the Dirac transformation, (see chapter 7), such a function will contain additional errors due to the numerical integrations involved in the transformation. The transformation of a STO is, on the other hand, exact, and the resulting momentum space radial function contains no errors over and above those engendered by the curve-fitting process.

The Hartree, and Hartree-Fock functions first introduced in the late 1920's [3,4] were defined numerically in their radial parts. It was soon realized that this form was inconvenient for the purpose of carrying out calculations on wavefunctions so generated. In 1932 Slater [190] performed a fit on various atomic wavefunctions calculated by Hartree. He used a maximum of 3 STO's for each orbital, and varied only the linear coefficients. The small number of functions used in each fit meant that only limited agreement with the original numerical radial functions was achieved. His tabulated values for Rb^+ show relative errors typically of the order of 1%. In 1953 Löwdin [191], using a greater number of fitting STO's, performed fits on various atomic systems and attained a relative accuracy perhaps an order of magnitude better than that of Slater.

In the 1950's, analytic Hartree-Fock wavefunctions began to be produced [192,193], and soon became very popular. These functions have the advantage of being in an analytic form, without the disadvantage of having to perform a fitting procedure separate from the original wavefunction production. However, they have the slight disadvantage that they are in principle a less accurate representation of the true Hartree-Fock wavefunction for a given system than the corresponding numerical Hartree-Fock function. This is because a summation of STO's has *limited* flexibility, compared with a purely numerical function. Despite the advent of analytic wavefunctions, fitting of Hartree-Fock functions continued [194] and in 1965, Curl and Coulson [29] reported a fit of the ground state of H^- using 5 STO's, with a relative error of $\sim 0.01\%$.

A.2 Fitting Procedure

We introduce the fundamental equation for fitting with a linear combination of the radial parts of STO's as follows:

$$R_{HF}^{NUM}(r) \simeq R_{HF}^{STO}(r) = \sum_{i=1}^{N^{STO}} C_i^{STO} r^{n_i} e^{-\zeta_i r}, \quad (\text{A.1})$$

where C_i^{STO} and ζ_i are parameters used in the fitting process, and n_i are simply positive integers selected before the fitting process begins. It should be noted that the individual terms in the summation are not normalized, although the radial function in its entirety

is. A slightly different way of writing an STO can be seen in equation 7.4.

In order to carry out the fitting, we have used the program UNIFIT4, written by von Meerwall [195,196]. It is a χ^2 routine; that is, it aims to minimize the sum of the squares of the differences between the numerical data points and the fitting function evaluated at these points:

$$\chi^2 = \sum_{j=1}^{N^{Points}} \left[R_{HF}^{NUM}(r_j) - R_{HF}^{STO}(r_j) \right]^2, \quad (A.2)$$

where N^{Points} is the number of numerical points used. A slightly different procedure was used for H^- . That will be described in the discussion section of this chapter.

If we denote the fitting parameters C_i^{STO} and ζ_i by $P_1, P_2, \dots, P_{2N^{STO}}$, then we can regard the problem as that of finding the minimum point of the $2N^{STO}$ -dimensional surface, $\chi^2(P_1, P_2, \dots, P_{2N^{STO}})$. The UNIFIT4 program attempts to do this by first performing a coarse grid search whereby some parameters are varied by fixed amounts, in order to try to 'jump' out of local minima; it then finds the local minimum by evaluating the gradient of the surface at trial points. Clearly there is no certainty that our final fit is a global minimum, but, as our object is to find a fit sufficiently accurate for our purposes, this is not of great moment.

Obtaining a sufficient number of points, in the correct radial regions, was not a straightforward matter. The Froese Fischer Hartree-Fock code [112] produces points on an exponential scheme suited to the evaluation of energy. Thus many more points were produced close to the origin than at a larger radius. It was therefore necessary to run the program many times, using a slightly different starting point for the radius each time, in order to get a high enough density of points in the outer regions. The resulting enormous number of points had to be condensed in order to produce an equal density of points over the regions where the function had a significant magnitude.

Different values of n_i in equation A.1 denote different *kinds* of STO's. Large values of n_i will tend to produce STO's which contribute more to the outer regions of the fit than do low- n_i STO's. High- n_i STO's are thus useful if a given fit is found to be deficient at high- r , as they may be added in without disrupting the fit of the *inner*

regions to the same extent as low- n_i STO's. Nevertheless, as the radial function that is being fitted has $2p$ character, most of the STO's in each fit have $n_i = 1$. It should be noted that the ζ_i in equation A.1 are varied in the fitting procedure, unlike earlier fitting studies. The advantage of this is that the fitting function is thus much more flexible, and so, in principle, should produce a more accurate final fit. However, it has the disadvantage of possible *linear dependence*. That is to say, the fitting procedure may change the exponential parameters so that two ζ_i 's have similar values. This is clearly inefficient, as they effectively represent the same STO. When this occurred, the problem was overcome by replacing the two dependent STO's with one STO with a C_i value equal to the sum of the two original C_i 's, and with an exponent equal to the average of the two original ζ_i 's. Tabulated values of n_i , C_i and ζ_i for each system can be found in table A.1.

A.3 Tests of Goodness-of-Fit

There are a number of criteria that can be used to assess the quality of our fitted curve. The most basic criterion is the difference between the fitted radial and the original numerical radial:

$$\Delta R(r) = R_{HF}^{NUM}(r) - R_{HF}^{STO}(r). \quad (\text{A.3})$$

This curve is known as the *residual*, and obviously shows in which regions the fit is good, and in which regions it is deficient. It tends to have an oscillatory form.

If we take a fixed correlated $D(r_1)$, (for example, generated from the Drake wavefunction), then it is possible to compare $\Delta D(r_1)$ curves formed from the fitted and numerical Hartree-Fock wavefunctions. It was found that even in the worst case, these were barely visually distinguishable. This can be seen for He and Be^{++} in figure A.1. The two curves for H^- are not visually distinguishable, whereas the discrepancy for Li^+ is similar to that in the two systems that we have displayed. These differences are certainly not enough to affect any interpretation that might be made. It is possible to evaluate the expectation values, $\langle r_1^n \rangle$, using both kinds of radial functions. The dif-

ferences were found to be negligible compared with the differences between these values and the corresponding correlated values; this can be seen in table II.4.

As our study is concerned with correlation properties, we thought it essential to assess the effect of the curve-fitting on a subsequently calculated interparticle function. It is possible to evaluate $f(r_{12})$ for the numerical HF wavefunction. We have therefore examined $\Delta f(r_{12})$ for the fitted and numerical HF's, using the same correlated function. In no case are they visually distinguishable. Again, we examined the corresponding expectation values, $\langle r_{12}^n \rangle$, shown in table II.8 and found that the differences between the fitted and the numerical HF values were negligible with respect to the changes which arise from correlation effects.

It was important to ensure that the fitted function was an accurate representation of the numerical radial function in *momentum space* as well as in position space. To this end the numerical function was transformed into a numerical momentum space radial function, (see section 7.2). As the primary criterion of accuracy in momentum space, we form the difference between the fitted and numerical radial functions:

$$\Delta R(p) = R_{HF}^{NUM}(p) - R_{HF}^{STO}(p). \quad (\text{A.4})$$

We examined the correlation function $\Delta D(p_1)$ formed using both the fitted and the numerical $D(p_1)$ functions as representations of the HF description. For the correlated function the NA-CI wavefunction was used. It should be noted that evaluating the $D(p_1)$ for this wavefunction is dependent on using the fitted Hartree-Fock as its first configuration. We found that the differences between these two $\Delta D(p_1)$ curves were small and not of significance in the interpretation of the results. This can be seen for He and Be^{++} in figure A.2. It was not possible to discriminate between the two curves for H^- by eye, and the results for Li^+ were similar to those for the two systems that are shown. In addition, the expectation values $\langle p_1^n \rangle$ were evaluated for the fitted and numerical functions. It can be seen in table III.1 that the differences between them are small compared to the differences in the values due to correlation effects.

One can compare the energy of the numerical Hartree-Fock wavefunction with the energy of the fitted Hartree-Fock wavefunction, calculated with use of the expectation

values, $\langle r_1^{-1} \rangle$, $\langle r_{12}^{-1} \rangle$, $\langle p_1^2 \rangle$. A similar exercise can be conducted for the NA-CI wavefunctions. In no case was the fractional error in the energies greater than 10^{-5} , and in some cases it was less than 10^{-7} .

A.4 Discussion

It should be clear from the previous section that in evaluating the quality of our fitted wavefunctions we have concentrated on the extent to which the *differences* between the Hartree-Fock and the correlated level are reproduced. This highlights the fact that there is no single criterion of a ‘good’ fit. Whether a fit is good or not depends on the purpose for which it is intended. If we merely wished to reproduce the general shape of the radial function to a level where the eye could not tell the difference, 3 or 4 STO’s would suffice. But to reproduce accurately the correlation differences we found that between 7 and 10 were needed.

As the atomic number, Z , increases, the magnitude of the correlation effects becomes smaller. We would therefore expect that more STO’s would be needed to reproduce the correlation effects to an acceptable level. This, broadly speaking, is what is observed. He required 7 STO’s, Li^+ required 9, and Be^{++} needed 10. But H^- , in fact, also required 10 STO’s. This is explained mainly by the fact that the H^- Hartree-Fock radial is extremely diffuse, but partly by the fact that an alternative method of fitting was used in this case. The H^- radial function was the first curve to be fitted, and in an effort to produce a fitted curve that would produce an accurate $D(r_1)$ the χ^2 was evaluated on the difference between the numerical $D(r_1)$ and the $D(r_1)$ derived from the STO fit. That is,

$$\chi^2 = \sum_{j=1}^{N_{\text{Points}}} [D(r_{1j})^{\text{NUM}} - D(r_{1j})^{\text{STO}}]^2 = \sum_{j=1}^{N_{\text{Points}}} [r_{1j}^2 R^2(r_{1j})^{\text{NUM}} - r_{1j}^2 R^2(r_{1j})^{\text{STO}}]^2. \quad (\text{A.5})$$

Although the resulting fit was highly accurate over most values of the radius, the effect of the r_1^2 factor caused the error in the radial function at low- r_1 to become quite large. The extremely large magnitude of the correlation effects in this system render our fit

wholly acceptable, but for the other systems we chose to conduct the fit on the radial function, as has been conventional in other such curve-fitting studies. In fact, the relative error for the H^- radial function was approximately the same as for the more compact ground-state H^- radial fit of Curl and Coulson mentioned earlier [29]. The relative errors for our other fits were almost an order of magnitude better than this.

A fit that is good in position space is not necessarily good in momentum space. It was observed that when $\Delta D(p_1)$ was plotted using numerical and fitted HF wavefunctions, the proportionate difference was greater than the proportionate difference when $\Delta D(r_1)$ was plotted using different kinds of HF radial functions. This can be seen in figures A.1 and A.2. This feature is not unexpected, as the χ^2 is, after all, evaluated on a position space function. An additional problem is the well-known effect whereby the Dirac transformation changes the regions of emphasis. This means that relatively small errors over a region of large- r_1 may be enfolded into a large error at small- p_1 . In the cases of Li^+ and Be^{++} this problem is accentuated by the small magnitude of some of the $\Delta D(p_1)$ curves at small- p_1 (see figure A.2.b, for example). An initial fit of the Hartree-Fock radial functions for these two systems had to be rejected because, although the position space fit was quite satisfactory, the $\Delta D(p_1)$ curves were significantly different at low- p_1 for the fitted and the numerical Hartree-Fock wavefunctions. The fit was re-performed to remove this difficulty. Naturally, the results we give for these two systems are for the later, superior, fit.

Many studies of correlation effects are conducted using analytic Hartree-Fock wavefunctions. A comparison of the energies of some analytic and numerical Hartree-Fock wavefunctions [197,21] reveals a very good agreement between the energies. It is, however, frequently observed in quantum chemistry that a wavefunction that has an accurate energy may reproduce other properties poorly. A significant advantage of using fitted Hartree-Fock functions is the fact that, although the fitting process introduces errors that may be non-trivial, it is possible to assess these errors and thus estimate the accuracy of any subsequent results obtained by using the fitted wavefunctions.

A.5 Table and Figures

WF	i	n_i	C_i	ζ_i
H ⁻	1	1	1.7474344 E-03	2.7500063
	2	1	-3.2211735 E-03	1.5454308
	3	1	4.6890077 E-02	0.71250865
	4	1	5.0478879 E-02	0.44312299
	5	1	1.1561809 E-02	0.32964975
	6	1	1.2180033 E-02	0.21827531
	7	2	1.5823037 E-05	0.11874883
	8	4	-4.1499378 E-09	0.11489110
	9	10	7.6996254 E-19	0.17000000
He	1	1	1.5806417 E-03	14.300250
	2	1	-2.2976881 E-03	7.5778567
	3	1	3.7980493 E-01	1.3093095
	4	1	3.3094461 E-02	1.0698733
	5	1	3.9559915 E-01	0.78350066
	6	1	7.4529712 E-02	0.62521799
	7	2	3.8478334 E-03	3.2070735
Li ⁺	1	1	1.8205988 E-03	8.6554169
	2	1	-4.3418744 E-02	3.8076460
	3	1	8.0162055 E-01	2.1395418
	4	1	4.8205533 E-01	1.4287951
	5	1	1.2759679 E 00	1.2527676
	6	1	1.4501205 E-01	1.0266786
	7	1	2.6939209 E-05	0.87573390
	8	1	-3.5933012 E-04	0.51488248
	9	10	1.3342048 E-11	0.99998520
Be ⁺⁺	1	1	7.6210362 E-03	22.459214
	2	1	-2.4816728 E-03	9.1348474
	3	1	-2.3933433 E-02	8.4618855
	4	1	1.6487616 E 00	2.7183398
	5	1	3.6487335 E 00	1.7549715
	6	1	4.2651749 E-01	1.5917691
	7	1	1.3027452 E-02	1.3795948
	8	1	1.1404017 E-03	0.97586898
	9	1	2.7996919 E-05	0.54581043
	10	10	-1.2546361 E-09	1.5311403

Table A.1

The Slater-Type orbitals which comprise each fitted Hartree-Fock radial function. The n_i are integers which define the type of STO, whilst the C_i and ζ_i are the linear and exponential parameters respectively. See equation A.1 for further details. In the C_i column the number after 'E' denotes the power of ten by which the entry is to be multiplied.

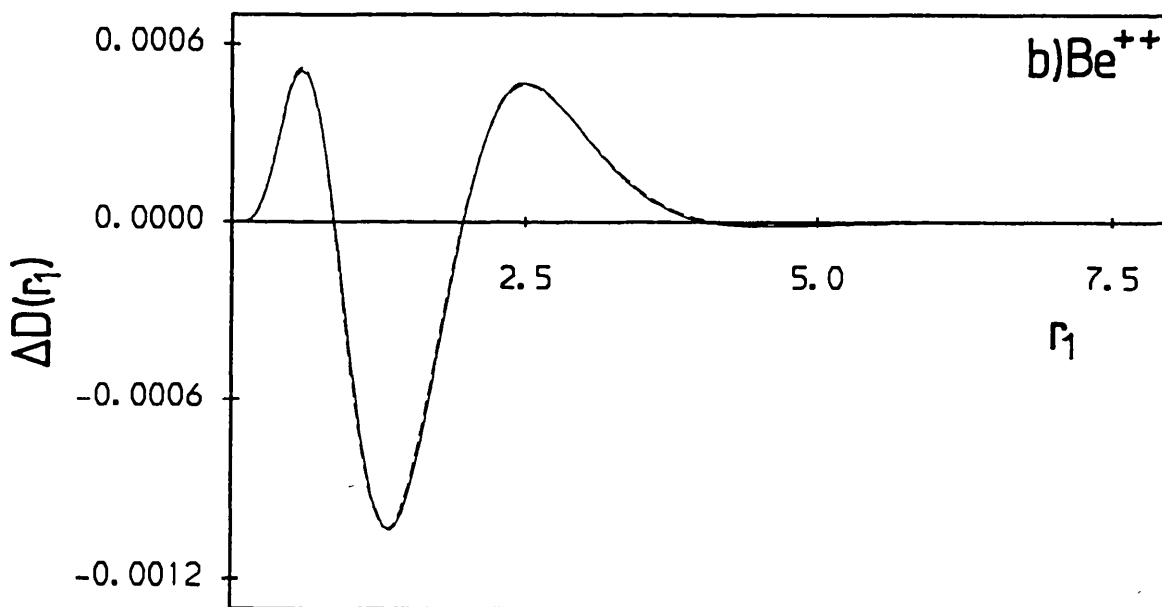
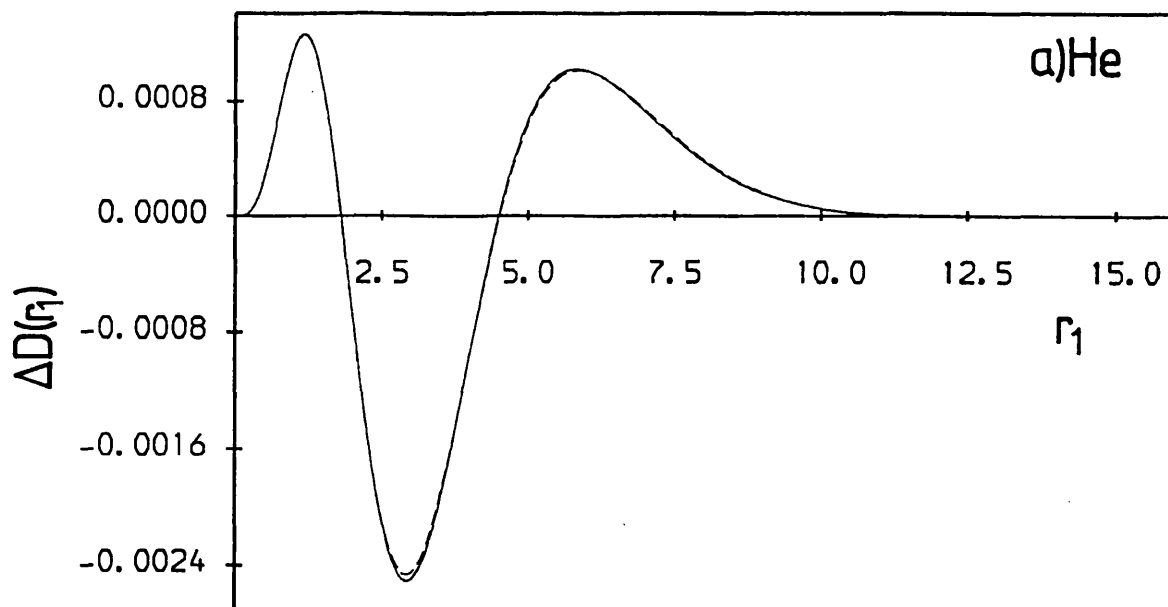


Figure A.1 a) & b)

The radial holes, $\Delta D(r_1)$, for a) He and b) Be^{++} are presented using both the numerical Hartree-Fock (full curve) and the STO-fitted Hartree-Fock (broken curve) as uncorrelated descriptions. In all curves the 13-term Drake wavefunction for the system is used as the correlated description.

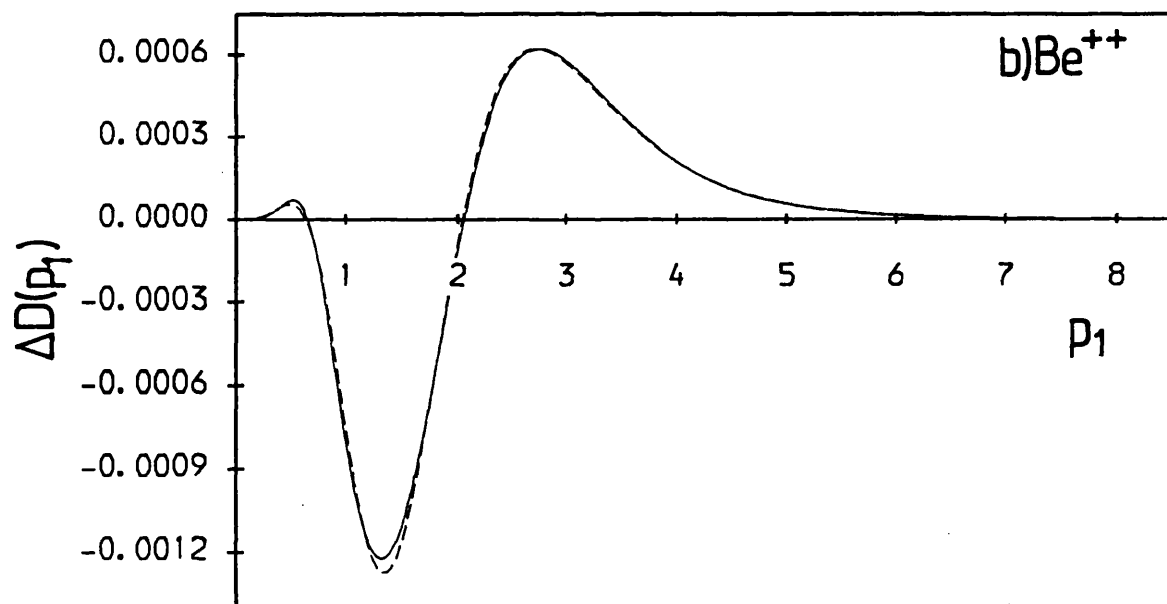
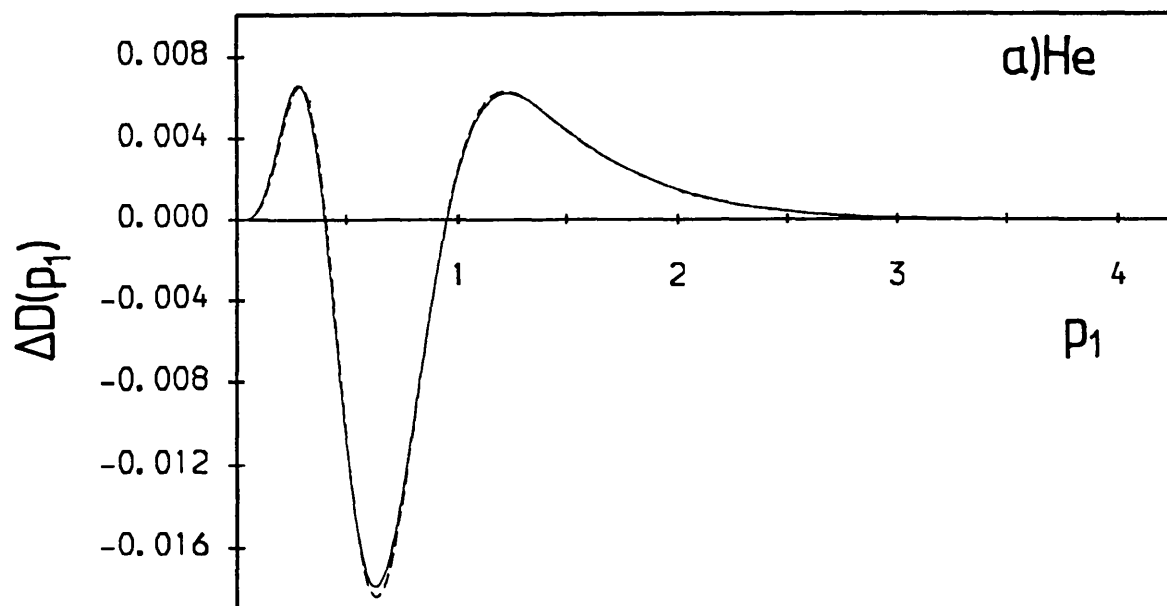


Figure A.2 a) & b)

The radial shifts, $\Delta D(p_1)$, for a) He and b) Be⁺⁺ are presented using both the numerical Hartree-Fock (full curve) and the STO-fitted Hartree-Fock (broken curve) as uncorrelated descriptions. In all curves the NA-CI wavefunction for the system is used as the correlated description.

Appendix B

Gram-Schmidt Orthogonalization

The Nicolaides and Aspromallis Configuration Interaction (NA-CI) wavefunction contains radial functions $R_i(r)$ which comprise summations of Slater-type orbitals, (STO's) (see chapter 3). All radials which pertain to orbitals of the same angular symmetry form an orthonormal set:

$$\int_0^{\infty} R_i^*(r)R_j(r)r^2 dr = \delta_{ij}. \quad (\text{B.1})$$

To produce this orthonormal set, one starts from a set of primitive functions, $u_i(r)$ and employs the Gram-Schmidt orthogonalization procedure [198] to produce $R_i(r)$, which are a linear combination of $u_i(r)$. In the case of the first p-type radial function, which is the fitted HF-radial function, the primitive function is a summation of STO's, produced by the curve fitting process, (see Appendix A).

It should be noted that the *form* of the following analysis, which is adapted from Arfken [199], is essentially independent of the nature of the functions which we wish to orthogonalize, and the definition of orthogonality that we employ. As all our radial functions are real, we may drop the complex conjugation in equation B.1, and write:

$$\int_0^{\infty} R_i(r)R_j(r)r^2 dr = \delta_{ij}. \quad (\text{B.2})$$

We take the un-normalized, non-orthogonal, primitive functions $u_i(r)$, form the orthogonal, but un-normalized, functions $\psi_i(r)$, and then form the orthonormal functions $R_i(r)$.

The $\psi_i(r)$ are, by definition, given by:

$$\psi_i(r) = u_i + a_{i0}R_0(r) + a_{i1}R_1 + \cdots + a_{ii-1}R_{i-1}, \quad (\text{B.3})$$

where it may be shown that:

$$a_{ij} = - \int_0^\infty u_i(r)R_j(r)r^2 dr. \quad (\text{B.4})$$

Equation B.4 may be derived by multiplying equation B.3 by $r^2 R_j(r)$ and then integrating from 0 to ∞ with respect to r . In order to evaluate $R_i(r)$, we must know $R_0(r), R_1(r), R_2(r) \dots R_{i-1}(r)$. Therefore we start, taking $\psi_0(r) = u_0(r)$, and proceed with increasing index i . Normalized functions are achieved by means of the expression:

$$R_i(r) = \frac{\psi_i}{\sqrt{\int_0^\infty \psi_i^2 r^2 dr}}. \quad (\text{B.5})$$

We will also need to express $R_i(r)$ in terms of $R_0(r)$ to $R_{i-1}(r)$:

$$R_i(r) = N_1 u_i + b_{i0}R_0(r) + b_{i1}R_1 + \cdots + b_{ii-1}R_{i-1}, \quad (\text{B.6})$$

where N_1 is a normalization constant produced using equation B.5. As each of the functions $R_1(r)$ to $R_{i-1}(r)$ in equation B.6 is composed, ultimately, of primitive functions $u_i(r)$, it will be most efficient to express the orthonormalized functions in terms of $u_i(r)$:

$$R_i(r) = c_{i0}u_0 + c_{i1}u_1 + \cdots + c_{ii}u_i. \quad (\text{B.7})$$

The orthonormal functions $R_i(r)$ that we have just generated are not a unique set. Even if we specify the order in which the functions are to be orthogonalized, the signs of the $R_i(r)$ are not uniquely determined. It is clear that if the functions we have constructed obey equation B.3, then if we multiply an arbitrary number of $R_i(r)$ by -1 , the resulting set will still obey equation B.3. The sign convention that is used in the NA-CI wavefunction is to demand that c_{ii} in equation B.7 is positive.

Appendix C

Natural Orbital Analysis

C.1 Introduction

In 1955, Löwdin[200] defined the natural spin-orbitals of a state as that orthonormal basis set of spin-orbitals which diagonalizes the single-particle reduced density matrix, $\gamma(\underline{x}_1'|\underline{x}_1)$. In general, for an N-electron system, $\gamma(\underline{x}_1'|\underline{x}_1)$ is given by:

$$\gamma(\underline{x}_1'|\underline{x}_1) = N \int \Psi^*(\underline{x}_1', \underline{x}_2, \dots, \underline{x}_N) \Psi(\underline{x}_1, \underline{x}_2, \dots, \underline{x}_N) d\underline{x}_2 \dots d\underline{x}_N, \quad (\text{C.1})$$

where \underline{x}_1 represents the space-spin coordinates of electron 1. The prime on the first \underline{x}_1 within the integrand indicates that if an operator were being used it would only apply to the unprimed \underline{x}_1 . This a useful convention, as it allows this density matrix to be used to discuss all one-electron properties. For our purposes, however, this additional complexity is redundant, and we henceforth do not use it. In this case, the density matrix is equal to the single-particle density function, $\rho(\underline{x}_1)$. In the case of two-electron wavefunctions, it is possible to write the wavefunction as the product of a spatial part and a spin part. This means that we may neglect the spin part in our natural orbital analysis. We therefore only refer to natural orbitals, rather than natural spin-orbitals.

In practice, of course, it is impossible to determine the natural orbitals exactly, because it is not possible to determine the single-particle density exactly. It is feasible, however, to find *approximate* natural orbitals. A common way of doing this is to perform a configuration interaction (CI) calculation, using a given basis set, and then form an

orthonormal basis set which is a linear combination of the original basis functions. This new basis is formed so that the total wavefunction is unaltered, but the approximate single-particle density is diagonal when expressed in this new basis set.

The point of finding the natural orbitals (NO's) is that it may be shown [148,149,201] that for a two-electron system a CI expansion containing natural orbitals will have certain optimal convergence properties. That is, a wavefunction formed by truncating a natural expansion to a certain number of terms and re-normalizing will have the minimum quadratic deviation from the exact wavefunction for any wavefunction of this length. Or, equivalently, such a truncation will have the highest overlap with the exact wavefunction. It is therefore to be expected that the truncated natural expansion has approximately the best energy for a wavefunction of this form [202]. The natural expansion consists of the natural configurations (symmetry-adapted combinations of natural orbitals) ordered in decreasing order of importance in the wavefunction.

Unfortunately, as it is necessary to perform a CI calculation to obtain the natural orbitals in the first place, this result cannot be directly applied. It is, however, possible to obtain a CI wavefunction, produce approximate natural orbitals from this wavefunction, and then perform a further CI calculation using the most important configurations containing the natural orbitals together with some new configurations. This procedure can be repeated, and the final energy is generally substantially lower than the energy obtained from the original CI calculation. This is the so-called iterative natural orbital method [203,204]. Also, it has been found [205] that approximate *atomic* natural orbitals can be employed profitably in subsequent molecular calculations.

For our purposes, the convergence properties of natural expansions make them extremely useful for the study of correlation effects. Because the energy of the first natural configuration is usually a good approximation to the Hartree-Fock energy, the addition of further natural configurations may be seen as adding correlation effects. This addition of correlation effects is occurring in the most efficient way possible, owing to the energy convergence properties mentioned above. Natural expansions have been used extensively in the analysis of correlation effects in the ground state of He-like [126,137,138,139] sys-

tems and the H_2 molecule [140,141,142]. An additional reason for studying natural orbitals is that they are, in principle, independent of any particular calculation. That is, they are a property of the wavefunction of the state. In practice, one can, of course, only deal with approximate natural orbitals. The accuracy of these will clearly depend on the accuracy of the approximate wavefunction from which they are derived.

We have evaluated approximate natural orbitals from the Nicolaides and Aspromalis configuration interaction (NA-CI) wavefunctions [111]. These are highly accurate wavefunctions, as may be seen by inspecting table II.1. It would have been possible to produce natural expansions based on the Drake wavefunctions, but the presence in them of powers of r_{12} renders such an exercise difficult.

It is appropriate to comment here on the nature of the first natural orbital. It is customary to state that the first natural orbital is a good approximation to the Hartree-Fock orbital [149]. In fact, for two-electron systems the first two natural orbitals are equivalent to the first two Brueckner orbitals [145,206]. The radial parts of these orbitals may be shown to be approximately equal to the Hartree-Fock radial functions with the appropriate Sinanoğlu f -orbital correction functions, (see chapter 1) added to them [155] (with renormalization of the resulting functions). A normalized determinant formed from Brueckner orbitals will be the determinant with the greatest overlap with the complete wavefunction [147]. For many properties, including the energy, the difference between the Hartree-Fock and the Brueckner wavefunctions is frequently negligible. For some single-particle properties, however, this is not so, as may be seen from the results presented in this thesis (see especially figures II.18 and III.3).

C.2 Method

The procedure used to obtain an approximate natural expansion from the NA-CI wavefunction will now be described. It must be emphasized that this account is specific to the $2p^2\ ^3P$ state of He-like systems. Similar accounts have been given for other systems [142,207,208].

It is possible to write the NA-CI wavefunction in the form:

$$\Psi(\mathbf{r}_1, \mathbf{r}_2) = \sum_{k,l} C_{kl} \phi_k(\mathbf{r}_1) \phi_l(\mathbf{r}_2), \quad (\text{C.2})$$

where $\phi(\mathbf{r})$ are orthonormal orbitals, and C_{kl} are real constants, such that: $C_{kl} = -C_{lk}$, in order to ensure antisymmetry. The spin part of the wavefunction is not included. We may rewrite this more conveniently in matrix form:

$$\Psi(\mathbf{r}_1, \mathbf{r}_2) = \phi(\mathbf{r}_1) \mathbf{C} \phi(\mathbf{r}_2)^T, \quad (\text{C.3})$$

where \mathbf{C} is a square matrix containing the coefficients C_{kl} , and $\phi(\mathbf{r}_1)$ is a row matrix containing the orbitals $\phi_k(\mathbf{r}_1)$. In this chapter matrices are denoted by the use of bold type. The 'T' superscript denotes the transpose of the matrix to which it is applied. The elements C_{kl} are zero when k and l label orbitals of different angular symmetry. This means that the matrix \mathbf{C} has a block-diagonal form. The natural orbital analysis can thus be carried out separately on each block of a given angular type.

For this wavefunction, the single-particle density function may be written:

$$\rho(\mathbf{r}_1) = \int \Psi(\mathbf{r}_1, \mathbf{r}_2)^* \Psi(\mathbf{r}_1, \mathbf{r}_2) d\tau_2 = \sum_{k,l} C_{kl}^D \phi_k^*(\mathbf{r}_1) \phi_l(\mathbf{r}_1), \quad (\text{C.4})$$

where C_{kl}^D are real constants such that $C_{kl}^D = C_{lk}^D$, and τ_2 is the volume element for electron 2. Again, we rewrite this in matrix form:

$$\rho(\mathbf{r}_1) = \phi^*(\mathbf{r}_1) \mathbf{C}^D \phi(\mathbf{r}_1)^T, \quad (\text{C.5})$$

where \mathbf{C}^D contains the constants C_{kl}^D . It is important to note that the matrices introduced so far are simply expressions of information that we already have about the wavefunction. They are therefore treated as known quantities in the following analysis.

The natural orbitals are each a linear combination of the original basis set. Expressed in matrix form:

$$\chi(\mathbf{r}) = \phi(\mathbf{r}) \mathbf{A}, \quad (\text{C.6})$$

where $\chi(\mathbf{r})$ is a row matrix containing the natural orbitals, and \mathbf{A} is a square matrix containing the linear combining coefficients. We require by definition that the single

particle density expressed in the natural basis, $\chi(\mathbf{r})$, is diagonal. Therefore, if we write

$$\rho(\mathbf{r}_1) = \chi^*(\mathbf{r}_1) \mathbf{C}^{NO} \chi(\mathbf{r}_1)^T, \quad (\text{C.7})$$

\mathbf{C}^{NO} must be diagonal. Our problem is to determine $\chi(\mathbf{r})$, \mathbf{A} and \mathbf{C}^{NO} .

Equation C.6 entails that:

$$\phi(\mathbf{r}) = \chi(\mathbf{r}) \mathbf{A}^{-1}, \quad (\text{C.8})$$

$$\phi(\mathbf{r})^T = (\mathbf{A}^{-1})^T \chi(\mathbf{r})^T. \quad (\text{C.9})$$

Substituting equation C.8 and equation C.9 into equation C.5 gives:

$$\rho(\mathbf{r}_1) = \chi^*(\mathbf{r}_1) (\mathbf{A}^{-1})^* \mathbf{C}^D (\mathbf{A}^{-1})^T \chi(\mathbf{r}_1)^T. \quad (\text{C.10})$$

Thus, from equation C.7, we may define:

$$\mathbf{C}^{NO} = (\mathbf{A}^{-1})^* \mathbf{C}^D (\mathbf{A}^{-1})^T. \quad (\text{C.11})$$

We require from their definition that the natural orbitals be orthonormal; that is,

$$\langle \chi(\mathbf{r}_1)^T | \chi(\mathbf{r}_1) \rangle = \mathbf{I}, \quad (\text{C.12})$$

where \mathbf{I} is the identity matrix. If we substitute equation C.6 into this expression we obtain:

$$\langle \mathbf{A}^T \phi(\mathbf{r}_1)^T | \phi(\mathbf{r}_1) \mathbf{A} \rangle = \mathbf{I}. \quad (\text{C.13})$$

But the orthogonality property of our original basis set, $\langle \phi(\mathbf{r}_1)^T | \phi(\mathbf{r}_1) \rangle = \mathbf{I}$, implies that:

$$(\mathbf{A}^T)^* \mathbf{A} = \mathbf{I}, \quad (\text{C.14})$$

and therefore:

$$\mathbf{A}^* = (\mathbf{A}^{-1})^T. \quad (\text{C.15})$$

Substitution of this relation into equation C.11 gives:

$$\mathbf{C}^{NO} = (\mathbf{A}^{-1})^* \mathbf{C}^D \mathbf{A}^*, \quad (\text{C.16})$$

and by a simple rearrangement:

$$\mathbf{C}^D \mathbf{A}^* = \mathbf{A}^* \mathbf{C}^{NO}. \quad (\text{C.17})$$

Remembering that \mathbf{C}^{NO} is defined to be diagonal, we can see that this expression is equivalent to the matrix eigenequation:

$$\mathbf{C}^D \mathbf{A}_i^* = \lambda_i \mathbf{A}_i^*, \quad (\text{C.18})$$

where λ_i is the i th eigenvalue and \mathbf{A}_i^* is the i th eigenfunction. Each \mathbf{A}_i^* is a column matrix, and together they form \mathbf{A}^* . In other words, we must now find the eigenvalues and eigenfunctions of the matrix \mathbf{C}^D . The λ_i form the diagonal elements of the matrix \mathbf{C}^{NO} . Solution of the eigenproblem was achieved by means of a standard NAG library routine [209].

Having found \mathbf{A} , we can determine $\chi(\mathbf{r})$ by the use of equation C.6. The matrix \mathbf{C}^{NO} is determined by the λ_i values. We may reconstruct the original wavefunction using equations C.3, C.8 and C.9:

$$\Psi(\mathbf{r}_1, \mathbf{r}_2) = \chi(\mathbf{r}_1) \mathbf{A}^{-1} \mathbf{C} (\mathbf{A}^{-1})^T \chi(\mathbf{r}_2)^T. \quad (\text{C.19})$$

We can write this:

$$\Psi(\mathbf{r}_1, \mathbf{r}_2) = \chi(\mathbf{r}_1) \mathbf{C}^x \chi(\mathbf{r}_2)^T, \quad (\text{C.20})$$

where:

$$\mathbf{C}^x = \mathbf{A}^{-1} \mathbf{C} (\mathbf{A}^{-1})^T. \quad (\text{C.21})$$

Writing this in non-matrix form, we have:

$$\Psi(\mathbf{r}_1, \mathbf{r}_2) = \sum_{k,l} C_{kl}^x \chi_k(\mathbf{r}_1) \chi_l(\mathbf{r}_2), \quad (\text{C.22})$$

where C_{kl}^x are elements of \mathbf{C}^x , and $\chi_k(\mathbf{r}_1)$ are the individual natural orbital elements of the matrix $\chi(\mathbf{r})$. It is of interest to note that any given $\chi_i(\mathbf{r})$ will be composed of a linear combination of orbitals with *identical* angular parts. Thus the natural orbital analysis only affects the *radial* parts of the orbitals. Therefore we may speak of natural *radials*. In fact, equation C.22 only gives a simple expression in terms of orbital products. It

is possible to reconstruct natural configurations from this equation. Nomenclature for the resulting expression is given in chapter 3. It should be noted that the natural configurations will each contain only one natural radial function.

Bibliography

- [1] E.Schrödinger, *Phys. Rev.* **28** (1926) 1049.
- [2] F.L.Pilar, *Elementary Quantum Chemistry*, McGraw-Hill Book Company: New York (1968).
- [3] D.R.Hartree, *Proc. Cambridge Phil. Soc.* **24** (1927) 89 and 111.
- [4] V.Fock, *Z. Physik* **61** (1930) 126.
- [5] J.C.Slater, *Phys. Rev.* **34** (1929) 1293.
- [6] P.O.Löwdin, *Advan. Chem. Phys.* **2** (1959) 207.
- [7] C.A.Coulson and A.H.Neilson, *Proc. Phys. Soc.* **78** (1961) 831.
- [8] J.M.Ugalde and R.J.Boyd, *Int. J. Quantum. Chem.* **27** (1985) 439.
- [9] *Methods in Computational Chemistry, Volume 1: Electron Correlation in Atoms and Molecules*, edited by S.Wilson, Plenum Press: New York (1987) 121.
- [10] E.Hylleraas, *Z. Physik* **54** (1929) 347.
- [11] E.Hylleraas, *Z. Physik* **48** (1928) 469.
- [12] L.Pauling and E.B.Wilson, *Introduction to Quantum Mechanics*, McGraw-Hill Book Company: Singapore (1935).
- [13] B.H.Bransden and C.J.Joachain, *Physics of Atoms and Molecules*, Longman Group Limited: New York (1983) 275.

- [14] C.L.Pekeris, Phys. Rev. **112** (1958) 1649.
- [15] K.Frankowski and C.L.Pekeris, Phys. Rev. **146** (1966) 46; **150** (1966) 366E.
- [16] D.E.Freund, B.D.Huxtable and J.D.Morgan III, Phys. Rev. A **29** (1984) 980.
- [17] H.M.James, Phys. Rev. **49** (1936) 688.
- [18] R.McWeeny and B.T.Sutcliffe, *Methods of Molecular Quantum Mechanics*, Academic Press: London (1969) 271.
- [19] A.R.Edmonds, *Angular Momentum in Quantum Mechanics*, Second Edition, Princeton University Press: Princeton (1960) 21.
- [20] H.Eyring, J.Walter and G.E.Kimball, *Quantum Chemistry*, John Wiley & Sons: New York (1944) 369.
- [21] C.Froese Fischer, *The Hartree-Fock Method for Atoms*, John Wiley & Sons: New York (1977).
- [22] O.Sinanoğlu and K.A.Brueckner, *Three Approaches to Electron Correlation in Atoms*, Yale University: New Haven (1970).
- [23] X.Feng and J.P.Dahl, Int. J. Quantum Chem. **36** (1989) 689.
- [24] O.Sinanoğlu, Rev. Mod. Phys. **35** (1963) 517.
- [25] G.K.Taylor and K.E.Banyard, Phys. Rev. A **8** (1973) 1157.
- [26] T.L.Gilbert, Rev. Mod. Phys. **35** (1963) 491.
- [27] H.Tatewaki and K.Tanaka, J. Chem. Phys. **60** (1974) 601.
- [28] A.J.Thakkar, *Extracules, Intracules, Correlation Holes, Potentials, Coefficients and All That*, in *Density Matrices and Density Functionals* edited by R.M.Erdahl and V.H.Smith Jr, Reidel: Dordrecht (1987) 553.
- [29] R.F.Curl and C.A.Coulson, Proc. Phys. Soc. **85** (1965) 647.

- [30] W.A.Lester Jr and M.Krauss, J. Chem. Phys. **41** (1964) 1407.
- [31] R.J.Boyd and C.A.Coulson, J. Phys. B **6** (1973) 782.
- [32] K.E.Banyard and C.E.Reed, J. Phys. B **11** (1978) 2957.
- [33] G.R.Taylor and R.G.Parr, Proc. Natl. Acad. Sci. U.S. **38** (1952) 154.
- [34] K.E.Banyard and D.J.Ellis, Mol. Phys. **24** (1972) 1291.
- [35] K.E.Banyard and P.K.Youngman, J. Phys. B **15** (1982) 853.
- [36] A.J.Thakkar, J. Phys. B **20** (1987) 3939.
- [37] K.E.Banyard and M.M.Mashat, J. Chem. Phys. **67** (1977) 1405.
- [38] R.J.Mobbs and K.E.Banyard, J. Chem. Phys. **78** (1983) 6106.
- [39] Liu Tong-jiang, Zhang Zhi-jie and Zhao Yi-jun, J. Phys. B **21** (1988) 535.
- [40] K.E.Banyard and K.H.Al-Bayati, J. Phys. B **19** (1986) 2211.
- [41] K.H.Al-Bayati and K.E.Banyard, J. Phys. B **20** (1987) 465.
- [42] *Compton Scattering: The Investigation of Electron Momentum Distributions*, edited by B.Williams, McGraw-Hill International Book Company: New York (1977).
- [43] P.K.Youngman and K.E.Banyard, J. Phys. B **20** (1987) 3313.
- [44] K.E.Banyard and P.K.Youngman, J. Phys. B **20** (1987) 5585.
- [45] K.E.Banyard, K.H.Al-Bayati and P.K.Youngman, J. Phys. B **21** (1988) 3177.
- [46] K.E.Banyard, J. Phys. B **23** (1990) 777.
- [47] N.Koyama et al., J. Phys. B **19** (1986) L331.
- [48] O.Robaux, J. Phys. B **20** (1987) 2347.
- [49] K.Molmer and K.Taulbjerg, J. Phys. B **21** (1988) 1739.

- [50] J.M.Rost and J.S.Briggs, *J. Phys. B* **21** (1988) L233.
- [51] J.Burgdörfer and R.Morgenstern, *Phys. Rev. A* **38** (1988) 5520.
- [52] I.K.Dmitrieva and G.I.Plindov, *J. Phys. B* **21** (1988) 3055.
- [53] H.Bachau, *J. Phys. B* **21** (1988) 3547.
- [54] H.Y.Wong and A.R.P.Rau, *Phys. Rev. A* **38** (1988) 4446.
- [55] A.R.P.Rau and Q.Molina, *J. Phys. B* **22** (1989) 189.
- [56] C.D.Lin, *Phys. Rev. A* **29** (1984) 1019.
- [57] R.S.Berry, *How Much are Atoms Like Molecules?*, seminar at the University of York, March 1987.
- [58] O.Sinanoğlu, *J. Chem. Phys.* **36** (1962) 706.
- [59] D.R.Herrick and O.Sinanoğlu, *Phys. Rev. A* **11** (1975) 97.
- [60] D.R.Herrick and M.E.Kellman, *Phys. Rev. A* **21** (1980) 418.
- [61] J.H.Bartlett, *Phys. Rev.* **51** (1937) 661.
- [62] C.D.Lin, *Phys. Rev. A* **27** (1983) 22.
- [63] P.Rehmus, M.E.Kellman and R.S.Berry, *Chem. Phys.* **31** (1978) 239.
- [64] J.L.Krause, J.D.Morgan III and R.S.Berry, *Phys. Rev. A* **35** (1987) 3189.
- [65] G.S.Ezra and R.S.Berry, *Phys. Rev. A* **28** (1983) 1974.
- [66] P.Rehmus and R.S.Berry, *Chem. Phys.* **38** (1979) 257.
- [67] C.A.Nicolaidis, N.Makri and Y.Komninos, *J. Phys. B* **20** (1987) 4963.
- [68] Y.Komninos, N.Makri and C.A.Nicolaidis, *Z. Phys. D* **2** (1986) 105.
- [69] G.W.F.Drake and A.Dalgarno, *Phys. Rev. A* **1** (1970) 1325.
- [70] V.A.Boiko et al., *Mon. Not. R. astr. Soc.* **181** (1977) 107.

- [71] C.A.Nicolaidis, IEEE J. Quantum Electronics **QE-19** (1983) 1781.
- [72] P.G.Kruger, Phys. Rev. **36** (1930) 855.
- [73] T.Y.Wu, Phys. Rev. **66** (1944) 291.
- [74] J.L.Tech and J.F.Ward, Phys. Rev. Lett. **27** (1971) 367.
- [75] K.Aashamar, Nucl. Instr. Meth. **90** (1970) 263.
- [76] W.B.Westerveld et al., J. Phys. B **12** (1979) 2575.
- [77] P.D.Burrow, Phys. Rev. A **2** (1970) 1774.
- [78] H.B. van Linden van den Heuvell et al., J. Phys. B **13** (1980) 2475.
- [79] J.P.Buchet et al., Phys. Rev. A **7** (1973) 922.
- [80] T.Andersen, S.M.Bentzen and O.Poulsen, Physica Scripta, **22** (1980) 119.
- [81] K.R.Karim and C.P.Bhalla, Phys. Rev. A **37** (1988) 1507.
- [82] J.M.Bañón, M.Koenig and H.Nguyen, J. Phys. B **18** (1985) 4195.
- [83] P.Audebert, Phys. Rev. A **30** (1984) 768.
- [84] J.G.Lunney and J.F.Seely, J. Phys. B **15** (1982) L121.
- [85] J.Dunn, Ph.D. Thesis, *High Resolution Spectroscopy of Laboratory Sources*, University of Leicester (1990).
- [86] R.Jáuregui and C.F.Bunge, J. Chem. Phys. **71** (1979) 4611.
- [87] T.Nagata, J. Phys. Soc. Jap. **39** (1975) 1334.
- [88] A.van Wijngaarden, J.Patel, K.Becker and G.W.F.Drake, *Fourteenth International Conference on the Physics of Electronic and Atomic Collisions*, Palo Alto, USA, North-Holland: Amsterdam (1985) 383.
- [89] A.van Wijngaarden, J.Patel, K.Becker and G.W.F.Drake, Phys. Rev. A **32** (1985) 2150.

- [90] N.A.Doughty, P.A.Fraser and R.P.McEachran, *Mon. Not. R. astr. Soc.* **132** (1966) 255.
- [91] R.Wildt, *Ap. J.* **95** (1939) 295.
- [92] G.W.F.Drake, *Ap. J.* **189** (1974) 161.
- [93] S.R.Heap and T.P.Stecher, *Ap. J.* **187** (1974) L27.
- [94] P.L.Bernacca and L.Bianchi, *Astron. Astrophys.* **75** (1979) 61.
- [95] G.W.F.Drake, *Ap. J.* **184** (1973) 145.
- [96] V.L.Jacobs, A.K.Bhatia and A.Temkin, *Ap. J.* **191** (1974) 785.
- [97] V.L.Jacobs, A.K.Bhatia and A.Temkin, *Ap. J.* **200** (1975) 239.
- [98] T.Y.Wu, *Phys. Rev.* **46** (1934) 239.
- [99] W.S.Wilson, *Phys. Rev.* **48** (1935) 536.
- [100] E.Hylleraas, *Ap. J.* **111** (1950) 209.
- [101] E.Holøien, *Physica Norvegica* **1** (1961) 53.
- [102] E.Holøien, *Nucl. Instr. Meth.* **90** (1970) 229.
- [103] E.Holøien and J.Midtdal, *J. Phys. B* **4** (1971) 1243.
- [104] J.Midtdal et al., *Physica Norvegica* **5** (1971) 177.
- [105] G.W.F.Drake, *Phys. Rev. Lett.* **24** (1970) 126.
- [106] A.K.Bhatia, *Phys. Rev. A* **2** (1970) 1667.
- [107] D.R.Beck and C.A.Nicolaides, *Chem. Phys. Lett.* **59** (1978) 525.
- [108] C.Froese Fischer, *Computer Phys. Commun.* **4** (1972) 126.
- [109] G.W.F.Drake, Private Communication, September 1986.
- [110] G.W.F.Drake, Private Communication, December 1986.

- [111] C.A.Nicolaides and G.Aspromallis, Private Communication, July 1987.
- [112] C.Froese Fischer, *Computer Phys. Commun.* **43** (1987) 355.
- [113] H.Margenau and G.M.Murphy, *The Mathematics of Physics and Chemistry*, D.Van Nostrand Company Inc.: Princeton, New Jersey, 2nd Edition, (1956).
- [114] R.Benesch, *Int. J. Quantum Chem.* **6** (1972) 181.
- [115] J.L.Calais and P.O.Löwdin, *J. Mol. Spect.* **8** (1962) 203.
- [116] G.W.F.Drake, *Phys. Rev. A* **18** (1978) 820.
- [117] S.Fraga and G.Malli, *Many-Electron Systems: Properties and Interactions*, W.B.Saunders: Philadelphia, (1968).
- [118] J.H. Van Vleck, *The Theory of Electric and Magnetic Susceptibilities*, Oxford University Press: Oxford (1932).
- [119] *Numerical Algorithm Fortran Library Manual, Mark 13*, (1989).
- [120] D.J.Ellis, Ph.D. Thesis, *Angular Correlation in Atoms and the Calculation of Molecular Wavefunctions*, University of Leicester (1974).
- [121] A.Dalgarno, *Advanc. Phys.* **11** (1962) 281.
- [122] W.A.Bingel, *Chem. Phys. Lett.* **5** (1970) 367.
- [123] K.E.Banyard and J.C.Moore, *J. Phys. B* **10** (1977) 2781.
- [124] K.E.Banyard and R.J.Mobbs, *J. Chem. Phys.* **75** (1981) 3433.
- [125] W.Kutzelnigg, G.Del Re and G.Berththier, *Phys. Rev.* **172** (1968) 49.
- [126] K.E.Banyard and C.C.Baker, *J. Chem. Phys.* **51** (1969) 2680.
- [127] P.K.Youngman, Ph.D. Thesis, *Electron Correlation Effects in Some S and P States of Helium and Lithium*, University of Leicester (1986).
- [128] J.Lennard-Jones and J.A.Pople, *Phil. Mag.* **43** (1952) 581.

- [129] K.H.Al-Bayati, Ph.D. Thesis, *Electron Correlation in the $(1s^22s)^2P$ and $(1s^22p)^2S$ States of the Lithium Isoelectronic Sequence in Position and Momentum Space*, University of Leicester (1984).
- [130] K.E.Banyard and G.J.Seddon, *J. Chem. Phys.* **58** (1973) 1132.
- [131] G.J.Seddon, Ph.D. Thesis, *A Study of Electron Correlation Effects in Two-Electron Atoms*, University of Leicester (1973).
- [132] K.E.Banyard and C.E.Reed, *J. Phys. B* **14** (1981) 411.
- [133] A.J.Thakkar and V.H.Smith Jr., *Chem. Phys. Lett.* **42** (1976) 476.
- [134] T.Kato, *Commun. Pure Appl. Math.* **10** (1957) 151.
- [135] A.J.Thakkar, *J. Chem. Phys.* **84** (1986) 6830.
- [136] D.R.Beck and C.A.Nicolaides, *Theory of the Electronic Structure of Excited states in Small Systems with Numerical Applications to Atomic States*, in *Excited States in Quantum Chemistry* edited by C.A.Nicolaides and D.R.Beck, Reidel: Dordrecht (1978) 105.
- [137] H.Shull and P.O.Löwdin, *J. Chem. Phys.* **30** (1959) 617.
- [138] R.Ahlrichs, W.Kutzelnigg and W.A.Bingel, *Theor. Chim.* **5** (1966) 289.
- [139] E.R.Davidson, *J. Chem. Phys.* **39** (1963) 875. *Acta.* **5** (1966) 289.
- [140] E.R.Davidson and L.L.Jones, *J. Chem. Phys.* **37** (1962) 2966.
- [141] S.Hagstrom and H.Shull, *Rev. Mod. Phys.* **35** (1963) 624.
- [142] J.Sanders, Ph.D. Thesis, *Electron Correlation Effects in H_2 and H_3^+ and a Study of Fluctuation Potentials in Atoms*, University of Leicester (1988).
- [143] C.E.Reed, Ph.D. Thesis, *Properties of Electron Momentum Distributions: A Study of Correlation Effects in Some Two-Electron Systems and an Examination of Directional Compton Profiles for the Lithium Halides*, University of Leicester (1980).

- [144] B.Roos, *The Configuration Interaction Method*, in *Computational Techniques in Quantum Chemistry and Molecular Physics* edited by G.H.F.Diercksen, B.T.Sutcliffe and A.Veillard, Reidel: Dordrecht (1975) 251.
- [145] S.Larsson, *Chem. Phys. Lett.* **7** (1970) 165.
- [146] K.A.Brueckner, *Phys. Rev.* **96** (1957) 508.
- [147] V.H.Smith Jr. and W.Kutzelnigg, *Arkiv. Fysik.* **38** (1968) 309.
- [148] A.J.Coleman, *Rev. Mod. Phys.* **35** (1963) 668.
- [149] P.O.Löwdin and H.Shull, *Phys. Rev.* **101** (1956) 1730.
- [150] O.Sinanoğlu and D.B.Tuan, *J. Chem. Phys.* **38** (1963) 219.
- [151] R.E.Stanton, *J. Chem. Phys.* **42** (1965) 2353.
- [152] A.J.Duben and J.P.Lowe, *J. Chem. Phys.* **55** (1971) 4276.
- [153] C.F.Bender and E.R.Davidson, *J. Chem. Phys.* **49** (1968) 4222.
- [154] F.Grimaldi, *Adv. Chem. Phys.* **14** (1969) 341.
- [155] G.K.Taylor, Ph.D. Thesis, *Cluster Analysis and Pair Function Synthesis of Correlated Wavefunctions*, University of Leicester (1973).
- [156] C.F.Bunge and A.V.Bunge, *Int. J. Quantum Chem. Symp.* **12** (1978) 345.
- [157] G.W.F.Drake, Private Communication, January 1988.
- [158] S.H.Patil, *J. Phys. B* **23** (1990) 1.
- [159] S.Gasiorowicz, *Quantum Physics*, John Wiley and Sons: New York, (1974) 119.
- [160] H.E.Hall, *Solid State Physics*, John Wiley and Sons: New York, (1974) 128.
- [161] A.H.Compton, *Bull. Natl. Res. Counc.* **4** (1922).
- [162] A.H.Compton, *Phys. Rev.* **21** (1923) 483.

- [163] A.H.Compton, Phys. Rev. **22** (1923) 409.
- [164] a) G.E.M.Jauncey, Phys. Rev. **24** (1924) 204.
b) G.E.M.Jauncey, Phys. Rev. **25** (1925) 314.
c) G.E.M.Jauncey, Phys. Rev. **24** (1924) 723.
- [165] J.W.M.DuMond, Phys. Rev. **33** (1929) 643.
- [166] B.Podolsky and L.Pauling, Phys. Rev. **34** (1929) 109.
- [167] C.A.Coulson, Proc. Camb. Phil. Soc. **37** (1941) 55.
- [168] C.A.Coulson and W.E.Duncanson, Proc. Camb. Phil. Soc. **37** (1941) 67.
- [169] C.A.Coulson, Proc. Camb. Phil. Soc. **37** (1941) 74.
- [170] W.E.Duncanson, Proc. Camb. Phil. Soc. **37** (1941) 397.
- [171] W.E.Duncanson and C.A.Coulson, Proc. Camb. Phil. Soc. **37** (1941) 406.
- [172] C.A.Coulson and W.E.Duncanson, Proc. Camb. Phil. Soc. **38** (1942) 100.
- [173] N.Svartholm, Ph.D. Thesis, *The Binding Energies of the Lightest Atomic Nuclei*, University of Lund (1945).
- [174] R.McWeeny and C.A.Coulson, Proc. Phys. Soc. (London) **62A** (1949) 509.
- [175] R.McWeeny, Proc. Phys. Soc. (London) **62A** (1949) 519.
- [176] P.E.Regier and A.J.Thakkar, Phys. Rev. A **30** (1984) 30.
- [177] P.A.M.Dirac, *The Principles of Quantum Mechanics*, Oxford University Press: Oxford, 4th Edition (1958).
- [178] B.Williams, see reference [42], 211.
- [179] K.E.Banyard and R.J.Mobbs, J. Chem. Phys. **88** (1988) 3788.
- [180] D.L.Cooper, Private Communication, May 1989.

- [181] R.J.Weiss, *Acta. Cryst.* **25a** (1969) 248.
- [182] B.Williams, see reference [42], 213.
- [183] C.E.Reed and K.E.Banyard, *J. Phys. B* **13** (1980) 1519.
- [184] R.Benesch and S.Thomas, *Phys. Rev. A* **19** (1979) 931.
- [185] P.Kajiser and V.H.Smith Jr., *Adv. Quant. Chem.* **10** (1977) 37.
- [186] J.L.Powell and B.Crasemann, *Quantum Mechanics*, Addison-Wesley Publishing Company Inc.: Reading, Massachusetts, U.S.A. (1961).
- [187] R.Benesch and V.H.Smith Jr., in *Wave Mechanics—The First Fifty Years*, edited by W.C.Price, S.S.Chissick and T.Ravensdale, Butterworths: London (1973).
- [188] B.Williams, see reference [42], 117.
- [189] H.A.Bethe and E.E.Salpeter, *Quantum Mechanics of One- and Two-Electron Atoms*, Springer-Verlag: Berlin (1957).
- [190] J.C.Slater, *Phys. Rev.* **42** (1932) 33.
- [191] P.O.Löwdin, *Phys. Rev.* **90** (1953) 120.
- [192] G.G.Hall, *Proc. R. Soc. A* **205** (1951) 541.
- [193] C.C.J.Roothaan, *Rev. Mod. Phys.* **23** (1951) 69.
- [194] J.T.Zung and R.G.Parr, *J. Chem. Phys.* **41** (1964) 2888.
- [195] E.von Meerwall, *Computer Phys. Commun.* **11** (1976) 211.
- [196] E.von Meerwall, *Computer Phys. Commun.* **18** (1979) 411.
- [197] E.Clementi and C.Roetti, *Atomic Data and Nuclear Data Tables*, **14**, Academic Press Inc.: New York (1974).
- [198] F.B.Hildebrand, *Methods of Applied Mathematics*, Prentice-Hall Inc.: New Jersey (1965) 34.

- [199] G.Arken, *Mathematical Methods for Physicists*, 3rd Ed., Academic Press Inc.: San Diego, (1985) 516.
- [200] P.O.Löwdin, *Phys. Rev.* **97** (1954) 1474.
- [201] E.Schmidt, *Math. Annln.* **63** (1907) 433.
- [202] P.O.Löwdin, *Advan. Phys.* **5** (1956) 150.
- [203] C.F.Bender and E.R.Davidson, *J. Phys. Chem.* **70** (1966) 2675.
- [204] H.F.Schaefer III, *The Electronic Structure of Atoms and Molecules*, Addison-Wesley Publishing Company: Reading, Massachusetts (1972) 52.
- [205] J.Almlöf and P.R.Taylor, *J. Chem. Phys.* **92** (1990) 551.
- [206] N.C.Handy, J.A.Pople et al., *Chem. Phys. Lett.* **164** (1989) 185.
- [207] A.D.Tait, Ph.D. Thesis, *Configuration Interaction Studies of Small Molecules*, University of Leicester (1972).
- [208] C.C.Baker, Ph.D. Thesis, *Correlation Effects and Electron Densities in Some Two-Electron Systems*, University of Leicester (1969).
- [209] The NAG routine F02AGF was used to solve the matrix eigenequation. For documentation relating to the most recent implementation of the NAG library, see *Numerical Algorithm Fortran Library Manual, Mark 13* (1989).

The $2p^2\ ^3P$ State of Some He-Like Systems: Electron Correlation Effects

David Robert Trevena Keeble

ABSTRACT

In Part I the nature of the electron correlation problem is briefly discussed and some approaches to its solution and analysis are described. In addition, some previous work concerning the $2p^2\ ^3P$ state of helium-like systems is reviewed.

In Part II, position space electron correlation effects in the $2p^2\ ^3P$ state of H^- , He, Li^+ and Be^{++} are investigated. This study is conducted by examining the effects of correlation on a variety of radial, angular and interparticle distribution functions and expectation values. A number of different correlated and uncorrelated wavefunctions are employed for this purpose, allowing the merits of different approaches to be assessed. In particular, a natural orbital analysis performed on a configuration interaction wavefunction is used to gauge the relative importance of the angular and radial components of correlation, which are found to act in unison. It is seen that the correlation effects are similar in kind to those found in the ground state systems, though they are of a greater magnitude in this doubly excited state. The variation of the correlation effects with the atomic number, Z , is also examined.

To complement the results for position space, a parallel study of electron correlation effects in *momentum* space is presented in Part III. In contrast to the position space investigation, the radial and angular components of correlation are found to have *opposing* effects, producing a rich and informative total correlation effect. As in position space, the Z -dependent correlation behaviour is studied and it is seen to be more informative in momentum space. The correlation effects in momentum space are similar to the effects in ground state systems, but are of a greater magnitude.

Some techniques used in this research are described in three appendices in Part IV.

